UNIVERSITY OF TRENTO

Doctoral School in Civil, Environmental and Mechanical Engineering

Curriculum 2. Mechanics, Materials, Chemistry and Energy

Francesco Boggian

Timber shear walls for a sustainable build future

2022 - Doctoral thesis

UNIVERSITY OF TRENTO - Italy
Department of Civil, Environmental
and Mechanical Engineering

Doctoral School in Civil, Environmental and Mechanical Engineering
Topic 2. Mechanics, Materials, Chemistry and Energy - XXXIV cycle 2021/2022

Doctoral Thesis

Francesco Boggian

Timber shear walls for a sustainable build future

Supervisor
Prof. Roberto Tomasi
Norwegian University of Life Sciences

Credits of the cover image:
Francesco Boggian, 10/01/2021, Nordbytjernet, Norway

University of Trento
Doctoral School in Civil, Environmental and Mechanical Engineering
http://web.unitn.it/en/dricam
Via Mesiano 77, I-38123 Trento
Tel. +39 0461 282670 / 2611 - *dicamphd@unitn.it*

Abstract

This research is inserted in the topic of timber buildings. Many construction systems are available for building using timber, with the two main systems in residential ambit being Cross Laminated Timber and Light Timber Frame. Both systems reckon on the presence of shear walls to bear the effects of horizontal loads like seismic events or wind. This thesis deals with timber shear walls, and is divided into two parts: the first part is related to the ultimate and serviceability limit states rules to be included in upcoming versions of the building codes, while the second part presents a novel use of CLT walls as seismic renovation for existing buildings, as part of a European project.

The first part of the thesis, which is presented in three papers, is closely related to the process of producing new building codes, and aims at an easier integration between research and codification. The initial focus is the behaviour of Cross Laminated Timber subjected to in-plane loading. Eurocode 5 currently lacks a part concerning this product and the discussion is still ongoing regarding the methods for stresses evaluation and on the strength values to adopt for safety verifications.

The first paper tackles this problem by analysing different calculation methods currently available for the evaluation of the in-plane shear stresses, a common notation is introduced in order to have a meaningful comparison between methods proposed by different authors. All methods are then applied to a real case of existing experimental data regarding a four point bending test of CLT beams. Stiffness and strength of CLT are essential parameters for the definition of models to be adopted in codes regarding timber buildings, in particular for the calculation of shear walls.

Another very common timber construction system is called Light Timber Frame: an assembly comprising a timber frame and an external sheathing layer mechanically joined to the frame. Consequently LTF walls are considered, the study is directed towards shear wall models for the evaluation of deformations. The second paper focuses on the evaluation of the displacement at the top of LTF walls subjected to horizontal loads. This is a key aspect for designers, since the limitation of deformations ensures that the building retains a satisfactory performance at serviceability limit states. The displacement is due to many different contributions, with the sheathing-to-framing deformation being one of the major ones. The paper presents a comparison between two of the proposed methods to calculate the sheathing-to-framing deformation of LTF shear walls. The influence of the nail slip contribution on the overall displacement of the top of the wall is studied also with parametric analyses, by varying both mechanical properties and geometrical dimensions. Comparison with existing experimental

data is also provided. The study on shear walls regards also their lateral capacity, as well as the comparison between LTF and CLT walls of equal aspect ratio and similar restraining. In the third paper, existing cyclic test data on LTF and CLT walls were used to study the different displacement contributions and estimate the influence of the hold-down on the lateral response of the walls. A simplified capacity model is proposed for the walls, based solely on the hold-down forces.

The second part of the thesis deals with the use of CLT shear walls as a mean for the retrofit of existing buildings. The need for sustainable renovation solutions and improvement of the performance of existing buildings is at the base of the European project e-Safe. The project presents a multidisciplinary approach on building renovation, from mechanical, energetic, technological and architectural point of view. In this thesis the focus is on the seismic retrofit system called e-CLT: a CLT panel is attached to the outside of existing buildings with a novel connector that acts as a friction dissipation device, thus offering additional energy dissipation in case of strong earthquakes.

The fourth paper presents the first experimental campaign on this novel friction connector. Different geometries for the connector are studied and optimised, before being tested under cyclic protocol. The connector is tested on a steel setup, in order to isolate the friction behaviour and study the stability of the hysteresis loops. The results permitted to acquire new information useful for further developments on the system.

The fifth paper presents a subsequent experimental campaign on the friction connector. The shape is changed and improved in light of the previous results. The setup is improved and includes also a screw connection between friction connector and CLT panel. The goal is to study the influence of the timber connection on the friction dissipative performance. An analytical model is proposed, fitted on the experimental data.

Contents

Part 1

Introduction, background and overview of the work

1. Introduction

The work of this thesis focuses on timber walls for construction, and in particular Light Timber Frame (LTF) and Cross Laminated Timber (CLT). The first system, widely used for residential buildings in the US and Northern Europe is composed by a timber frame: vertical studs with a regular spacing are connected with a top and bottom rail elements. Bracing is provided by applying on one or both sides a sheathing layer, usually OSB or GFB, that is fixed to the frame elements with small diameter metal fasteners, usually nails or staples. The wall is then restrained against sliding and overturning by means of metal plates that fix the bottom rail to the foundation. Hold-downs are the most common system to resist the uplift, and angle brackets to restrain against sliding. Cross Laminated Timber (CLT) is a newer product that became popular in Europe over the last 20 years. It is usually produced in a plate-like shape, and is constituted by multiple layers of timber boards, with glue between each layer. The grain orientation of each layer is perpendicular with respect to the adjacent ones. This gives CLT panels good mechanical performances for both in plane and out of plane actions. CLT walls are restrained at the base with the same connections used also for LTF. The high degree of prefabrication opens up new possibilities of use for CLT panels, among others in the renovation interventions. CLT panels are lightweight and made from sustainable material, thus can represent an interesting solution for seismic retrofitting interventions.

1.1 Motivation

This thesis aims at giving a contribution to the knowledge and use of timber structures in two aspects: standardisation and renovation.
The process of producing building codes, standardisation/codification, is very long and requires a continuous dialogue and collaboration between different professional figures. The Eurocode for timber structures, EN1995, was published at first in 2004, after a development process that lasted over 20 years. Nevertheless, technology, construction materials and methods evolve, and in 2012 the European Commission invited the CEN (European Committee for Standardization, the

body producing the Eurocodes) to start the process of review of the existing Eurocode in order to publish a new updated version. Some key aspects, focus of the review process, are related to enhancing the ease of use and including CLT products. The papers attached to this thesis attempt to give a useful contribution in this process. The first paper will focus on the evaluation of in-plane shear stresses for CLT panels. The second paper will focus on the calculation of the displacement at the top of an LTF shear wall. The third paper will compare the rocking behavior of LTF and CLT walls in order to propose a unified simple mechanical model.
The renovation of existing buildings is a key topic of the present days, when awareness has been raised to sustainability, resources management and energy efficiency. The European Union has sponsored research on the topic "Decarbonisation of the EU building stock: innovative approaches and affordable solutions changing the market for buildings renovation" within the Horizon 2020 programme. The funded program *e-Safe* -Energy and Seismic AFfordable rEnovation solutions- aims at proposing an innovative approach to building renovation, which covers multiple aspects of the process. The contribution of this thesis to the progress of the project lies in the seismic retrofit system called e-CLT: CLT panels attached to the outside of existing buildings and connected with a novel steel friction connection. The fourth paper presents the preliminary results of the testing campaign on these new friction connections. The fifth paper will present a subsequent experimental campaign, with new prototypes and with the influence of the CLT.

1.2 Structure of the thesis

This thesis is paper based and is divided into 3 parts.
Part 1 contains *Introduction*, *Background* and *Overview of the present work*. The section *Background* will give a brief state of the art regarding the subject of the appended papers, while the section *Overview of the present work* will summarise each of the appended papers, by keeping a structure based on *Goals and method* and *Main findings*.
Part 2 contains the 3 appended papers regarding the shear wall codification topic.
Part 3 contains the 2 appended papers regarding the shear wall renovation topic.

2. Background

The background chapter will be divided into two sections concerning different aspects of the timber shear walls: the first section will be regarding codification, so related to building codes and rules for design; the second section will be regarding the use of timber walls for a renovation intervention. The part regarding codification will contain three main topics, which are reflected in the papers appended to this thesis: ULS CLT part, where both in-plane shear stress calculation methods and experimental data on CLT will be discussed (related to Paper I); SLS LTF part, which will be regarding the calculation of the elastic displacement on the top of an LTF shear wall (related to Paper II); ULS rocking timber walls part, which deals with the theory for the analysis of rocking timber shear walls (related to Paper III). The renovation part (related to both Paper IV and Paper V), will deal with the innovative seismic retrofit intervention called e-CLT, part of the European project e-Safe, and will offer a state of the art on friction connections.

2.1 Shear Walls - Codification

2.1.1 ULS - CLT in-plane shear stress

The evaluation of the in-plane shear stresses for CLT panels is a topic of the utmost importance, and even if different calculation methods are currently available no common agreement has been reached so far. In plane shear stresses in CLT are transferred through the glued interface, and thus the two usual stresses to be considered are:

Net shear stresses acting perpendicular to the grain of the lamellas of a specific layer, denoted as τ_{yx} τ_{yx} in Fig.2.1;

Torsional shear stresses acting within the glue interface between two layers, denoted as τ_T.

Five different calculation methods will be considered: a method based on the equilibrium, developed by [4] (Equilibrium method), a method based on the

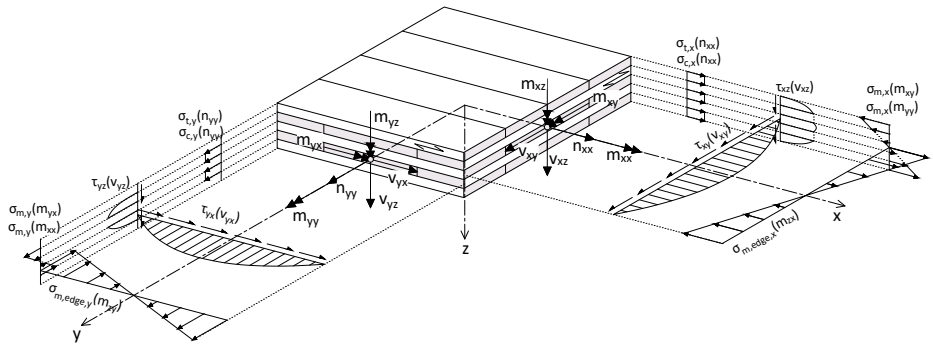

Fig. 2.1. Shear stresses, modified from COST document ([11]).

Representative Sub Element Volume method, developed by [8] (RVSE method), the method for beams developed by Flaig [30] and adopted also in COST document ([11], Beam method), and the method of the Austrian annex K to ÖNORM B 1995 [86] (AT-annex method). Fig. 2.1 will serve as a common notation for comparisons between the different calculation methods. The first index indicates the plane normal to the action, the second index indicates the axis the action is parallel to. The shear force ν is expressed as force per unit length and for rotational equilibrium:

$$v_{xy} = v_{yx} = v \tag{2.1}$$

For a complete nomenclature regarding this subsection the reader is referred to I.9.

Equilibrium method

The equilibrium method was presented in [4] and is developed from equilibrium equations. The initial assumption is that shear stresses are only present in the cross section of the boards oriented perpendicular respect to the shear action. The equations for net shear are as follows:

$$\begin{cases} \tau_{xy} = \dfrac{v}{t_1 + t_3} & \text{3-layer} \\ \tau_{yx} = \dfrac{v}{t_2} & \text{3-layer} \end{cases} \qquad \begin{cases} \tau_{xy} = \dfrac{v}{(t_1 + t_3 + t_5)} & \text{5-layer} \\ \tau_{yx} = \dfrac{v}{t_2 + t4} & \text{5-layer} \end{cases} \tag{2.2}$$

or with a general notation:

$$\begin{cases} \tau_{xy} = \dfrac{v}{t_x} \\ \tau_{yx} = \dfrac{v}{t_y} \end{cases} \tag{2.3}$$

The equations for torsional shear stress differ in the case of 3 or 5 layers panel:

$$\tau_T == 3 \cdot \frac{\tau_{xy} \cdot t_1}{b_l} \qquad \text{3-layer} \tag{2.4}$$

$$\begin{cases} \tau_{T,\text{ext}} = 3 \cdot \frac{\tau_{xy} \cdot t_1}{b_l} \\ \tau_{T,\text{int}} = \dfrac{3}{2} \cdot \frac{\tau_{xy} \cdot t_1}{b_l} \end{cases} \qquad \text{5-layer} \tag{2.5}$$

In the case of a 5 layers panel the torsional shear stresses are not equal for all glued interfaces: the value is major for external interfaces and minor for the internal one.

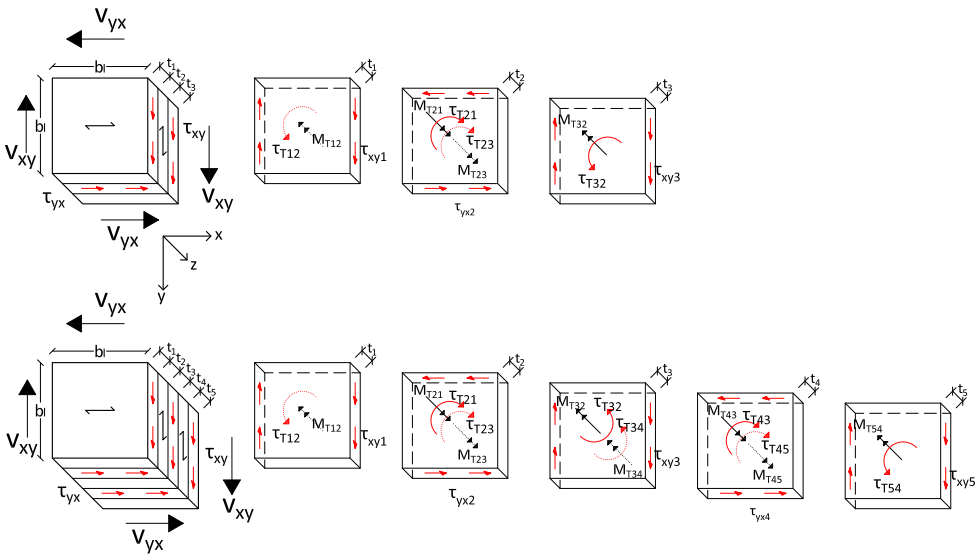

Fig. 2.2. Shear stresses for the equilibrium method.

RVSE method

This model is developed by referring to an ideal CLT panel with an infinite number of layers and considering a crossing interface with width equal to the width of the laminations, see [8]. This element is then simplified to obtain a Representative Volume Sub Element (RVSE) of CLT which has a thickness t and a nominal shear stresses τ_0 distributed on its entire thickness t (see fig.2.3). The equations in this case are then referred to the fictitious values $\tau_0^* \quad t_{tot}^*$:

$$\tau_0^* = \frac{v}{t_{tot}^*} \tag{2.6}$$

$$\tau_{yx} = \tau_v^* = 2 \cdot \tau_0^* \tag{2.7}$$

$$\tau_T = \tau_T^* = 3 \cdot \tau_0^* \cdot \frac{t_i^*}{b_l} \tag{2.8}$$

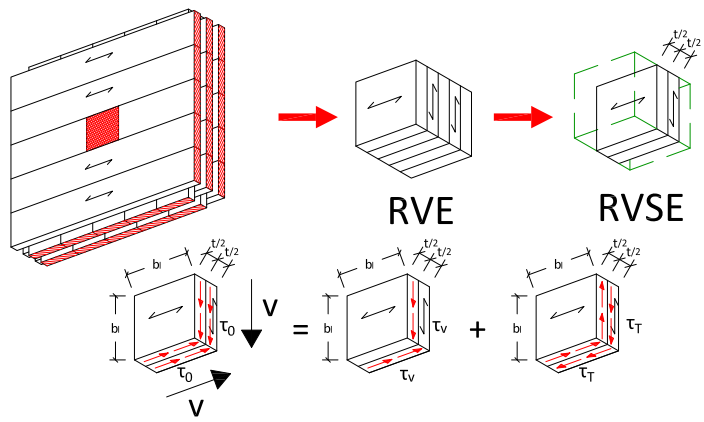

Fig. 2.3. Shear stresses for RVSE model.

Where the following apply:

$$t_{tot}^* = \sum_{1}^{n_{CA}} t_i^* \tag{2.9}$$

$$t_i^* = \begin{cases} \min(2 \cdot t_1; t_2) & \text{for the case of } t_1 \text{ external layer and } t_2 \text{ internal} \\ \min(t_3; t_4) & \text{for the case of } t_3 \text{ and } t_4 \text{ both internal layers} \end{cases} \tag{2.10}$$

Beam method

This method was developed by Flaig [30] by referring to the equilibrium of a beam and is also present in COST document ([11] and [23]), which will be the base for a new part in the EN 1995 regarding CLT products. For shear stresses the calculus is carried out separately considering net areas for both directions; the only difference between Flaig theory and COST document is that the second one advises to reduce by 0,20 the area comprising outer layers. For 3 layer panel:

$$\begin{cases} \tau_{xy} = \dfrac{v}{t_1 + t_3} & \text{Flaig} \\ \tau_{xy} = \dfrac{v}{0,8 \cdot (t_1 + t_3)} & \text{COST} \end{cases} \qquad \begin{cases} \tau_{yx} = \dfrac{v}{t_2} & \text{Flaig} \\ \tau_{yx} = \dfrac{v}{t_2} & \text{COST} \end{cases} \tag{2.11}$$

And for a 5 layer panel:

$$\begin{cases} \tau_{xy} = \dfrac{v}{t_1 + t_3 + t_5} & \text{Flaig} \\ \tau_{xy} = \dfrac{v}{0,8 \cdot (t_1 + t_5) + t_3} & \text{COST} \end{cases} \qquad \begin{cases} \tau_{yx} = \dfrac{v}{t_2 + t_4} & \text{Flaig} \\ \tau_{yx} = \dfrac{v}{t_2 + t_4} & \text{COST} \end{cases} \tag{2.12}$$

Torsional shear stresses are calculated as:

$$\tau_T = \frac{3V_{xy}}{b_l^2 \cdot n_{CA}} \left(\frac{1}{n_l} - \frac{1}{n_l^3} \right) \tag{2.13}$$

where V_{xy} is the applied shear force, $n_{CA} = n_{\text{lay}} - 1$ is the number of glued interfaces, $n_l = \frac{h_{\text{CL}}}{b_l}$ is the number of laminations in the height of the beam.

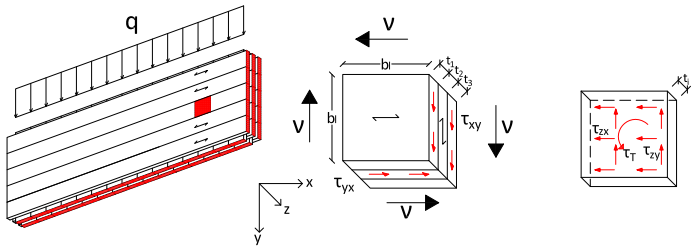

Fig. 2.4. Shear stresses for the beam method, on the right part a representative glue interface is shown.

AT-annex

The Austrian annex K to ÖNORM B 1995 [86] proposes, regarding shear stresses, a verification with reference to the net area in the two directions:

$$\tau_{xy} = \frac{v}{t_1 + t_3} \quad \tau_{yx} = \frac{v}{t_2} \qquad \text{3 layer panel} \tag{2.14}$$

$$\tau_{xy} = \frac{v}{t_1 + t_3 + t_5} \quad \tau_{yx} = \frac{v}{t_2 + t_4} \qquad \text{5 layer panel} \tag{2.15}$$

For what regards torsional shear stresses the proposed formulation is (adopting the previous conventions, where for usual panels the major shear stress is τ_{yx}):

$$\tau_T = 3 \cdot \tau_{yx} \cdot \frac{t_{i,max}}{b_l} \tag{2.16}$$

2.1.2 SLS - LTF Elastic displacement

The evaluation the displacement at the top of a LTF wall subjected to lateral loads is becoming increasingly important, both to limit the inter-storey drift in relation to serviceability limit states (SLS) and to determine the building period for the ultimate limit state (ULS) calculations. The typical wall segment is assembled of a timber frame on which a structural sheathing material, such as OSB or plywood panels, is attached using metal fasteners, usually nails or staples. Wall segments are then mechanically anchored at the base, using discrete hold-downs and/or continuous fastening along the bottom rail, to provide stability against uplift generated by the overturning moment. This difference in the anchoring technique corresponds to two categories of LTF shear walls respectively: fully anchored and partially anchored, seen in Figure 2.5. The calculation of the horizontal deflection

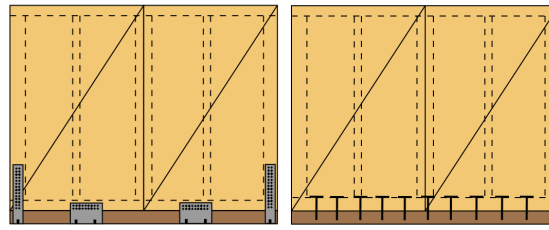

Fig. 2.5. Fully anchored LTF shear wall vs. partially anchored on the left and right sides, respectively.

of an LTF shear wall segment in the new Eurocode 5 proposal [1] includes six contributions, as shown in Figure 2.6:

1. u_{Kser} - deformation due to slip of sheathing-to-framing fasteners;
2. u_N - deformation of the chords;
3. u_A - rigid body rotation of the wall segment, due to the elongation in the wall anchorage system;
4. u_V - rigid body translation of the wall segment, due to the horizontal movement at the base;
5. u_C - deformation of the framing due to compression perpendicular to grain in the bottom rail;
6. u_G - in-plane shear deformation of the sheathing panel.

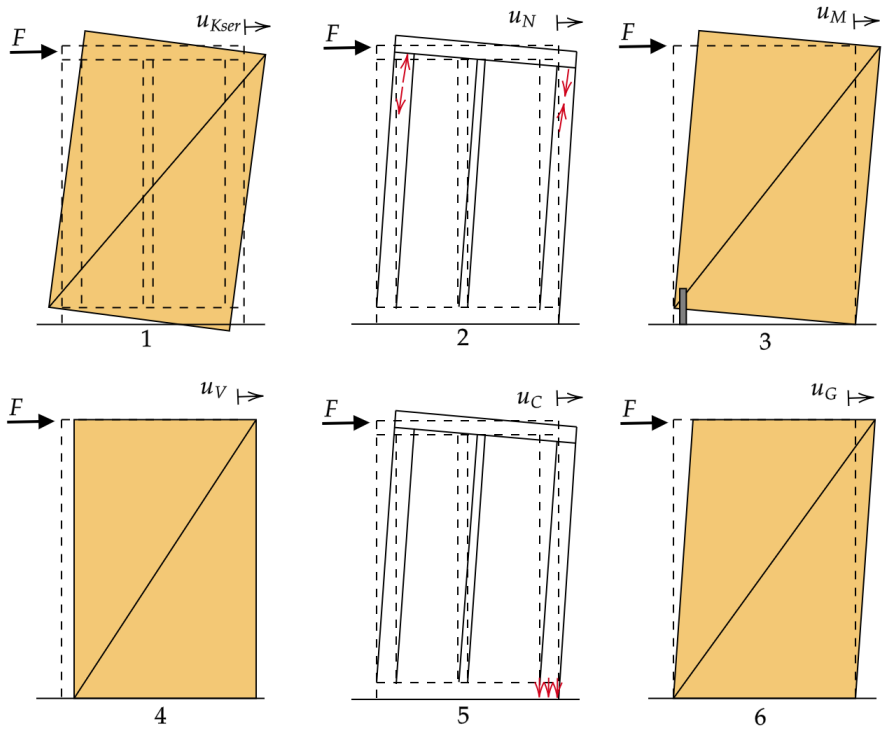

Fig. 2.6. Shear wall displacements contributions.

The relevant expressions read:

$$u_{Kser} = \frac{F_{v,Ed}\,\lambda(\alpha)\,a_1}{K_{ser,f}\,l\,n_p} \tag{2.17}$$

$$u_N = \frac{2}{3}\frac{F_{v,Ed}}{E_{0,m}}\left(\frac{l}{A_{rail}} + \frac{h^3}{A_{stud}\,l^2}\right) \tag{2.18}$$

$$u_A = \frac{h}{\tau\,l}\,u_{z,A} \qquad u_{z,A} = \frac{N_{net,Ed}}{K_{ser,A}} \qquad N_{net,Ed} = \frac{M_{net,Ed}}{\tau\,l} \tag{2.19}$$

$$u_V = \frac{F_{v,Ed}}{K_{ser,v}\,n_v} \tag{2.20}$$

$$u_C = \frac{F_{v,Ed}\,h_{rail}\,h^2}{E_{90,m}\,A_{eff}\,l^2} \tag{2.21}$$

$$u_G = \frac{F_{v,Ed}\,h}{G_p\,t_p\,n_p\,l} \tag{2.22}$$

where the symbols denote: $F_{v,Ed}$ - design horizontal force applied to the shear wall segment, $\lambda(\alpha)$ - shape coefficient depending on the aspect ratio of the sheathing panel, $\alpha = h/b_p$ - aspect ratio, b_p = width of the sheathing panel, l - length of the shear wall segment, h - height of the wall, a_1 - fastener spacing along the perimeter of the sheathing panel, $K_{ser,f}$ - stiffness of the sheathing-to-framing connections, n_p - number of sheathed sides of the wall, $E_{0,m}$ - mean modulus of elasticity parallel to the grain of the external studs, A_{rail} - average cross-sectional area of the top and bottom rails, A_{stud} - average cross-sectional area of the leading and trailing studs, τ - factor taking into account the reduced lever arm stabilising the wall, $u_{z,A}$ - vertical elongation of the wall anchorage system, $N_{net,Ed}$ - net tensile action resisting overturning in the connection at the leading edge, $M_{net,Ed}$ - net resulting overturning moment acting about the bottom trailing edge of the wall segment and producing a tensile action in the connection at the leading edge, $K_{ser,A}$ - stiffness of the connection against overturning, $K_{ser,v}$ - stiffness of the diaphragm base connection with respect to horizontal translation, n_v - number of base connections with respect to horizontal translation, $E_{90,m}$ - mean modulus of elasticity perpendicular to the grain, h_{rail} - cross-section height of the bottom rail, A_{eff} - effective contact area between the bottom rail and the trailing stud, G_p - shear modulus of the sheathing panels, t_p - thickness of the sheathing panels. Equation 2.17 stems from an elastic analysis [45], whereas the shape coefficient can assume two different values depending on the bending stiffness of the frame elements. Equation 2.18 is derived from elastic analysis using the principle of virtual work. Equations 2.19,2.20,2.22 are mere equilibrium equations, which consider the stiffness of the respective restraining element. Equation 2.21 stems from elastic analysis; more details on its background are presented in [75] and [71]. A notable remark is worth on the derivation of equations 2.17,2.18,2.19,2.21:

they are all based on the theory of a fully anchored wall, therefore with a strong anchorage at its leading stud. The extension of equations 2.17,2.18,2.21 to the case of partially anchored wall is still under discussion, while for equation 2.19 a new formulation may be required.

Fastener slip contribution

Equation 2.17 for fastener slip contribution presents a shape function λ, which depends on the aspect ratio of the sheathing panels α:

$$\lambda(\alpha) = \lambda_1 + \lambda_2 \alpha \qquad \alpha = h/b_p \tag{2.23}$$

Coefficients λ_1, λ_2 can assume two possible sets of values, depending on the analysis and hypothesis used for their computation:

- case 1 stems from the elastic analysis in [45], where the initial hypothesis assumes the framing members as fully rigid, and the outcome, linearised in [12], is $\lambda_1 = 0.81, \lambda_2 = 1.85$;

- case 2 supposes the framing members are fully flexible, as done in [45] through an elastic analysis and in [46] and [47] using a plastic approach, leading in both cases to $\lambda_1 = 2, \lambda_2 = 2$. The functions relevant to the cases above are plotted in Figure 2.7, and they are seen to differ by 34%.

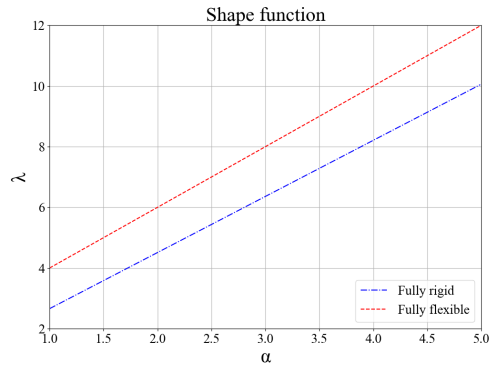

Fig. 2.7. Fastener slip formulation λ function.

2.1.3 ULS - Rocking shear walls

This section gives a brief description on the lateral capacity models for timber shear walls, both LTF and CLT. Much research was dedicated at developing predictive capacity models useful to calibrate simplified design methods [3]. Predictive capacity models require experimental data for a proper calibration: numerous experimental campaigns evaluated the lateral responses of the two systems following distinct loading protocols and under diverse structural configurations [74, 44, 82, 40, 85, 2, 63].
The capacity models may gather in two main groups: those based on Finite Element (F.E.) and structural analysis [83, 38, 24, 72, 37, 50], and empirical models [31, 51, 77, 76]. The first ones attempt to follow the experimental data and could be used in extrapolating the response of structural configurations different from those used for calibration. Conversely, empirical hysteresis models consist of algebraic or differential equations, which follow closely the experimental data, with no concern of the mechanical meaning of the employed parameters. These models cannot be used in extrapolating structural behaviours beyond those associated with the experimental data. However, the so-called empirical models are less time consuming than F.E. models and can be used to perform simulations in a relatively short time. Di Gangi et al. recently [20] reviewed the modeling strategies of timber shear walls from 1978 to 2018.
There are numerous and diverse capacity models in the scientific literature. Some researches merely attempt to elaborate closed-form models which best seize the observed response. Others, like [13], append to the mentioned efforts, an interpretative framework useful in developing simplified and reliable tools for the prediction of the lateral response. Specifically, [13] developed an analytical procedure and a simplified numerical model for the elastic response of LTF and CLT shear walls. They found that, in the elastic response range of CLT shear walls, 77% of the total displacement is due to rigid-body rotation, 16% to the rigid-body translation and 7% to the panel deformation. Conversely, in LTF shear walls, 45% is expected to the rigid-body rotation, 6% to the rigid body translation, and 45% and 4% to the sheathing-to-framing connection and sheathing panel deformation, respectively.
The scientific literature presents several models for assessing the strength of CLT and LTF timber shear walls. The capacity models of LTF walls, like the ones by Källsner and Girhammar [52], [53], focus on the role of the sheathing-to-framing connections, by evaluating the resistance of the wall related to that sort of failure. That is also the base for the prediction models present in the current Eurocode 5 proposal. Conversely, many scholars consider CLT walls as rigid bodies: the capacity of the wall depends on the strength of its anchorage system, due to its intrinsic considerable in-plane strength and stiffness[61]. The CLT capacity models merely descend from the equilibrium equations of the wall, see Fig.2.8,

while the main differences between them lie on two main points: the inclusion or not of the angle brackets contribution in the tension resisting mechanism, and the shape and contribution of the compression zone. Casagrande [13] and Tomasi [66] both neglect the contribution of angle brackets: the first does not make any specific assumptions about the compression stresses distribution and proposes a conventional lever arm equals to $0.9l$, the second assumes a rectangular stress block distribution in the compression zone, with size $0.8x$. Wallner-Novak [84] proposes a model similar to [66] but with compression zone equals to $0.25l$. Pei [65], Reynolds [70], Gavric [32] presented models that include the tensile contribution of angle brackets. Pei [65] assumes an elastic triangular distribution of tensile forces, by considering the rigid body rotation around one edge of the shear wall. Reynolds [70] presented three different models, which all include the presence of a compression zone, but differ in the size of that zone and the distribution of tensile forces between angle brackets and hold-down. Gavric [32] presents a model similar to [65], but considers the interaction between horizontal and vertical forces on the angle brackets.

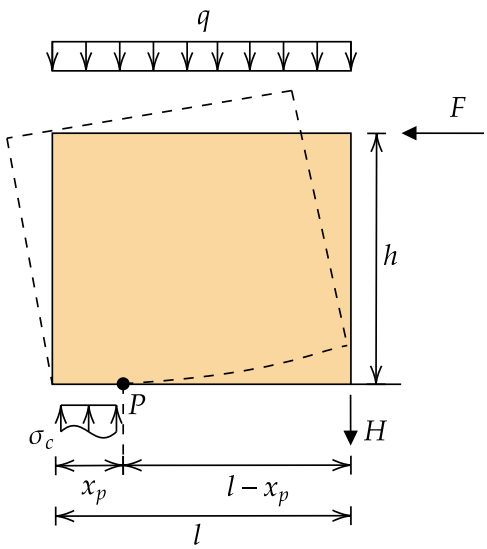

Fig. 2.8. Mechanical model of a rocking timber shear wall.

2.2 Shear walls - Renovation

2.2.1 Seismic renovation methods: e-CLT

The seismic retrofitting of existing buildings is a comprehensive and contemporary research topic with diverse economic, social and environmental entanglements, especially in earthquake-prone areas in southern Europe. As an example, 60% of Italian residential buildings were built between 1946 and 1990, while 25% before 1946 [41]. The Italian seismic hazard and the inadequacy of seismic provisions before the 1980s confirm the Italian territory's significant seismic risk. There are several solutions for the seismic retrofitting of reinforced-concrete (RC) buildings. Specifically, there are two types of interventions, those aiming to reduce the seismic demand and those aiming to increase the structural capacity [64, 21, 14]. The structural capacity may be increased by adopting strengthening interventions or by installing stiffening elements. So far the strengthening interventions are the most widespread. They can be traditional (e.g., steel jacketing of beams and columns [25]) or based on the use of advanced materials (wrapping with fibre-reinforced polymers (FRP) or textile-reinforced mortar [19, 10]). Properly designed stiffening elements (e.g., RC shear walls, X-bracing [68, 69]) could partially adsorb the seismic load. However, the seismic vulnerability could also be reduced by lessening the seismic demand. These interventions include the use of dissipation devices [43, 22, 5] or base isolation [18, 80, 6]. The solutions aiming at increasing the structural capacity are invasive and generally expensive. The interventions that reduce the seismic demand could be advantageous, being low-invasive and reducing installation time. In this field, friction connections (FC) could be considered possible candidates for increasing the structural dissipation capacity [49, 9]. Still, these devices are not common due to difficulties in their practical installation and the uncertainty of the RC building's coupled response. So far, full-scale experimental tests on the effect of AFC on RC frames are lacking [67, 48]. On the other side, many scholars started investigating the possibility of using timber as a strengthening solution for existing buildings, particularly Cross Laminated Timber (CLT) panels [7]. In RC buildings with masonry infill, CLT panels can be used in addition or substitution [79, 78] of the existing masonry infill. The main issue related to these interventions is implementing an appropriate connection system between the CLT panel and the existing structure.
The innovative system presenter here is called e-CLT, see Fig.2.9, and consists of installing the CLT panel from the outside of the building, while leaving the masonry infills unchanged, without discomfort for the people living inside the building [81]. This system is part of the European e-SAFE (Energy and Seismic AFfordable rEnovation solutions) project [26, 27], which presents a multidisciplinary approach on renovation solutions for existing buildings, in the

framework of the Horizon 2020 European goal [39]. CLT panels have light weight (around 470 kg/m3), thus not increasing too much the mass of existing buildings. Other advantages that make CLT attractive for retrofitting uses are the high level of prefabrication and the benefits of dry interventions, such as quick and easy installation, material recyclability and reversibility of the retrofit intervention. The central innovation of the e-CLT retrofitting intervention stands in the connection system between CLT and existing building: a Friction Connection (FC). The FC is constituted by a couple of steel profiles, one connected to the existing beam and the other to the CLT panel, clamped together by preloaded bolts. One of the two profiles presents a slotted hole, which enables their mutual sliding. Single CLT panels are connected to the RC beams of the existing structure by at least two FCs. The size of the CLT panels is related to that of the bays without openings where they are applied. In common RC framed buildings, the story height is generally equal to 3 m, while the width of each bay does not exceed 6 m. The e-CLT technology can be combined with non-structural framed panels, that may be applied to the walls with openings and are equipped with high-performing windows that replace the existing ones. Both panels integrate insulation materials, to improve the energy efficiency of the building, and finishing layer. The retrofit system also provides technological solutions to cover the FC devices after the panels installation and to ensure their inspection and maintenance [62].

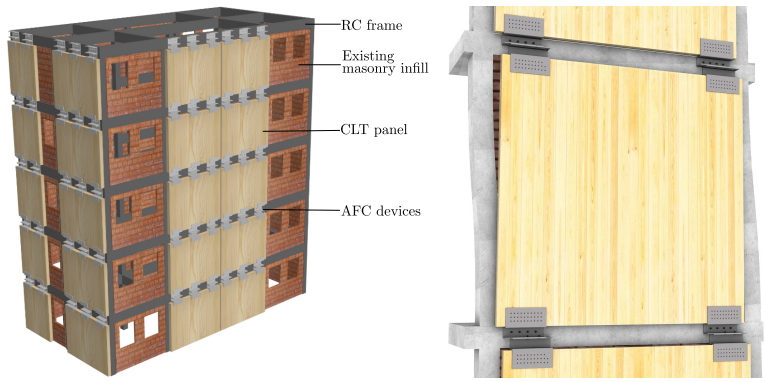

Fig. 2.9. (a) Components of the e-CLT retrofitting system and (b) e-CLT panel subjected to seismic action

2.2.2 Friction connections

Several researchers investigated the friction connections performance in their basic form, usually divided into two classes: symmetric friction connections (SFC) and asymmetric friction connections (AFC) [54, 57], see Fig.2.10. Symmetric friction connections present one central plate with an elongated hole and two lateral plates with round holes. In this connection, the central plate slides while the two lateral plates are restrained, determining symmetric loading conditions. In asymmetric friction connections, instead, one plate is restrained while the other slides. This configuration determines asymmetric loading condition. A third plate with round holes may be used to close the connection as a "cap" plate. Additionally, shim layers made from various materials may be used between the three plates, in order to increase the stability of the friction behaviour. An example of the tested specimen for the e-CLT system, which are classified as AFC, is shown in Fig.IV.9.
[56] initially began investigating with a numerical study the possibility of using SFC instead of hold-down for restraining timber shear walls against uplift, to cap the force transmitted to the wall, and reduce inelastic damage. Consequently, [60] and [55] presented two experimental campaigns: the first on single SFCs and the second on full-scale timber walls. In [60] the focus was on the single connectors, with different materials tested as shim layers, such as brake lining and different alloys. An innovative connection without shim layers was also tested, where the central slotted element was made directly with the high hardness alloy. They found that high hardness alloys offered the best sliding performances, like bisalloy 400, while steel vs steel sliding presented a more erratic behavior. In [55] the concept of SFC was applied to a full-scale timber wall, where the friction connections replaced the hold-downs. The results showed that these devices determined a global elastoplastic response of the entire wall under cycling loading. [58] further extended the concept, by modeling CLT walls and multistory buildings and by proposing a displacement-based design method. [59] tested SFC by adopting different methods of surface preparation of the sliding interface. Surfaces cleaned from loose rust and mill scale yielded the best hysteresis curves in terms of stability. [29] studied an SFC with self-tapping screws for CLT, which was then used also for a full-scale campaign in [28]. [17] investigated the performance of SFCs in steel buildings. [33] and [34] presented two experimental campaigns on AFCs. The first one, [33] aimed at understanding the behavior of the AFC when using different materials as shim layers. Materials with high hardness led to extremely stable loops, low hardness materials determined moderately stable loops, while an erratic behavior was observed with medium hardness materials (hardness values similar to steel plates). The second, [34], established a dependence between stability and shape of the loop and the clamping force level. [35] and [36] presented an experimental campaign on AFC focused on the bolt

length effects. They found that increasing the bolt length determined a decrease in AFC strength and a more pronounced preload loss, conversely the effective friction coefficient and its variability tended to decrease. [15] tested brake pads as shim material for AFC. [73] studied the dynamic effects on AFC for applications in steel structures, which further led to the design proposals in [16].
Friction connections were selected as appropriate for the e-CLT seismic retrofitting intervention due to their highly efficient energy dissipation mechanism, which contributes to reduce inter-story drift damage to the existing building. The damage-free energy dissipation mechanism also ensures the durability of its structural efficiency even after seismic events. This feature avoids the need for the removal and replacement of the FC, which in turn would involve the removal of the attached CLT panel too. After a seismic event it is sufficient to check and eventually replace the bolts and the shim layers. Another important feature, differently from visco-elastic devices, is that these connections present stable hysteresis loops which are not dependent on the speed [42].

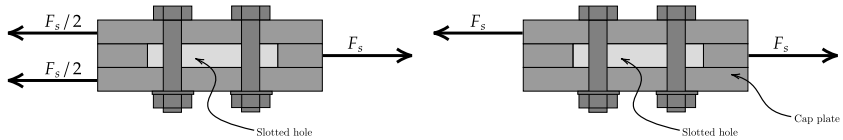

Fig. 2.10. (a) Symmetric and (b) Asymmetric Friction connections.

Bibliography

[1] SC5.PT3 final document, 2020.

[2] Farnaz Alinoori, Pezhman Sharafi, Farzad Moshiri, and Bijan Samali. Experimental investigation on load bearing capacity of full scaled light timber framed wall for mid-rise buildings. *Construction and Building Materials*, 231:117069, 2020.

[3] Angelo Aloisio, Rocco Alaggio, Jochen Köhler, and Massimo Fragiacomo. Extension of generalized bouc-wen hysteresis modeling of wood joints and structural systems. *Journal of Engineering Mechanics*, 146(3):04020001, 2020.

[4] Mauro Andreolli, Roberto Tomasi, and Andrea Polastri. Experimental investigation on in-plane behaviour of cross-laminated timber elements. In *Proceedings of CIB-W18*, 2012.

[5] Francesca Barbagallo, Melina Bosco, Edoardo M. Marino, Pier Paolo Rossi, and Paola R. Stramondo. A multi-performance design method for seismic upgrading of existing rc frames by brbs. *Earthquake Engineering & Structural Dynamics*, 46(7):1099–1119, 2017.

[6] Francesca Barbagallo, Ikumi Hamashima, Hongsong Hu, Masahiro Kurata, and Masayoshi Nakashima. Base shear capping buildings with graphite-lubricated bases for collapse prevention in extreme earthquakes. *Earthquake Engineering & Structural Dynamics*, 46(6):1003–1021, 2017.

[7] Anders Björnfot, Francesco Boggian, Anders Nygård, and Roberto Tomasi. Strengthening of traditional buildings with slim panels of cross-laminated timber (clt). In *International Conference on Structural Health Assessment of Timber Structures*, 09 2017.

[8] Thomas Bogensperger, Thomas Moosbrugger, and Gregor Silly. Verification of CLT-plates under loads in plane. In *Proceedings of WCTE-World Conference on Timber Engineering*, 2010.

[9] J Borzouie, GA MacRae, JG Chase, GW Rodgers, and GC Clifton. Experimental studies on cyclic performance of column base strong axis–aligned asymmetric friction connections. *Journal of Structural Engineering*, 142(1):04015078, 2016.

[10] Dionysios A Bournas, Thanasis C Triantafillou, K Zygouris, and F Stavropoulos. Textile-reinforced mortar versus frp jacketing in seismic retrofitting of rc columns with continuous or lap-spliced deformed bars. *Journal of Composites for Construction*, 13(5):360–371, 2009.

[11] Reinhard Brandner, Roberto Tomasi, Thomas Moosbrugger, Erik Serrano, and Philipp Dietsch. *Properties, Testing and Design of Cross Laminated Timber, a state-of-the-art report by COST Action FP1402 / WG 2.* 2018.

[12] Daniele Casagrande, Simone Rossi, Tiziano Sartori, and Roberto Tomasi. Proposal of an analytical procedure and a simplified numerical model for elastic response of single-storey timber shear-walls. *Construction and Building Materials*, 102:1101–1112, January 2016.

[13] Daniele Casagrande, Simone Rossi, Tiziano Sartori, and Roberto Tomasi. Proposal of an analytical procedure and a simplified numerical model for elastic response of single-storey timber shear-walls. *Construction and Building Materials*, 102:1101–1112, 2016.

[14] Nicola Caterino, Iunio Iervolino, Gaetano Manfredi, and Edoardo Cosenza. Multi-criteria decision making for seismic retrofitting of rc structures. *Journal of Earthquake Engineering*, 12(4):555–583, 2008.

[15] Jose Christian Chanchi Golondrino, Gregory Anthony MacRae, James Geoffrey Chase, Geoffrey William Rodgers, and George Charles Clifton. Hysteretic behaviour of asymmetrical friction connections using brake pads of d3923. *Structures*, 16:164–175, 2018.

[16] Jose Christian Chanchi Golondrino, Gregory Anthony MacRae, James Geoffrey Chase, Geoffrey William Rodgers, and George Charles Clifton. Asymmetric friction connection (afc) design for seismic energy dissipation. *Journal of Constructional Steel Research*, 157:70–81, 2019.

[17] Jose Christian Chanchi Golondrino, Gregory Anthony MacRae, James Geoffrey Chase, Geoffrey William Rodgers, and George Charles Clifton. Seismic behaviour of symmetric friction connections for steel buildings. *Engineering Structures*, 224:111200, 2020.

[18] Paolo Clemente and Giacomo Buffarini. Base isolation: design and optimization criteria. *Seismic isolation and protection systems*, 1(1):17–40, 2010.

[19] Ciro Del Vecchio, Marco Di Ludovico, Alberto Balsamo, Andrea Prota, Gaetano Manfredi, and Mauro Dolce. Experimental investigation of exterior rc beam-column joints retrofitted with frp systems. *Journal of Composites for Construction*, 18(4):04014002, 2014.

[20] Giorgia Di Gangi, Cristoforo Demartino, Giuseppe Quaranta, and Giorgio Monti. Dissipation in sheathing-to-framing connections of light-frame timber shear walls under seismic loads. *Engineering Structures*, 208:110246, 2020.

[21] Marco Di Ludovico, Andrea Prota, Claudio Moroni, Gaetano Manfredi, and Mauro Dolce. Reconstruction process of damaged residential buildings outside historical centres after the l'aquila earthquake: part i—" light damage" reconstruction. *Bulletin of Earthquake Engineering*, 15(2):667–692, 2017.

[22] L Di Sarno and G Manfredi. Seismic retrofitting with buckling restrained braces: Application to an existing non-ductile rc framed building. *Soil Dynamics and Earthquake Engineering*, 30(11):1279–1297, 2010.

[23] Philipp Dietsch, Gerhard Schickhofer, Alfons Brunauer, Roberto Tomasi, Ulrich Hübner, Harald Krenn, Peter Mestek, Thomas Moosbrugger, and Tobias

Wiegand. Eurocode 5:2022 – Einführung in die neuen Abschnitte Brettsperrholz und Verstärkungen. In Rainer Görlacher and Carmen Sandhaas, editors, *Karlsruher Tage 2018 - Holzbau*, pages 65–84, 10 2018.

[24] JD Dolan and RO Foschi. Structural analysis model for static loads on timber shear walls. *Journal of Structural Engineering*, 117(3):851–861, 1991.

[25] Rahul Dubey and Pardeep Kumar. Experimental study of the effectiveness of retrofitting rc cylindrical columns using self-compacting concrete jackets. *Construction and Building Materials*, 124:104–117, 2016.

[26] e-SAFE. Energy and seismic affordable renovation solutions. `https://cordis.europa.eu/project/id/893135`. Accessed: 2021-03-23.

[27] e-SAFE. Energy and seismic affordable renovation solutions. `http://esafe-buildings.eu/`. `http://esafe-buildings.eu/`.

[28] D. Fitzgerald, T.H. Miller, A. Sinha, and J.A. Nairn. Cross-laminated timber rocking walls with slip-friction connections. *Engineering Structures*, 220, 2020.

[29] Dillon Fitzgerald, Arijit Sinha, Thomas H. Miller, and John A. Nairn. Axial slip-friction connections for cross-laminated timber. *Engineering Structures*, 228:111478, 2021.

[30] Marcus Flaig and Hans Joachim Blass. Shear strength and shear stiffness of CLT-beams loaded in plane. In *Proceedings of CIB-W18*, 2013.

[31] Greg C Foliente. Hysteresis modeling of wood joints and structural systems. *Journal of Structural Engineering*, 121(6):1013–1022, 1995.

[32] I. Gavric and M. Popovski. Design models for clt shearwalls and assemblies based on connection properties. In *Proceedings of International Network on Timber Engineering Research, INTER/47-15-4*, 2014.

[33] JC Golondrino, GA MacRae, JG Chase, and GW Rodgers. Behaviour of asymmetrical friction connections using different shim materials. In *New Zealand Society for Earthquake Engineering Conference*, 2012.

[34] JC Golondrino, GA MacRae, JG Chase, GW Rodgers, and C Clifton. Clamping force effects on the behaviour of asymmetrical friction connections (afc). In *15th World Conference on Earthquake Engineering*, Lisboa, Portugal, 2012.

[35] JC Golondrino, GA MacRae, JG Chase, GW Rodgers, and C Clifton. Effects of the bolt grip length on the behaviour of asymmetrical friction connections (afc). In *New Zealand Society for Earthquake Engineering Conference*, 2016.

[36] Jose Christian Chanchi Golondrino, Gregory Anthony MacRae, James Geoffrey Chase, Geoffrey William Rodgers, and George Charles Clifton. Asymmetric friction connection bolt lever arm effects on hysteretic behaviour. *Journal of Earthquake Engineering*, 0(0):1–22, 2020.

[37] Paolo Grossi, Tiziano Sartori, Ivan Giongo, and Roberto Tomasi. Analysis of timber log-house construction system via experimental testing and analytical modelling. *Construction and Building Materials*, 102:1127–1144, 2016.

[38] Ajaya K Gupta and George P Kuo. Behavior of wood-framed shear walls. *Journal of Structural Engineering*, 111(8):1722–1733, 1985.

[39] Horizon 2020. Reducing energy consumption and carbon footprint by smart and sustainable use. `https://cordis.europa.eu/programme/id/H2020-EU.3.3.1.` Accessed: 2021-03-23.

[40] Asif Iqbal, Massimo Fragiacomo, Stefano Pampanin, and Andrew Buchanan. Seismic resilience of plywood-coupled lvl wall panels. *Engineering Structures*, 167:750–759, 2018.

[41] Istat. *Annuario Statistico Italiano*. Istituto nazionale di statistica, Roma, 2015. `https://www.istat.it/it/files//2015/12/Asi-2015.pdf` Accessed: 2021-03-23.

[42] Sujit Jaisee, Feng Yue, and Yi Hao Ooi. A state-of-the-art review on passive friction dampers and their applications. *Engineering Structures*, 235:112022, 2021.

[43] Pasha Javadi, Ali Tizchang, AmirHosein GhafourianHesami, and MohammadJavad Askari. A friction-based connection for retrofitting rc frames by steel braced frames. In *Structures*, volume 24, pages 627–639. Elsevier, 2020.

[44] Johnn P Judd and Fernando S Fonseca. Analytical model for sheathing-to-framing connections in wood shear walls and diaphragms. *Journal of structural engineering*, 131(2):345–352, 2005.

[45] Bo Källsner and Ulf Arne Girhammar. Analysis of fully anchored light-frame timber shear walls-elastic model. *Materials and Structures*, 42:301–320, January 2009.

[46] Bo Källsner and Ulf Arne Girhammar. Plastic models for analysis of fully anchored light-frame timber shear walls. *Engineering Structures*, 31:2171–2181320, 2009.

[47] Martin Kessel. Tafeln - eine linear elastische beschreibung. *Holzbau Kalender*, 2003.

[48] Hsen-Han Khoo, Charles Clifton, John Butterworth, and Gregory MacRae. Experimental study of full-scale self-centering sliding hinge joint connections with friction ring springs. *Journal of Earthquake Engineering*, 17(7):972–997, 2013.

[49] Hsen-Han Khoo, Charles Clifton, Gregory MacRae, Hao Zhou, and Shahab Ramhormozian. Proposed design models for the asymmetric friction connection. *Earthquake Engineering & Structural Dynamics*, 44(8):1309–1324, 2015.

[50] Maria Koliou, John W van de Lindt, and Ronald O Hamburger. Nonlinear modeling of wood-frame shear wall systems for performance-based earthquake engineering: Recommendations for the asce 41 standard. *Journal of Structural Engineering*, 144(8):04018095, 2018.

[51] AK Kottari, AE Charalampakis, and VK Koumousis. A consistent degrading bouc–wen model. *Engineering structures*, 60:235–240, 2014.

[52] B. Källsner and U.A. Girhammar. Analysis of fully anchored light-frame timber shear walls-elastic model. *Materials and Structures/Materiaux et Constructions*, 42(3):301–320, 2009.

[53] B. Källsner and U.A. Girhammar. Plastic models for analysis of fully anchored light-frame timber shear walls. *Engineering Structures*, 31(9):2171–2181, 2009.

[54] Massimo Latour, Gianvittorio Rizzano, Aldina Santiago, and Luis Simões da Silva. Experimental response of a low-yielding, self-centering, rocking column base joint with friction dampers. *Soil Dynamics and Earthquake Engineering*, 116:580–592, 2019.

[55] Wei Y. Loo, Chern Kun, Pierre Quenneville, and Nawawi Chouw. Experimental testing of a rocking timber shear wall with slip-friction connectors. *Earthquake Engineering & Structural Dynamics*, 43(11):1621–1639, 2014.

[56] Wei Y. Loo, Pierre Quenneville, and Nawawi Chouw. A numerical study of the seismic behaviour of timber shear walls with slip-friction connectors. *Engineering Structures*, 34:233–243, 2012.

[57] Wei Y Loo, Pierre Quenneville, and Nawawi Chouw. A new type of symmetric slip-friction connector. *Journal of Constructional Steel Research*, 94:11–22, 2014.

[58] Wei Y. Loo, Pierre Quenneville, and Nawawi Chouw. Rocking timber structure with slip-friction connectors conceptualized as a plastically deformable hinge within a multistory shear wall. *Journal of Structural Engineering*, 142(4):E4015010, 2016.

[59] Wei Y. Loo, Pierre Quenneville, and Nawawi Chouw. The influence of surface preparation and the lubricating effect of mill scale on the performance of slip-friction connectors. *Construction and Building Materials*, 155:1025–1038, 2017.

[60] W.Y. Loo, P. Quenneville, and N. Chouw. A new type of symmetric slip-friction connector. *Journal of Constructional Steel Research*, 94:11–22, 2014.

[61] Ildiko Lukacs, Anders Björnfot, and Roberto Tomasi. Strength and stiffness of cross-laminated timber (clt) shear walls: State-of-the-art of analytical approaches. *Engineering Structures*, 178:136–147, 2019.

[62] Giuseppe Margani, Gianpiero Evola, Carola Tardo, and Edoardo Michele Marino. Energy, seismic, and architectural renovation of rc framed buildings with prefabricated timber panels. *Sustainability*, 12(12), 2020.

[63] Tu T Nguyen, Thang N Dao, Sriram Aaleti, John W van de Lindt, and Kenneth J Fridley. Seismic assessment of a three-story wood building with an integrated clt-lightframe system using rths. *Engineering Structures*, 167:695–704, 2018.

[64] Stavroula J Pantazopoulou, Souzana P Tastani, Georgia E Thermou, Thanasis Triantafillou, Giorgio Monti, Dionysios Bournas, and Maurizio Guadagnini. Background to the european seismic design provisions for retrofitting rc elements using frp materials. *Structural Concrete*, 17(2):194–219, 2016.

[65] S. Pei, J. Lindt, and M. Popovski. Approximate r-factor for cross-laminated timber walls in multistory buildings. *Journal of Architectural Engineering*, 19:245–255, 2013.

[66] S. Pei, J. Lindt, and M. Popovski. Enhance mechanical properties of timber, engineered wood products and timber structures. *CLT course at FPS COST Action FP1004. CLT Training School*, 2014.

[67] Ali A Rad, Gregory A MacRae, Nikoo K Hazaveh, and Quincy Ma. Shake table testing of a low damage steel building with asymmetric friction connections (afc). *Journal of Constructional Steel Research*, 155:129–143, 2019.

[68] A Rahimi and Mahmoud R Maheri. The effects of retrofitting rc frames by x-bracing on the seismic performance of columns. *Engineering Structures*, 173:813–830, 2018.

[69] A Rahimi and Mahmoud R Maheri. The effects of steel x-brace retrofitting of rc frames on the seismic performance of frames and their elements. *Engineering Structures*, 206:110149, 2020.

[70] T. Reynolds, R. M. Foster, J. Bregulla, Wen shao Chang, R. Harris, and M. Ramage. Lateral load resistance of cross-laminated timber shear walls. *Journal of Structural Engineering-asce*, 143:06017006, 2017.

[71] Elena Ricci. Design methods for Light Timber Frame shear walls: validation with experimental data. Master's thesis, University of Trento, 2020.

[72] Giovanni Rinaldin, Claudio Amadio, and Massimo Fragiacomo. A component approach for the hysteretic behaviour of connections in cross-laminated wooden structures. *Earthquake engineering & structural dynamics*, 42(13):2023–2042, 2013.

[73] Geoffrey W. Rodgers, Robin Herve, Gregory A. MacRae, Jose Chanchi Golondrino, and J. Geoffrey Chase. Dynamic friction coefficient and performance of asymmetric friction connections. *Structures*, 14:416–423, 2018.

[74] Alexander J Salenikovich. *The racking performance of light-frame shear walls*. PhD thesis, Virginia Tech, 2000.

[75] Werner Seim, Johannes Hummel, and Tobias Vogt. Earthquake design of timber structures - Remarks on force-based design procedures for different wall systems. *Engineering Structures*, 76:124–137, 2014.

[76] Salvatore Sessa, Nicoló Vaiana, Massimo Paradiso, and Luciano Rosati. An inverse identification strategy for the mechanical parameters of a phenomenological hysteretic constitutive model. *Mechanical Systems and Signal Processing*, 139:106622, 2020.

[77] Junho Song and Armen Der Kiureghian. Generalized bouc–wen model for highly asymmetric hysteresis. *Journal of engineering mechanics*, 132(6):610–618, 2006.

[78] F. Stazi, M. Serpilli, G. Maracchini, and A. Pavone. An experimental and numerical study on clt panels used as infill shear walls for rc buildings retrofit. *Construction and Building Materials*, 211:605–616, 2019.

[79] Iztok Sustersic and Bruno Dujic. Seismic strengthening of existing urm and rc structures using xlam timber panels. In *International conference on Earthquake Engineering*, 01 2013.

[80] M TahamouliRoudsari, MB Eslamimanesh, AR Entezari, O Noori, and M Torkaman. Experimental assessment of retrofitting rc moment resisting frames with adas and tadas yielding dampers. In *Structures*, volume 14, pages 75–87. Elsevier, 2018.

[81] Carola Tardo, Francesco Boggian, Magnus Hatletveit, Edoardo Marino, Giuseppe Margani, and Roberto Tomasi. Mechanical characterization of energy dissipation devices in retrofit solution of reinforced concrete frames coupled with solid wood panels. In *Proceedings of the 12th International Conference on Structural Analysis of Historical Constructions*, 2020.

[82] Roberto Tomasi and Tiziano Sartori. Mechanical behaviour of connections between wood framed shear walls and foundations under monotonic and cyclic load. *Construction and Building Materials*, 44:682–690, 2013.

[83] Roger L Tuomi and William J McCutcheon. Racking strength of light-frame nailed walls. *Journal of the Structural Division*, 104(7):1131–1140, 1978.

[84] M. Wallner-Novak, J. Koppelhuber, and K. Pock. *Brettsperrholz Bemessung Grundlagen für Statik und Konstruktion nach Eurocode.* proHolz Austria, 2013.

[85] Daniel Way, Arijit Sinha, and Frederick A Kamke. Performance of light-frame timber shear walls produced with weathered sheathing. *Journal of Architectural Engineering*, 26(1):04019022, 2020.

[86] ÖNORM B 1995-1-1. Ausgabe: 2015-06-15, Eurocode 5: Bemessung und Konstruktion von Holzbauten Teil 1-1: Allgemeines — Allgemeine Regeln und Regeln für den Hochbau. Austrian Standards, Vienna. 2015.

3. Overview of the work

This chapter will give a brief and schematic description of each of the papers attached to this thesis.

3.1 I Paper

F. Boggian, M. Andreolli, and R. Tomasi, "Cross laminated timber (CLT) beams loaded in plane: testing stiffness and shear strength," *Frontiers in Built Environment*, vol. 5, p. 58, 2019. Doi.
Included in chapter I.

3.1.1 Goals and method

The first paper tackles the problem of the in-plane shear stress calculation for CLT panels, focusing on net-shear and torsional shear. Many different methods are present in literature, a state of the art is proposed and an analytical comparison between the methods guides the analysis. The discussion is still ongoing both regarding the evaluation of strength values and standard testing procedures to obtain those values. The goal of the paper is to offer a comparison between the available methods and study their applicability, while also presenting an experimental campaign and investigating the strength values obtained.
An four point bending test campaign is presented, see Fig.3.2, which investigated a total of 10 CLT beams. The beam geometry was adapted from the prescriptions of [8] in the attempt to obtain a shear failure. Four different types of specimen have been tested, with differences regarding: the number and thickness of layers, the presence of narrow edge glued interface, the board width, and presence of cracks or cuts to improve shrinkage behaviour; see fig.3.1.
The shear stresses were calculated with all the methods presented in the introduction (see sec.2.1.1, but the Equilibrium method will be used as reference:

A-3	A-5	B-5	C-5
			
Glued narrow surface	Glued narrow surface and cracks	Not glued narrow surface and cuts	Not glued narrow surface

Fig. 3.1. Tested specimens: for each series of specimen an image is provided showing the layup in the thickness direction and underlining differences.

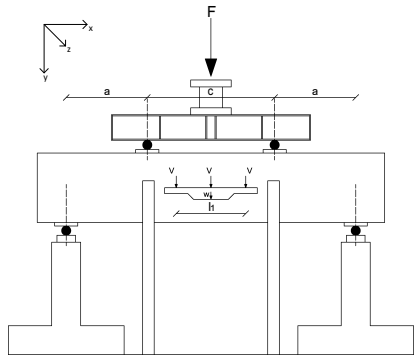

Fig. 3.2. Four point bending test.

$$\begin{cases} \tau_{xy} = \dfrac{v}{t_x} \\ \\ \tau_{yx} = \dfrac{v}{t_y} \end{cases} \tag{3.1}$$

The equations for torsional shear stress differ in the case of three or 5 layer panel:

$$\tau_T == 3 \cdot \frac{\tau_{xy} \cdot t_1}{b_l} \qquad \text{3-layer} \tag{3.2}$$

$$\begin{cases} \tau_{T,\text{ext}} = 3 \cdot \frac{\tau_{xy} \cdot t_1}{b_l} \\ \tau_{T,\text{int}} = \dfrac{3}{2} \cdot \frac{\tau_{xy} \cdot t_1}{b_l} \end{cases} \qquad \text{5-layer} \tag{3.3}$$

The bending stresses were calculated according to the following equation:

$$\sigma_{\mathrm{m,edge,x}} = \frac{M_{xz}}{I_{net}} \cdot \frac{h_{\mathrm{CL}}}{2} \tag{3.4}$$

I_{net} moment of inertia referred to net section of the beam (layers parallel to x axis) [mm^4]

$h_{\mathbf{CL}}$ height of the CLT beam [mm]

3.1.2 Main findings

The main results from the experimental campaign are reported below: Tab.3.2 presents the stress values at failure and Fig.3.3 shows the different failure modes.

	MoE [MPa]
Series	Mean
A3	11648
A5	15302
B5	15553
C5	11634

Table 3.1. Modulus of Elasticity values [MPa].

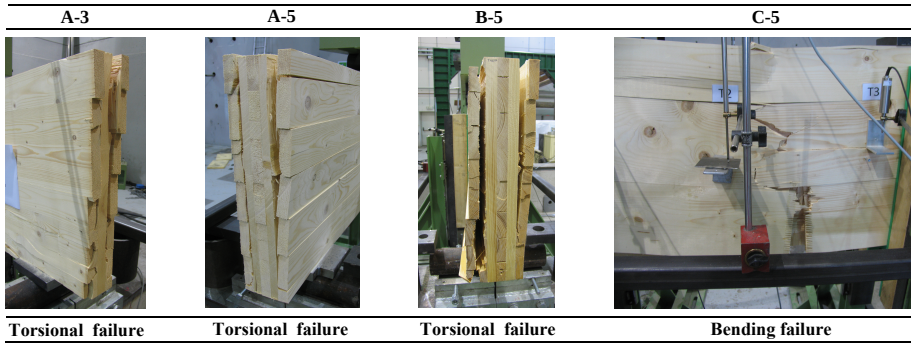

Fig. 3.3. Failure modes.

The main findings are summarized:

Stresses at failure [MPa]						
Series	$\sigma_{m,\text{edge},x}$	τ_{xy}	τ_{yx}	$\tau_{T,\text{ext}}$	$\tau_{T,\text{int}}$	Failure
A3	35.42	6.88	13.75	6.19	/	Torsional
A5	34.20	7.34	15.21	6.39	3.19	Torsional
B5	29.59	6.34	9.51	6.42	3.21	Torsional
C5	30.31	6.50	15.77	4.42	2.21	Bending

Table 3.2. Stresses at failure, shear stresses calculated with the equilibrium method.

- Net shear stresses calculation: under usual symmetry and layup conditions the Equilibrium method and RVSE method provide the same value for the maximum net shear stress (see the appendix of Paper I for detailed demonstration I.9). The beam method coincides with the Equilibrium method (except for a 0.2 reduction coefficient suggested in the COST document). The AT-Annex method also provides the same values.

- Torsional shear stresses calculation: the Equilibrium method is the only one that provides two different values for 5-layer panel: a major value in the outer interfaces and minor in the internal interface. With the same geometric assumptions as the previous point, the RVSE method provides the same torsional shear stress as the Equilibrium method for a 3 layer panel, and the average of the two values for a 5 layer panel. The Beam method tends to coincide with the RVSE method for a high number of lamellas in the section. The AT-Annex method provides values which are exactly the double than the other two methods.

- The specimens failed mainly in torsional shear, and the failure always started from the external layers. This suggests that the value may be higher in those layers, as described by the Equilibrium method-

- The EN408 standard four point bending test is not suitable for obtaining net shear failure. Different testing procedures have been proposed by [29], [5] and [6].

- The values of net shear stress obtained from the test can not be directly compared with other values from literature, since in the current campaign net shear failure was not obtained. Nevertheless the values of $f_{v,\text{mean}}$ obtained by [29], [5] and [6] present significant differences, which are respectively: 12.8; 9 and 7.5 MPa. This suggests a strong dependence on the specific test setup.

- The values of torsional shear obtained are much higher than the tests on single crossing interfaces present in literature. This suggests that the tests on single CLT crossing interfaces may not representative of the behaviour of a bigger element.

3.2 II Paper

F. Boggian, E. Ricci, A. Salenikovich, R. Springhetti, and R. Tomasi, "Deflections of light timber frame shear wall segments: Validation of a standard proposal," in *Proceedings of the World Conference of Timber Engineering-WCTE*, (Chile), 2021. Link.
Included in chapter II.

3.2.1 Goals and methods

The second paper focuses on the new Eurocode 5 (EC5) proposal for the elastic displacement on top of an LFT wall subjected to an horizontal force. The goal is to study applicability of current EC5 proposal, analysing in particular the sheathing to framing contribution and to validate the formulas with available experimental data.
First a FE model based on the formulas of EC5 was set up in *SAP2000* and the results from a sample case were compared with the analytical formulation. Then the model was used to perform a parametric analysis to study the sheathing-to-framing contribution. Last, the model was adapted to different geometries of available experimental data, and the results compared.
Frame elements connected with hinges at corners were used for the wall frame. The sheathing panels were modelled using shell elements. For connections and restraints three types of elements were used: linear links for the sheathing-to-framing connections and sliding restraints, nonlinear hook links for the hold-downs and and nonlinear gap elements the compression interface between bottom rail and ground. The analysis was nonlinear elastic. The non-linearity derives from the use of hook and gap elements, which may be active or inactive. The model was then used to calculate the horizontal deflection of a fully anchored wall with standard 1:1 aspect ratio (2.5m x 2.5m, taken from [12], see Fig.3.4) as reference case. First, the horizontal force applied to the top of the wall was set to 10 kN, and five cases of vertical distributed load were then considered, with values increasing from 0 to 30 kN/m. After validating the model with respect to the analytical formulas, the same model was used for a parametric analysis studying the sheathing-to-framing contribution. In the end the model was also used for comparison with the result of existing experimental tests on LTF timber walls.

3.2.2 Main findings

Table 3.3 shows the comparison for the first reference case, from which it is evident that the FE model accurately mimics the analytical formulation, with a 1% discrepancy on the global deflection value. The comparison of each contribution

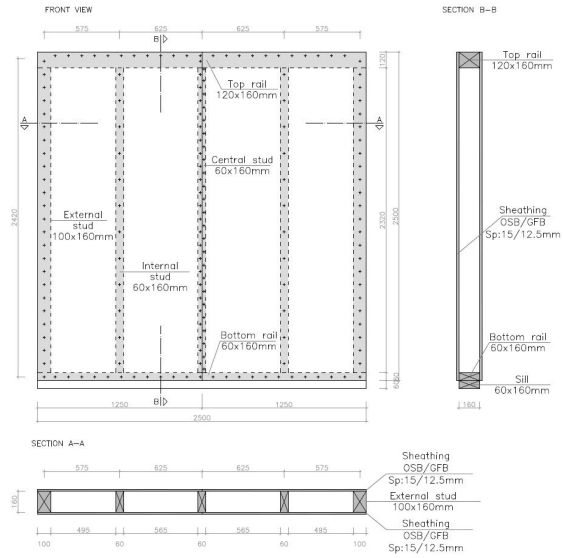

Fig. 3.4. Wall configuration in [12].

also shows generally a good agreement, as seen from Fig. 3.5. The difference is large for the framing and bottom rail contributions, but they represent the two smallest contributions to the overall displacement.

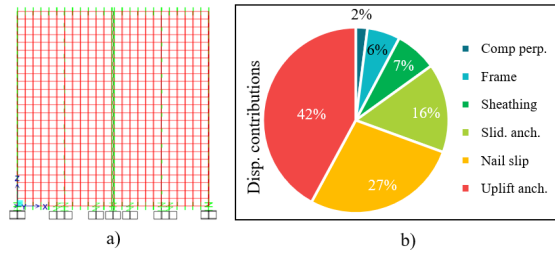

Fig. 3.5. a) FEM model and b) percentages of the different contributions.

The two possible approaches for modelling the sheathing-to-framing contribution were studied with a parametric analysis on the same wall model, varying the section and the flexibility of the frame members by means of a *Python OAPI* script. The results are plotted in Figure 3.6 along with the analytical values predicted by Equation 2.17 Fully flexible (red) refers to case 1 in 2.1.2, while fully rigid (blue) refers to case 2 in 2.1.2. Frame elements groups from A to E are

Table 3.3. Results of the comparison between analytical formulation and FEM, for F=10 kN and q=0 kN/m.

Contribution	u_{anal} [mm]	u_{FEM} [mm]	Diff. %
(1) Fastener slip	1.18	1.17	0.1
(2) Framing deformation	0.24	0.18	27.1
(3) Uplift of anchorage	1.81	1.81	0.1
(4) Sliding of anchorage	0.67	0.67	0.1
(5) Compression perp. def.	0.09	0.07	21.4
(6) Sheathing deformation	0.31	0.32	0.1
Total deflection	4.3	4.26	1.0

increasing size of cross sections (group C represent the reference size from [10], while the analysis "Inf J and A" uses an infinite multiplier for the moment of inertia J and the area A of the frame elements, to simulate the fully rigid formula case. The graphs shows that the analysis "Inf J and A" matches with the rigid analytical formula, while the real case lies between the two formulas.

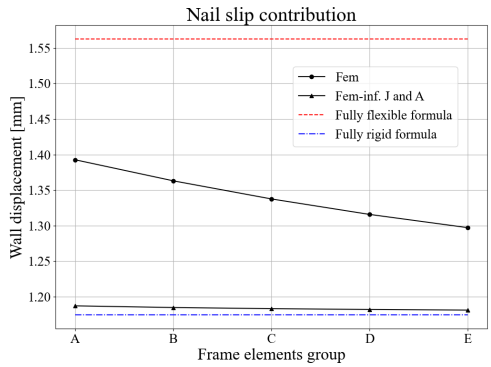

Fig. 3.6. Parametric analysis on nail slip contribution.

The FE model then was used for calculating the horizontal displacement at the top of the shear wall segments tested in recent experimental campaigns in North and South Americas and in Europe. The results can be see in Tab.3.4 for fully anchored walls and in Tab.3.5 for partially anchored walls. The differences in this case are higher, between 7% and 47% for fully anchored walls, and between 3% and 47% for partially anchored walls.

Table 3.4. Comparisons for fully anchored walls.

Experimental campaign	u_{test} [mm]	u_{FEM} [mm]	Diff. %
Grossi [12],[13]	7.37	8.54	-13
Salenikovich [21]	6.4	4.29	33
Seim [25],[26]	10.3	11.08	7
Payeur [19],[22]	9.7	5.14	47
Seaders [24]	4.08	5.18	-21
Lebeda [15]	7.86	5.72	27
Santa Maria [14],[23]	10.06	8.69	13

Table 3.5. Comparisons for partially anchored walls.

Experimental campaign	u_{test} [mm]	u_{FEM} [mm]	Diff. %
Salenikovich [21]	3.94	2.1	47
Payeur [19]	5.11	4.02	21
Seaders [24]	2.64	2.71	-3
Ni [18]	4.27	2.61	39

The main findings are summarized:

- The FEM model accurately mimics the analytical formulas of the Eurocode 5 proposal, the discrepancies on the total displacement are around 1%.
- The parametric analysis highlights the dependence of the sheathing-to-framing contribution on the framing cross section size and stiffness. The analytical formulation has two limit hypothesis, fully flexible or fully rigid members, the FEM model provides results which lay in between.
- The discrepancies between the FE model and the experimental data vary between 3% and 47%. The constructive details strongly influence the results. While this inconsistency could potentially be reduced, the results still show that the new EC5 proposal represents an improvement with respect to the current formulation adopted in the U.S. and Canada, which lead to differences up to 200% [17].

3.3 III Paper

A. Aloisio, F. Boggian, R. Tomasi, and M. Fragiacomo, "The role of the hold-down in the capacity model of LTF and CLT shear walls based on the experimental lateral response", *Construction and Building Materials*, vol. 289, 2021. Doi.
This paper is included in chapter III.

3.3.1 Goals and methods

In this paper existing experimental data on LTF and CLT shear walls are used for analysing the lateral response and calibrate a simple failure model for rocking timber walls. The goal is to study the lateral behaviour of timber shear walls in the post-elastic phase, find similarities between the two technologies and propose a simplified model that can work for both.
The experimental data used in this paper derives from LTF and CLT shear wall tests performed at the University of Trento. [11] have partially published the outcomes on LTF shear walls, while very limited results on CLT were published in [2, 28, 3]. Both LTF and CLT shear walls with dimensions of 2.5×2.5 m were tested. The test set-up, shown in Fig.3.7, follows the EN 594:2011 prescriptions [1]. Various vertical loads and different types of hold-downs, angle brackets and sheathing, drove a comparative assessment about the performance of the specimens. The total number of tests was 9 for LTF and 8 for CLT. An extract of the results is show in the load-displacement graphs of Fig.3.8.

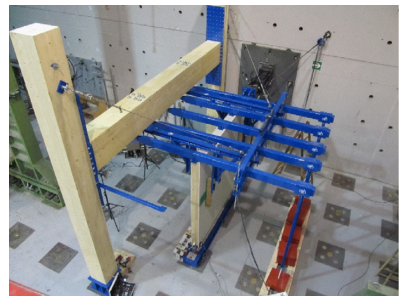

Fig. 3.7. LTF test setup.

The experimental data, with measures of displacements from different parts of the walls, see Fig.3.9, was used to divide the wall response in three different contributions and study their distribution in ultimate condition:

s Sliding u_D: describes the contribution to displacement due to the deformation of the anchorage against sliding, taken from the measure in point D;

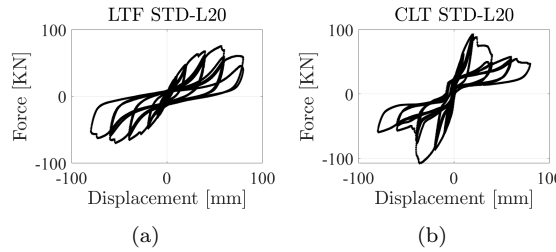

Fig. 3.8. Example of cyclic test results.

d Deformation δ: describes the contribution to displacement due to the deformation of the timber parts of the wall, taken from the measures of the displacement in the diagonals;

r Rocking $\theta \cdot l$: describes the contribution to displacement due to the elongation of the anchorage against uplift, taken as the difference between the total applied displacement u_b and the two previous contributions.

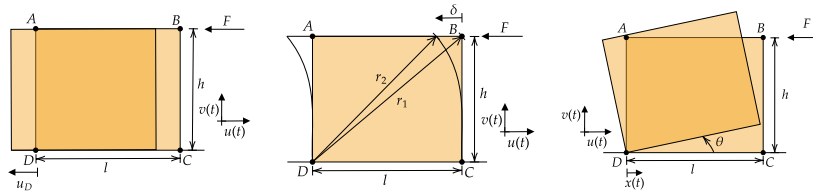

Fig. 3.9. Different contribution to displacement: (a) sliding, (b) deformation, (c) rocking.

In the end, previous data and conclusions were also used to evaluate the position of the pivot point at failure during the rocking behaviour of the shear walls, see Fig.3.10, and propose a simple mechanical model of the wall.

3.3.2 Main findings

The study of the three displacement contributions defined earlier permitted to assess that, for higher levels of the input displacement during testing, each component has an asymptotic behaviour towards a final value, see Fig.3.11. This

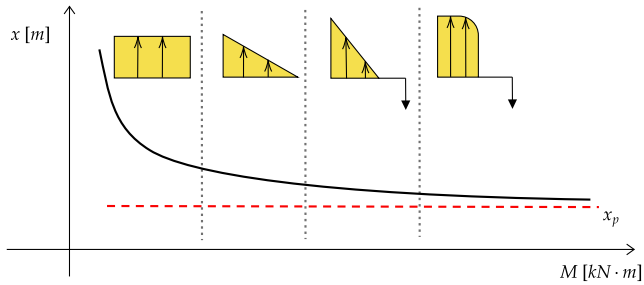

Fig. 3.10. Qualitative evolution of the neutral axis as a function of the base moment.

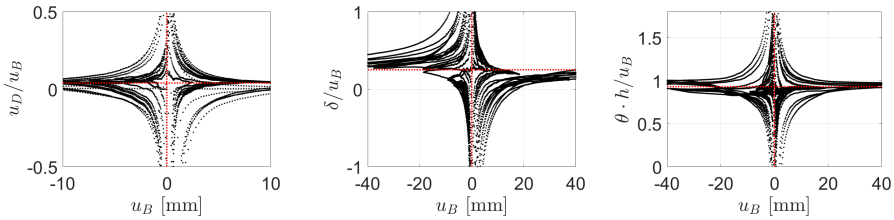

(a) (b) (c)

Fig. 3.11. Ratio between each displacement contribution and the applied input displacement on top: (a) s-sliding; (b) d-deformation; (c) r-rocking.

finding pis illustrated graphically in Fig.3.12, which shows the average values of the s,d,r components for the two typologies of walls both during the elastic phase and post-elastic. This finding confirms that, in ultimate conditions, the behaviour of the walls is mainly influenced by their rocking contribution. This also permitted to estimate the extension of the neutral axis at failure x_P, see Fig.3.10 and 3.13, for each tested wall.
The previous findings inspired the following mechanical model, that is based purely on the hold-down reaction and neglects the compression zone (σ_c is neglected in the equilibrium equations), see Fig.3.13:

$$F = H \cdot \frac{\tau \cdot l}{h} + q \cdot \frac{l}{h}\left(\tau \cdot l - \frac{l}{2}\right) \quad | \quad \tau = \frac{l - x_p}{l} \tag{3.5}$$

where q is the distributed vertical load, l the wall length, F the top horizontal force, h the wall height, H the hold down reaction force, x_p the extension of the neutral axis, t_{eff} is the thickness of the wall reacting in compression, l_c is the lever

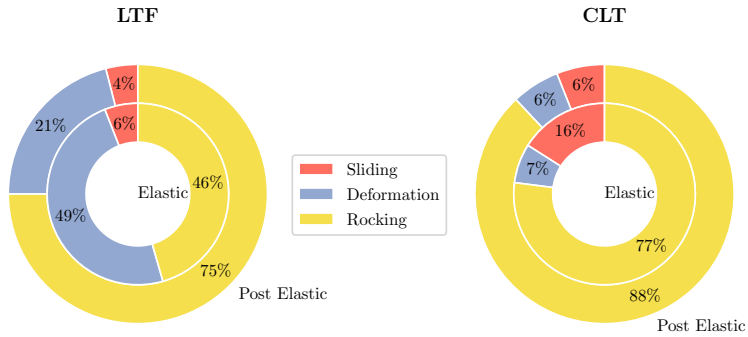

Fig. 3.12. Percentage of displacement on top of the shear walls due to each single contribution in both the elastic (calculated by [7]) and post-elastic range (as calculated from the experimental data in this paper).

arm of the compression region. The authors validated this model by comparing,

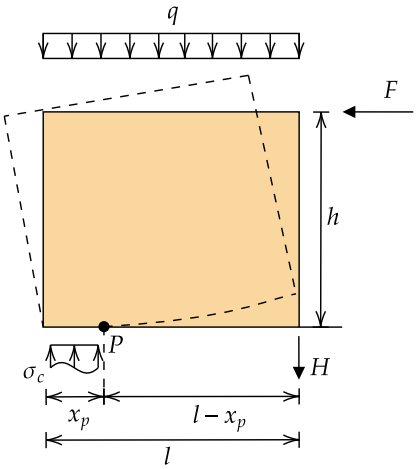

Fig. 3.13. Mechanical model of the shear wall.

in terms of cyclic curves and maximum force values, the forces measured in point B of the shear wall, with the horizontal force $F(t)$. $F(t)$ is obtained from the simplified model in Eq.III.11, using the forces measured on the hold-downs $H(t)$ and the pivot point x_p value estimated earlier. Examples of comparison are shown in Fig.3.14. Two values of lever arm reduction factor τ are proposed, based on

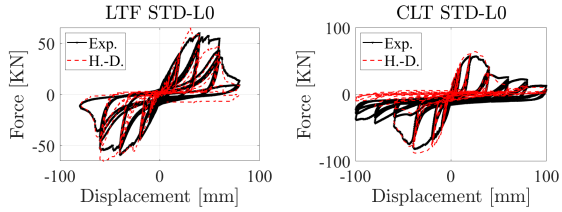

Fig. 3.14. Comparison between the experimental cyclic response of the timber walls and the capacity model based on hold-down measured forces.

the previous experimental data and on the assumption of a Gauss distribution:

$$\begin{aligned} \tau_{\mathrm{LTF},95\%} &= 0.81 \\ \tau_{\mathrm{CLT},95\%} &= 0.86 \end{aligned} \tag{3.6}$$

The main findings are summarised:

- In ultimate conditions the rocking behaviour is dominant, for both CLT and LTF shear walls.
- A simple mechanical model, based solely on the hold-down reaction force, accurately predicts the maximum capacity of the walls.
- It is important to consider the reduction of lever arm during rocking, as the simplification of using the corner of the wall leads to over estimation of the capacity. Two values are proposed: 0.81 for LTF and 0.85 for CLT.

3.4 IV Paper

F. Boggian, C. Tardo, A. Aloisio, E. Marino, and R. Tomasi, "Experimental cyclic response of a novel friction connection for seismic retrofitting of RC buildings with CLT panels", *Journal of Structural Engineering*, 2022 Doi.
This paper is included in chapter IV.

3.4.1 Goals and methods

This paper will report a testing campaign on the novel Friction Connector developed within the e-CLT retrofitting technology, part of the e-Safe European project, see Fig.3.15. The cyclic response of four different prototypes was investigated, by focusing on their dissipative performance. The goal was to understand the prototypes' behaviour for a mindful assessment of their potential for future developments. The main novelty of this paper lies in the development and testing of a new AFC for seismic retrofitting intervention coupled with CLT panels, both design choices regarding the shape and mechanical behaviour of the system will be discussed.

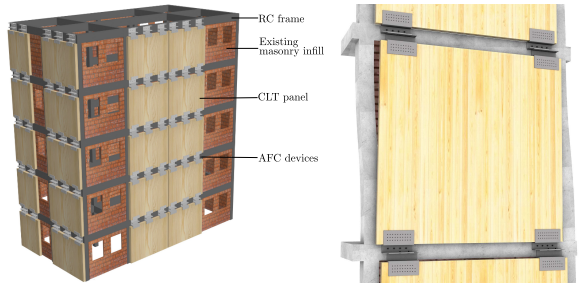

Fig. 3.15. (a) Components of the e-CLT retrofitting system and (b) e-CLT panel subjected to seismic action when the FC are sliding.

Specimen and setup

The prototypes have four different geometries, all fabricated from 8mm cold-bent S235 steel plates. The first one is labelled STD: the standard design in Fig.3.17(a), with an overall 450mm width, 325mm height and a 105mm depth, which matches with a 100mm thick CLT panel. The "top" profile has holes for

the connections with the RC beam and round holes on the interface surface with the "bottom" profile. The bottom profile has two slotted holes, which guarantee the sliding between the two profiles. Each hole hosts a preloaded 10.9 class M14 bolt. Both profiles present holes in the outer plates for screwed connections with the CLT panels. The STD is the initial design of the FC, that worked as a base configuration. Other three different designs were obtained by modifying the STD, in order to improve the mechanical behavior and the possible weaknesses evidenced in FEM modeling [27]. Three main features were changed: the number and position of the slotted holes, the out of plane eccentricity -between friction connection and bottom profile (see Fig.3.16)-, and the number of bends of the bottom profile. The prototype STD-R was built to add strength to the STD in the

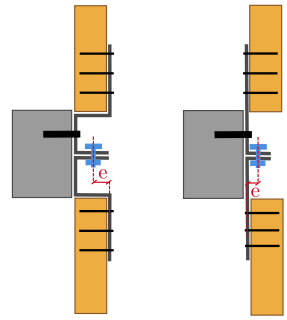

Fig. 3.16. Scheme illustrating the out of plane eccentricity of the system: (a) STD design, (b) ALT design.

box-like area, so two welded plates were added as reinforcements, see Fig.3.17(c). The two plates guarantee the same installation of the STD, without any grooves required in the CLT. The prototype STD-1H has the same geometry as the STD with one significant difference: there is a single and centered slotted hole with both preloaded bolts sliding inside, see Fig.3.18(a). The ALT design presents a shape different from that of the STD design, as shown in Fig.3.18(c). In addition, the connection to the CLT panel was moved to the back, thus making both the profiles L shaped elements. In this way, only one bend was necessary, and also the out of plane eccentricity could be slightly reduced. However, the downside of this design is represented by a more difficult mounting and maintenance procedure. The connection to the CLT panel is on the backside, adjacent to the existing masonry.

The specimens used for the experimental campaign are shown in Fig.3.17(b), 3.17(d), 3.18(b), 3.18(d). They present some modifications with respect to the prototypes, mainly to fit the setup and to isolate and study the sole friction

Table 3.6. Nomenclature and parameters of the prototypes

Prototype	Description	e [mm]	Slotted hole	n_{bend}
STD	Standard	46.1	Double	3
STD-R	Standard with reinforcements	46.1	Double	3
STD-1H	Standard with 1 elongated hole	46.1	Single	3
ALT	Alternative	32.8	Single	1

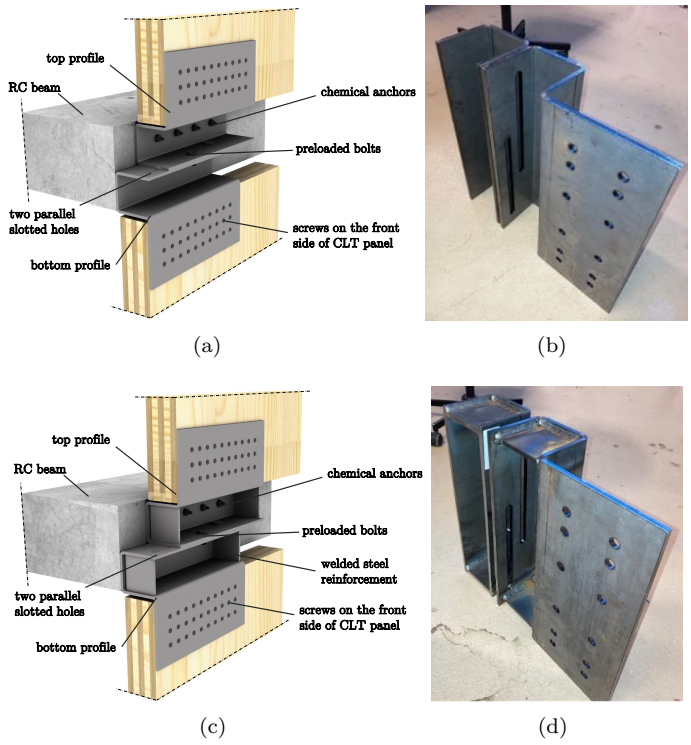

Fig. 3.17. (a) STD prototype; (b) STD specimen; (c) STD-R prototype; (d) STD-R specimen.

connection. The "top" profile was simplified to a C-shape for connection with the cross-head of the press. The vertical displacement protocol of the press simulates the horizontal displacement of the RC beam of the existing building. The setup was conceived to reproduce a loading condition that applies a sliding movement

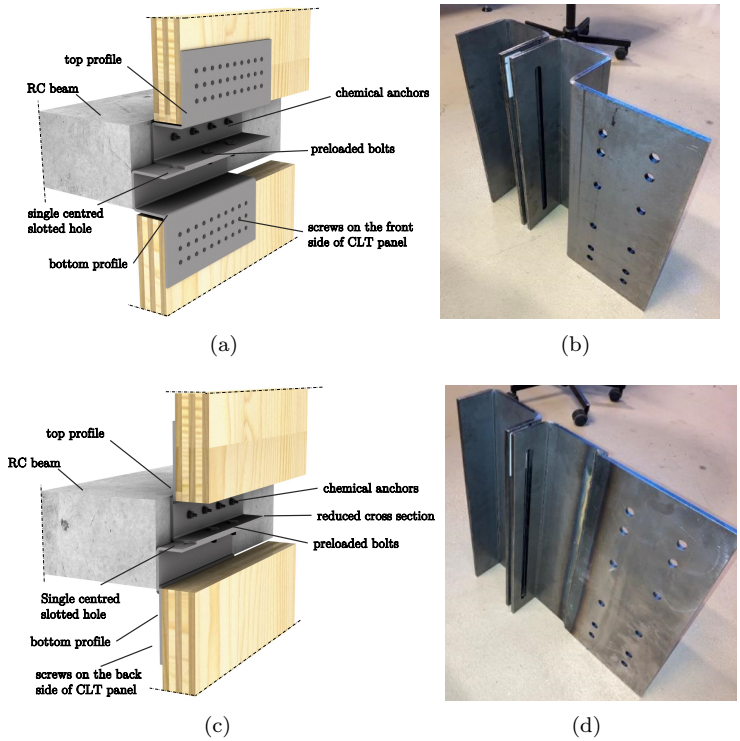

Fig. 3.18. (a) STD-1H prototype; (b) STD-1H specimen; (c) ALT prototype; (d) ALT specimen.

to the FC, in order to isolate and study the friction behaviour. The setup consists of a rigid steel frame embedded in a universal *Instron* electromechanical testing machine, as seen in Fig.3.19.

Testing and data elaboration

Table 3.7 lists the tests carried out in this campaign and a description of the loading protocol. For tests starting from STD.5 the authors included an 8mm cap plate and 2mm aluminium shim layers, as shown in Fig.3.20, thus reproducing an Asymmetric Friction Connection (see section 2.2.2). The definition of the slip force F_{slip} from the experimental data is neither straightforward nor unique. The author decided to use the same approach used by [16], which adopts a definition

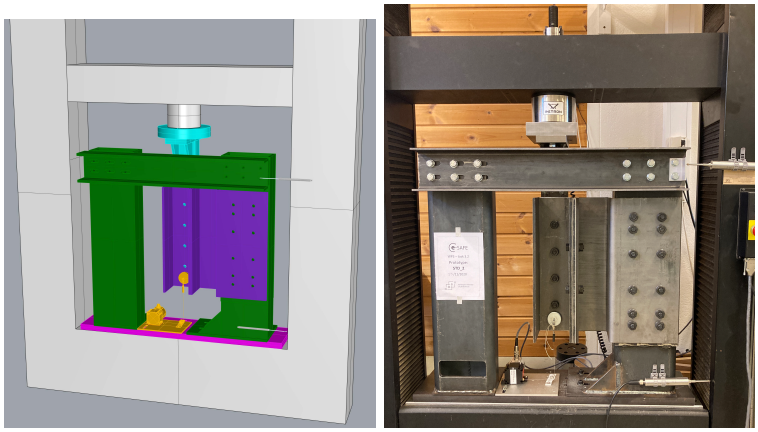

(a) (b)

Fig. 3.19. (a) 3D model of the setup; (b) setup.

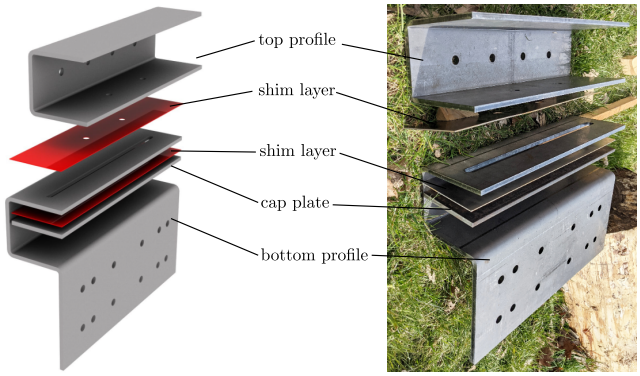

Fig. 3.20. Illustration and photo of the parts of a specimen.

related to the dissipated energy E:

$$E = \sum_{i=0}^{n} E_i = \sum_{i=0}^{n} \left| \frac{F_{i+1} + F_i}{2} \cdot (\delta_{i+1} - \delta_i) \right| \tag{3.7}$$

where E_i denotes the energy at the $i-$th time step, F_i and δ_i are the force and displacement at the same time step, respectively. The slip force is defined as the

Table 3.7. Test overview

Test Label	Specimen	Protocol	Speed [mm/s]	Shim	Preload [kN]
STD.1	STD_0	M	4.0	\	80.5
STD.2	STD_1	A	0.5	\	24.1
STD.3	STD_1	B	0.5	\	24.1
STD.4	STD_1	B	0.5	\	24.1
STD.5	STD_2	B	0.5	Alum.	24.1
STD-R.1	STD-R_1	B	0.5	Alum.	24.1
STD-1H.1	STD-1H_1	B	0.5	Alum.	24.1
STD-1H.2	STD-1H_1	B	0.5	Alum.	45.3
ALT.1	ALT_1	B	0.5	Alum.	24.1
ALT.2	ALT_1	B	0.5	Alum.	36.0
ALT.3	ALT_1	C	2.0	Alum.	36.0
ALT.4	ALT_1	D	2.0	Alum.	36.0

M: monotonic
Cyclic A: 1x5mm+3x10-20-30mm; speed 0.5 mm/s
Cyclic B: 1x5mm+3x10-20-30-40-50mm; speed 0.5 mm/s
Cyclic C: 1x5mm+3x10-20-30-40-50mm; speed 2 mm/s
Cyclic D: 1x5-10mm+3x20-40-60-80-100mm; speed 2 mm/s

work per unit of length:

$$F_{\text{slip}} = \frac{E}{D} \qquad F_{sd} = \sqrt{\frac{\sum_{i=0}^{n} |F_i - F_{\text{slip}}|^2}{n-1}} \tag{3.8}$$

where $D = \sum_{i=0}^{n} |\delta_{i+1} - \delta_i|$ is cumulative distance of travel and F_{sd} is the standard deviation is calculated with reference to the F_{slip} value. The experimental friction coefficient μ is calculated as follows:

$$\mu = \frac{F_{\text{slip}}}{n_s n_b F_P} \tag{3.9}$$

where F_{slip} is the slip force calculated in Eq.(3.8), n_s is the number of shear surfaces, n_b is the number of the preloaded bolts and F_P is the preload force from Tab.3.7.

3.4.2 Main findings

Tab.3.8 reports the results by in terms of slip force and friction coefficient, while Fig. 3.21 present the results in graphical form as force displacement loops. The

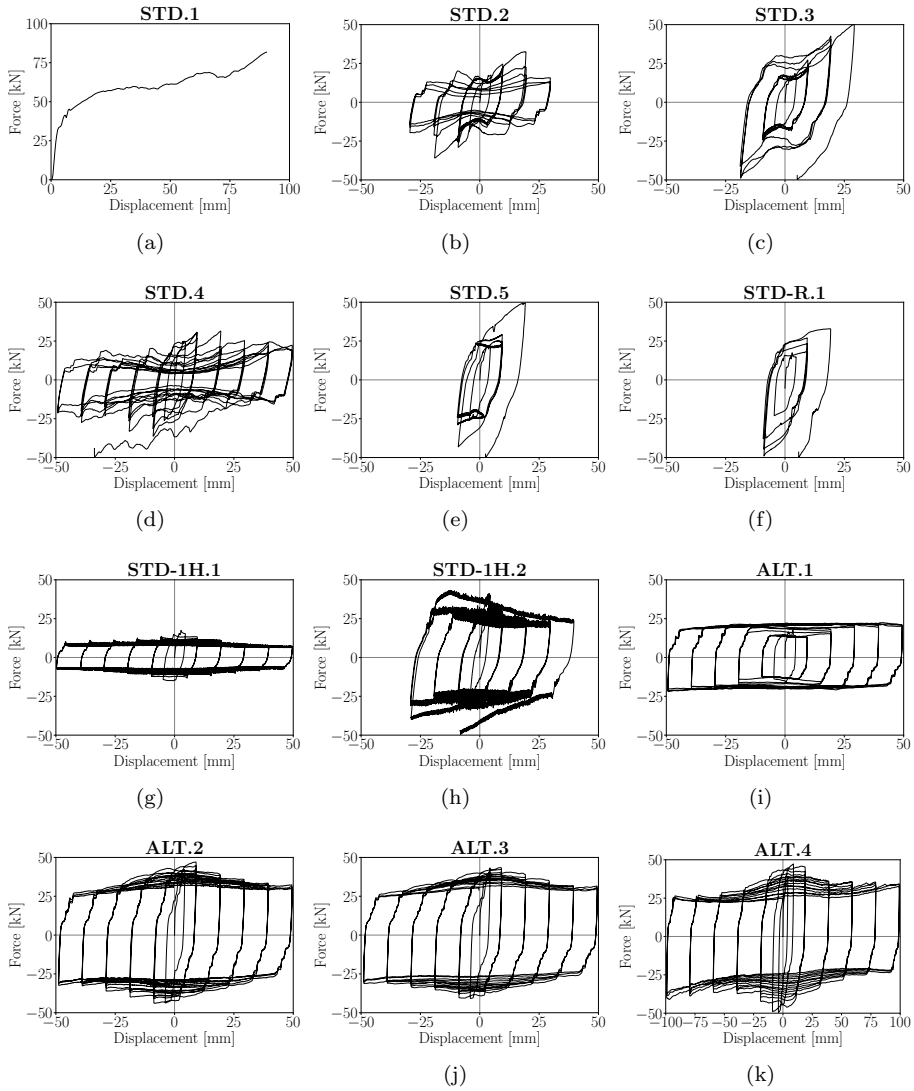

Fig. 3.21. Cyclic test results of ALT specimens.

Table 3.8. Results of cyclic tests

Test	F_{slip} [kN]	F_{sd} [kN]	μ
STD.1	59.94	12.11	0.19
STD.2	10.61	5.62	0.11
STD.3	19.99	12.02	0.21
STD.4	12.00	10.59	0.12
STD.5	19.51	14.78	0.20
STD-R.1	20.49	12.79	0.21
STD-1H.1	8.10	1.44	0.08
STD-1H.2	22.74	8.53	0.13
ALT.1	18.20	3.62	0.19
ALT.2	30.79	7.51	0.21
ALT.3	29.57	7.27	0.21
ALT.4	28.79	6.80	0.20

main findings are that STD and STD-R suffer from major deformations (see Fig.3.22 due to bending and twisting which brought their test to an early stop, and the reason lies in two features: an intrinsic weakness of the outer bend of the bottom profile, because of the eccentricity, and the presence of two not aligned elongated holes. STD-1H and ALT showed promising results, indicating that the

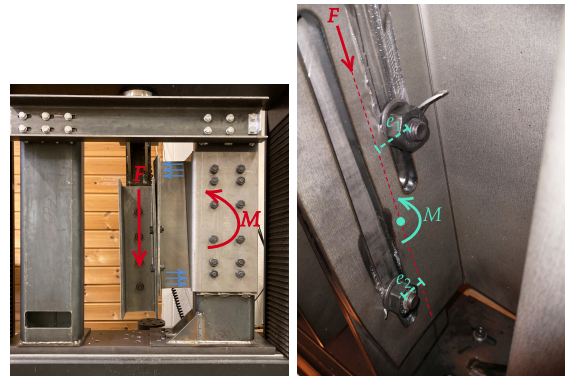

(a) (b)

Fig. 3.22. Test STD.1: schemes illustrating the observed deformations.

arrangement of a single elongated hole solved some of the deformation problems,

and that the reduced eccentricity and lower number of bends of ALT design were effective in isolating the friction behaviour. The authors obtained acceptable results using aluminium for the shim layer, whose friction coefficient, nearly equal to 0.2, agree with literature formulations. Aluminium as shim material provided stable hysteresis curves, while its absence caused an erratic response (e.g. steel-to-steel friction). ALT tests also confirmed the independence from loading speed of the friction connections.
In general then the main conclusions are that:

- Two geometric features play an important role: the out of plane eccentricity -between the sliding force and the CLT restraint on the bottom profile-, and the number of bends. A limited depth of the connectors, aimed reducing the eccentricity, and a single bend are effective in limiting unwanted deformations and isolating the friction behaviour.

- The arrangement of the bolts in two unaligned slotted holes is cause of additional eccentricities during the sliding movement: a single slotted hole with both bolts aligned is preferable to limit twisting deformations.

- A cap plate and shim layers are necessary to obtain an acceptable loop stability: aluminium shims provided satisfactory frictional behaviour with an estimated 0.2 friction coefficient.

3.5 V Paper

F. Boggian, A. Aloisio, and R. Tomasi, "Experimental and analytical study of friction connection for seismic retrofit with CLT panels," *Earthquake Engineering and Structural Dynamics*, 2022. Doi
This paper is included in chapter V.

3.5.1 Goals and methods

This paper can be considered a continuation of Paper IV, as the testing campaign on the AFC for the e-CLT system was extended with the use of new specimens and a new setup. The experimental campaign was carried out on AFCs fixed with screws to a CLT panel, to observe the contribution of timber to the total dissipation performance. The investigation is based on 20 cyclic test with two different setups. The main one includes a CLT panel and screw connection, while the second one is only made with steel. The goal is to compare the tests on AFC with and without connection to the CLT specimen, in order to estimate the effect of the timber connection on the hysteretic response.

Specimens and setup

The specimen is called HYB (Hybrid), since its design originated from the results of the previous campaign [4]: STD offered the positive feature of the front mounting possibility, while ALT offered better mechanical performances due to the single bend L shape. HYB attempts to combine the best features of the two previous designs: front mounting and simple L shape, see Fig. 3.23. The specimen is made of two 8mm thick cold bent S355 steel profiles: the anchor profile is connected to the moving head of the press (the existing RC beam for the real world case), while the free profile is connected to the CLT panel. The two profiles are clamped together to form an asymmetric friction connection (AFC) by adding an 8mm steel cap plate and two 2mm aluminum shim layers. The connection between the two profiles is ensured by two high strength M16 10.9 bolts [9], that will slide in a 17mm wide elongated hole.

Five total specimens were tested. The free profile of the first 4 specimens presented 33 holes for 10x80mm HBS Plate Evo screws from Rothoblaas [20]. These specimens were tested on the main setup, with a piece of CLT panel that was 100mm thick, had 5 layers and of dimensions 400x800mm. Fig.3.24 shows the main setup, where the machine applied a vertical sliding movement, which would be equivalent to the horizontal movement of an RC beam in a real case building. One specimen, called HYB_s (1 sample), was tested on a different setup: a steel column was used as support for the free profile instead of a CLT panel, thus the hole pattern was different since bolts were used instead of screws, see Fig. 3.25.

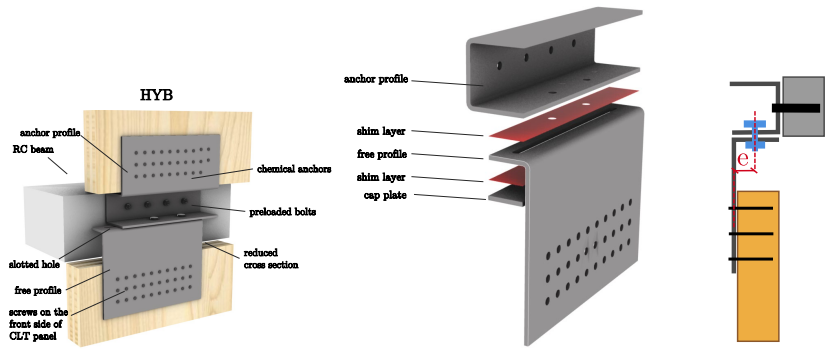

(a) (b) (c)

Fig. 3.23. Specimen HYB tested in the current experimental campaign: (a) parts of the system in a real building, (b) parts of the specimen used for testing, (c) eccentricity of the specimen.

This specimen was made in order to have a direct comparison regarding the effect of the screw connection on the friction behavior of the system.

Table 3.9. Description of the specimens.

Prototype	n	e [mm]	Setup
HYB	3	52.5	with CLT
HYB_e	1	43.5	with CLT
HYB_s	1	52.5	no CLT

Testing and data elaboration

Tab.3.10 summarizes the 20 tests that are presented in this paper. The first part of the testing campaign (on specimens with design HYB and HYB_e) was carried out on the main setup that includes the CLT panel. The last 5 tests, on the HYB_s specimen, were performed on the secondary setup which was made of steel and didn't include the CLT panel. The labels of the tests are as follows: ¡name of design¿-¡number of sample¿.¡number of repetition¿, so for example the label *HYB-2.3* indicates the third test on the second sample with HYB design. Data elaboration was performed in the same way as the previous paper, with some small modifications in order to account for the additional deformability introduced by the screw connection, see V.3 for a complete explanation.

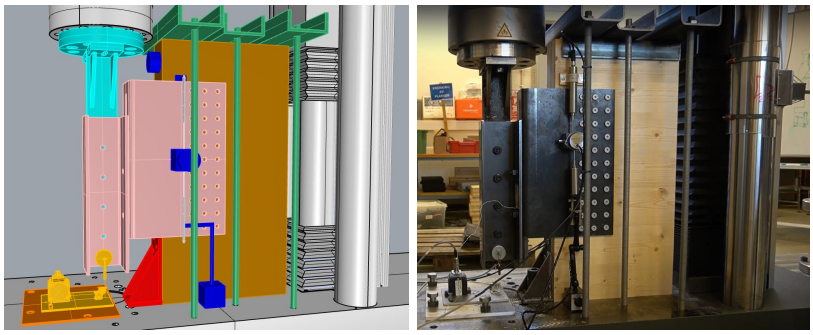

(a) (b)

Fig. 3.24. (a) Model of the setup, (b) picture of the setup. In both images the press is pushing down 100mm.

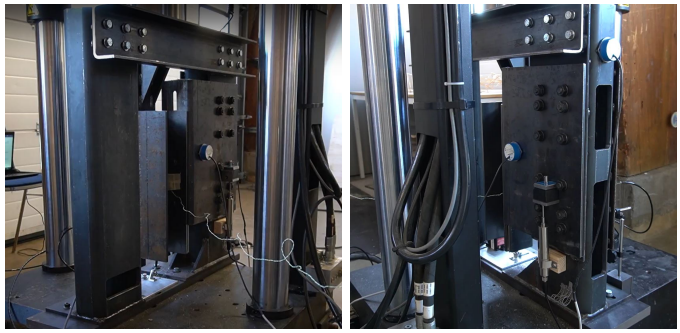

(a) (b)

Fig. 3.25. (a) Setup for HYB_s experiments, (b) detail of the free profile bolted to the steel column. In both images the press is pushing down 100mm.

Table 3.10. Overview of the tests.

Test Label	Specimen	Protocol	Setup	Preload [kN]
HYB-1.1	HYB-1	A	CLT	25.0
HYB-1.2		A	CLT	25.0
HYB-2.1	HYB-2	B	CLT	25.0
HYB-2.2		B	CLT	25.0
HYB-2.3		B	CLT	25.0
HYB-2.4		B	CLT	25.0
HYB-3.1	HYB-3	B	CLT	25.0
HYB-3.2		B	CLT	25.0
HYB-3.3		B	CLT	25.0
HYB-3.4		B	CLT	25.0
HYB_e-1.1	HYB_e-1	B	CLT	25.0
HYB_e-1.2		B	CLT	25.0
HYB_e-1.3		B	CLT	37.5
HYB_e-1.4		B	CLT	37.5
HYB_e-1.5		B	CLT	37.5
HYB_s-1.1	HYB_s-1	B	no CLT	25.0
HYB_s-1.2		B	no CLT	25.0
HYB_s-1.3		B	no CLT	37.5
HYB_s-1.4		B	no CLT	37.5
HYB_s-1.5		B	no CLT	37.5

Protocol A: 1x5mm+3x10-20-30-40-50mm; 2mm/s
Protocol B: 1x5-10mm+3x20-40-60-80-100mm; 2mm/s

3.5.2 Main findings

Tab.3.11 reports the results by in terms of slip force and friction coefficient, while Fig. 3.26,3.27,3.28,3.29 present the results in graphical form as force displacement loops. The immediate observation from the graphs is that the friction behaviour is satisfactory for this new shape of specimen, since all the cycles present a shape similar to a rectangle that offers high energy dissipation. In general there is also not a big difference between the graphs of the tests on the timber setup and the ones without, suggesting that the influence of the timber connection on the friction behaviour is limited. One key difference in the slightly better shape of the loops with the steel setup, which are more rectangular and with higher initial stiffness of the graphs referring to the CLT setup, that show pinching behaviour in the first cycles. For both the setup the friction coefficient value was calculated to be around 0.21, which is in line with values for aluminium and in accordance with the previous experimental campaign.

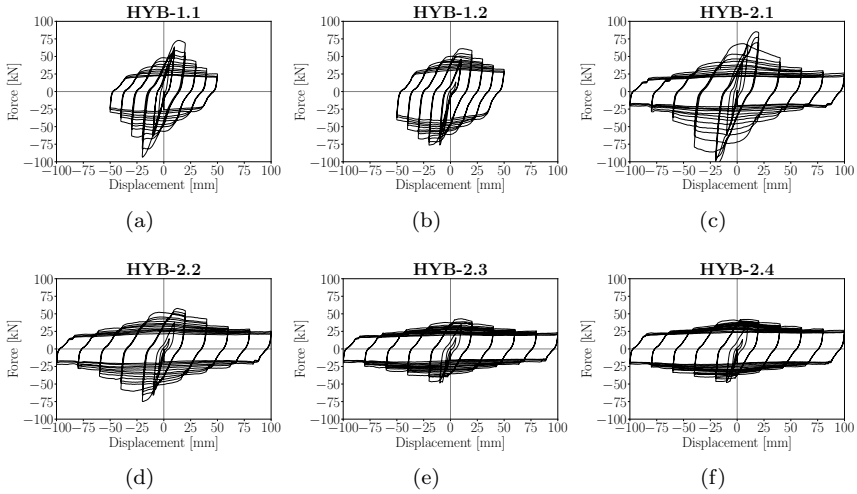

Fig. 3.26. Test results of specimen HYB-1 and HYB-2, all with preload 25kN.

The main findings are summarised:

- The HYB shape of specimen can represent a valid solution.
- The hysteresis loops of tests with CLT show a certain level of pinching-S shape, typical of timber connections.
- The hysteresis loops of tests without CLT present a more rectangular shape.

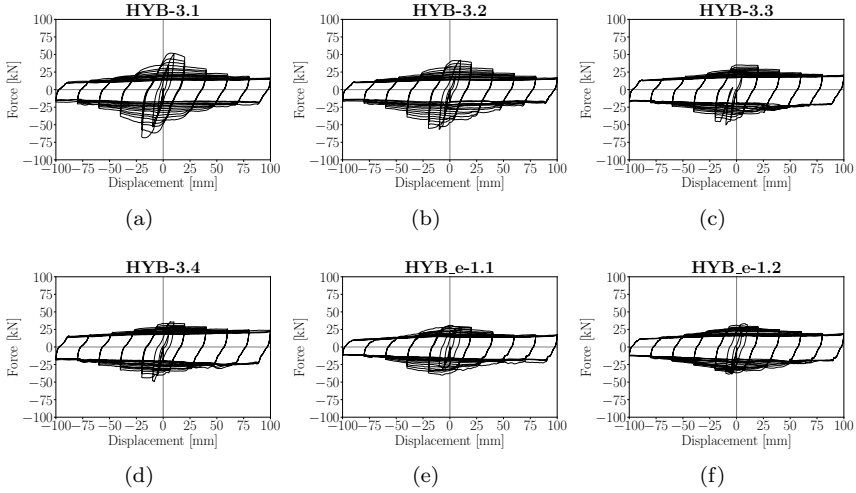

Fig. 3.27. Test results of specimen HYB-3 and part of HYB_e.1, all with preload 25kN.

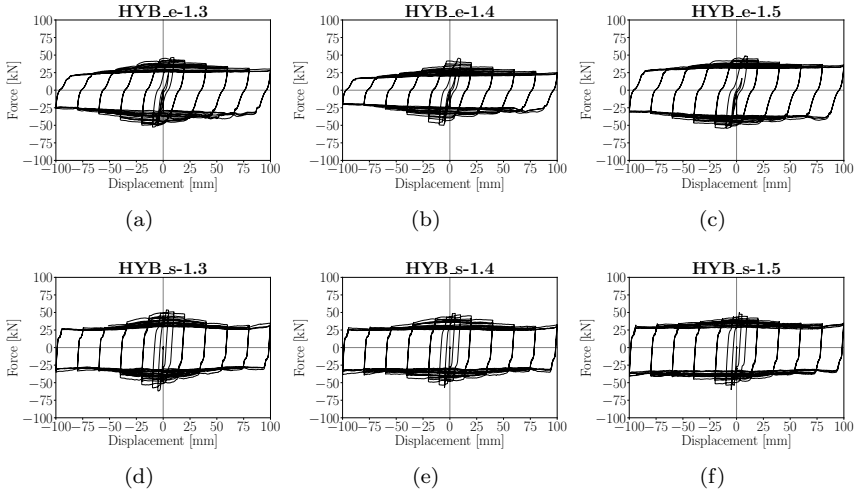

Fig. 3.28. Test results for specimen HYB_e-1 HYB_s-1 with preload 37.5kN.

- Overall the CLT connection doesn't influence the friction behaviour in a great manner.

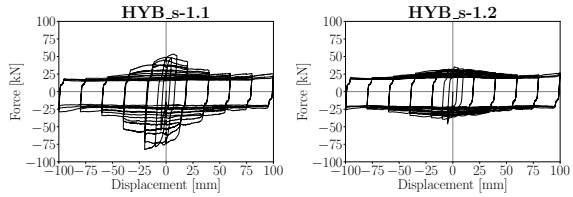

(a) (b)

Fig. 3.29. Test results for specimen HYB_s-1 with preload 25kN.

- The indirect comparison between tests with CLT and tests without highlights an energy loss of around 10%. This performance in considere acceptable.
- Slip force and friction coefficient are similar in both the setups and in accordance with literature and previous findings.

Table 3.11. Results in terms of slip force, standard deviation, coefficient of variation, stability coefficient and friction coefficient.

Test	F_{slip} [kN]	StDev[kN]	COV	μ
HYB-1.1	29.61	12.92	0.44	0.30
HYB-1.2	36.07	14.68	0.41	0.36
mean				0.33
HYB-2.1	28.35	13.70	0.48	0.28
HYB-2.2	26.91	10.35	0.38	0.27
HYB-2.3	22.49	6.91	0.31	0.22
HYB-2.4	25.52	7.40	0.29	0.26
HYB-3.1	19.86	7.98	0.40	0.20
HYB-3.2	19.73	7.52	0.38	0.20
HYB-3.3	20.55	5.67	0.28	0.21
HYB-3.4	21.58	5.73	0.27	0.22
HYB_e-1.1	17.03	5.32	0.31	0.17
HYB_e-1.2	19.21	5.52	0.29	0.19
HYB_e-1.3	30.38	8.15	0.27	0.20
HYB_e-1.4	24.79	6.43	0.26	0.17
HYB_e-1.5	34.41	8.53	0.25	0.23
mean				0.22
HYB_s-1.1	18.94	8.92	0.47	0.19
HYB_s-1.2	23.45	4.28	0.18	0.23
HYB_s-1.3	31.53	5.35	0.17	0.21
HYB_s-1.4	31.25	5.45	0.17	0.21
HYB_s-1.5	33.87	5.12	0.15	0.23
mean				0.21

Bibliography

[1] EN 594:2011 Timber structures, Test methods - Racking strength and stiffness of timber frame wall panels. *BSI, London UK*, 2011.

[2] Ermanno Acler and Roberto Tomasi. Monotonic and cyclic in-plane behavior of clt panels tested by using different types of metal devices. In *COST Action FP1004 - Early Stage Researchers Conference Enhance mechanical properties of timber, engineered wood products and timber structures - Zagreb, Croatia*, 2012.

[3] Mauro Andreolli and Roberto Tomasi. Bemessung von gebäuden in brettsperrholzbauweise unter erdbebenbeanspruchung. *Bautechnik*, 2016.

[4] Francesco Boggian, Carola Tardo, Angelo Aloisio, Edoardo Marino, and Roberto Tomasi. Experimental cyclic response of a novel friction connection for seismic retrofitting of rc buildings with clt panels. *Journal of Structural Engineering*, 2022.

[5] Reinhard Brandner, Thomas Bogensperger, and Gerhard Schickhofer. In plane shear strength of cross laminated timber (clt): test configuration, quantification and influencing parameters. In *Proceedings of 46th CIB-W18 Meeting, Vancouver*, 2013.

[6] Reinhard Brandner, Philipp Dietsch, Julia Dröscher, Michael Schulte-Wrede, Heinrich Kreuzinger, and Mike Sieder. Cross laminated timber (clt) diaphragms under shear: Test configuration, properties and design. *Construction and Building Materials*, 147:312–327, 2017.

[7] Daniele Casagrande, Simone Rossi, Tiziano Sartori, and Roberto Tomasi. Proposal of an analytical procedure and a simplified numerical model for elastic response of single-storey timber shear-walls. *Construction and Building Materials*, 102:1101–1112, 2016.

[8] EN 408. Timber structures–Structural timber and glue-laminated timber–Determination of some physical and mechanical properties. Comité Européen de Normalisation CEN. 2012.

[9] EN14399-4. High-strength structural bolting assemblies for preloading - part 4: System hv - hexagon bolt and nut assemblies, 2015.

[10] Paolo Grossi. Experimental investigations on seismic behaviour of light timber framed buildings and log-house traditional constructive system. Master's thesis, University of Trento, 2013.

[11] Paolo Grossi, Tiziano Sartori, and Roberto Tomasi. Tests on timber frame walls under in-plane forces: part 2. *Proceedings of the Institution of Civil Engineers-Structures and Buildings*, 168(11):840–852, 2015.

[12] Paolo Grossi, Roberto Tomasi, and Tiziano Sartori. Tests on timber frame walls under in-plane forces: Part 1. *Proceedings of the Institution of Civil Engineers: Structures and Buildings*, 168:826–839, November 2015.

[13] Paolo Grossi, Roberto Tomasi, and Tiziano Sartori. Tests on timber frame walls under in-plane forces: Part 2. *Proceedings of the Institution of Civil Engineers: Structures and Buildings*, 168:840–852, November 2015.

[14] Guíñez, Felipe and Santa María, Hernán and Almazán, José Luis. Monotonic and cyclic behaviour of wood frame shear walls for mid-height timber buildings. *Engineering structures*, 2019.

[15] Daňa Lebeda. The effect of hold-down misplacement on the strength and stiffness of wood shear walls. Master's thesis, Oregon State University, 2002.

[16] W.Y. Loo, P. Quenneville, and N. Chouw. A new type of symmetric slip-friction connector. *Journal of Constructional Steel Research*, 94:11–22, 2014.

[17] Zeno A. Martin and Thomas D. Skaggs. APA Report T2001L-65: Shear wall deflection and predictive equations. Technical report, APA- The Engineerd Wood Association, 2002.

[18] Chun Ni and Erol Karacabeyli. Performance of braced walls under various boundary conditions. In *World Conference on Timber Engineering*, 2010.

[19] Mario Payeur. Influence des charges verticales sur les performances laterales des murs de refend en bois a ossature legere. Master's thesis, Université Laval, 2011.

[20] Rothoblaas. Screws and connectors for wood-carpentry, structures and outdoor. Accessed: 2022-01-12.

[21] Alexander Salenikovich. The racking performance of light-frame shear walls. Master's thesis, Virginia Polytechnic Institute and State University, 2000.

[22] Alexander Salenikovich and Mario Payeur. Influence of vertical loads on lateral resistance of light-frame shear walls. In *World Conference on Timber Engineering*, 2010.

[23] Santa María, H. and Salinas, A. and Montaño, J. and Ugarte, JJ. and Almazán, JL. and Guindos, P. and Opazo, A. and Benedetti, F. and Rosales, V. nd Estrella, V. and Guiñez, F. and Berwart, S. and Cárcamo, S. and

Jara, A. Assessment of seismic design factors and proposal of modification to Chilean seis- mic building design code (NCh 433) for mid-rise wood-frame buildings. *International Network on Timber Engineering Research*, 2020.

[24] Peter Seaders, Rakesh Gupta, and Thomas H. Miller. Monotonic and cyclic load testing of partially and fully anchored wood-frame shear walls. *Wood and Fiber Science*, 41(2):145–156, April 2009.

[25] Werner Seim, Johannes Hummel, and Tobias Vogt. Earthquake design of timber structures - Remarks on force-based design procedures for different wall systems. *Engineering Structures*, 76:124–137, 2014.

[26] Werner Seim, Miha Kramar, Tomaž Pazlar, and Tobias Vogt. OSB and GFB As Sheathing Materials for Timber-Framed Shear Walls: Comparative Study of Seismic Resistance. *Journal of Structural Engineering*, 142(4), April 2016.

[27] Carola Tardo, Francesco Boggian, Magnus Hatletveit, Edoardo Marino, Giuseppe Margani, and Roberto Tomasi. Mechanical characterization of energy dissipation devices in retrofit solution of reinforced concrete frames coupled with solid wood panels. In *Proceedings of the 12th International Conference on Structural Analysis of Historical Constructions*, 2020.

[28] Roberto Tomasi. Seismic behavior of connections for buildings in clt. In *COST Action FP1004 - Focus Solid Timber Solutions European Conference on Cross Laminated Timber (CLT) - Graz, Austria*, 2013.

[29] Georg Wallner. Versuchstechnische ermittlung der verdrehungskenngrössen von orthogonal verklebten brettlamellen. Master's thesis, TU Graz, 2004.

4. Conclusion and future works

The main conclusions regarding the part on codification are:

- The available methods for the calculation of net shear stresses all provide similar results for usual CLT layups. In the choice of which one to adopt for the new Eurocode 5 particular attention should be payed to ease of use and consistency with non usual CLT layups. The Equilibrium method is the only one providing different torsional shear values depending on the interface considered, and the experimental data seem to confirm this difference. Regarding the evaluation of in-plane net shear strength it can be concluded that the four point bending test by the EN408 is not suitable to the scope, so additional test procedures are needed in this sense.

- The formulas for the calculation of the displacement at the top of an LTF shear wall, part of the new Eurocode 5 draft, can be considered adequate. Even if they show some discrepancies with existing experimental data, they can be considered an improvement with respect to accepted formulas in other standards. Further development may be directed in two directions: giving a criteria for choosing Flexible/Rigid members in the formula of the sheathing-to-framing contribution, and new proposals for the partially anchored walls.

- In ultimate conditions the rocking behaviour of both LTF and CLT walls is mainly governed by the hold downs. For both walls the maximum force can be predicted with a simplified model that takes into account only the hold-down contribution and with a proper reduction of the lever arm (0.81 for LTF and 0.85 for CLT). Further developments of the model may include the contribution of the compression region in timber and of the angle brackets. It is important to stress that this is related only to the ultimate capacity, LTF and CLT walls differ in other aspects such as ductility/dissipation capabilities, ease of manufacturing, possibilities of fabrication and application.

For what concerns the e-CLT retrofit system and the new friction connection the main conclusion is that the system showed great potential during the the first two stages of the experimental campaign. These testing campaigns at component level permitted to understand the behaviour of the connector and highlight the key points in the design of the AFC:

- The shape of the friction connection should have only 1 bend, in that way the undesired deformations due to eccentricities are limited;
- the cap plate and shim layers are necessary to obtain a stable friction behaviour. Aluminium is considered an appropriate choice given its satisfactory mechanical results, ease of manufacturing and cost;
- the coupling of the friction device with a steel-to-timber screw connection gives a slight reduction in total dissipated energy, but nevertheless the overall friction behaviour is maintained and the performance is deemed acceptable.

Further studies and developments are needed before the real world application of the e-CLT system. Research effort can be directed at studying the possible treatments of the shim layers in order to increase the friction loop stability. Furthermore, a real scale test on a concrete frame with masonry, with and without e-CLT retrofit, is already planned within the research project. Another useful potential development would be a real scale test on the shake table of a small pilot building.

Part 2

Papers Shear Walls-codification

I. Cross Laminated Timber (CLT) Beams Loaded in Plane: Testing Stiffness and Shear Strength

Bibliographic data

F. Boggian, M. Andreolli, and R. Tomasi, "Cross laminated timber (CLT) beams loaded in plane: testing stiffness and shear strength," *Frontiers in Built Environment*, vol. 5, p. 58, 2019. Doi

Contents

abstract

Cross Laminated Timber (CLT) is a relatively new timber product used in constructions that gained lots of popularity over the last decade. The product itself is constituted by multiple glued layers of juxtaposed boards, usually arranged in an orthogonal direction between one layer and the adjacent ones. This particular structure brings several benefits, such as the possibility to use the same product both for walls and slabs, since it can bear in plane and out of plane loads. However, the mechanical behavior differs from usual timber products, and research is still ongoing to achieve common agreement on standard procedures for testing products and theories for evaluating stresses for safety verifications. This paper focuses on the in-plane shear behaviour of CLT and analyzes the existing methods to evaluate shear stresses. An experimental part then presents a four point bending test of CLT beams with a specific geometry to induce shear failure. Results are reported both for the elastic range test, measuring the Modulus of Elasticity, and for the failure test to investigate shear behavior with regard to different mechanisms. Previously exposed methods are used for the calculation of shear stresses and to analyze correspondence between them, results are then compared with other existing tests and values in literature. A new test setup for future research is eventually proposed.

Keywords:

CLT, cross laminated timber, shear, in plane, shear stress, testing, shear strength

I.1 Introduction

Cross Laminated Timber is one of the many systems of building with timber, it can be seen as a development of glued laminated timber by applying a similar concept on 2D elements instead of linear elements and with a new layup; its employment in construction is recent and it became widely used mostly in Europe in the past 15 years. This product is usually produced in plate-like shape and its alternated orthogonal board layers structure makes it apt to bear loads in and out of plane; hence the great benefit given by the possibility to use the same element both as a wall and as a floor slab. Another big advantage of this building system is the high degree of prefabrication it offers: this means more control during production process which translates in small tolerances, CLT members are produced and if necessary cut in personalized shapes directly in the production site using CNC machines. Regarding the building site this also means faster times and cleaner area since the elements only need to be assembled and connected

to each other to constitute the load bearing structure of the building; it further permits faster application of additional insulation layers and finishes (see [7]). The use of this construction system is relatively new so the process of producing standards is still ongoing. The problem regards two different but closely related areas: which test procedures to use for the evaluation of the strength properties of CLT and also which methods to adopt for the calculation of stresses. The work of this paper is inserted in this scope, particularly regarding the in-plane shear properties: a four point bending test has been performed on CLT beams according to [13] procedure to investigate the values of the modulus of elasticity and shear stresses at failure. On the matter of evaluating shear stresses, a review is provided presenting the available methods in literature, and then a test is also used for comparison.

I.2 Materials

The experimental campaign investigated a total number of 10 CLT beams, coming from different producers. The beams were cut from bigger panels and geometry was modified from the prescriptions of [13] to induce a shear failure. All beams had a span $l = 3\,\mathrm{m}$ and a height $h_{\mathrm{CL}} = 600\,\mathrm{mm}$, the thickness varied depending on the number of layers and the producer, as seen in tableI.1. Four different

Series	n. of spec.	$b_{l,\mathrm{mean}}$ [mm]	t_{CL} [mm]	t_i [mm]	Edge gluing
A3	4	100	90	30-30-30	yes
A5	2	100	130	29-21-29-21-29	yes
B5	2	80	135	27-27-27-27-27	no
C5	2	150	144	34-21-34-21-34	no

Table I.1. Characteristics of tested CLT beams.

types of specimen have been tested, with differences in the number and thickness of layers, presence of narrow edge glued interface, board width and presence of cracks or cuts to improve shrinkage behavior, see fig.I.1. For all panels the technical certificate of the producer indicated a minimum of 90% C24 strength class boards for each layer, with a maximum 10% of C16 boards (for strength classes of structural timber in Europe see [12]).

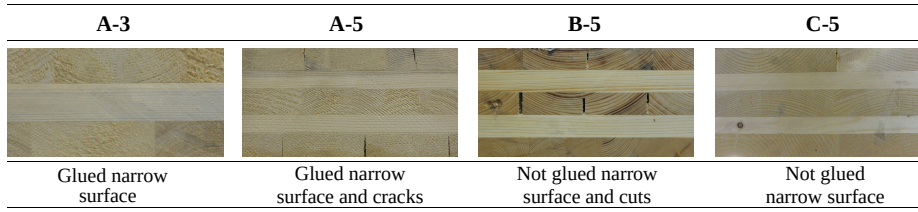

Fig. I.1. Tested specimen: for each series of specimen an image is provided showing the layup in the thickness direction and underlining differences.

I.3 Test Setup

The beams were tested using a four point bending test in accordance to the procedures of [13] and [11], see fig.I.2. The test was conducted in a displacement control method with a loading ratio of $0,03\,\mathrm{mm/s}$ till reaching a maximum force $F \leq 0,4F_{\mathrm{max,est}}$ to obtain the load/displacement curve in order to calculate the modulus of elasticity. The load was applied by a hydraulic actuator and the integrated load cell was used to measure the force. A rigid steel beam was used to equally distribute the load in two centred points at a distance $c = 1100\,\mathrm{mm}$ ($a = 700\,\mathrm{mm}$; $c = 800\,\mathrm{mm}$ and $a = 850\,\mathrm{mm}$ only for the first two specimen of series A3), in order to avoid local concentration of stresses the load was transferred with two steel plates screwed on the beam. The beam itself was simply supported by two concrete foundations, with one end functioning as a slider allowing movement in the longitudinal axis direction. Given the particular slenderness of the beam two additional restraints were placed to avoid instability out of plane, with internal surfaces of frictionless plastic material in order to allow free movement of the beam in its bending plane. Displacement measures were taken with 4 LVDT on each side of the beam: three of them were measuring absolute displacements at neutral axis height (one in the center and two additional centred with $l_1 = 800\,\mathrm{mm}$, $l_1 = 600\,\mathrm{mm}$ only for the first two specimen of series A3) while the fourth one was measuring relative displacement.

I.4 Modulus of Elasticity calculation

The modulus of elasticity was calculated in accordance with [13]. Experimental load-displacement curves were analyzed through a linear regression analysis and for each specimen the modulus was calculated considering the longest line between $0{,}1F_{\mathrm{max}}$ and $0{,}4F_{\mathrm{max}}$ with a minimum correlation coefficient of 0,99 (the line must at least include the interval between $0{,}2F_{\mathrm{max}}$ and $0{,}3F_{\mathrm{max}}$). The equation

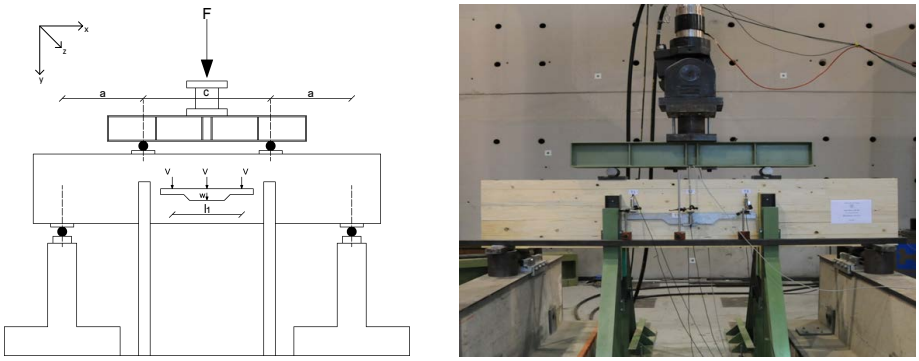

Fig. I.2. Test setup presented in EN 408.

used is the following:

$$E_{m,l} = \frac{al_1^2(F_2 - F_1)}{16I_{net}(w_2 - w_1)} \tag{I.1}$$

- $(F_2 - F_1)$: load increase [N]
- $(w_2 - w_1)$: displacement increase in the corresponding interval [mm]
- a: distance between the loading point and the support [mm]
- l_1: reference length for MoE determination [mm]
- I_{net}: moment of inertia referred to net section of the beam (layers parallel to x axis) [mm^4]

I.5 Shear Stresses calculation

In this section various methods for calculating in plane shear stresses will be presented and compared: a method based on the equilibrium, developed by [1] (Equilibrium method), a method based on the Representative Sub Element Volume method, developed by [3] (RVSE method), the method for beams developed [14] and adopted also in COST document ([8], Beam method), and the method of Austrian annex K to [21] (AT-annex method). In order to obtain a simple and significant exposition a common notation will be used: the one present in the COST document ([8]) and [9], see fig.I.3, which will also be the base for the future Eurocode section regarding CLT products. The first index indicates the plane normal to the action, the second index indicates the axis the action is parallel to;

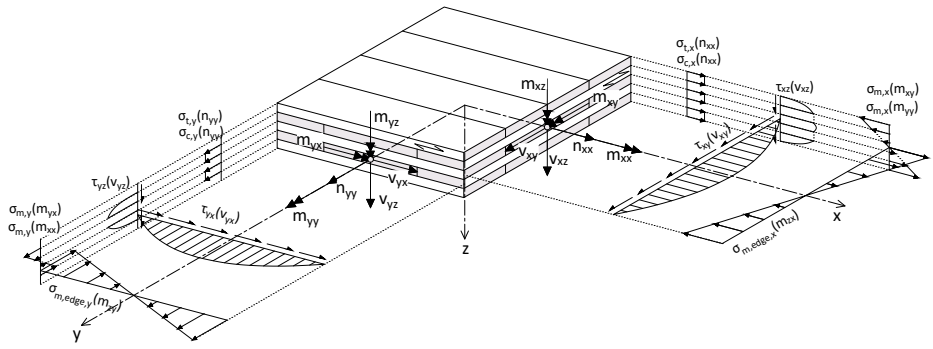

Fig. I.3. Shear stresses, modified from COST document ([8]).

for the following section then the direction y would be the vertical one (parallel to the height h_{CL} of the beam), x is horizontal (parallel to the longitudinal axis of the beam), z is horizontal through the thickness t_{CL} of the beam. The shear force is expressed as force per unit length and for rotational equilibrium:

$$v_{xy} = v_{yx} = v \tag{I.2}$$

The layers oriented as the x axis (so the major number of layers for a usual panel with an odd total number of layers) will have thickness $t_1\, t_3\, t_5$, while the layers oriented as the y axis (so the minor number of layers) will have thickness $t_2\, t_4$. The width of the laminations b_l is assumed to be equal for boards oriented in both directions, if cracks are present or it is not constant for each board then $b_{l,\mathrm{mean}}$ is to be used (unless otherwise specified).

I.5.1 Equilibrium method

This method is based on equilibrium equations for each layer and glued interfaces and was presented in [1]. As seen from fig.I.4 the base assumption is that shear stresses are only present in the cross section of the boards oriented perpendicular respect to the shear action.

3 Layer panel

Shear stresses τ_{xy} and τ_{yx} are calculated using the thicknesses of the layers oriented as the respective direction:

$$\tau_{xy} = \frac{v}{t_1 + t_3} \tag{I.3}$$

$$\tau_{yx} = \frac{v}{t_2} \tag{I.4}$$

For panels with symmetric layup $t_1 = t_3$ the stress τ_{yx} can be expressed as a function of τ_{xy}:

$$\tau_{yx} = \tau_{xy} \cdot \frac{2 \cdot t_1}{t_2} \tag{I.5}$$

The global equilibrium to rotation poses:

$$M_{T12} - M_{T21} - M_{T23} + M_{T32} = 0 \tag{I.6}$$

At each glued interface, for action reaction:

$$\begin{cases} M_{T12} = M_{T21} \\ M_{T23} = M_{T32} \end{cases} \tag{I.7}$$

Rotational equilibrium is calculated for each layer:

$$\begin{cases} M_{T12} - \tau_{xy1} \cdot b_l^2 \cdot t_1 = 0 \\ M_{T21} - \tau_{yx2} \cdot b_l^2 \cdot t_2 + M_{T23} = 0 \\ M_{T32} - \tau_{xy3} \cdot b_l^2 \cdot t_3 = 0 \end{cases} \tag{I.8}$$

So considering that $\tau_{xy1} = \tau_{xy3} = \tau_{xy}$ and $\tau_{yx2} = \tau_{yx}$ and using the relations previously found it can be obtained:

$$M_T = M_{T12} = M_{T21} = M_{T23} = M_{T32} = \tau_{xy} \cdot b_l^2 \cdot t_1 \tag{I.9}$$

It is then possible to evaluate torsional shear stresses as a function of τ_{xy} considering that $W = W_1 = W_2 = W_3 = \frac{b_l^3}{3}$:

$$\tau_T = \tau_{T12} = \tau_{T21} = \tau_{T23} = \tau_{T32} = \frac{M_T}{W} = 3 \cdot \frac{\tau_{xy} \cdot t_1}{b_l} \tag{I.10}$$

5 layer panel

Shear stresses τ_{xy} and τ_{yx} are calculated using the thicknesses of the layers oriented as the respective direction:

$$\tau_{xy} = \frac{v}{t_1 + t_3 + t_5} \tag{I.11}$$

$$\tau_{yx} = \frac{v}{t_2 + t_4} \tag{I.12}$$

For panels with symmetric layup $t_1 = t_3 = t_5$ and $t_2 = t_4$ the stress τ_{yx} can be expressed as a function of τ_{xy}:

$$\tau_{yx} = \tau_{xy} \cdot \frac{3t_1}{2t_2} \tag{I.13}$$

Similarly to the previous 3 layer case the same calculations are done, arriving at:

$$\begin{cases} M_{T,\text{ext}} = M_{T12} = M_{T21} = M_{T45} = M_{T54} = \tau_{xy} \cdot b_l^2 \cdot t_1 \\ M_{T,\text{int}} = M_{T23} = M_{T32} = M_{T34} = M_{T43} = \dfrac{\tau_{xy}}{2} \cdot b_l^2 \cdot t_1 \end{cases} \tag{I.14}$$

It is then possible to evaluate torsional shear stresses as a function of τ_{xy} considering that $W = W_1 = W_2 = W_3 = W_4 = W_5 = \frac{b_l^3}{3}$:

$$\begin{cases} \tau_{T,\text{ext}} = \tau_{T12} = \tau_{T21} = \tau_{T45} = \tau_{T54} = \dfrac{M_{T,\text{ext}}}{W} = 3 \cdot \dfrac{\tau_{xy} \cdot t_1}{b_l} \\ \tau_{T,\text{int}} = \tau_{T23} = \tau_{T32} = \tau_{T34} = \tau_{T43} = \dfrac{M_{T,\text{int}}}{W} = \dfrac{3}{2} \cdot \dfrac{\tau_{xy} \cdot t_1}{b_l} \end{cases} \tag{I.15}$$

So differently from the case of a 3 layer panel torsional shear stresses are not equal for all glued interfaces, but are major on external ones.

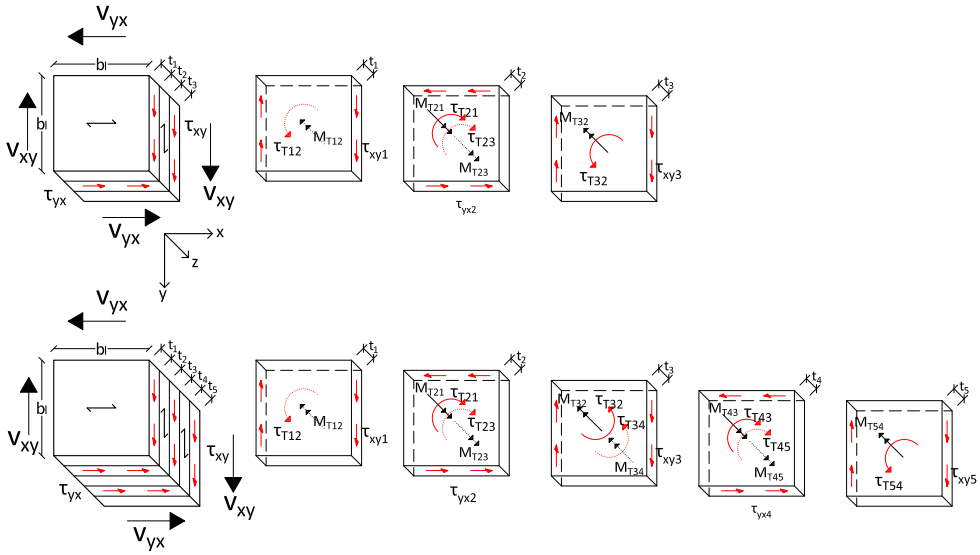

Fig. I.4. Shear stresses for the equilibrium method.

I.5.2 RVSE method

This model is developed by referring to an ideal CLT panel with an infinite number of layers and considering a crossing interface with width equal to the width of the laminations, see [3]. This element is then simplified to obtain a Representative Volume Sub Element (RVSE) of CLT which has a thickness t and a nominal shear stresses τ_0 distributed on its entire thickness t (see fig.I.5):

$$\tau_0 = \frac{v}{t} \tag{I.16}$$

This stress can be considered as the composition of two parts: an effective shear stress on the cross section with orientation perpendicular to grain

$$\tau_v = 2 \cdot \tau_0 \tag{I.17}$$

and a torsional shear stress

$$\tau_T = 3 \cdot \tau_0 \cdot \frac{t}{b_l} \tag{I.18}$$

Since the real CLT panel has a finite number of layers it is necessary to refer to fictitious thicknesses of RVSE t_i^* ($n_{CA} = n_{\text{lay}} - 1$ is the number of glued interfaces):

$$t_{tot}^* = \sum_1^{n_{CA}} t_i^* \tag{I.19}$$

$$t_i^* = \begin{cases} \min(2 \cdot t_1; t_2) & \text{for the case of } t_1 \text{ external layer and } t_2 \text{ internal} \\ \min(t_3; t_4) & \text{for the case of } t_3 \text{ and } t_4 \text{ both internal layers} \end{cases} \tag{I.20}$$

So for a real CLT panel we get:

$$\tau_0^* = \frac{v}{t_{tot}^*} \tag{I.21}$$

$$\tau_{yx} = \tau_v^* = 2 \cdot \tau_0^* \tag{I.22}$$

$$\tau_T = \tau_T^* = 3 \cdot \tau_0^* \cdot \frac{t_i^*}{b_l} \tag{I.23}$$

It can be seen that τ_v^* corresponds to the major of the shear stresses calculated before with the equilibrium method, which is τ_{yx} for "usual" cases of symmetrical CLT panels with an odd number of layers and where the total thickness t_x of layers oriented as x axis is larger or equal to the total thickness t_y of the other layers oriented as y axis. Under the same assumptions it is also true that the torsional shear stress calculated with this method coincides precisely with the one calculated for a 3 layer panel with the equilibrium method, while for a 5 layer panel the result of the RVSE method is the average of the two values obtained with the equilibrium method. A detailed demonstration of these observation is provided in the annex.

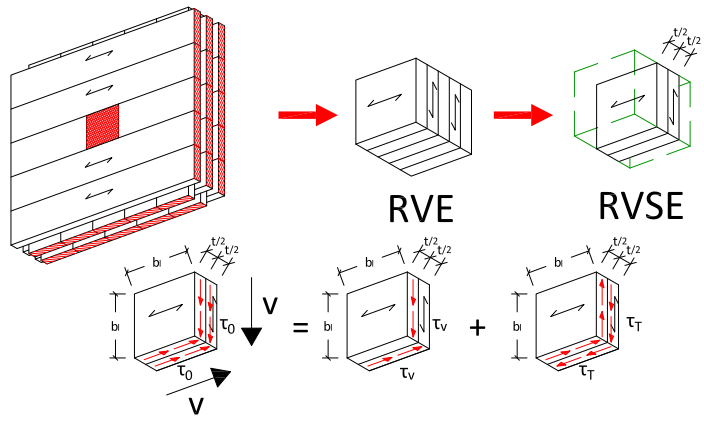

Fig. I.5. Shear stresses for RVSE model.

I.5.3 Beam method

This method was developed in [14] by referring to the equilibrium of a beam and is also present in COST document ([8]) and [9] which will be the base for a new part in the EN 1995 regarding CLT products. For shear stresses the calculus is carried out separately considering net areas for both directions; the only difference between Flaig theory and COST document is that the second one advises to reduce by 0,20 the area comprising outer layers. For 3 layer panel:

$$\begin{cases} \tau_{xy} = \dfrac{v}{t_1 + t_3} & \text{Flaig} \\ \tau_{xy} = \dfrac{v}{0,8 \cdot (t_1 + t_3)} & \text{COST} \end{cases} \qquad \begin{cases} \tau_{yx} = \dfrac{v}{t_2} & \text{Flaig} \\ \tau_{yx} = \dfrac{v}{t_2} & \text{COST} \end{cases} \tag{I.24}$$

And for a 5 layer panel:

$$\begin{cases} \tau_{xy} = \dfrac{v}{t_1 + t_3 + t_5} & \text{Flaig} \\ \tau_{xy} = \dfrac{v}{0,8 \cdot (t_1 + t_5) + t_3} & \text{COST} \end{cases} \qquad \begin{cases} \tau_{yx} = \dfrac{v}{t_2 + t_4} & \text{Flaig} \\ \tau_{yx} = \dfrac{v}{t_2 + t_4} & \text{COST} \end{cases} \tag{I.25}$$

With this method then the shear stresses are exactly the same as the Equilibrium method (except for the 0,20 reduction factor in the COST document). Torsional shear stresses are calculated as:

$$\tau_T = \frac{3V_{xy}}{b_l^2 \cdot n_{CA}} \left(\frac{1}{n_l} - \frac{1}{n_l^3} \right) \tag{I.26}$$

where V_{xy} is the applied shear force, $n_{CA} = n_{\text{lay}} - 1$ is the number of glued interfaces, $n_l = \frac{h_{\text{CL}}}{b_l}$ is the number of laminations in the height of the beam. This formula gives torsional shear stresses values very close to the ones of the RVSE method and for high n_l values they coincide, indeed for the limit case of $1/n_l^3 \to 0$:

$$\tau_T = \frac{3V_{xy}}{b_l^2 \cdot n_{CA}} \cdot \frac{1}{n_l} = \frac{3V_{xy}}{b_l^2 \cdot n_{CA}} \cdot \frac{1}{\frac{h_{\text{CL}}}{b_l}} = \frac{3V_{xy}}{b_l \cdot h_{\text{CL}} \cdot n_{CA}} = 3 \cdot \frac{v}{b_l \cdot n_{CA}} \tag{I.27}$$

Remembering eq.I.19 and eq.I.21 and with the consideration that $t^*_{tot}/n_{CA} = t^*_i$ it is possible to obtain the same formula of the RVSE method (eq.I.23):

$$\tau_T = 3 \cdot \frac{v}{b_l \cdot n_{CA}} = 3 \cdot \frac{\tau^*_0 \cdot t^*_{tot}}{b_l \cdot n_{CA}} = 3 \cdot \tau^*_0 \cdot \frac{t^*_i}{b_l} \qquad \square \tag{I.28}$$

Two additional shear stresses on the glued interface are presented in this method, as seen in fig.I.6, which are not regarded in the other methods (so they will not be considered for the comparison with the other methods in the next section): τ_{zx} which lies in the intersection plane (z) and is parallel to the axis of the beam (x), τ_{zy} which lies in the same plane and is parallel to the axis of the beam height (y). Values are calculated according to following equations:

$$\tau_{zx} = \frac{6V_{xy}}{b_l^2 \cdot n_{CA}} \left(\frac{1}{n_l^2} - \frac{1}{n_l^3} \right) \tag{I.29}$$

$$\tau_{zy} = \frac{q}{n_l \cdot b_l} \tag{I.30}$$

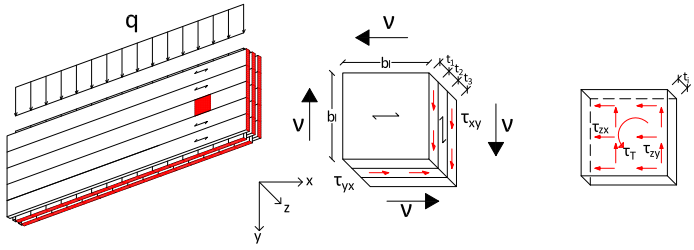

Fig. I.6. Shear stresses for the beam method, on the right part a representative glue interface is shown.

I.5.4 AT-annex

The Austrian annex K to [21] proposes, regarding shear stresses, a verification with reference to the net area in the two directions:

$$\tau_{V,0,d} = \frac{n_{xy,d}}{\min(A_x; A_y)} \tag{I.31}$$

which then yields, with the previous conventions:

$$\tau_{xy} = \frac{v}{t_1 + t_3} \quad \tau_{yx} = \frac{v}{t_2} \qquad \text{3 layer panel} \tag{I.32}$$

$$\tau_{xy} = \frac{v}{t_1 + t_3 + t_5} \quad \tau_{yx} = \frac{v}{t_2 + t_4} \qquad \text{5 layer panel} \tag{I.33}$$

In this case then, these values are exactly the same as the previous methods. For what regards torsional shear stresses the proposed formulation is (adopting the previous conventions, where for usual panels the major shear stress is τ_{yx}):

$$\tau_T = 3 \cdot \tau_{yx} \cdot \frac{t_{i,max}}{b_l} \tag{I.34}$$

The formula can be developed for a comparison:

$$\tau_T = 3 \cdot \frac{v}{n_{\text{lay,y}} \cdot t_{l,y}} \cdot \frac{t_{i,max}}{b_l} \tag{I.35}$$

$$\tau_T = 3 \cdot \frac{v}{t_{l,y}} \cdot \frac{t_{i,max}}{b_l} \qquad \text{3-layer CLT} \qquad\qquad \tau_T = \frac{3}{2} \cdot \frac{v}{t_{l,y}} \cdot \frac{t_{i,max}}{b_l} \qquad \text{5-layer CLT} \tag{I.36}$$

Equilibrium method

$$\tau_T = \frac{3}{2}\frac{v}{b_l} \qquad \text{3-layer CLT} \qquad\qquad \tau_{T,\text{mean}} = \frac{3}{4}\frac{v}{b_l} \qquad \text{5-layer CLT} \tag{I.37}$$

The two formulations are similar, but the results obtained are quite different: one considers the maximum lamination thickness and the other the mean, and even when the these two values coincide (i.e., when all layers have equal thickness) the Austrian formulation gives values which are exactly double those of the equilibrium method.

I.6 Bending stress calculation

Regarding bending stresses there is common agreement on the method of calculation, so with the usual convention of fig.I.3 the formula used for the maximum bending stress is:

$$\sigma_{\text{m,edge,x}} = \frac{M_{xz}}{I_{net}} \cdot \frac{h_{\text{CL}}}{2} \tag{I.38}$$

- I_{net}: moment of inertia referred to net section of the beam (layers parallel to x axis) [mm^4]
- h_{CL}: height of the CLT beam [mm]

I.7 Experimental results

In tableI.2 the results of the elastic part of the test are presented in term of Modulus of Elasticity, calculated as explained in sec.I.4. For the series A3 the first specimen was only tested to failure and the second one was discarded since it didn't respect all prescriptions of [13].

	MoE [MPa]				
Series	Spec. 1	Spec. 2	Spec. 3	Spec. 4	Mean
A3	-	-	12298	10997	11648
A5	15845	14758	-	-	15302
B5	14445	16661	-	-	15553
C5	12493	10775	-	-	11634

Table I.2. Modulus of Elasticity values [MPa].

The results regarding failure are instead presented in tableI.3 in term of the maximum force applied by the press, so then $V_{\max} = V_{xy}$ and $M_{\max} = M_{xz}$. The

	$F_{\max}$ [kN]					$V_{\max}$ [kN]	$M_{\max}$ [kNm]
Series	Spec. 1	Spec. 2	Spec. 3	Spec. 4	Mean	Mean	Mean
A3	313	324	372	310	330	165	128
A5	506	515	-	-	511	255	179
B5	417	405	-	-	411	206	144
C5	565	495	-	-	530	265	186

Table I.3. Values of applied force and relative shear and bending moment at failure.

result in terms of bending and shear stresses are presented in tableI.4, using the mean values of moment and shear force at failure. For the calculation of shear stresses the equilibrium method was used and to obtain the maximum value a Jourawski distribution was assumed. It is also interesting to see from figureI.8 a comparison between the values of shear stresses evaluated using all the different

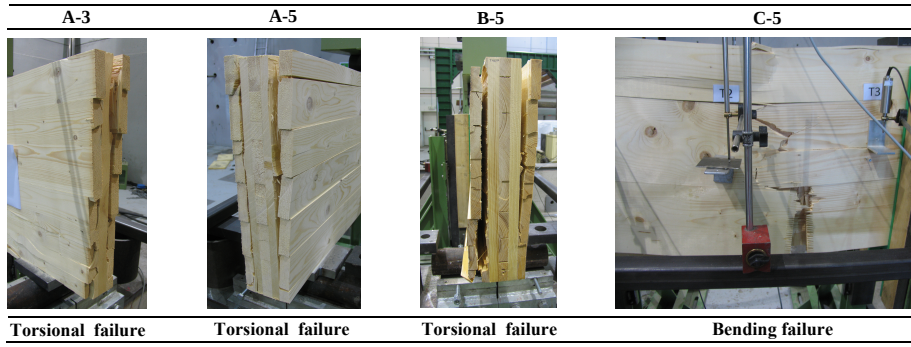

Fig. I.7. Failure modes.

Stresses at failure [MPa]						
Series	$\sigma_{m,\text{edge},x}$	τ_{xy}	τ_{yx}	$\tau_{T,\text{ext}}$	$\tau_{T,\text{int}}$	Failure
A3	35.42	6.88	13.75	6.19	/	Torsional
A5	34.20	7.34	15.21	6.39	3.19	Torsional
B5	29.59	6.34	9.51	6.42	3.21	Torsional
C5	30.31	6.50	15.77	4.42	2.21	Bending

Table I.4. Stresses at failure, shear stresses calculated with the equilibrium method.

methods previously explained. Shear stress τ_{xy} is the same value for all methods, except for COST method which results in a slightly higher value due to a 0,20 reduction factor for the thickness of outer layers. Shear stress τ_{yx} is the same value for all methods, while torsional shear stresses present some differences. The equilibrium method presents two different values, one for external and one for internal interfaces while the other methods present a single value which for RVSE, COST and Beam method is more or less the average of the previous values, while for the Austrian annex the value is much higher.

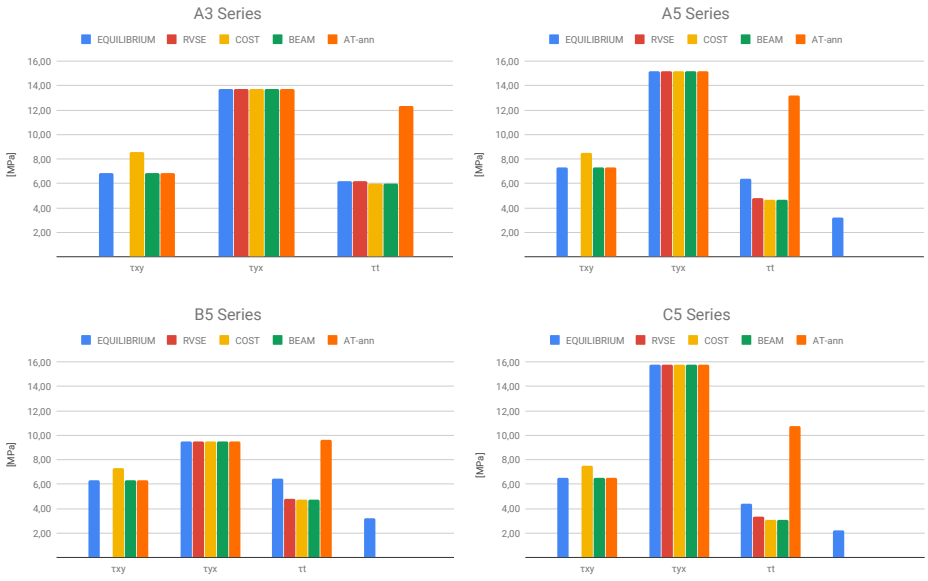

Fig. I.8. Comparison of shear stresses at failure. Note that for RVSE method there is no value for τ_{xy} since this method only provides the value of major stress τ_{yx}; note also that for 5 layer panels the equilibrium method provides two values of τ_T, one for the external and one for the internal glued interface.

I.8 Discussion and comparison

The different failures for the four types of specimen can be seen in fig.I.7. No specimen failed due to shear stresses in the laminations but two other types of failures were observed: specimen A3, A5, B5 all failed due torsional shear stresses in the glued interfaces, while the specimen C5 failed in bending. From the figures another interesting detail appears: torsional shear failure in 5 layer panels (A5 and B5) started from the outer glued interfaces, which is in accordance with the equilibrium method that hypothesizes different values of torsional shear stresses, major in external glued interfaces and minor in internal ones. Specimen series C5 failed in bending and this is probably due to a stress concentration near a defect present in both beams which brought to an early bending failure. The C5 series was also the one with the largest width of laminations, thus it had the highest polar moment of inertia which also contributed to prevent torsional shear failure like in the other three cases. The presence or absence of glue on the narrow surface of laminations doesn't seem to have an influence on the values of

torsional shear stresses of failure, as seen from the values in tableI.4.

A comparison can be done with stress values coming from other authors present in literature. Regarding bending stresses at failure a value $f_{m,\text{mean}} = 38,5\,\text{MPa}$ was obtained in [17] using the same four-point bending test procedure used in this article; the authors obtained bending failure for all specimen so the value obtained seems reliable and is indeed higher than all bending stresses in tableI.4. In the same paper a different setup is also tested (from [20]), presenting two possible failure sections which proved to be effective in obtaining shear failure in the lamellas. The value obtained for shear stresses at failure was $f_{v,\text{mean}} = 12,8\,\text{MPa}$, which is lower (except for B5 series) than the values obtained here. Two considerations can be done: the first is that, in the present testing campaign, shear failure in the lamellas was not obtained. The second is that the test devised in [20] presents a very specific geometry whose capacity to represent real cases of CLT beams and walls is difficult to prove. Another different test setup, based on a particular configuration with orientation of 14° respect to the compression force, is presented in [4] (from [15]) which achieves shear failure in lamellas with a value $f_{v,\text{mean}} = 9\,\text{MPa}$. Another test which succeeded in obtaining shear failure in lamellas is the one presented in [5] (taken also from [6], [10], [19]). It contemplates a compression test on a column specimen which has grain orientation at an angle respect to the applied force; results are provided for a series tested at TU Graz and another at TU Munich, which are, respectively, $f_{v,\text{mean}} = 7,3\,\text{MPa}$ and $f_{v,\text{mean}} = 7,6\,\text{MPa}$. Regarding torsional stresses, the majority of tests found in literature are on a single crossing interface, such as the ones present in [2] and [18] (from [16]). Torsional stresses values at failure obtained from these two works are, respectively, $f_{t,\text{mean}} = 3,6\,\text{MPa}$ and $f_{t,\text{mean}} = 3,5\,\text{MPa}$, which are well below the values obtained in the present article. This suggests probably that torsional shear strength is much higher in real scale CLT panels, which implies that torsional tests on single nodes may not be representative of the complexity of a complete CLT panel. It is also worth noting that in this paper a Jourawski shear stress distribution was assumed, thus the $1,5$ factor may imply an overestimation of real stress distribution, both for shear stresses in the lamellas and for torsional shear stresses at the glue interface.

I.9 Conclusion and future works

In-plane shear stresses for CLT still remain an open topic regarding which method to use for their evaluation and the test setup to measure strength values. This is due to the particular structure of this timber product which, differently from other simpler products like solid wood and GLT, presents different types of failure depending on loading, geometry and layup. In this paper a review and comparison between the available methods to calculate in-plane shear stresses for CLT panels

was presented, with particular effort directed at trying to uniformize the notation for all methods to match the one of fig.I.3, which will be probably used for the new Eurocode. From the comparison it is evident that for shear stresses in the laminations all methods provide the same values for usual CLT layups, while regarding torsional shear stresses there are still some differences. RVSE method, COST method, Beam method all provide the same single value for torsional shear stress, while the Equilibrium method provides two different values referred to external and internal glued interfaces (for 5 layers panels); for usual CLT layups the average of these two values corresponds to the values of the previous three methods. The method proposed in the Austrian annex to Eurocode instead provides much higher values than all other methods. An important topic for future developments could be to adopt a single method both for CLT walls and beams in the upcoming Eurocode, since for now two different method are present in the draft, referring to the wall case or beam case (see [9]).

A four-point bending test was then applied to four different types of CLT beams to investigate in-plane shear behaviour; in spite of the specifically chosen geometry no shear failure in the laminations was obtained–only torsional shear failure and bending failure in one case, which highlighted the inapplicability of such a testing setup to obtain information about shear strength. It is then necessary to devise a specific test capable of singling out the shear failure in laminations, promising first results are coming from a test setup based on the diagonal compression of a CLT panel which will be presented in a future paper. Nevertheless, the high values of torsional shear stresses obtained at failure in this paper indicate much higher strength than the values present nowadays in literature, underlying the importance of testing full scale CLT panels and not simply conducting torsional tests on single nodes or crossing interfaces, even though this is presently still suggested in [11].

List of Symbols

$\sigma_{\mathrm{m,edge,x}}$ in plane bending stresses, referred to layers parallel to the grain of the outermost layers (x-direction)

$\sigma_{\mathrm{m,edge,y}}$ in plane bending stresses, referred to layers perpendicular to the grain of the outermost layers (y-direction)

$\sigma_{c,x}$ compression stresses, referred to layers parallel to the grain of the outermost layers (x-direction)

$\sigma_{c,y}$ compression stresses, referred to layers perpendicular to the grain of the outermost layers (y-direction)

$\sigma_{m,x}$ out of plane bending stresses, referred to layers parallel to the grain of the outermost layers (x-direction)

$\sigma_{m,y}$ out of plane bending stresses, referred to layers perpendicular to the grain of the outermost layers (y-direction)

$\sigma_{t,x}$ tensile stresses, referred to layers parallel to the grain of the outermost layers (x-direction)

$\sigma_{t,y}$ tensile stresses, referred to layers perpendicular to the grain of the outermost layers (y-direction)

σ_{xy} in plane shear stresses stresses, referred to layers parallel to the grain of the outermost layers (x-direction)

σ_{xz} out of plane shear stresses stresses, referred to layers parallel to the grain of the outermost layers (x-direction)

τ_0 nominal shear stress (RVSE method)

τ_0^* nominal shear stress, referred to real panel (RVSE method)

τ_v effective shear stress (RVSE method)

τ_v^* effective shear stress, referred to real panel (RVSE method)

$\tau_{T,\mathrm{ext}}$ torsional stresses at glue interface, referred to external interfaces (Equilibrium method)

$\tau_{T,\mathrm{int}}$ torsional stresses at glue interface, referred to internal interfaces (Equilibrium method)

τ_T torsional stresses at glue interface

τ_{yx} in plane shear stresses, referred to layers perpendicular to the grain of the outermost layers (y-direction)

τ_{yz} out of plane shear stresses, referred to layers perpendicular to the grain of the outermost layers (y-direction)

b_l width of laminations or mean distance between the edge and a groove or mean spacing between grooves within a lamination

$b_{l,\mathrm{mean}}$ mean width of laminations or mean distance between the edge and a groove or mean spacing between grooves within a lamination

F force

$F_{\mathrm{max,est}}$ estimated maximum force at failure

F_{max} maximum force at failure

h_{CL} cross laminated timber height

I_{net} moment of inertia referred to net section

l length or span

M bending moment

m bending moment per unit length

M_T torsional moment at glued interface

n tension/compression force per unit length

n_l number of laminations in the height of the beam

$n_{\mathrm{lay,x}}$ number of layers in a cross laminated timber member with grain parallel to x-direction

$n_{\mathrm{lay,y}}$ number of layers in a cross laminated timber member with grain parallel to y-direction

n_{lay} number of layers of cross laminated timber member

n_{CA} number of glued interfaces

$t_1\, t_3\, t_5$ thickness of each lamination parallel to the grain of outermost layers (x-direction)

$t_2\, t_4$ thickness of each lamination perpendicular to the grain of outermost layers (y-direction)

t_i thickness of a single lamination

t_i^* fictitious thickness of a single lamination (RVSE method)

t_x sum of thicknesses of layers in x-direction

t_y sum of thicknesses of layers in y-direction

t_{CL} cross laminated timber thickness

$t_{l,x}$ equal thickness of each layer in a cross laminated timber member with grain parallel to x-direction ($t_{l,x} = t_1 = t_3 = t_5$)

$t_{l,y}$ equal thickness of each layer in a cross laminated timber member with grain parallel to y-direction ($t_{l,y} = t_2 = t_4$)

V shear force

v shear force per unit length

W torsional resistance moment

The raw data supporting the conclusions of this manuscript will be made available by the authors, without undue reservation, to any qualified researcher.

Annex

Comparison between equilibrium and RVSE method

For a 3 layer panel n_{lay} denotes the total number of layers, $n_{\mathrm{lay,x}}$ is the number of layers with grain oriented in the x direction, $t_{l,x}$ is the thickness of a single lamination oriented in the x direction):

$$n_{\mathrm{lay}} = 3 \tag{I.39}$$

$$n_{\mathrm{lay,y}} = \frac{n_{\mathrm{lay}} - 1}{2} = 1 \tag{I.40}$$

$$n_{\mathrm{lay,x}} = n_{\mathrm{lay}} - n_{\mathrm{lay,y}} = 2 \tag{I.41}$$

$$t_x = t_1 + t_3 = n_{\mathrm{lay,x}} \cdot t_{l,x} = 2 \cdot t_{l,x} \qquad \text{HYP: symmetry } t_1 = t_3 = t_{l,x} \tag{I.42}$$

$$t_y = t_2 = n_{\mathrm{lay,y}} \cdot t_{l,y} = 1 \cdot t_{l,y} \qquad t_2 = t_{l,y} \tag{I.43}$$

Equilibrium method

$$\tau_{xy} = \frac{v}{t_x} = \frac{v}{n_{\text{lay,x}} \cdot t_{l,x}} = \frac{v}{2 \cdot t_{l,x}} \tag{I.44}$$

$$\tau_{yx} = \frac{v}{t_y} = \frac{v}{n_{\text{lay,y}} \cdot t_{l,y}} = \frac{v}{t_{l,y}} \tag{I.45}$$

RVSE method

$$t^*_{tot} = \sum_{i=1}^{n_{\text{lay}}-1} t^*_i = \sum_{1}^{2} t^*_i = t_{l,y} + t_{l,y} = 2 \cdot t_{l,y} \tag{I.46}$$

with this additional HYP: $t_x \geq t_y \rightarrow n_{\text{lay,x}} \cdot t_{l,x} \geq n_{\text{lay,y}} \cdot t_{l,y} \rightarrow t_{l,y} \leq 2 \cdot t_{l,x}$ (I.47)

the fictitious thickness is obtained as: $t^*_i = t^*_1 = t^*_2 = \min(2 \cdot t_{l,x}; t_{l,y}) = t_{l,y}$ (I.48)

$$\tau^*_0 = \frac{v}{t^*_{tot}} = \frac{v}{2 \cdot t_{l,y}} \tag{I.49}$$

$$\tau^*_v = 2 \cdot \tau^*_0 = 2 \cdot \frac{v}{2 \cdot t_{l,y}} = \frac{v}{t_{l,y}} \equiv \tau_{yx} \qquad \square \tag{I.50}$$

For a 5 layer panels:

$$n_{\text{lay}} = 5 \tag{I.51}$$

$$n_{\text{lay,y}} = \frac{n_{\text{lay}} - 1}{2} = 2 \tag{I.52}$$

$$n_{\text{lay,x}} = n_{\text{lay}} - n_{\text{lay,y}} = 3 \tag{I.53}$$

$t_x = t_1 + t_3 + t_5 = n_{\text{lay,x}} \cdot t_{l,x} = 3 \cdot t_{l,x}$ HYP: symmetry and $t_3 = t_1$; so $t_1 = t_3 = t_5 = t_{l,x}$ (I.54)

$t_y = t_2 + t_4 = n_{\text{lay,y}} \cdot t_{l,y} = 2 \cdot t_{l,y}$ $t_2 = t_4 = t_{l,y}$ (I.55)

Equilibrium method

$$\tau_{xy} = \frac{v}{t_x} = \frac{v}{n_{\text{lay,x}} \cdot t_{l,x}} = \frac{v}{3 \cdot t_{l,x}} \tag{I.56}$$

$$\tau_{yx} = \frac{v}{t_y} = \frac{v}{n_{\text{lay,y}} \cdot t_{l,y}} = \frac{v}{2 \cdot t_{l,y}} \tag{I.57}$$

RVSE method

$$t^*_{tot} = \sum_{i=1}^{n_{\text{lay}}-1} t^*_i = \sum_{1}^{4} t^*_i = t_{l,y} + t_{l,y} + t_{l,y} + t_{l,y} = 4 \cdot t_{l,y} \tag{I.58}$$

with this additional HYP: $t_{l,y} \leq t_{l,x}$ (I.59)

we obtain: $t^*_i = t^*_1 = t^*_4 = \min(2 \cdot t_{l,x}; t_{l,y}) = t_{l,y} \qquad t^*_i = t^*_2 = t^*_3 = \min(t_{l,x}; t_{l,y}) = t_{l,y}$ (I.60)

$$\tau^*_0 = \frac{v}{t^*_{tot}} = \frac{v}{4 \cdot t_{l,y}} \tag{I.61}$$

$$\tau^*_v = 2 \cdot \tau^*_0 = 2 \cdot \frac{v}{4 \cdot t_{l,y}} = \frac{v}{2 \cdot t_{l,y}} \equiv \tau_{yx} \qquad \square \tag{I.62}$$

So for CLT panels (with an odd number of layers) where the layers oriented in the x direction have all the same thickness and this value is greater or equal than the thickness of the layers in the other direction there is coincidence between the two methods; these geometrical characteristics cover the majority of commercial CLT panels.

Keeping the same hypothesis made regarding shear stresses it is possible to compare torsional shear stresses. It can be seen that for a 3 layer panels it is the same value for both methods, while for a 5 layer panel a constant value is obtained from the RVSE method which is the average of the previous internal and external values of equilibrium method.

Equilibrium method

$$\tau_T = 3 \cdot \frac{\tau_{xy} \cdot t_1}{b_l} = 3 \cdot \frac{v}{n_{\text{lay,x}} \cdot t_{l,x}} \frac{t_{l,x}}{b_l} = \frac{3}{2} \frac{v}{b_l} \tag{I.63}$$

RVSE method

$$\tau^*_T = 3 \cdot \tau^*_0 \cdot \frac{t^*_i}{b_l} = 3 \cdot \frac{v}{2 \cdot t_{l,y}} \cdot \frac{t_{l,y}}{b_l} = \frac{3}{2} \frac{v}{b_l} \equiv \tau_T \qquad \square \tag{I.64}$$

For 5 layer panel

Equilibrium method

$$\tau_{T,\text{ext}} = 3 \cdot \frac{\tau_{xy} \cdot t_1}{b_l} = 3 \cdot \frac{v}{n_{\text{lay,x}} \cdot t_{l,x}} \frac{t_{l,x}}{b_l} = \frac{v}{b_l} \tag{I.65}$$

$$\tau_{T,\text{int}} = \frac{3}{2} \cdot \frac{\tau_{xy} \cdot t_1}{b_l} = \frac{3}{2} \cdot \frac{v}{n_{\text{lay,x}} \cdot t_{l,x}} \frac{t_{l,x}}{b_l} = \frac{1}{2} \frac{v}{b_l} \tag{I.66}$$

$$\tau_{T,\text{mean}} = \frac{\tau_{T,\text{ext}} + \tau_{T,\text{int}}}{2} = \frac{3}{4} \frac{v}{b_l} \tag{I.67}$$

RVSE method

$$\tau^*_T = 3 \cdot \tau^*_0 \cdot \frac{t^*_i}{b_l} = 3 \cdot \frac{v}{4 \cdot t_{l,y}} \cdot \frac{t_{l,y}}{b_l} = \frac{3}{4} \frac{v}{b_l} \equiv \tau_{T\text{mean}} \qquad \square \tag{I.68}$$

Bibliography

[1] Mauro Andreolli, Roberto Tomasi, and Andrea Polastri. Experimental investigation on in-plane behaviour of cross-laminated timber elements. In *Proceedings of CIB-W18*, 2012.

[2] HJ Blaß and R Görlacher. Zum trag- und verformungsverhalten von lignotrend elementen bei beanspruchung in plattenebene. Technical report, Universität Karlsruhe, 2001.

[3] Thomas Bogensperger, Thomas Moosbrugger, and Gregor Silly. Verification of CLT-plates under loads in plane. In *Proceedings of WCTE-World Conference on Timber Engineering*, 2010.

[4] Reinhard Brandner, Thomas Bogensperger, and Gerhard Schickhofer. In plane shear strength of cross laminated timber (clt): test configuration, quantification and influencing parameters. In *Proceedings of 46th CIB-W18 Meeting, Vancouver*, 2013.

[5] Reinhard Brandner, Philipp Dietsch, Julia Dröscher, Michael Schulte-Wrede, Heinrich Kreuzinger, and Mike Sieder. Cross laminated timber (clt) diaphragms under shear: Test configuration, properties and design. *Construction and Building Materials*, 147:312–327, 2017.

[6] Reinhard Brandner, Philipp Dietsch, Julia Dröscher, Michael Schulte-Wrede, Heinrich Kreuzinger, Mike Sieder, Gerhard Schickhofer, and Stefan Winter. Shear properties of cross laminated timber (clt) under in-plane load: Test configuration and experimental study. In *INTER Proceedings Meeting 48 2015*, pages 181–201, 2015.

[7] Reinhard Brandner, Georg Flatscher, Andreas Ringhofer, Gerhard Schickhofer, and Alexandra Thiel. Cross laminated timber (clt): overview and development. *European Journal of Wood and Wood Products*, 74:331–351, 2016.

[8] Reinhard Brandner, Roberto Tomasi, Thomas Moosbrugger, Erik Serrano, and Philipp Dietsch. *Properties, Testing and Design of Cross Laminated Timber, a state-of-the-art report by COST Action FP1402 / WG 2.* 2018.

[9] Philipp Dietsch, Gerhard Schickhofer, Alfons Brunauer, Roberto Tomasi, Ulrich Hübner, Harald Krenn, Peter Mestek, Thomas Moosbrugger, and Tobias Wiegand. Eurocode 5:2022 – Einführung in die neuen Abschnitte Brettsperrholz und Verstärkungen. In Rainer Görlacher and Carmen Sandhaas, editors, *Karlsruher Tage 2018 - Holzbau*, pages 65–84, 10 2018.

[10] Julia Dröscher. *Prüftechnische Ermittlung der Schubkenngrößen von BSP-Scheibenelementen und Studie ausgewählter Parameter.* PhD thesis, TU Graz, 2014.

[11] EN 16351. Timber structures–Cross laminated timber–Requirements. Comité Européen de Normalisation CEN. 2015.

[12] EN 338. Structural timber–strength classes. Comité Européen de Normalisation CEN. 2016.

[13] EN 408. Timber structures–Structural timber and glue-laminated timber–Determination of some physical and mechanical properties. Comité Européen de Normalisation CEN. 2012.

[14] Marcus Flaig and Hans Joachim Blass. Shear strength and shear stiffness of CLT-beams loaded in plane. In *Proceedings of CIB-W18*, 2013.

[15] B Hirschmann. *Ein Beitrag zur Bestimmung der Scheibenschubfestigkeit von Brettsperrholz [A contribution to the determination of in-plane shear strength of cross laminated timber].* PhD thesis, TU Graz, 2011.

[16] Georg Jeitler. *Versuchstechnische Ermittlung der Verdrehungskenngrößen von orthogonal verklebten Brettlamellen.* PhD thesis, TU Graz, 2004.

[17] RA Jöbstl, T Bogensperger, and G Schickhofer. In-plane shear strength of cross laminated timber. In *Proceedings of 41th CIB-W18 Meeting, St. Andrews*, 2008.

[18] Robert A Jöbstl, Thomas Bogensperger, Gerhard Schickhofer, and Georg Jeitler. Mechanical behaviour of two orthogonally glued boards. In *Proceedings of 8th World Conference on Timber Engineering (WCTE2004), Portland*, 2004.

[19] Heinrich Kreuzinger and Mike Sieder. Einfaches prüfverfahren zur bewertung der schubfestigkeit von kreuzlagenholz/brettsperrholz. *Bautechnik*, 90(5):314–316, 2013.

[20] Georg Wallner. Versuchstechnische ermittlung der verdrehungskenngrössen von orthogonal verklebten brettlamellen. Master's thesis, TU Graz, 2004.

[21] ÖNORM B 1995-1-1. Ausgabe: 2015-06-15, Eurocode 5: Bemessung und Konstruktion von Holzbauten Teil 1-1: Allgemeines — Allgemeine Regeln und Regeln für den Hochbau. Austrian Standards, Vienna. 2015.

II. Cross Laminated Timber (CLT) Beams Loaded in Plane: Testing Stiffness and Shear Strength

Bibliographic data

F. Boggian, E. Ricci, A. Salenikovich, R. Springhetti, and R. Tomasi, "Deflections of light timber frame shear wall segments: Validation of a standard proposal," in *Proceedings of the World Conference of Timber Engineering-WCTE*, (Chile), 2021. Link

Contents

abstract

This paper focuses on the evaluation of the horizontal displacement of a light timber frame shear wall, due to several components: fastener slip, rigid body rotation, rigid body translation and shear deformation. The approach of the working draft for the new Eurocode 5 is presented, also explaining background literature and the alternative current prescriptions adopted by the Canadian and American design standards. The new European proposal is used as a base for setting up a FEM model in SAP2000, which is then employed for establishing a benchmark for the comparisons. Lastly, past experimental campaigns are studied for the evaluation of the effectiveness of the Eurocode 5 proposal in predicting the deflection of fully anchored and partially anchored shear walls. In conclusion, strengths and weaknesses of the new Eurocode proposal are highlighted.

Keywords:

Light timber frame shear walls, serviceability limit state, standardisation

II.1 Introduction

Light timber frame (LTF) construction is a fast and easy way to build with timber and is the main system used in North America for low-rise residential buildings [1]. With the advancement of mid-rise LTF construction worldwide, evaluating the displacement of LTF walls and floors subjected to lateral loads becomes increasingly important, both to limit the inter-storey drift in relation to serviceability limit states (SLS) and to determine the building period for the ultimate limit state (ULS) calculations. Typical wall segment is assembled of a timber frame on which a structural sheathing material, such as OSB or plywood panels, is attached using metal fasteners, usually nails or staples. Wall segments are then mechanically anchored at the base, using discrete hold-downs and/or continuous fastening along the bottom rail, to provide stability against uplift generated by the overturning moment. This difference in the anchoring technique corresponds to two categories of LTF shear walls respectively: fully anchored and partially anchored, seen in Figure II.1. This constructive choice reflects on a different mechanical behaviour and thus different design equations. One of the first design provisions is the four-term equation used in the American and Canadian design standards [2],[3], which is based on the early shear wall tests carried out by the APA starting in the 1950s [4]. This paper focuses on the SLS horizontal deflection calculations, and specifically on the new proposal for the Eurocode 5. The equations proposed in Eurocode 5 are used to develop a FEM

model implemented in SAP2000. After validating the model for the case of one wall it is used for predicting the deflection values from recent experimental data. Finally, the effectiveness of the Eurocode 5 proposal is analysed, and conclusions are drawn.

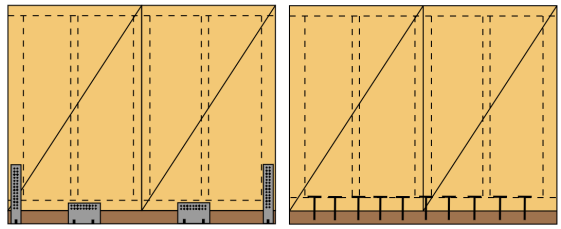

Fig. II.1. Fully anchored LTF shear wall vs. partially anchored on the left and right sides, respectively.

II.2 Eurocode 5 proposal

The calculation of the horizontal deflection of a LTF shear wall segment in the new Eurocode 5 proposal [5] includes six contributions, as shown in Figure II.2: (1) $u_K ser$ - deformation due to slip of sheathing-to-framing fasteners; (2) u_N - deformation of the chords; (3) u_A - rigid body rotation of the wall segment, due to the elongation in the wall anchorage system; (4) u_V - rigid body translation of the wall segment, due to the horizontal movement at the base; (5) u_C - deformation of the framing due to compression perpendicular to grain in the bottom rail; and (6) u_G - in-plane shear deformation of the sheathing panel. The relevant

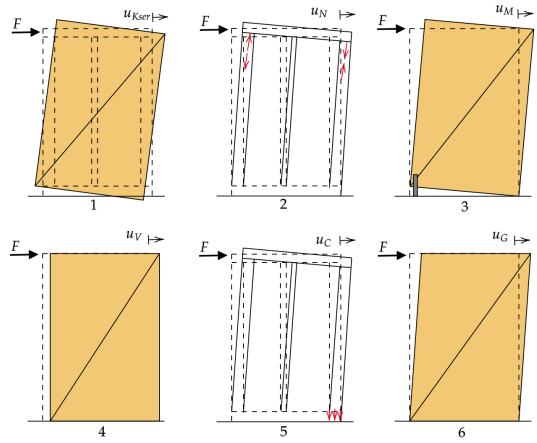

Fig. II.2. Shear wall displacements contributions.

expressions read:

$$u_{Kser} = \frac{F_{v,Ed}\,\lambda(\alpha)\,a_1}{K_{ser,f}\,l\,n_p} \tag{II.1}$$

$$u_N = \frac{2}{3}\frac{F_{v,Ed}}{E_{0,m}}\left(\frac{l}{A_{rail}} + \frac{h^3}{A_{stud}\,l^2}\right) \tag{II.2}$$

$$u_A = \frac{h}{\tau\,l}\,u_{z,A} \qquad u_{z,A} = \frac{N_{net,Ed}}{K_{ser,A}} \qquad N_{net,Ed} = \frac{M_{net,Ed}}{\tau\,l} \tag{II.3}$$

$$u_V = \frac{F_{v,Ed}}{K_{ser,v}\,n_v} \tag{II.4}$$

$$u_C = \frac{F_{v,Ed}\,h_{rail}\,h^2}{E_{90,m}\,A_{eff}\,l^2} \tag{II.5}$$

$$u_G = \frac{F_{v,Ed}\,h}{G_p\,t_p\,n_p\,l} \tag{II.6}$$

where the symbols denote: $F_{v,Ed}$ - design horizontal force applied to the shear wall segment, $\lambda(\alpha)$ - shape coefficient depending on the aspect ratio of the sheathing panel, $\alpha = h/b_p$ - aspect ratio, b_p = width of the sheathing panel, l - length of the shear wall segment, h - height of the wall, a_1 - fastener spacing along the perimeter of the sheathing panel, $K_{ser,f}$ - stiffness of the sheathing-to-framing connections, n_p - number of sheathed sides of the wall, $E_{0,m}$ - mean modulus of elasticity parallel to the grain of the external studs, A_{rail} - average cross-sectional area of the top and bottom rails, A_{stud} - average cross-sectional area of the leading

and trailing studs, τ - factor taking into account the reduced lever arm stabilising the wall, $u_{z,A}$ - vertical elongation of the wall anchorage system, $N_{net,Ed}$ - net tensile action resisting overturning in the connection at the leading edge, $M_{net,Ed}$ - net resulting overturning moment acting about the bottom trailing edge of the wall segment and producing a tensile action in the connection at the leading edge, $K_{ser,A}$ - stiffness of the connection against overturning, $K_{ser,v}$ - stiffness of the diaphragm base connection with respect to horizontal translation, n_v - number of base connections with respect to horizontal translation, $E_{90,m}$ - mean modulus of elasticity perpendicular to the grain, h_{rail} - cross-section height of the bottom rail, A_{eff} - effective contact area between the bottom rail and the trailing stud, G_p - shear modulus of the sheathing panels, t_p - thickness of the sheathing panels. Equation II.1 stems from an elastic analysis [6], whereas the shape coefficient can assume two different values depending on the bending stiffness of the frame elements. Equation II.2 is derived from elastic analysis using the principle of virtual work. Equations II.3,II.4,II.6 are mere equilibrium equations, which consider the stiffness of the respective restraining element. Equation II.5 stems from elastic analysis; more details on its background are presented in [7] and [8]. A notable remark is worth on the derivation of equations II.1,II.2,II.3,II.5: they are all based on the theory of a fully anchored wall, therefore with a strong anchorage at its leading stud. The extension of equations II.1,II.2,II.5 to the case of partially anchored wall is still under discussion, while for equation II.3 a new formulation may be required.

II.3 Fastener slip contribution

Equation II.1 for fastener slip contribution presents a shape function λ, which depends on the aspect ratio of the sheathing panels α:

$$\lambda(\alpha) = \lambda_1 + \lambda_2 \alpha \qquad \alpha = h/b_p \tag{II.7}$$

Coefficients λ_1, λ_2 can assume two possible sets of values, depending on the analysis and hypothesis used for their computation:

- case 1 stems from the elastic analysis in [6], where the initial hypothesis assumes the framing members as fully rigid, and the outcome, linearised in [9], is $\lambda_1 = 0.81, \lambda_2 = 1.85$
- case 2 supposes the framing members are fully flexible, as done in [6] through an elastic analysis and in [10] and [11] using a plastic approach, leading in both cases to $\lambda_1 = 2, \lambda_2 = 2$. The functions relevant to the cases above are plotted in Figure II.3, and they are seen to differ by 34%.

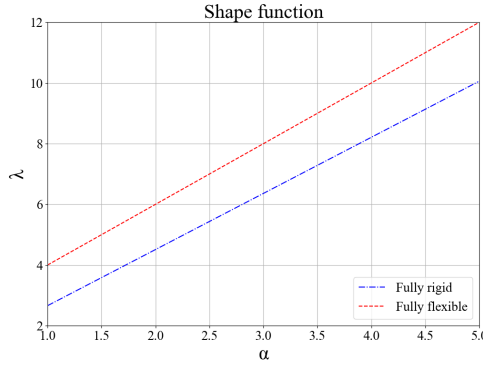

Fig. II.3. Fastener slip formulation λ function.

To check the reliability of these two different hypotheses, the authors performed a parametric analysis: a simple wall model was analysed in *SAP2000* (additional details on the modelling are presented in the following section), varying the section and the flexibility of the frame members by means of a *Python OAPI* script. The 1:1 LTF shear wall from [12], pictured in Figure II.4, was used as reference configuration corresponding to the frame members group C in Figure 5. The section of the frame elements was then increased or decreased by 10 mm in each direction for the other cases: -20 mm for case A, -10 mm for case B, +10 mm for case D and +20 mm for case E. Then, for each of the 5 sections, two different analyses were run: one with the correct dimension and parameters and an additional one assuming an infinite multiplier for the moment of inertia J and the area A of the frame elements, to simulate the fully rigid case. The results are plotted in Figure II.5 along with the analytical values predicted by Equation II.1. The curves in Figure II.5 disclose interesting information: the fully rigid formula and the FE model with infinite section multipliers closely match as expected, while the real case lies in an intermediate area between the fully rigid and fully flexible formulations. Interestingly, the FE wall displacement predicted on the basis of the current sections decreases with their dimensions, confirming that larger sections of the frame elements offer increased stiffness, thus reducing the fastener slip contribution and approaching the fully rigid formulation case.

II.4 FE model and validation

A FE model based on the formulas of Eurocode 5 was set up in *SAP2000*. Frame elements connected with hinges at corners were used for the wall frame, endowed

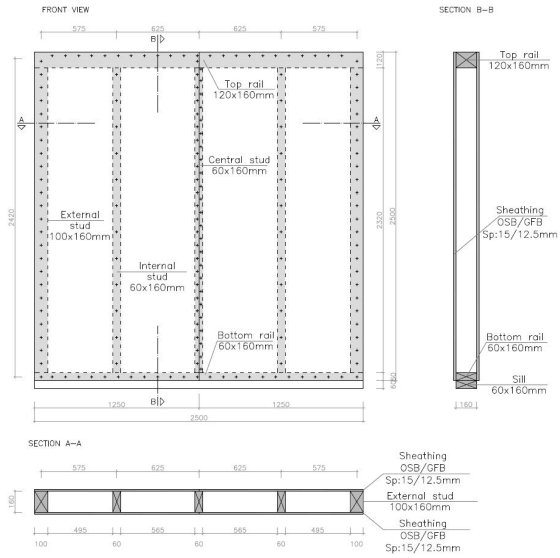

Fig. II.4. Wall configuration in [12].

with an elastic material with timber properties. The sheathing panels were modelled using shell elements with their respective in plane properties. For connections and restraints three types of link elements were used: linear links for the sheathing-to-framing connections and sliding restraints, nonlinear hook links and nonlinear gap elements for the hold-downs and the compression interface between bottom rail and ground, respectively. For the sheathing-to-framing connections, the fastener slip modulus equations in the Eurocode 5 [13] were used to estimate their stiffness. For the sliding restraints the values declared by the manufacturer or deduced from experimental tests were used. The nonlinear hook elements used for the hold-downs react only when an uplift (tensile) load is applied, and their stiffness was taken from the technical data sheet of the manufacturer. A nonlinear gap link was used to model the interface at the base of the studs, which deforms under compression perpendicular to grain: in this case the stiffness was set to $E_{90,m}A/h_{rail}$, with A - effective contact area between the stud and the bottom rail. The analysis was nonlinear elastic. The non-linearity was introduced using hook and gap element, which may be active or inactive. The model was then used to calculate the horizontal deflection of a fully anchored wall with standard 1:1 aspect ratio (2.5m x 2.5m, taken from [12]). First, the horizontal force applied to the top of the wall was set to 10 kN, and five cases of vertical distributed load were then considered, with values increasing from 0 to 30

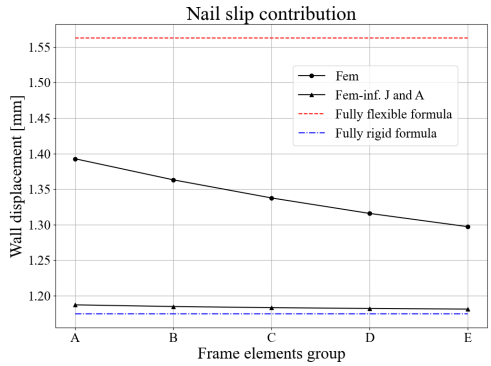

Fig. II.5. Parametric analysis on nail slip contribution.

kN/m. Table II.1 shows the comparison for the first load case (with no vertical distributed load), in which it is evident that the FE model accurately mimics the analytical formulation, with a 1% discrepancy on the global deflection value. The

Table II.1. Results of the comparison between analytical formulation and FEM, for F=10 kN and q=0 kN/m.

Contribution	u_{anal} [mm]	u_{FEM} [mm]	Diff. %
(1) Fastener slip	1.18	1.17	0.1
(2) Framing deformation	0.24	0.18	27.1
(3) Uplift of anchorage	1.81	1.81	0.1
(4) Sliding of anchorage	0.67	0.67	0.1
(5) Compression perp. def.	0.09	0.07	21.4
(6) Sheathing deformation	0.31	0.32	0.1
Total deflection	4.3	4.26	1.0

difference is large for the frame and bottom rail contributions, but they represent the two smallest contributions; hence, the comparison may not be relevant for these small values. For the other load cases, the discrepancy was always less than 10%. Figure II.6 shows the magnitude of the different displacement contributions, and confirms the findings of [9] that the hold-down and fastener slip represent the prevailing contributions for LTF shear walls. The next analysis was carried out, by keeping a constant vertical distributed load (10 kN/m) and varying the applied horizontal force between 0 and 30 kN. The results are shown in Table II.2 and

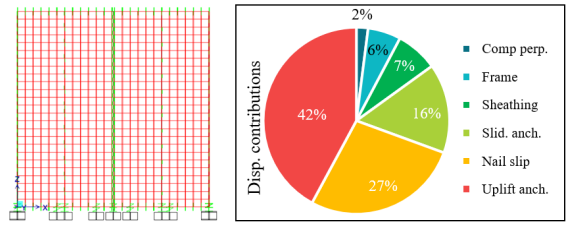

Fig. II.6. a) FEM model and b) percentages of the different contributions.

Figure II.7, where the FEM results are compared with the analytical Eurocode 5 formulation. As can be seen from the graph in Figure II.7, which plots the

Table II.2. Results of the comparison between analytical formulation and FEM, for increasing F values with q=10 kN/m.

F [kN]	u_{anal} [mm]	u_{FEM} [mm]	Diff. %
5	1.35	1.32	2.2
10	2.6	2.92	10.9
15	4.42	4.65	5.2
20	6.57	6.67	1.5
25	8.72	8.74	0.2
30	10.88	10.81	0.7

data of Table II.2, the FE model accurately describes the Eurocode 5 formulation for various levels of force. Regarding partially anchored walls a comparison with analytical formulation is not possible, because the current Eurocode 5 proposal does not offer specific provisions. The FE model was setup in the same way as for the fully anchored wall with one main difference, beyond the different uplift restraints: joints between the leading stud and the rail were substituted with a gap element, which transfers only compressive loads. This is to ensure that the FE model is coherent with the definition of partially anchored shear wall, where the leading stud does not transmit tensile forces to the foundation and the uplift is transferred to the ground only through the bottom rail. An interesting comparison was then made for the FE model of a fully anchored wall (with hold-down): the hinges on the frame were substituted with gap elements only transferring compressive forces. It was done to investigate the influence of the hypothesis regarding the presence of hinges in the frame corners, assumed by the analysis in [14], and thus check if an appropriate design of these connections

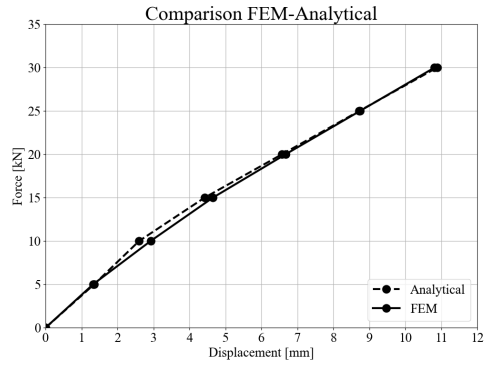

Fig. II.7. FEM results and Eurocode 5 formulas compared.

is required or not. For the same wall modelled in the previous analyses, and with a horizontal force F = 20 kN, the predicted deflection values were $u_{\text{hinged}} = 8.5$ mm and $u_{\text{unhinged}} = 8.8$ mm, suggesting that appropriate dimensioning and design of such connections may not be required.

II.5 Experimental data comparison: results and discussion

The FE model was used for calculating the horizontal displacement at the top of the shear wall segments tested in recent experimental campaigns in North and South Americas and in Europe. The considered testing campaigns are taken from the works listed below. Grossi [12], [15], and [16] tested fully anchored walls with 1:1 aspect ratio, varying vertical load, hold downs, spacing of sheathing nails, and sheathing material. Salenikovich [17] tested different aspect ratios of the walls, both fully and partially anchored, with no vertical load. Seim [7], [18] tested fully anchored walls with 1:1 aspect ratio, no vertical load and varied sheathing materials and connections. Payeur [19], [20] and Ni [21] tested both fully and partially anchored walls, with different aspect ratios and different vertical loads. Lebeda [22] and [23] tested 1:1 fully anchored walls with no vertical load. The same applies to the testing campaign of Seaders [24], [25] and [26], with the addition of partially anchored walls. Last, Guíñez [27] and [28] tested different aspect ratios of both fully and partially anchored walls, with no vertical load. The comparison was then carried out for a configuration present in all campaigns: a 1:1 aspect ratio wall with no vertical load is modelled for a total of 11 FE

simulations. The criteria for applying the force to the FE model and evaluating the displacement was the following: the ultimate force was retrieved for each experimental campaign, then 40% of such value was applied to the FE model to ensure that the comparison was made in the elastic part of the wall behaviour. Tables II.3 and II.4 present the results comparing the displacements obtained through the FE model and the experimental campaigns and listing the relevant discrepancies, where a plus symbol indicates that the FE model was more rigid than the test. For both fully and partially anchored walls the discrepancies

Table II.3. Comparisons for fully anchored walls.

Experimental campaign	u_{test} [mm]	u_{FEM} [mm]	Diff. %
Grossi [12],[15]	7.37	8.54	-13
Salenikovich [17]	6.4	4.29	33
Seim [7],[18]	10.3	11.08	7
Payeur [19],[20]	9.7	5.14	47
Seaders [24]	4.08	5.18	-21
Lebeda [23]	7.86	5.72	27
Santa Maria [27],[28]	10.06	8.69	13

Table II.4. Comparisons for partially anchored walls.

Experimental campaign	u_{test} [mm]	u_{FEM} [mm]	Diff. %
Salenikovich [17]	3.94	2.1	47
Payeur [19]	5.11	4.02	21
Seaders [24]	2.64	2.71	-3
Ni [21]	4.27	2.61	39

between FE model and tests were found to be always less than 47%, with the FE model being generally stiffer than the tested walls. In two cases the FEM deflection was greater than the experimental one, which is normally unexpected. The reason could be ascribed to the specific construction detailing of the tested walls. In particular, for the test in Grossi [12], the hold-down was positioned on the face of the wall over the sheathing, as seen in Figure II.8. As a consequence, the hold-down was restraining not only the leading stud, but also the sheathing panel, offering an additional increase in stiffness which was not captured by a unified FE model and the analytical formulation. To prove this hypothesis another FE model of the Grossi [12] shear wall was analysed to mimic in detail the role of the hold-down. Some additional joint constraints were added in the

FE model at the bottom corner of the wall to force a part of the sheathing to be restrained by the hold-down. The new predicted displacement was $u_{FEM} = 7.62$mm, which is just 3.3% greater than the experimental result. This proves that construction detailing of the wall plays a crucial role influencing the stiffness, therefore it is to be expected that a general analytical formulation as well as FE model can deviate significantly from the experimental test results and vice-versa.

Fig. II.8. Details of the wall tested by [29]

II.6 Conclusion

The comparisons underline discrepancies between the Eurocode approach and the analysed experimental campaigns. These differences vary between 7% and 47% for fully anchored wall segments and 3% and 47% for partially anchored shear wall segments. While this inconsistency could potentially be reduced, the results illustrated in this paper show that the Eurocode prescriptions represent an improvement with respect to the current formulation adopted in the U.S. and Canada, which lead to differences up to 200% [4]. It is important to bear in mind that the adoption of standardised equations is always a trade-off between simplicity of use for the designers and precision, so a choice has to be made taking into consideration both aspects. Another open topic is represented by the equations for partially anchored walls still lacking in the Eurocode proposal, therefore additional research and comparisons with other standards are required and will be addressed in future publications.

Bibliography

[1] G. Beyer, M. Defays, M. Fischer, J. Fletcher, E. DeMunck, F. DeJaeger, C. Van Riet, K. Vandeweghe, and K. Wijnendaele, *Tackle climate change:*

use wood. CEI Bois, 2006.

[2] *CSA O86-19: Engineering design in wood*, 2019.

[3] *SDPWS: Special design provisions for wind and seismic*, 2015.

[4] Z. A. Martin and T. D. Skaggs, "APA Report T2001L-65: Shear wall deflection and predictive equations," tech. rep., APA- The Engineerd Wood Association, 2002.

[5] "SC5.PT3 final document," 2020.

[6] B. Källsner and U. A. Girhammar, "Analysis of fully anchored light-frame timber shear walls-elastic model," *Materials and Structures*, vol. 42, pp. 301–320, January 2009.

[7] W. Seim, J. Hummel, and T. Vogt, "Earthquake design of timber structures - Remarks on force-based design procedures for different wall systems," *Engineering Structures*, vol. 76, pp. 124–137, 2014.

[8] E. Ricci, "Design methods for Light Timber Frame shear walls: validation with experimental data," Master's thesis, University of Trento, 2020.

[9] D. Casagrande, S. Rossi, T. Sartori, and R. Tomasi, "Proposal of an analytical procedure and a simplified numerical model for elastic response of single-storey timber shear-walls," *Construction and Building Materials*, vol. 102, pp. 1101–1112, January 2016.

[10] B. Källsner and U. A. Girhammar, "Plastic models for analysis of fully anchored light-frame timber shear walls," *Engineering Structures*, vol. 31, pp. 2171–2181320, 2009.

[11] M. Kessel, "Tafeln - eine linear elastische beschreibung," *Holzbau Kalender*, 2003.

[12] P. Grossi, R. Tomasi, and T. Sartori, "Tests on timber frame walls under in-plane forces: Part 1," *Proceedings of the Institution of Civil Engineers: Structures and Buildings*, vol. 168, pp. 826–839, November 2015.

[13] EN 1995-1-1, "Design of timber structures Part 1-1: General - Common rules and rules for buildings.," Comité Européen de Normalisation CEN, 2014.

[14] B. Källsner, U. A. Girhammar, and J. Vessby, "Evaluation of two analytical plastic design models for light-frame shear walls," in *World Conference on Timber Engineering*, vol. 5, pp. 479–488, July 2012.

[15] P. Grossi, R. Tomasi, and T. Sartori, "Tests on timber frame walls under in-plane forces: Part 2," *Proceedings of the Institution of Civil Engineers: Structures and Buildings*, vol. 168, pp. 840–852, November 2015.

[16] P. Grossi, "PARETI INTELAIATE IN LEGNO: indagine sul comportamento meccanico tramite prove sperimentali a scala reale," Master's thesis, University of Trento, 2011.

[17] A. Salenikovich, "The racking performance of light-frame shear walls," Master's thesis, Virginia Polytechnic Institute and State University, 2000.

[18] W. Seim, M. Kramar, T. Pazlar, and T. Vogt, "OSB and GFB As Sheathing Materials for Timber-Framed Shear Walls: Comparative Study of Seismic Resistance," *Journal of Structural Engineering*, vol. 142, April 2016.

[19] M. Payeur, "Influence des charges verticales sur les performances laterales des murs de refend en bois a ossature legere," Master's thesis, Université Laval, 2011.

[20] A. Salenikovich and M. Payeur, "Influence of vertical loads on lateral resistance of light-frame shear walls," in *World Conference on Timber Engineering*, 2010.

[21] C. Ni and E. Karacabeyli, "Performance of braced walls under various boundary conditions," in *World Conference on Timber Engineering*, 2010.

[22] D. Lebeda, R. Gupta, D. Rosowsky, and D. Dolan, "Effect of Hold-down displacement on strength and stiffness of wood shear walls," *Practice Periodical on Structural Design and Construction*, vol. 10, pp. 79–87, May 2005.

[23] D. Lebeda, "The effect of hold-down misplacement on the strength and stiffness of wood shear walls.," Master's thesis, Oregon State University, 2002.

[24] P. Seaders, R. Gupta, and T. H. Miller, "Monotonic and cyclic load testing of partially and fully anchored wood-frame shear walls," *Wood and Fiber Science*, vol. 41, pp. 145–156, April 2009.

[25] P. Seaders, R. Gupta, and T. H. Miller, "Performance of Code-Prescribed Wood Shear Walls," in *World Conference on Timber Engineering*, 2004.

[26] P. Seaders, "Performance of partially and fully anchored wood frame shear walls under monotonic, cyclic and earthquake loads," Master's thesis, Oregon State University, 2004.

[27] Guíñez, Felipe and Santa María, Hernán and Almazán, José Luis, "Monotonic and cyclic behaviour of wood frame shear walls for mid-height timber buildings," *Engineering structures*, 2019.

[28] Santa María, H. and Salinas, A. and Montaño, J. and Ugarte, JJ. and Almazán, JL. and Guindos, P. and Opazo, A. and Benedetti, F. and Rosales, V. nd Estrella, V. and Guiñez, F. and Berwart, S. and Cárcamo, S. and Jara, A., "Assessment of seismic design factors and proposal of modification to Chilean seis- mic building design code (NCh 433) for mid-rise wood-frame buildings," *International Network on Timber Engineering Research*, 2020.

[29] P. Grossi, "Experimental investigations on seismic behaviour of light timber framed buildings and log-house traditional constructive system," Master's thesis, University of Trento, 2013.

III. The role of the hold-down in the capacity model of LTF and CLT shear walls based on the experimental lateral response

Bibliographic data

A. Aloisio, F. Boggian, R. Tomasi, and M. Fragiacomo, "The role of the hold-down in the capacity model of LTF and CLT shear walls based on the experimental lateral response", *Construction and Building Materials*, vol. 289, 2021. Doi

Contents

abstract

This paper compares the experimental cyclic responses of Cross Laminated Timber (CLT) and Light Timber Frame (LTF) shear walls. In specific configurations, the shear wall rigid-body rotation prevails over the deformation and rigid-body translation in the post-elastic displacement range. Consequently, a generalised capacity model based on the sole hold-down response accurately seizes the observed cyclic response, ignoring other resisting contributions. The authors discuss a novel capacity model based on the sole hold-down restraints. Additionally, they examine the overstrength of the CLT panel, and LTF sheathing to the shear walls collapse due to the hold-down failure.

Keywords:

Experimental cyclic response; timber engineering; shear walls; rocking; Cross Laminated Timber; Light Timber Frame.

III.1 Introduction

The use of timber in structural engineering is diverse across the centuries [1, 2] and between geographical areas [3]. Currently, the most diffuse timber constructive systems in Europe are based on the use of Light Timber Frame (LTF) and Cross Laminated Timber (CLT) shear walls. LTF walls are made by a pinned-frame braced by OSB (Oriented Strand Board) or GFP (Gypsum Fiber Panel) sheathing panels, whereas CLT walls are solid-timber panels composed by layers of timber planks glued together [4, 5]. The boost to the use of engineered wood products and timber engineering *tout court* stems from multiple reasons, e.g. the growing dominance of green engineering, and the economic and structural benefits in using timber products [6]. Additionally, the spreading of timber technologies in seismic-prone areas fed copious research activities devoted to the assessment of the lateral response of LTF and CLT structural systems via numerical and experimental investigations [7, 8, 9].
Many scholars attempt to develop structural systems alternative to the standard CLT and LTF shear walls by coupling dissipation devices [10, 11], tuned mass dampers [12], and structural components which enhance ductility [13, 14, 15]. Most of the research pointed at developing predictive capacity models likely useful

to calibrate simplified design methods [16]. Predictive capacity models require experimental data for a proper calibration: numerous experimental campaigns evaluated the lateral responses of the two systems following distinct loading protocols and under diverse structural configurations [17, 18, 19, 20, 21, 22, 23]. The capacity model may gather in two main groups: those based on Finite Element (F.E.) and structural analysis [24, 25, 26, 27, 28, 29], and empirical models [30, 31, 32, 33]. The former ones strive to follow the experimental data and could be used in extrapolating the response of structural configurations different from those used for calibration. Conversely, empirical hysteresis models consist of algebraic or differential equations, which follow the experimental data, with no concern of the mechanical meaning of the employed parameters. These models cannot be used in extrapolating structural behaviours beyond those associated with the experimental data. However, the so-called empirical models are less time consuming than F.E. models and can be used to perform simulations in a relatively short time. Di Gangi et al. recently [34] reviewed the modeling strategies of timber shear walls from 1978 to 2018.

There are numerous and diverse capacity models in the scientific literature. Some researches merely attempt to elaborate closed-form models which best seize the observed response. Others, like [35], append to the mentioned efforts, an interpretative framework useful in developing simplified and reliable tools for the prediction of the lateral response. Specifically, [35] developed an analytical procedure and a simplified numerical model for the elastic response of LTF and CLT shear walls. They found that, in the elastic response range of CLT shear walls, 77% of the total displacement is due to rigid-body rotation, 16% to the rigid-body translation and 7% to the panel deformation. Conversely, in LTF shear walls, 45% is expected to the rigid-body rotation, 6% to the rigid body translation, and 45% and 4% to the sheathing-to-framing connection and sheathing panel deformation, respectively.

In this paper, the authors investigate CLT and LTF systems in the post-elastic range. The rigor and straightforwardness of elastic analysis vanishes when dissipative phenomena arise. The authors devoted their efforts in interpreting experimental data by clustering the displacement response in rocking, sliding and deformation components. In a second step, based on the observed results, an elementary capacity model based on the sole hold-down experimental response is compared to the experimental results to estimate the related approximation. The closeness between the experimental data of CLT and LTF shear walls inspire a conclusive remark about the disguised difference between them: the overstrength of the panel to the hold-downs. The different overstrength of the CLT and LTF panels is the actual feature which best distinguishes the natures of the two structural systems.

The first two sections describe the experimental cyclic tests of LTF and CLT

shear walls, respectively. The third section analyses the displacement response by decomposing the rocking, sliding and deformation fractions. The fourth and fifth sections estimate the equivalent elastic stiffness in the elastic response range and the approximation in using a hold-down based capacity model. The last part addresses the differences between the two systems in term of overstrength.

III.2 Experimental cyclic tests of LTF and CLT shear walls

The results presented in this paper descend from the experimental data on LTF and CLT shear wall tests performed at the University of Trento. [36] have partially published the outcomes on LTF shear walls, while very limited results on CLT were published in [37, 38, 39]. The first part of this paper focuses on the description of the test setup and the experimental responses. The second part attempts to understand the leading deformation contributes to the shear walls lateral response and proposes a capacity model based on the hold-down contribution. The research novelty of this paper, with respect to [36, 37], derives from the (1) complete report of the cyclic test results on CLT shear walls, (2) comparing CLT and LTF by decomposing the experimental response into rocking, sliding and deformation fractions, (3) the proposal of a novel capacity model driven by hold-down reactions, and (4) the estimation of overstrength factors.
The full description of the test setup of LTF and CLT shear walls is detailed in [40, 41]. In this section, the authors will limit to a short description of the tested shear walls and features of the setup. LTF shear walls with dimensions of 2.5×2.5 m were tested. The test set-up, shown in Fig.III.1, follows the EN 594:2011 protocol [42]. Various vertical loads and different types of hold-downs, angle brackets and sheathing, drove a comparative assessment about the performance of the specimens. The LTF shear walls have the following characteristics: the frame elements are C24, with sections reported in Fig. III.1. There are two types of sheathing: OSB/3 and GFP, with nails or staples as fasteners. The spacing of the sheathing-to-framing fasteners on the perimeter is also varied, and the spacing in the inner stubs always doubles the spacing of the perimeter, as shown in Tab.III.1. Angle brackets or inclined screws resist against the shear wall sliding. Two types of hold-downs were tested, in addition to a specimen without any. The specimens labels follow this nomenclature: "LTF/CLT label-L number", where the label refers to the configuration explained in Tab.III.1 and L identifies the vertical load in kN.

Tab.III.2 summaries the primary outcomes of the cyclic tests. Tab.III.2 reports only F_u and v_u, F_u measuring the strength capacity, while v_u the displacement capacity. The former expresses ultimate resistance; the latter is related to

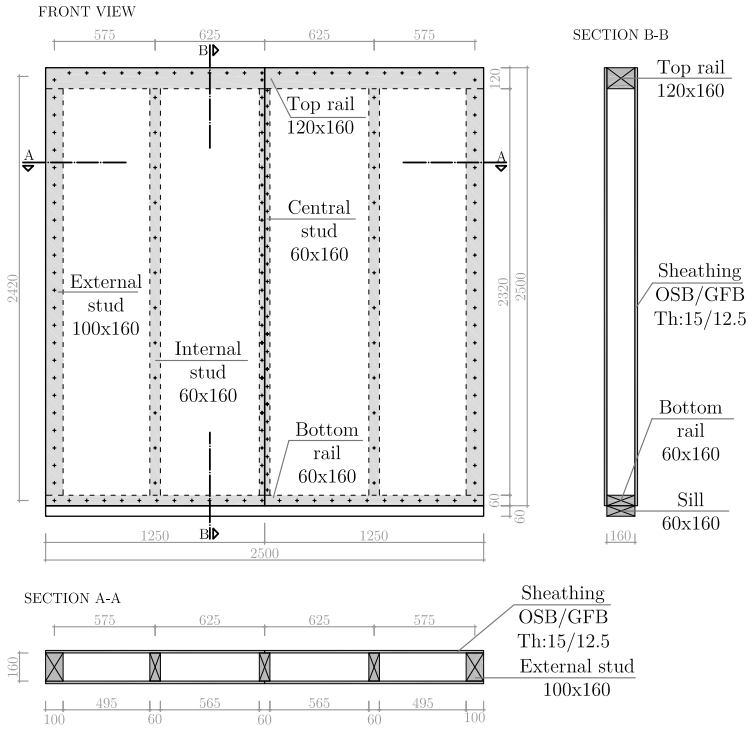

(a)

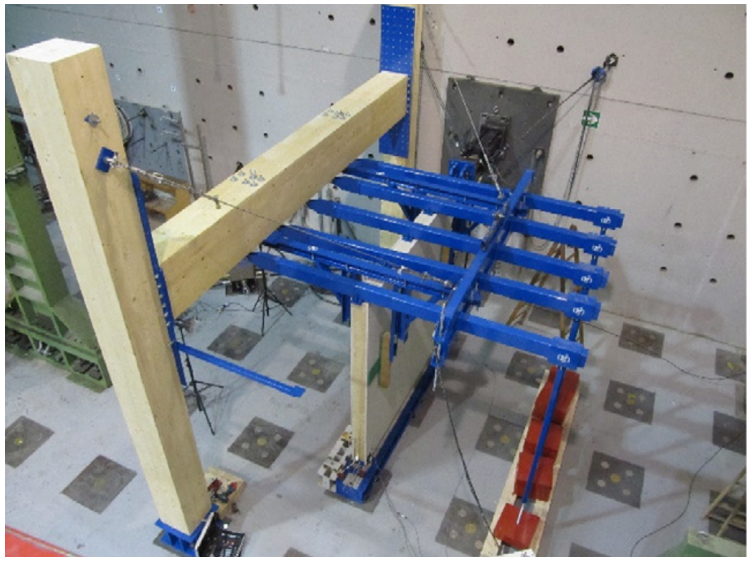

(b)

Fig. III.1. (a) LTF specimen; (b) LTF test setup.

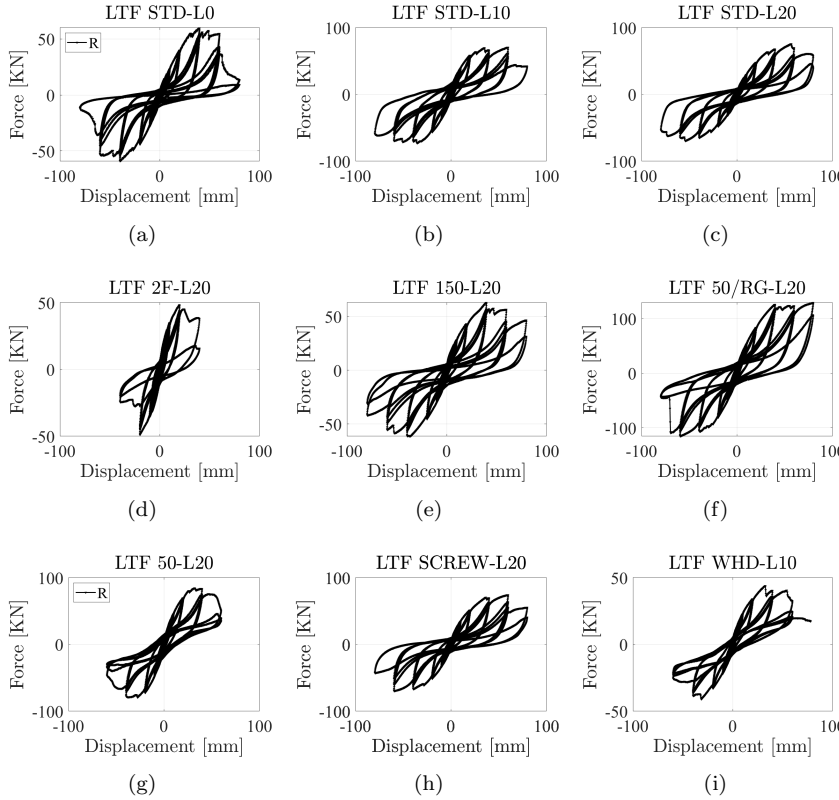

Fig. III.2. Cyclic test results of LTF shear walls.

Table III.1. Characteristics of the tested LTF shear walls.

Specimen LTF	**STD**	**2F**	**150**	**50/RG**	**50**	**SCREW**	**WHD**
Sheathing	OSB/3	GFB	OSB/3	OSB/3	OSB/3	OSB/3	OSB/3
Thickness [mm]	15	12.5	15	15	15	15	15
Fastener type	Ring nails	Staples	Ring nails	Ring nails	Ring nails	Ring nails	Ring nails
⌀ [mm]	2.8	1.4x1.6	2.8	2.8	2.8	2.8	2.8
l [mm]	60	55	60	60	60	60	60
Perimeter spacing [mm]	100	100	150	50	50	100	100
Sliding restraint	New150	New150	New150	New150	New150	HBS	New150
n°	4	4	4	4	4	/	4
Fastener type	Anker nails	Anker nails	Anker nails	Anker nails	Anker nails	Screws	Anker nails
n°	12	12	12	12	12	25	12
⌀ [mm]	4	4	4	4	4	8	4
l [mm]	60	60	60	60	60	180	60
Uplift restraint	WHT340	WHT340	WHT340	WHT620	WHT340	WHT340	/
n°	2	2	2	2	2	2	/
Fastener type	Anker nails	Anker nails	Anker nails	Anker nails	Anker nails	Anker nails	/
n°	20	20	20	52	20	20	/
⌀ [mm]	4	4	4	4	4	4	/
l [mm]	60	60	60	60	60	60	/

ductility. The optimum performance of a structural system derives from the optimum balance between resistance and ductility. Therefore, F_u and v_u may be suitable synthetic indicators of the experimental structural performance. Fig.III.2 presents the results in the form of force-displacement curves.

Table III.2. Cyclic test results: F_u, ultimate experimental racking load; v_u, slip corresponding to the ultimate load; both evaluated according to EN12512.

LTF			**CLT**		
Test	$\boldsymbol{F_u}$ [kN]	$\boldsymbol{v_u}$ [mm]	**Test**	$\boldsymbol{F_u}$ [kN]	$\boldsymbol{v_u}$ [mm]
STD-L0	47.6	60.6	STD-L0	55.6	42.2
STD-L10	58.1	78.4	STD-L20	80.2	43.3
STD-L20	57.5	74.5	NA620-L0	124.0	29.1
2F-L20	38.9	33.5	NA620-L20	146.5	28.6
150-L20	49.6	70.8	ND620-L0	132.9	30.4
50/RG-L20	97.6	76.0	ND620-L20	160.5	32.6
50-L20	65.5	53.5	NA340-L20	83.6	57.4
SCREW-L20	57.6	74.9	NAWH-L20	66.6	57.7
WHD-L10	34.0	54.1			

The CLT shear walls have the following characteristics: three layers (thickness 30-30-30 mm) of C24 boards. Different vertical loads, various connections to the ground headed a comparative assessment between the specimens: precisely, three types of angle brackets, two types of hold-down and a specimen without hold-down—Tab.III.2 reports the preliminary results of the cyclic tests. Fig.III.4 depicts the force-displacement curves of the tested specimens.

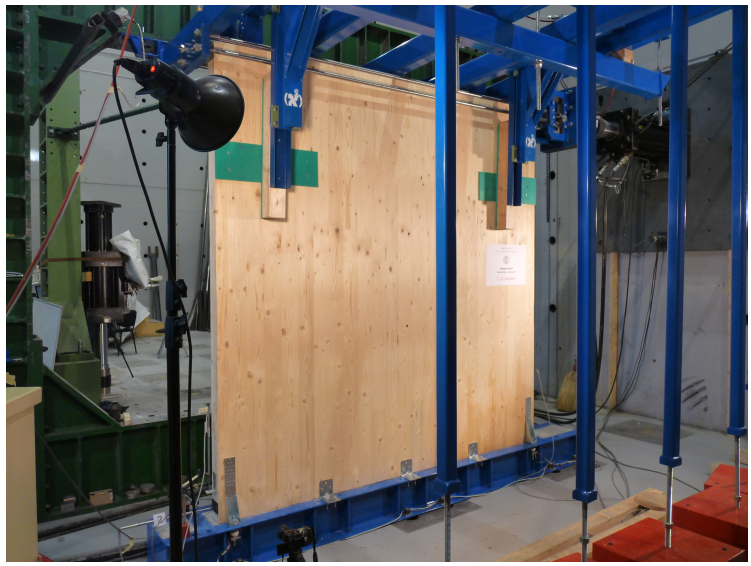

Fig. III.3. CLT test setup.

Table III.3. Characteristics of the tested CLT shear walls.

Specimen CLT	**STD**	**NA620**	**ND620**	**NA340**	**NAWH**
Sliding restraint	100CR	10060newA	10060newD	10060newA	10060newA
n°	3	3	3	3	3
Fastener type	Anker nails	Anker nails	Anker nails	Anker nails	Anker nails
n°	12	30	30	30	30
⌀ [mm]	4	4	4	4	4
l [mm]	60	60	60	60	60
Uplift restraint	WHT340	WHT620	WHT620	WHT340	/
n°	2	2	2	2	/
Fastener type	Anker nails	Anker nails	Anker nails	Anker nails	/
n°	20	52	52	20	/
⌀ [mm]	4	4	4	4	/
l [mm]	60	60	60	60	/

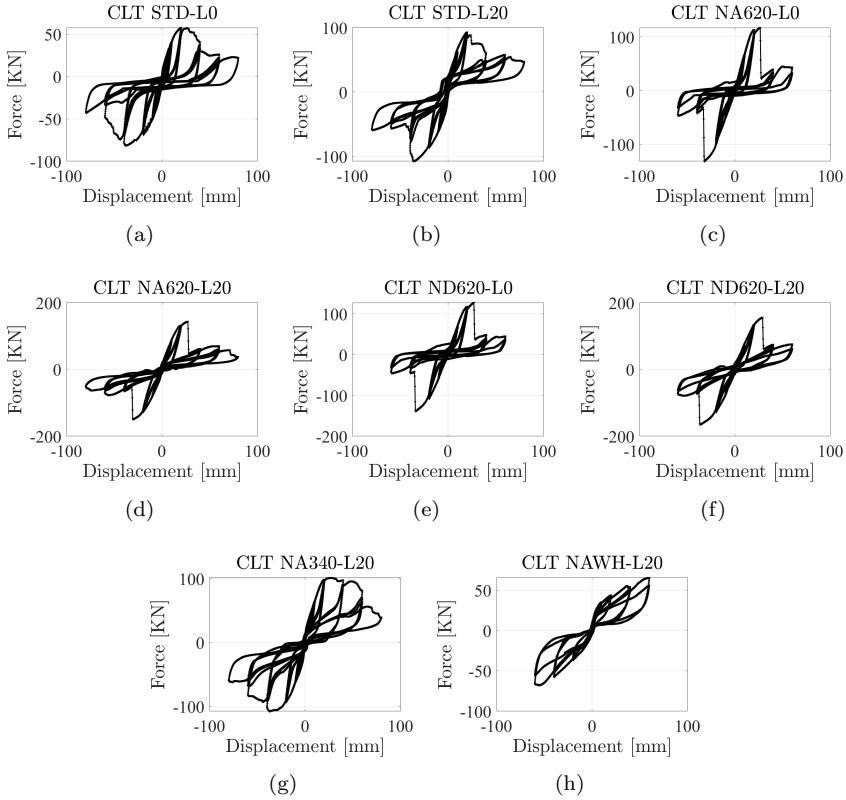

Fig. III.4. Cyclic test results of CLT shear walls.

The experimental data deserve several and special considerations about the effect of the different connection layouts, vertical load, stiffness of the panel or the frame. Nevertheless, several research papers comment on this sort of results [7, 36, 28, 19], and a mere comparative analysis between specimens would not add significant information to what is already published or acknowledged by the scientific community.
Still, the authors would comment on the analogies between the performances exhibited by the LTF and CLT shear walls. Tab.III.2 attempts to compare the two structural typologies: in many specimens, the force and displacement data are quite similar. Averagely, the resistance of the CLT is higher than the LTF, whereas the ultimate displacement of the LTF is higher than the CLT. The crude conclusion is that the CLT and LTF shear walls exhibit an analogous behaviour, although the CLT system has a lower ductility than LTF.
The differences and analogies between the two classes of specimens may depend on the fact that the panel is adequately rigid to transfer the horizontal forces to the hold-downs. In particular, the discrepancies may depend on the different panel rigidity and the analogies on the use of the same connection layouts. The CLT and LTF shear wall in-plane stiffness determines a predominant rigid rocking, which causes the failure of the hold-downs. Accordingly, the entire panel testing is likely a test on its hold down connections, subjected to asymmetric cyclic loading. Therefore, the cyclic test of LTF and CLT shear walls would reduce to a sort of pull-out test of the hold-downs, since the wall assemblies behave like a rigid lever that transfers the load. The validation of this hypothesis entails the assessment of the different contributions to the total displacement in the post-elastic range: rigid-body rotation, rigid-body translation and panel deformation. In this paper, the wall deformation encompasses all sorts of deformation related to the connection elements and the panel itself, namely: the nail slip between the sheathing (OSB, plywood, gypsum, plasterboard) and the timber frame, the shear distortion of the sheathing or the panel, the flexural deformation of the frame, and the slip of the wall relative to its base due to the flexibility of the hold-down and shear base connections.

III.3 Decomposition of the experimental cyclic response

The horizontal displacement of a shear wall may originate by summing the contributions of deformations from three primary sources: the rigid-body translation (sliding) and rotation (rocking), and the panel deformation (which includes all the contribution not included in the previous ones, such as sheathing-to-framing deformation for LTF and OSB/CLT in plane shear deformation). Differently

from the elastic range, the influence of the three contributions changes with the load and the history of displacement. Still, it is attempted to derive the three parts which averagely comprise the total displacement at higher deformation. The authors assume that the displacement measured in point D, Fig.III.5(a), is representative of the sliding component. The deformation component arises from the relative displacement measured along the diagonals, while the rocking component arises from the vertical and horizontal displacements measured in C and B, respectively. The comparison between the sliding, rocking and deformation contributions of the considered shear walls will drive the assessment of the approximation associated with an elementary capacity model.

III.3.1 Sliding

The sliding fraction is estimated as the limit of the ratio between the horizontal displacements in points D and B, as illustrated in Fig.III.5(a):

$$\mathrm{s} := \lim_{u_B \to \infty} \left| \frac{u_D(t)}{u_B(t)} \right| \tag{III.1}$$

The values of $u_D(t)$ and $u_B(t)$ are direct measures from the experimental campaign, and when plotted, they reveal an hyperbolic behaviour, with a clearly visible asymptote for higher values of the imposed displacement as seen in fig. III.5(c). The ratio in Eq.III.1 is illustrated in a sample case by Figs.III.5(c)-(d). At a lower displacement, the ratio tends to infinity: this is due to the division with almost zero displacement values imposed in B, while u_D may rest approximately constant at a low value. At higher displacement, the fraction tends towards two horizontal asymptotes. The main comments about Figs.III.5(c)-(d) follow:

- The ratios between the displacement measured in D and that imposed in B likely gather into beams of hyperbolae. In this case, it is focused on the first quadrant. The hyperbolae in the other quadrants derive from the combination of negative or positive components (Fig.III.5(b)). Fig.III.5(b) manifests that the displacements are not always concordant due to the "dragging" related to hysteresis phenomena.

- The higher is the imposed displacement, the higher is the sliding fraction. The horizontal asymptote of the beams of hyperbolae is non-negative, and it is likely a property of the test configuration, almost independent from the displacement value after a certain load level; The asymptote evidences the linear proportion between displacement in B and D at higher displacement values (Fig.III.5(d)). The asymptote can be rightfully assumed as the sliding fraction of the imposed displacement.

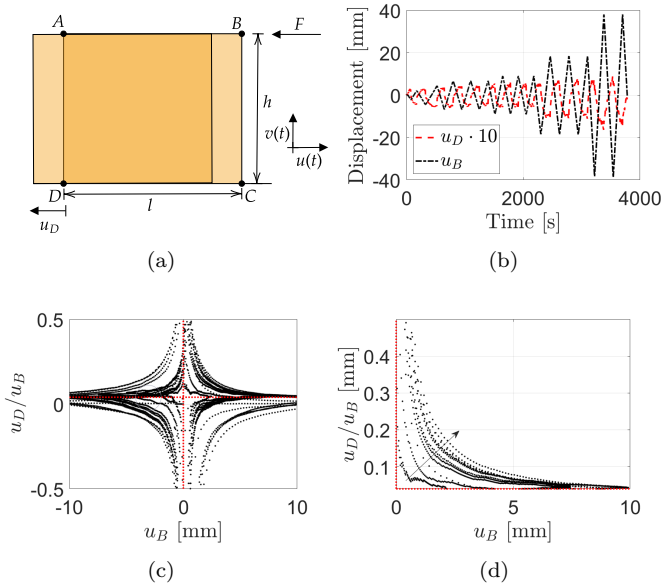

Fig. III.5. (a) Illustration of the rigid-body translation of the panel and the adopted notation; (b) superposition between the displacements in B and D; (c)-(d) ratio between the displacement in D and B as a function of the imposed displacement according to the loading protocol.

- The curve followed in approaching the asymptote depends on the number of cycles. The arrow indicates the direction: the higher the cycle, the more the curve moves towards the upper right part of the quadrant. It possibly depends on the following evidence: a sliding fraction inherited by the previous cycle rises the u_D/u_B values when there are lower displacement values. The higher the cycle, the higher is the sliding fraction originated from the previous cycles: the growing plasticization of the shear wall components raises the fraction of permanent deformation on the total displacement.

III.3.2 Panel deformation

The relative displacement between the points A-C and B-D is a measure of the diagonal deformations in the East and West directions identified by d_E and d_W respectively. At this stage, the authors assume that the panel manifests a predominant shear deformation.

$$d_{E,W} = r_2 - r_1 \tag{III.2}$$

The shear displacement δ derives from Eq.III.2 by expliciting the two radii r_2 and r_1, see Fig.III.5(a):

$$\delta = l - \left[(h\sqrt{2} - d_{E,W})^2 - h^2\right]^{0.5} \tag{III.3}$$

The ratio between δ and u_B approaches a constant value at higher displacement values. The following definition of the deformation fraction, d, attempts to grasp the approaching asymptot.

$$\mathrm{d} := \lim_{u_B \to \infty} \left| \frac{\delta}{u_B} \right| \tag{III.4}$$

At a lower displacement, the ratio tends to infinity: this is due to the division with almost zero displacement values imposed in B, while δ maintains a small plastic deformation which never approaches zero. The main comments about Fig.III.6 follow:

- The sample relative displacement in Fig.III.6(b) shows that the panel deformation almost follows the loading protocol, except for the last three cycles. At that stage, localized plastic deformations occur due to timber compression, and the definition in Eq.III.4 may lose its accuracy.

- The ratio between δ and u_B tends to a constant value, although the beams of hyperbolae are not symmetric, as explained in the previous paragraphs, see Fig.III.6(c).

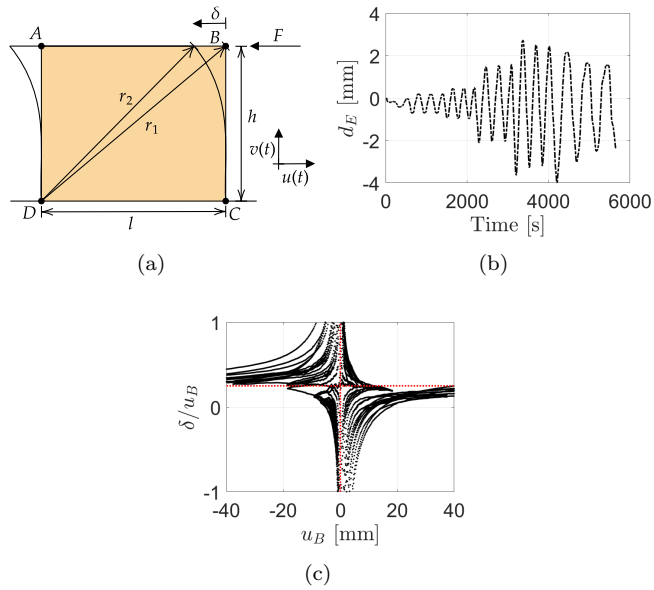

Fig. III.6. (a) Illustration of the shear deformation of the panel and the adopted notation; (b) displacement-time curve of a sample diagonal relative displacement δ; (c) ratio between δ and u_B as a function of the imposed displacement according to the loading protocol.

III.3.3 Rocking

The rocking component is estimated as a complement to one of the already estimated sliding and deformation contributions:

$$r = 1 - (s + d) \tag{III.5}$$

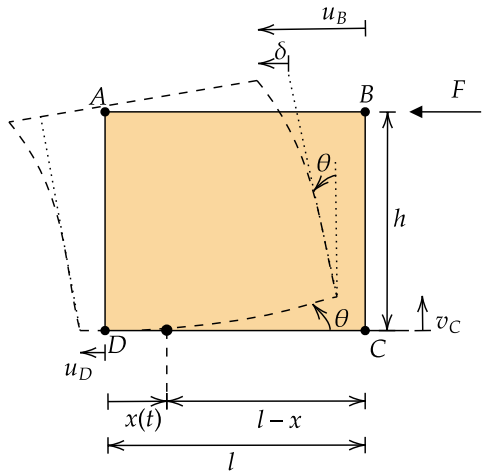

Fig. III.7. Displacements field of the wall.

The whole displacement field of the shear wall is illustrated in Fig.III.7, where all the contribution to the top displacement u_B are highlighted: u_D represents the sliding contribution while δ represents the deformation contribution, both evaluated in the previous sections. The rocking component can be expressed by θh. By assuming small displacements, the displacements can be written as:

$$u_B - u_D - \delta = \theta h \tag{III.6}$$

$$v_C = \theta(l - x) \tag{III.7}$$

Eq.III.6 then permits the direct evaluation of the rocking component, which is plotted in Fig.III.8(b). By inserting the estimated value of the rotation angle θ in eq.III.7 it is possible to obtain the position of the neutral axis x, which is plotted in fig.III.8(c).

The main remarks about the r fraction and the rocking behaviour illustrated in Fig.III.8 follow:

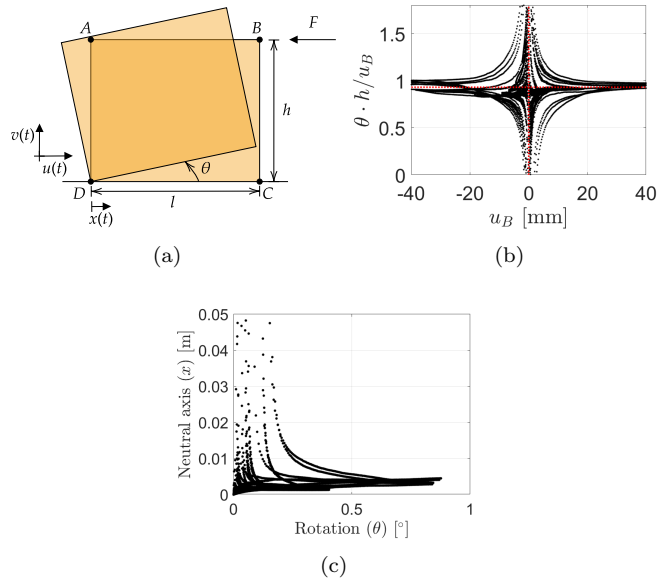

Fig. III.8. (a) Illustration of the rigid-body rotation of the panel and the adopted notation; (b) ratio between the displacement in D and B as a function of the imposed displacement according to the loading protocol; (c) Relationship between the neutral axis position and the angle rotation.

- The ratios between the rocking component and the total displacement group into beams of hyperbolae, like in Fig.III.8(b). The higher is the imposed displacement, the higher is the rocking fraction. Nonetheless, the values corresponding to lower displacements are not entirely reliable: they originate from the division with almost zero values.

- The position of the pivot point x is not zero when the panel rotates: the edges of the panel plasticize and the extension of the compressed area changes. The x value tends to infinity when the panel's rotation approaches zero. When the rotation mounts, the extension of the contact area changes due to plasticization. Fig.III.8(c) evidence a sample increment of the contact area as the rotation angle rises. The x value depends on both the rotation angle θ and the past displacement history: the depth of the neutral axis advances as the plasticization raises, given the same rotation angles.

- The horizontal asymptote is a feature of the test configuration, almost independent from the displacement value after a certain load level. The asymptote likely expresses the rocking fraction of the imposed displacement, see Fig.III.8(b).

III.3.4 Rocking, sliding and deformation components: LTF vs CLT

Tab.III.4 reports the three displacement contributions in all the tested specimens, expressed as percentages. The displacement components in Tab.III.4 refer to the post-elastic behaviour. They originate from Eqs.III.1,III.4,III.5 respectively, which present an asymptotic definition of the three displacement fractions. The experimental data reveal that the three displacement components rapidly converge towards a definite value after the elastic phase. The values stationarity proves that the excitation amplitude does not modify the balance between the three contributions after a certain post elastic displacement value.

The prevalent contribution to the total displacement comes from the rigid-body rotation. The rocking motion of LTF shear walls is lower than CLT: LTF shear walls are more deformable than CLT. Tab.III.5 proves and quantifies the diverse in-plane stiffness between the two structural typologies: the first column shows the bending stiffness obtained from the tangent to the first loading curve. In contrast, the second column collects the equivalent elastic modulus obtained by assuming a cantilevered-like behaviour of the panel. The vertical load has almost the same effects in both the shear walls: the load increment reduces the rocking component. The vertical load acts as a rotation restraint. The reduction of the base connections determines a significant increment of the rocking motion, like in the case without hold-downs (WHD). Interestingly the test LTF SCREW, which

Table III.4. The table attempts to synthesize the displacement components due to sliding, deformation and rocking, expressed as a fraction of the imposed displacement in point B, estimated using Eqs.III.1,III.4,III.5 respectively.

Test	**Sliding-s**[%]	**Deformation-d** [%]	**Rocking-r**[%]
LTF STD-L0	9.5	4.7	85.9
LTF STD-L10	2.1	17.8	80.1
LTF STD-L20	5.1	21.7	73.2
LTF 2F-L20	3.8	33.4	62.8
LTF 150-L20	7.6	34.6	57.8
LTF 50/RG-L20	7.7	18.8	73.5
LTF 50-L20	0.8	15.4	83.9
LTF SCREW L20	2.0	34.5	63.5
LTF WHD-L10	1.4	8.1	90.5
CLT STD-L0	5.6	4.2	90.2
CLT STD-L20	5.0	12.8	82.3
CLT NA620-L0	7.7	3.8	88.5
CLT NA620-L20	3.6	7.9	88.6
CLT ND620-L0	4.0	8.6	87.4
CLT ND620-L20	8.5	5.7	85.8
CLT NA340-L20	4.1	2.2	93.7
CLT NAWH-L20	6.8	0.1	93.0

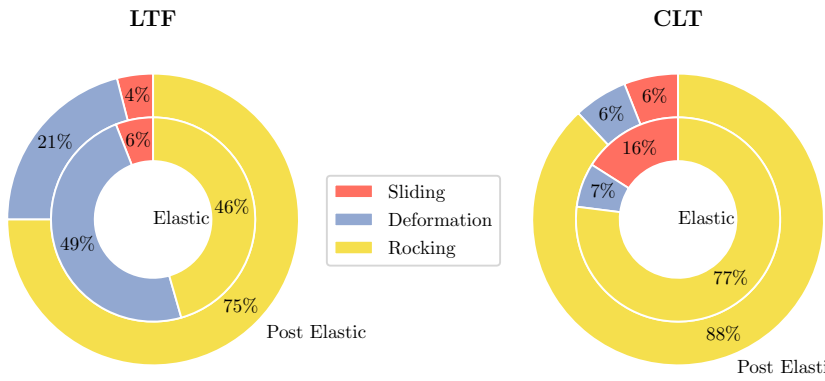

Fig. III.9. Percentage of displacement on top of the shear walls due to each single contribution in both the elastic (calculated by [35]) and post-elastic range (as calculated from the experimental data in this paper).

uses screws distributed uniformly on the bottom rail as a sliding restraint, shows that the presence of screws may influence the rocking mechanism, by offering an additional uplift restraint, thus limiting the rocking percentage as seen from Tab.III.4.
The sliding component does not significantly change between LTF and CLT shear walls. The rigid-body translation mainly depends on the transverse resistance of the base connections and does not likely depend on the vertical load. This shred of information conveys some details about the occurring of friction phenomena. The amount of the Coulomb-type friction restraint depends on the vertical load: the substantial independence of the sliding fraction on the vertical load proves the possible independence of friction in the sliding restraints, primarily provided by the base connections. In the current setup, friction phenomena are then negligible compared to the restraining capacity of the connections.
Additionally, Tab.III.4 proves the substantial independence of the sliding component on the angle brackets. The CLT shear wall has four angle brackets, while the LTF shear wall has two. Nonetheless, the CLT sliding is lower than LTF. The sliding fractions are quite similar between the two structural typologies and the increment in the number of the angle brackets does not enhance the sliding restraint, likely.
The panel deformation changes between LTF and CLT as expected. The impact of deformation on shear walls with low load values and a few base connections (WHD) is shallow and very similar between the two structural typologies. However, as the load increases as well as the base connections, the impact of deformation increases in LTF, while CLT does not deform significantly.
Tab.III.4 stores critical information, which may feed copious comments and research considerations. However, the authors preferred to lighten the presentation by reporting four pie charts in Fig.III.9, which compare the average contributions in the post-elastic phase shown in Tab.III.4 and the contributions in the elastic phase, estimated by [35] via analytical investigations. In conclusion, the rocking fraction is dominant in all structural typologies and increases compared to elastic behaviour. The sliding fraction does not change significantly between CLT and LTF shear walls and between elastic and post-elastic behaviours. The deformation fraction is predominant in LTF shear walls. Still, it tends to reduce between elastic and post-elastic in both structural typologies, due to the predominance of rocking, i.e. the deformation of the hold-downs.

Table III.5. Estimate of the initial stiffness of the LTF and CLT shear walls and the equivalent elastic modulus.

Test	**Bending stiffness**[kN/mm]	**Equivalent E** [MPa]
LTF STD-L0	7.6	337.3
LTF STD-L10	4.1	180.9
LTF STD-L20	10.6	469.8
LTF 2F-L20	10.8	481.8
LTF 150-L20	9.4	419.1
LTF 50/RG-L20	9.4	416.9
LTF 50-L20	6.5	288.9
LTF SCREW L20	20.4	906.2
LTF WHD-L10	7.7	341.3
CLT STD-L0	12.6	561.3
CLT STD-L20	19.6	870.7
CLT NA620-L0	12.2	542.4
CLT NA620-L20	15.4	685.3
CLT ND620-L0	12.4	552.0
CLT ND620-L20	19.6	871.6
CLT NA340-L20	17.5	779.6
CLT NAWH-L20	13.0	576.4

III.4 Discussion: the effect of timber plasticization to force redistribution

The dominance of the rocking response due to the hold-downs deformation may inspire the proposal of an elementary capacity model based on the sole hold down reactions. However, the accuracy of the model mostly depends on an accurate estimation of the extension of the compressed area. In contrast with the elastic behaviour, the extension of the compressed area tends towards a sort of plastic asymptote due to the stress redistribution. The definition of the neutral axis is the following:

$$x_p := \lim_{u_B \to \infty} \left| l - \frac{v_C}{\theta} \right| \tag{III.8}$$

Fig.III.10 shows a qualitative evolution of the neutral axis as the base moment increases and the vertical stress redistribute. There are no studies about the trend of the stress in the compressed area, which depends on several factors: e.g. the planarity of contact areas, timber grading and the slenderness of the panel. Tab.III.6 attests that the extension of the compressed area depends on the vertical load, the in-plane stiffness of the panel and the boundary restraints. The compressed area expands significantly when the vertical load raises, the in-plane stiffness reduces, and there are fewer base connections. An analytical correlation between the x_p variable and the three mentioned variables (vertical load, in-plane

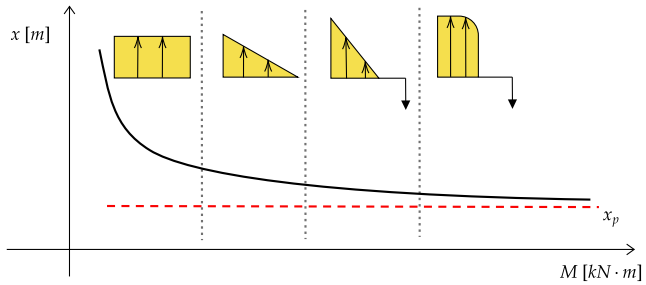

Fig. III.10. Qualitative evolution of the neutral axis as a function of the base moment.

stiffness and boundary conditions) is critical for a conservative estimation of forces acting on the base connections. Specifically, the estimation of the pivot point is essential when assessing the force on the hold-downs: the assumption of the pivot point by one edge of the panel would significantly underestimate the hold-down reactions. Tab.III.6 lists the expected extension of the compressed

Table III.6. Estimate of the asymptotic neutral axis in the considered test configurations.

Test	x_p [m]	x_p/l [%]	**Rocking-r** [%]
LTF STD-L0	0.01	0.4	85.9
LTF STD-L10	0.43	17.2	80.1
LTF STD-L20	0.71	28.2	73.2
LTF 2F-L20	0.72	28.8	62.8
LTF 150-L20	0.02	0.8	57.8
LTF 50/RG-L20	0.01	0.4	73.5
LTF 50-L20	0.01	0.4	83.9
LTF SCREW L20	0.59	23.7	63.5
LTF WHD-L10	0.09	3.6	90.5
CLT STD-L0	0.19	7.5	90.2
CLT STD-L20	0.88	35.4	82.3
CLT NA620-L0	0.20	8.0	88.5
CLT NA620-L20	0.13	5.3	88.6
CLT ND620-L0	0.05	2.0	87.4
CLT ND620-L20	0.70	27.9	85.8
CLT NA340-L20	0.37	14.9	93.7
CLT NAWH-L20	0.48	19.2	93.0

area. The second column presents the percentage ratio between the estimated x_p value and the base length l. The x_p extension depends on the balance between deformation and rocking components: the increment of the deformation fraction

yields an increment of the x_p value. In this paper, the authors do not investigate the compressed area extension based on mechanical analytical models. This step would entail dedicated research efforts based on adequate mechanical models of the shear wall post-elastic response.

III.5 Capacity models for timber shear walls

The scientific literature presents several models for assessing the strength of CLT and LTF timber shear walls. The capacity models of LTF walls, like the ones by Källsner and Girhammar [43], [44], focus on the role of the sheathing-to-framing connections, by evaluating the resistance of the wall related to that sort of failure. That is also the base for the prediction models present in the current Eurocode 5 proposal. Conversely, many scholars consider CLT walls as rigid bodies: the capacity of the wall depends on the strength of its anchorage system, due to its intrinsic considerable in-plane strength and stiffness[45]. The CLT capacity models merely descend from the equilibrium equations of the wall, while the main differences between them lie on two main points: the inclusion or not of the angle brackets contribution in the tension resisting mechanism, and the shape and contribution of the compression zone. Casagrande [35] and Tomasi [46] both neglect the contribution of angle brackets: the first does not make any specific assumptions about the compression stresses distribution and proposes a conventional lever arm equals to $0.9l$, the second assumes a rectangular stress block distribution in the compression zone, with size $0.8x$. Wallner-Novak [47] proposes a model similar to [46] but with compression zone equals to $0.25l$. Pei [48], Reynolds [49], Gavric [50] presented models that include the tensile contribution of angle brackets. Pei [48] assumes an elastic triangular distribution of tensile forces, by considering the rigid body rotation around one edge of the shear wall. Reynolds [49] presented three different models, which all include the presence of a compression zone, but differ in the size of that zone and the distribution of tensile forces between angle brackets and hold-down. Gavric [50] presents a model similar to [48], but considers the interaction between horizontal and vertical forces on the angle brackets.

The simplified capacity model presented in this paper, based on equilibrium equations, is the same in both LTF and CLT walls. As evidenced by the experimental campaign and the previous sections, the behaviour of LTF walls is mainly governed by the hold-down connections. As shown in Fig.III.11, the wall is assumed to pivot around the position P of its neutral axis, characterized by a compression region of extension x_p; no specific assumption is made regarding the shape of the stress distribution in the compression zone. The contribution of angle brackets to the racking mechanism is neglected. Hereafter follows the

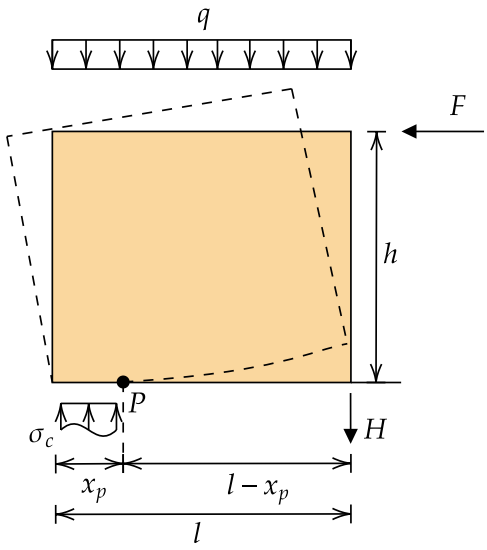

Fig. III.11. Mechanical model of the shear wall.

equilibrium equations:

$$\uparrow \quad -q \cdot l - H + k_C \sigma_C \cdot x_p \cdot t_{\text{eff}} = 0 \tag{III.9}$$

$$\circlearrowleft \quad F \cdot h - q \cdot l \cdot \left(\frac{l}{2} - x_p \right) - H \cdot (l - x_p) + k_C \sigma_C \cdot x_p \cdot t_{\text{eff}} \cdot l_c = 0 \tag{III.10}$$

where q is the distributed vertical load, l the wall length, F the top horizontal force, h the wall height, H the hold down reaction force, σ_c the averaged compression stress on timber, k_c a modification parameter which accounts for the increment of resistance due to compression hardening and the shape feature of the stress diagram, x_p the extension of the neutral axis, t_{eff} is the thickness of the wall reacting in compression, l_c is the lever arm of the compression region. The k_c and the l_c factors are in fact unknown. The goal of this section is to demonstrate that the cyclic behaviour of the tested shear walls is mainly dependent on the hold-down. The force acting on the wall is then evaluated by considering the sole hold-down contribution to the rotational equilibrium, and neglecting the contribution of the unknown compression stresses in timber:

$$F = H \cdot \frac{\tau \cdot l}{h} + q \cdot \frac{l}{h} \left(\tau \cdot l - \frac{l}{2} \right) \quad | \quad \tau = \frac{l - x_p}{l} \tag{III.11}$$

Eq.III.11 bestows the top horizontal force acting on the wall, given the hold-down force H, the vertical load q and the position of the pivot point x_p. The authors validated this model by comparing, in terms of cyclic curves and maximum force values, the forces measured in point B of the shear wall, with the horizontal force $F(t)$. $F(t)$ is obtained from the simplified model in Eq.III.11, using the forces measured on the hold-downs $H(t)$ and the pivot point x_p value estimated in Tab.III.6.

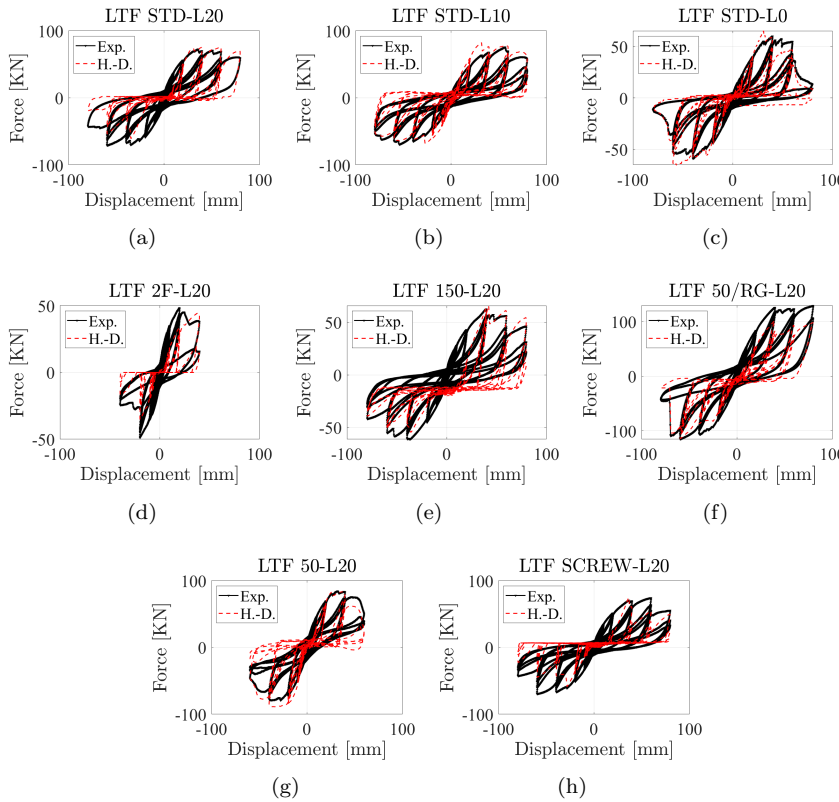

Fig. III.12. Comparison between the experimental cyclic response of LTF shear walls and the capacity model based on hold-down measured forces.

Figs.III.12-III.13 show the two comparing curves: the dotted red curve is the simplified model in Eq.III.11, while the solid black one is the force measured in B. Accurately, the dotted red curves Figs.III.12-III.13 derive from plugging the hold down reaction H measured during the experimental test into Eq.III.11. The

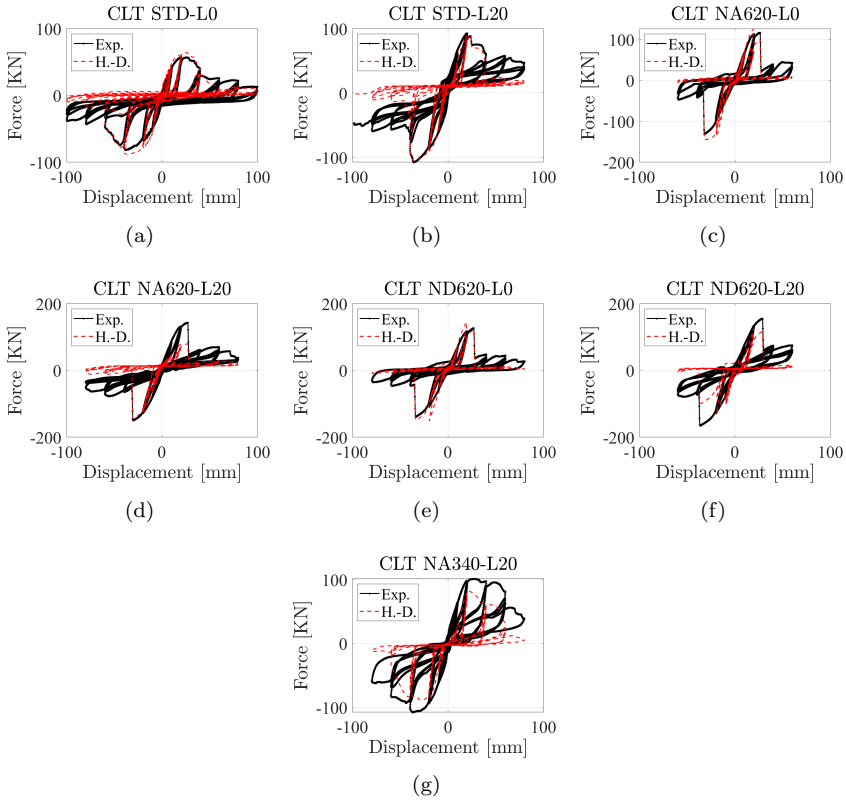

Fig. III.13. Comparison between the experimental cyclic response of CLT shear walls and the capacity model based on hold-down measured forces.

positive and negative reaction values originate from the sense of rotation: if the panel rotates anticlockwise, the authors used the force values measured by the right hold-down with a positive sign. If the panel rotates clockwise, the left hold-down reaction is used with a negative sign. Consequently, the top force values are positive or negative depending on the sense of rotation and the particular hold-down subjected to tension loading, see Fig.III.11. The visual inspection of the pictures suggests an optimal matching. Tab.III.7 quantifies the discrepancies between the two curves in terms of the maximum forces.

Table III.7. Comparison between the maximum forces attained by the experimental cyclic tests and the capacity model based on the sole hold-down reactions.

Test	**Experimental data** $\boldsymbol{F}_{\max}$[kN]	**Analytical model** $\boldsymbol{F}_{\max}$ [kN]	**Error**[%]
LTF STD-L0	72.8	75.9	−4.3
LTF STD-L10	75.6	82.7	−9.3
LTF STD-L20	75.6	68.1	10.0
LTF 2F-L20	60.0	54.6	9.0
LTF 150-L20	62.7	65.9	−5.2
LTF 50/RG-L20	128.9	116.1	9.9
LTF 50-L20	84.4	89.0	−5.4
LTF SCREW L20	74.2	74.7	−0.6
		Avg —Error—	6.7
CLT STD-L0	81.3	87.9	−8.1
CLT STD-L20	107.6	105.5	1.9
CLT NA620-L0	131.1	144.9	−105
CLT NA620-L20	143.6	149.5	−4.2
CLT ND620-L0	138.8	151.6	−9.2
CLT NDS20-L20	165.2	148.7	10.0
CLT NA340-L20	107.5	98.4	8.5
		Avg —Error—	7.5

The agreement between the two curves may be considered entirely satisfactory, given the roughness of the model and the numerous restrictions. The presented capacity model grasps the maximum forces attained by the experimental curves. Conversely, the model fails in following the loading and unloading paths closely. The experimental curves exhibit a more gradual force increment/reduction compared to the dotted lines. This difference likely depends on the lack of the angle brackets contribution, which offer a definite resistance in both the loading and unloading phases, and the contribution of the compression stresses in timber. The percentage error is below 10% in the worst cases. Tab.III.7 proves that a capacity model based on the sole hold down reaction is quite faithful, and an elementary formula for the prediction of the hold-down response could descend by taking the 95% percentile of a Gaussian distribution of the τ factor in Eq.III.11. Accurately,

the 95% percentiles of the τ factor in the LTF and CLT shear walls are:

$$\begin{aligned} \tau_{\mathrm{LTF},95\%} &= 0.81 \\ \tau_{\mathrm{CLT},95\%} &= 0.86 \end{aligned} \tag{III.12}$$

These values suggest that the estimate of F needs a proper reduction of the pivot point of the hold-downs. The decrease is higher in the case of LTF shear walls due to the higher deformability. Eqs.III.11-III.12 represent simplified formulations possibly useful for engineering purposes, which attempts to avoid underestimating the hold-down reaction by reducing the distance of the rotation point. In conclusion, LTF and CLT shear walls do not display significant differences in the considered configurations. This fact is essentially due to the overstrength of the panel to the base resistance derived from the base connections. Fig.III.14 illustrates the probability distributions of two resisting mechanisms: the failure reached during testing, mainly due to hold-down collapse, and the OSB sheathing/CLT panel collapse. The experimental probability density functions of the

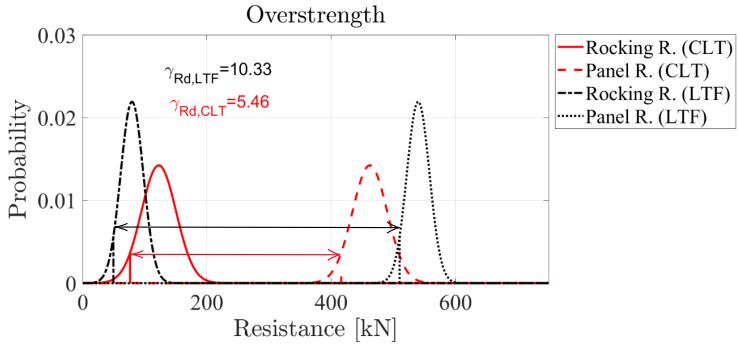

Fig. III.14. Comparison between the experimental cyclic response of CLT shear walls and the capacity model based on Hold-Down measured forces.

CLT and LTF shear walls are calculated directly from the values of failure of the cyclic tests. The probability density functions related to the capacity of the CLT panel / OSB sheathings derive by assuming the same variance of the corresponding experimental curves, and by assuming the shear failure of the OSB sheathing in LTF walls and the in-plane torsional shear failure in CLT panels (see [51] and [52]). The authors used the following values of strength: $f_{v,k} = 6.8$ MPa for OSB/3 and $f_{v,\mathrm{tor},k} = 2.5$ MPa for CLT [53] [54]. Fig.III.14 expresses the true nature of the considered structural systems. The two systems behave likewise due to the similarity of the base connections. Still, the CLT panel is far more resistant than the LTF when different boundary restraints and loads may activate other resisting mechanisms.

$$\gamma_{RD} = \frac{R_{k,b}}{R_{k,d}} \tag{III.13}$$

The authors reported the overstrength values, estimated as shown in Eq.III.13. $R_{k,b}$ is the characteristic load bearing capacity of the panel assuming the timber failure mode (brittle), while $R_{k,d}$ the characteristic load bearing capacity of the panel assuming the hold-down failure mode (ductile). The characteristic values are set equal to the 5-th percentile of the corresponding strength distributions. In the considered cases, the overstrength of LTF shear walls is almost two times of that of CLT. The obtained overstrength values are not general and depend from the specific structural configurations and the considered failure modes. The extension of these results to different structural arrangements must be the object of devoted efforts by the authors.

III.6 Concluding remarks

Light Timber Frame (LTF) and Cross Laminated Timber (CLT) shear walls exhibit similar response under cyclic loading. The authors compared the experimental test of LTF and CLT wall assemblies characterised by similar geometric features. The first part of the paper describes the test results on nine LTF and eight CLT specimens. Then, the multi-channels force and displacement acquisitions are used to extract three deformation contributions from the shear walls lateral displacement in the post-elastic range: the rigid-body translation (sliding) and rotation (rocking), and the panel deformation (which includes all the contribution not included in the previous ones, such as sheathing-to-framing deformation for LTF and OSB/CLT in-plane shear deformation). The rigid-body rotation is the predominant contribution. This contribution, expressed in percentage to the total deformation, is on average 75% and 88% in LTF and CLT specimens, respectively. The rocking response dominance, due to the hold-down deformation contribution, inspired an elementary capacity model based on the hold down reactions and the assumption of a pivot point. The 95^{th} percentile of the Gaussian probability distribution of the ratio between the extension of the compressed area and the panel length is about 0.2: the adoption of the panel edge as a rotation point would determine an approximate 20% underestimation of the hold down reactions in the considered capacity model.
The simplified capacity model based on the measured hold-down reactions and the estimated pivot point led to an excellent agreement with the experimental lateral response. The error in term of the maximum force attained during the cycles is less than 10%. The two systems, LTF and CLT, behave likewise due to the similarity of the base connections. This fact is essentially due to the wall

assembly overstrength to the resistance of the base connections. The overstrength ratios between the CLT panel/OSB sheathing and the panel resistance due to the hold down collapse are approximately 5.46 and 10.33 for the CLT and LTF shear walls respectively. The overstrength ratio features the intrinsic difference between the two structural systems, although the hold-down failure mode conceals such diversity. The authors will aim at assessing the approximation related to more accurate capacity model and will endeavour to determine the shape of the stress distribution of the compressed area. The estimation of the stress distribution would yield the estimate of the shape factor of an equivalent rectangular stress-block. The assessment of the compressed timber resisting contribution would drive mindful reinforcement methods for compression perpendicular to grain in top/bottom plates of Light Timber Frames, like in [55].

Acknowledgements

The authors acknowledge the research efforts of Paolo Grossi, Paolo Endrizzi, Tiziano Sartori and Ermanno Acler, who carried out the experimental tests with the support of the staff of the University of Trento.

Bibliography

[1] A. Aloisio, M. Fragiacomo, and G. D'Alò, "Traditional tf masonries in the city centre of l'aquila–the baraccato aquilano," *International Journal of Architectural Heritage*, pp. 1–18, 2019.

[2] A. Aloisio, M. Fragiacomo, and G. D'Alò, "The 18th-century baraccato of l'aquila," *International Journal of Architectural Heritage*, pp. 1–15, 2019.

[3] S. Thelandersson and H. J. Larsen, *Timber engineering*. John Wiley & Sons, 2003.

[4] M. Piazza, R. Tomasi, and R. Modena, "Strutture in legno," *Materiale, calcolo e progetto secondo le nuove normative europee (Wooden structures. Material, calculation and design according to the new European regulations). Biblioteca Tecnica Hoepli Milano, Milano*, pp. 512–558, 2005.

[5] A. Aloisio, D. Pasca, R. Tomasi, and M. Fragiacomo, "Dynamic identification and model updating of an eight-storey clt building," *Engineering Structures*, vol. 213, p. 110593, 2020.

[6] V. A. De Araujo, J. Cortez-Barbosa, J. N. Garcia, M. Gava, C. Laroca, and S. F. César, "Woodframe: light framing houses for developing countries," *Journal of Construction*, vol. 15, no. 2, pp. 78–87, 2020.

[7] I. Gavric, M. Fragiacomo, and A. Ceccotti, "Cyclic behavior of clt wall systems: Experimental tests and analytical prediction models," *Journal of Structural Engineering*, vol. 141, no. 11, p. 04015034, 2015.

[8] D. Casagrande, S. Rossi, R. Tomasi, and G. Mischi, "A predictive analytical model for the elasto-plastic behaviour of a light timber-frame shear-wall," *Construction and Building Materials*, vol. 102, pp. 1113–1126, 2016.

[9] A. Aloisio, R. Alaggio, and M. Fragiacomo, "Fragility functions and behavior factors estimation of multi-story cross-laminated timber structures characterized by an energy-dependent hysteretic model," *Earthquake Spectra*, p. 8755293020936696, 2020.

[10] A. Hashemi, P. Zarnani, and P. Quenneville, "Seismic assessment of rocking timber walls with energy dissipation devices," *Engineering Structures*, vol. 221, p. 111053, 2020.

[11] D. Fitzgerald, T. H. Miller, A. Sinha, and J. A. Nairn, "Cross-laminated timber rocking walls with slip-friction connections," *Engineering Structures*, vol. 220, p. 110973, 2020.

[12] G. Poh'Sie, C. Chisari, G. Rinaldin, C. Amadio, and M. Fragiacomo, "Optimal design of tuned mass dampers for a multi-storey cross laminated timber building against seismic loads," *Earthquake Engineering & Structural Dynamics*, vol. 45, no. 12, pp. 1977–1995, 2016.

[13] M. Koliou and A. Filiatrault, "Development of wood and steel diaphragm hysteretic connector database for performance-based earthquake engineering," *Bulletin of Earthquake Engineering*, vol. 15, no. 10, pp. 4319–4347, 2017.

[14] Z. Chen, M. Popovski, and A. Iqbal, "Structural performance of post-tensioned clt shear walls with energy dissipators," *Journal of Structural Engineering*, vol. 146, no. 4, p. 04020035, 2020.

[15] Y. Cui, Z. Shu, R. Zhou, Z. Li, F. Chen, and Z. Ma, "Self-centering steel–timber hybrid shear wall with slip friction dampers: Theoretical analysis and experimental investigation," *The Structural Design of Tall and Special Buildings*, p. e1789, 2020.

[16] A. Aloisio, R. Alaggio, J. Köhler, and M. Fragiacomo, "Extension of generalized bouc-wen hysteresis modeling of wood joints and structural systems," *Journal of Engineering Mechanics*, vol. 146, no. 3, p. 04020001, 2020.

[17] A. J. Salenikovich, *The racking performance of light-frame shear walls.* PhD thesis, Virginia Tech, 2000.

[18] J. P. Judd and F. S. Fonseca, "Analytical model for sheathing-to-framing connections in wood shear walls and diaphragms," *Journal of structural engineering*, vol. 131, no. 2, pp. 345–352, 2005.

[19] R. Tomasi and T. Sartori, "Mechanical behaviour of connections between wood framed shear walls and foundations under monotonic and cyclic load," *Construction and Building Materials*, vol. 44, pp. 682–690, 2013.

[20] A. Iqbal, M. Fragiacomo, S. Pampanin, and A. Buchanan, "Seismic resilience of plywood-coupled lvl wall panels," *Engineering Structures*, vol. 167, pp. 750–759, 2018.

[21] D. Way, A. Sinha, and F. A. Kamke, "Performance of light-frame timber shear walls produced with weathered sheathing," *Journal of Architectural Engineering*, vol. 26, no. 1, p. 04019022, 2020.

[22] F. Alinoori, P. Sharafi, F. Moshiri, and B. Samali, "Experimental investigation on load bearing capacity of full scaled light timber framed wall for mid-rise buildings," *Construction and Building Materials*, vol. 231, p. 117069, 2020.

[23] T. T. Nguyen, T. N. Dao, S. Aaleti, J. W. van de Lindt, and K. J. Fridley, "Seismic assessment of a three-story wood building with an integrated clt-lightframe system using rths," *Engineering Structures*, vol. 167, pp. 695–704, 2018.

[24] R. L. Tuomi and W. J. McCutcheon, "Racking strength of light-frame nailed walls," *Journal of the Structural Division*, vol. 104, no. 7, pp. 1131–1140, 1978.

[25] A. K. Gupta and G. P. Kuo, "Behavior of wood-framed shear walls," *Journal of Structural Engineering*, vol. 111, no. 8, pp. 1722–1733, 1985.

[26] J. Dolan and R. Foschi, "Structural analysis model for static loads on timber shear walls," *Journal of Structural Engineering*, vol. 117, no. 3, pp. 851–861, 1991.

[27] G. Rinaldin, C. Amadio, and M. Fragiacomo, "A component approach for the hysteretic behaviour of connections in cross-laminated wooden structures," *Earthquake engineering & structural dynamics*, vol. 42, no. 13, pp. 2023–2042, 2013.

[28] P. Grossi, T. Sartori, I. Giongo, and R. Tomasi, "Analysis of timber log-house construction system via experimental testing and analytical modelling," *Construction and Building Materials*, vol. 102, pp. 1127–1144, 2016.

[29] M. Koliou, J. W. van de Lindt, and R. O. Hamburger, "Nonlinear modeling of wood-frame shear wall systems for performance-based earthquake engineering: Recommendations for the asce 41 standard," *Journal of Structural Engineering*, vol. 144, no. 8, p. 04018095, 2018.

[30] G. C. Foliente, "Hysteresis modeling of wood joints and structural systems," *Journal of Structural Engineering*, vol. 121, no. 6, pp. 1013–1022, 1995.

[31] A. Kottari, A. Charalampakis, and V. Koumousis, "A consistent degrading bouc–wen model," *Engineering structures*, vol. 60, pp. 235–240, 2014.

[32] J. Song and A. Der Kiureghian, "Generalized bouc–wen model for highly asymmetric hysteresis," *Journal of engineering mechanics*, vol. 132, no. 6, pp. 610–618, 2006.

[33] S. Sessa, N. Vaiana, M. Paradiso, and L. Rosati, "An inverse identification strategy for the mechanical parameters of a phenomenological hysteretic constitutive model," *Mechanical Systems and Signal Processing*, vol. 139, p. 106622, 2020.

[34] G. Di Gangi, C. Demartino, G. Quaranta, and G. Monti, "Dissipation in sheathing-to-framing connections of light-frame timber shear walls under seismic loads," *Engineering Structures*, vol. 208, p. 110246, 2020.

[35] D. Casagrande, S. Rossi, T. Sartori, and R. Tomasi, "Proposal of an analytical procedure and a simplified numerical model for elastic response of single-storey timber shear-walls," *Construction and Building Materials*, vol. 102, pp. 1101–1112, 2016.

[36] P. Grossi, T. Sartori, and R. Tomasi, "Tests on timber frame walls under in-plane forces: part 2," *Proceedings of the Institution of Civil Engineers-Structures and Buildings*, vol. 168, no. 11, pp. 840–852, 2015.

[37] E. Acler and R. Tomasi, "Monotonic and cyclic in-plane behavior of clt panels tested by using different types of metal devices," in *COST Action FP1004 - Early Stage Researchers Conference Enhance mechanical properties of timber, engineered wood products and timber structures - Zagreb, Croatia*, 2012.

[38] R. Tomasi, "Seismic behavior of connections for buildings in clt," in *COST Action FP1004 - Focus Solid Timber Solutions European Conference on Cross Laminated Timber (CLT) - Graz, Austria*, 2013.

[39] M. Andreolli and R. Tomasi, "Bemessung von gebäuden in brettsperrholzbauweise unter erdbebenbeanspruchung," *Bautechnik*, 2016.

[40] P. Grossi, "PARETI INTELAIATE IN LEGNO: indagine sul comportamento meccanico tramite prove sperimentali a scala reale," Master's thesis, University of Trento, 2011.

[41] P. Endrizzi, "I sistemi di connessione di base del pannello xlam compensato di tavole indagine sperimentale in scala reale e modellazione numerica della capacità portante globale di parete ottenuta con l'impiego di una nuova tipologia di angolare a taglio," Master's thesis, University of Trento, 2011.

[42] "EN 594:2011 Timber structures, Test methods - Racking strength and stiffness of timber frame wall panels," *BSI, London UK*, 2011.

[43] B. Källsner and U. Girhammar, "Analysis of fully anchored light-frame timber shear walls-elastic model," *Materials and Structures/Materiaux et Constructions*, vol. 42, no. 3, pp. 301–320, 2009.

[44] B. Källsner and U. Girhammar, "Plastic models for analysis of fully anchored light-frame timber shear walls," *Engineering Structures*, vol. 31, no. 9, pp. 2171–2181, 2009.

[45] I. Lukacs, A. Björnfot, and R. Tomasi, "Strength and stiffness of cross-laminated timber (clt) shear walls: State-of-the-art of analytical approaches," *Engineering Structures*, vol. 178, pp. 136–147, 2019.

[46] S. Pei, J. Lindt, and M. Popovski, "Enhance mechanical properties of timber, engineered wood products and timber structures," *CLT course at FPS COST Action FP1004. CLT Training School*, 2014.

[47] M. Wallner-Novak, J. Koppelhuber, and K. Pock, *Brettsperrholz Bemessung Grundlagen für Statik und Konstruktion nach Eurocode.* proHolz Austria, 2013.

[48] S. Pei, J. Lindt, and M. Popovski, "Approximate r-factor for cross-laminated timber walls in multistory buildings," *Journal of Architectural Engineering*, vol. 19, pp. 245–255, 2013.

[49] T. Reynolds, R. M. Foster, J. Bregulla, W. shao Chang, R. Harris, and M. Ramage, "Lateral load resistance of cross-laminated timber shear walls," *Journal of Structural Engineering-asce*, vol. 143, p. 06017006, 2017.

[50] I. Gavric and M. Popovski, "Design models for clt shearwalls and assemblies based on connection properties," in *Proceedings of International Network on Timber Engineering Research, INTER/47-15-4*, 2014.

[51] D. Casagrande, T. Sartori, and R. Tomasi, "Capacity design approach for multi-storey timber-frame buildings," in *Proceedings of International Network on Timber Engineering Research, INTER/47-15-3*, 2014.

[52] F. Boggian, M. Andreolli, and R. Tomasi, "Cross laminated timber (clt) beams loaded in plane: testing stiffness and shear strength," *Frontiers in Built Environment*, vol. 5, p. 58, 2019.

[53] "EN 300:2006, Oriented strand boards (OSB). Definitions, classification and specifications," 2006.

[54] R. Brandner, G. Flatscher, A. Ringhofer, G. Schickhofer, and A. Thiel, "Cross laminated timber (clt): overview and development," *European Journal of Wood and Wood Products*, vol. 74, no. 3, pp. 331–351, 2016.

[55] F. Alinoori, F. Moshiri, P. Sharafi, and B. Samali, "Reinforcement methods for compression perpendicular to grain in top/bottom plates of light timber frames," *Construction and Building Materials*, vol. 231, p. 116377, 2020.

Part 3

Papers Shear Walls-Renovation

IV. Experimental cyclic response of a novel friction connection for seismic retrofitting of RC buildings with CLT panels

Bibliographic data

F. Boggian, C. Tardo, A. Aloisio, E. Marino, and R. Tomasi, "Experimental cyclic response of a novel friction connection for seismic retrofitting of RC buildings with CLT panels", *Journal of Structural Engineering*, 2022 Doi

Contents

abstract

The seismic vulnerability of existing reinforced concrete (RC) framed buildings in seismic prone areas entails affordable and practice-oriented solutions for their retrofitting. In this paper, the authors present a retrofitting solution for RC building based on the combined use of Cross-Laminated Timber (CLT) panels and asymmetric friction connections (AFC). The AFC connection is activated when the force level reaches the design threshold. The energy dissipation of the AFC increases the structural dissipation capacity, and reduces the displacement demand. This research presents the outcomes of an experimental campaign on selected prototypes of these AFC connectors. The authors assess their dissipative capacity from cyclic load tests in four different connector arrangements, and examine the contribution of aluminum shim layers. The first results highlight the significant dissipation potential of the AFC, despite they also evidence the notable sensitivity on the design and constructive details. The authors present a modeling approach to simulate the experimental results.

IV.1 Introduction

The seismic retrofitting of existing buildings is a comprehensive and contemporary research topic with diverse economic, social and environmental entanglements. This paper is part of the European e-SAFE (Energy and Seismic AFfordable rEnovation solutions) project [1, 2], which presents a multidisciplinary approach on renovation solutions for existing buildings, in the framework of the Horizon 2020 European goal [3]. The authors will focus on seismic retrofitting, which represents an all-embracing challenge, especially in earthquake-prone areas in southern Europe. As an example, 60% of Italian residential buildings were built between 1946 and 1990, while 25% before 1946 [4]. The Italian seismic hazard and the inadequacy of seismic provisions before the 1980s confirm the Italian territory's significant seismic risk. There are several solutions for seismic retrofitting of reinforced-concrete (RC) buildings. Specifically, there are two types of interventions, those aiming to reduce the seismic demand and those aiming to increase the structural capacity [5, 6, 7]. The structural capacity may be increased by adopting strengthening interventions or by installing stiffening elements. So far the strengthening interventions are the most widespread. They can be traditional (e.g., steel jacketing of beams and columns [8]) or based on the use of advanced materials (wrapping with fibre-reinforced polymers (FRP) or textile-reinforced mortar [9, 10]). Properly designed stiffening elements (e.g., RC shear walls, X-bracing [11, 12]) could partially adsorb the seismic load. However, the seismic vulnerability could also be reduced by lessening the seismic demand.

These interventions include the use of dissipation devices [13, 14, 15] or base isolation [16, 17, 18]. The solutions aiming at increasing the structural capacity are invasive and generally expensive. The interventions that reduce the seismic demand could be advantageous, being low-invasive and reducing installation time. In this field, friction connections (FC) could be considered possible candidates for increasing the structural dissipation capacity [19, 20]. Still, these devices are not common due to difficulties in their practical installation and the uncertainty of the RC building's coupled response. So far, full-scale experimental tests on the effect of AFC on RC frames are lacking [21, 22]. On the other side, many scholars started investigating the possibility of using timber as a strengthening solution for existing buildings, particularly Cross Laminated Timber (CLT) panels [23]. In RC buildings with masonry infill, CLT panels can be used in addition or substitution [24, 25] of existing masonry infill. The main issue related to these interventions is implementing an appropriate connection system between the CLT panel and the existing structure. The system proposed by the authors is called e-CLT, see Fig.IV.1, and consists of installing CLT panel from the outside of the building while leaving the masonry infills unchanged, without discomfort for the people living inside the building [26]. CLT panels have light weight (around 470 kg/m3), thus not increasing too much the mass of existing buildings. Other advantages that make CLT attractive for retrofitting uses are the high level of prefabrication and the benefits of dry interventions, such as quick and easy installation, material recyclability and reversibility of the retrofit intervention. The central innovation of the e-CLT retrofitting intervention stands in the connection system between CLT and existing building: a friction connection. The FC is constituted by a couple of steel profiles, one connected to the existing beam and the other to the CLT panel, clamped together by preloaded bolts. One of the two profiles presents a slotted hole, which enables their mutual sliding. Single CLT panels are connected to the RC beams of the structure by at least two FC. The size of the CLT panels is related to that of the bays without openings where they are applied. In common RC framed buildings, the story height is generally equal to 3 m, while the width of each bay does not exceed 6 m. The e-CLT technology can be combined with non-structural framed panels, that may be applied to the walls with openings and are equipped with high-performing windows that replace the existing ones. Both panels integrate insulation materials, to improve the energy efficiency of the building, and finishing layer. The retrofit system also provides technological solutions to cover the FC devices after the panels installation and to ensure their inspection and maintenance [27]. This paper will report a testing campaign on the novel FC developed within the e-CLT retrofitting technology, but also applicable to other type of structural panels or retrofit systems. The authors investigated the cyclic response of four different prototypes by focusing on their dissipative performance. The goal is to understand the prototypes'

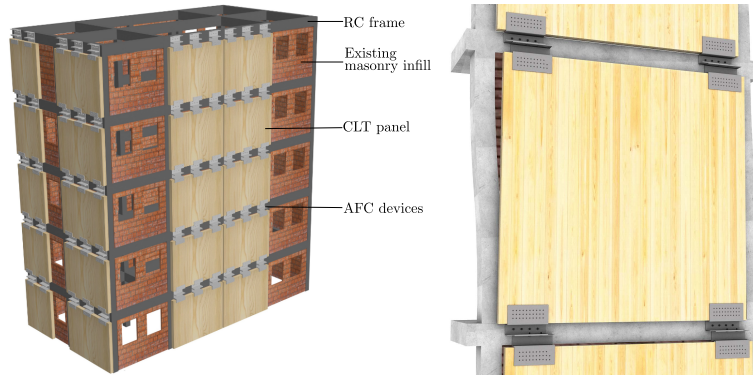

Fig. IV.1. (a) Components of the e-CLT retrofitting system and (b) e-CLT panel subjected to seismic action

behavior for a mindful assessment of their potential for future developments. The main novelty of this paper lies in the development and testing of a new AFC for seismic retrofitting intervention coupled with CLT panels, both design choices regarding the shape and mechanical behavior of the system will be discussed. The investigation of the connection between FC and CLT panel, and between FC and concrete beam, is outside the scope of the current paper. The experimental activity was directed at isolating and studying the friction behavior of the FC, representing the innovative part of the system. The connection to the CLT panel and to the concrete are known from literature and standards. Their design will follow the capacity design rules, with respect to the sliding force of the FC. The structure of the paper is the following: after an overview of previous investigations on friction connections, tested specimens and setup are described; results are presented in graphical and tabulated form, along with brief explanation on the data elaboration; a discussion completes the presentation of results, along with a possible modeling approach, and in the end conclusions are drawn.

IV.2 Friction connections

Several researchers investigated friction connections performance in their basic form, usually divided into two classes: symmetric friction connections (SFC) and asymmetric friction connections (AFC) [28, 29]. Symmetric friction connections present one central plate with an elongated hole and two lateral plates with

round holes. In this connection, the central plate slides while the two lateral plates are restrained, determining symmetric loading conditions. In asymmetric friction connections, instead, one plate is restrained while the other slides. This configuration determines asymmetric loading condition. A third plate with round holes may be used to close the connection as a "cap" plate. Additionally, shim layers made from various materials may be used between the three plates, in order to increase the stability of the friction behavior. An example of the tested specimen, which are classified as AFC, is shown in Fig.IV.9.
[30] initially began investigating with a numerical study the possibility of using SFC instead of hold-down for restraining timber shear walls against uplift, to cap the force transmitted to the wall, and reduce inelastic damage. Consequently, [31] and [32] presented two experimental campaigns: the first on single SFCs and the second on full-scale timber walls. In [31] the focus was on the single connectors, with different materials tested as shim layers, such as brake lining and different alloys. An innovative connection without shim layers was also tested, where the central slotted element was made directly with the high hardness alloy. They found that high hardness alloys offered the best sliding performances, like bisalloy 400, while steel vs steel sliding presented a more erratic behavior. In [32] the concept of SFC was applied to a full-scale timber wall, where the friction connections replaced the hold-downs. The results showed that these devices determined a global elastoplastic response of the entire wall under cycling loading. [33] further extended the concept, by modeling CLT walls and multistory buildings and by proposing a displacement-based design method. [34] tested SFC by adopting different methods of surface preparation of the sliding interface. Surfaces cleaned from loose rust and mill scale yielded the best hysteresis curves in terms of stability. [35] studied an SFC with self-tapping screws for CLT, which was then used also for a full-scale campaign in [36]. [37] investigated the performance of SFCs in steel buildings. [38] and [39] presented two experimental campaigns on AFCs. The first one, [38] aimed at understanding the behavior of the AFC when using different materials as shim layers. Materials with high hardness led to extremely stable loops, low hardness materials determined moderately stable loops, while an erratic behavior was observed with medium hardness materials (hardness values similar to steel plates). The second, [39], established a dependence between stability and shape of the loop and the clamping force level. [40] and [41] presented an experimental campaign on AFC focused on the bolt length effects. They found that increasing the bolt length determined a decrease in AFC strength and a more pronounced preload loss, conversely the effective friction coefficient and its variability tended to decrease. [42] tested brake pads as shim material for AFC. [43] studied the dynamic effects on AFC for applications in steel structures, which further led to the design proposals in [44].
Friction connections were selected as appropriate for the e-CLT seismic retrofitting

intervention due to their highly efficient energy dissipation mechanism, which contributes to reduce inter-story drift damage to the existing building. The damage-free energy dissipation mechanism also ensures the durability of its structural efficiency even after seismic events. This feature avoids the need for the removal and replacement of the FC, which in turn would involve the removal of the attached CLT panel too. After a seismic event it is sufficient to check and eventually replace the bolts and the shim layers. Another important feature, differently from visco-elastic devices, is that these connections present stable hysteresis loops which are not dependent on the speed [45].

IV.3 Materials and methods

IV.3.1 Specimen

The prototypes have four different geometries, all fabricated from 8mm cold-bent S235 steel plates. The first one is labeled STD, the standard design in Fig.IV.4(a), with an overall 450mm width, 325mm height and a 105mm depth, which matches with a 100mm thick CLT panel. Detailed dimensions are present in the appendix section. The prototype consists of a couple of plates with different holes. The "top" profile has holes for the connections with the RC beam and round holes on the interface surface with the "bottom" profile. The bottom profile has two slotted holes, which guarantee the sliding between the two profiles. Each hole hosts a preloaded 10.9 class M14 bolt. The clearance of movement is 100mm in each direction, plus some tolerance. Both profiles present holes in the outer plates for screwed connections with the CLT panels. The STD is the initial design of the FC, that worked as a base configuration. This configuration has been conceived for the potential advantages also in terms of industrial and technological efficiency. On an industrial scale, the innovative design enables an easy and efficient manufacturing process, since the profiles are produced by cutting, drilling and press bending of steel sheets. These manufacturing processes are ordinary and commonly performed workshops specialized in metal processing. Furthermore, the device allows for a fast and easy installation of the e-CLT system by means of mobile lifting equipment, thus avoiding the costs and time needed for the scaffolding set-up. The inspection and maintenance interventions (e.g. preloading the friction bolts that may have loosened after a seismic event) are also facilitated by the front mounting and by adopting a proper cladding solution that covers the FC devices after the installation of the CLT panels. Even the swift removal and replacement of the dampers is possible, since the steel profiles are connected to the external side of CLT panels.
Other three different designs were obtained by modifying the STD, in order to improve the mechanical behavior and the possible weaknesses evidenced in

FEM modeling [26]. The FEM analysis carried out in *Ansys* by [26] on the STD design highlighted significant stress concentrations and deformations around the bend of the bottom profile, see Fig.IV.3(a), which is the profile that is free to slide. Therefore, three different prototype designs were derived from the STD, by changing mainly the following features: the number and position of the slotted holes, the out of plane eccentricity -between friction connection and bottom profile (see Fig.IV.2)-, and the number of bends of the bottom profile. Table IV.1 lists the names and features of all the designs. The prototype STD-R was built to add strength to the STD in the box-like area, so two welded plates were added as reinforcements, see Fig.IV.4(c). The two plates guarantee the same installation of the STD, without any grooves required in the CLT. The FEM analysis showed a partial improvement to the STD, even if the point of weakness remained in the area of the outer bend of the bottom profile, as seen from Fig.IV.3(b). The prototype STD-1H has the same geometry as the STD with one significant difference: there is a single and centered slotted hole with both preloaded bolts sliding inside, see Fig.IV.5(a). This design originated from the simpler production process, faster mounting phase, and a more uniform force distribution between the two aligned bolts. The FEM investigations presented in [26] evidenced significant deformability of all the previous STD shaped prototypes due to (1) the eccentricity between the points of application of the slip force and the reaction force transmitted by the CLT panel, and (2) the multiple bends that characterize their geometry. Hence, in order to improve the expected performance, the authors developed the ALT prototype. The ALT design presents a shape different from that of the STD design, as shown in Fig.IV.5(c). In addition, the connection to the CLT panel was moved to the back, thus making both the profiles L shaped elements. In this way, only one bend was necessary, and also the out of plane eccentricity could be slightly reduced. Furthermore, only one slotted hole is used for the bolts sliding, like the STD-1H prototype. As a result, the FEM analysis showed lower values of stresses and deformations if compared to the other designs, as seen from Fig.IV.3(c). However, the downside of this design is represented by a more difficult mounting and maintenance procedure. The connection to the CLT panel is on the backside, adjacent to the existing masonry.

The specimens used for the experimental campaign are shown in Fig.IV.4(b), IV.4(d), IV.5(b), IV.5(d). They present some modifications with respect to the prototypes, mainly related to the choice of test setup and goal of the campaign, being the study of the sole friction connection. Each specimen is composed by two profiles. One profile is shaped as the "bottom" profile of the corresponding prototype, and presents 12 holes to be fixed by means of bolts to a steel column, which simulates the CLT panel. Instead, the other profile is C-shaped and simulates the "top" profile fixed to the RC beam, which is replicated by a

Table IV.1. Nomenclature and parameters of the prototypes

Prototype	Description	e [mm]	Slotted hole	n_{bend}
STD	Standard	46.1	Double	3
STD-R	Standard with reinforcements	46.1	Double	3
STD-1H	Standard with 1 elongated hole	46.1	Single	3
ALT	Alternative	32.8	Single	1

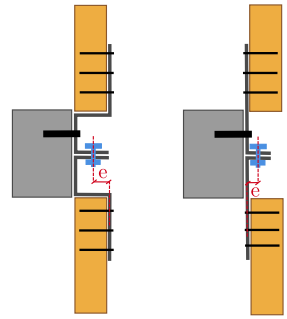

(a) (b)

Fig. IV.2. Scheme illustrating the out of plane eccentricity of the system: (a) STD design, (b) ALT design.

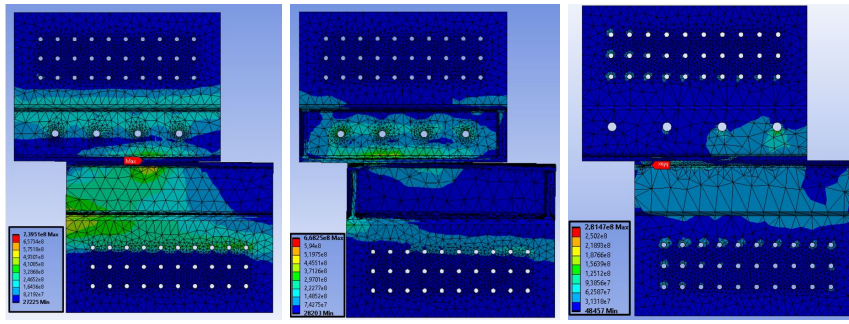

(a) (b) (c)

Fig. IV.3. FEM models from [26], showing equivalent von-Mises stress [N/m^2] for a 30kN sliding force. The specimen shown are (a) STD design; (b) STD-R design; (c) ALT design.(Images used courtesy of *ANSYS, Inc.*)

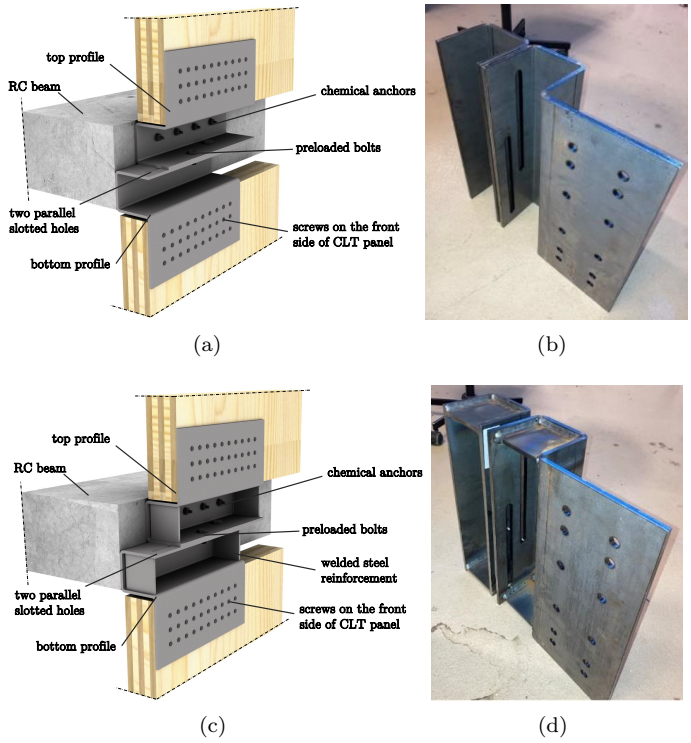

Fig. IV.4. (a) STD prototype; (b) STD specimen; (c) STD-R prototype; (d) STD-R specimen.

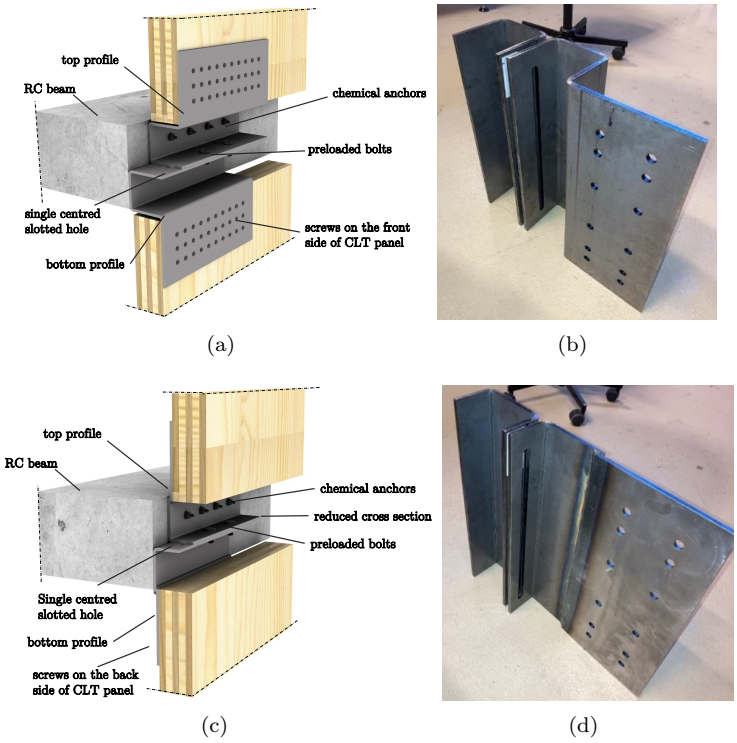

Fig. IV.5. (a) STD-1H prototype; (b) STD-1H specimen; (c) ALT prototype; (d) ALT specimen.

steel element. The displacement protocol of the press simulates the horizontal displacement of the RC beam of the existing building. The authors assumed the possible application of the e-CLT technology in RC buildings characterized by a prevalent shear-type behavior. Therefore, the floors mainly exhibit a horizontal displacement, and no uplift is allowed to the CLT panel.

IV.3.2 Setup and load protocol

The authors devised the setup to test the four different specimens with minor adjustments, despite the STD and the ALT specimens have different geometry. The setup was conceived to reproduce a loading condition that applies a sliding movement to the FC, in order to isolate and study the friction behavior. The setup consists of a rigid steel frame embedded in a universal *Instron* electromechanical testing machine, as seen in Fig.IV.6 and IV.7. The two columns present a rectangular hollow steel section, 12.5mm thick and 100x120mm dimension. The bottom profile of each specimen is fixed on the right column from the outside, using 12 pre-screwed bolts. A T-shaped element ensures the load transfer to the specimen: its base stands below the load cell, while the C-shaped top profile is connected to its wing, which simulates the RC beam movement. The column-base connection of the right column, the left beam-to-column connection and the connection between the T-element and press plate are realized by means of slotted holes. The clearance of the slotted holes has been designed to accommodate manufacturing tolerances of the specimens. With a 100kN and 50kN capacity in

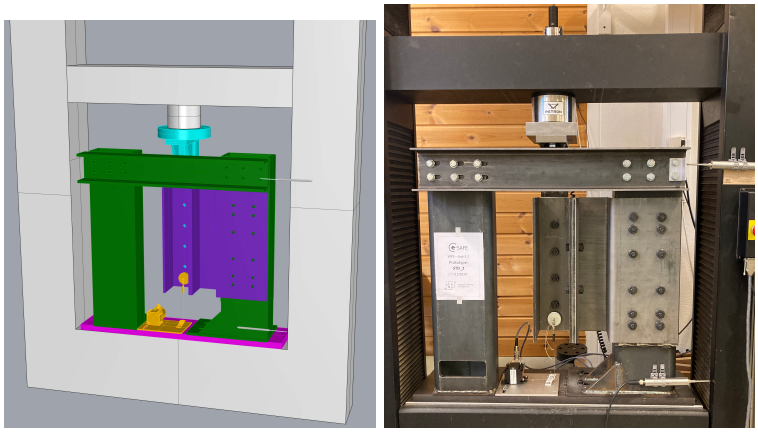

(a) (b)

Fig. IV.6. (a) 3D model of the setup; (b) setup.

monotonic and cyclic testing, respectively, the press load cell measures the force. Two sensors measure the top profile displacement: the sensor embedded in the press, which drives the displacement-controlled test, and an external wire sensor attached to the bottom profile with a magnet. LVDTs also acquired two displacement measures on the right column: by its base and top, to detect undesired sliding or rotations for assessing the adequacy of the setup stiffness. A scheme of the measuring setup is provided in Fig.IV.7. The displacement-controlled

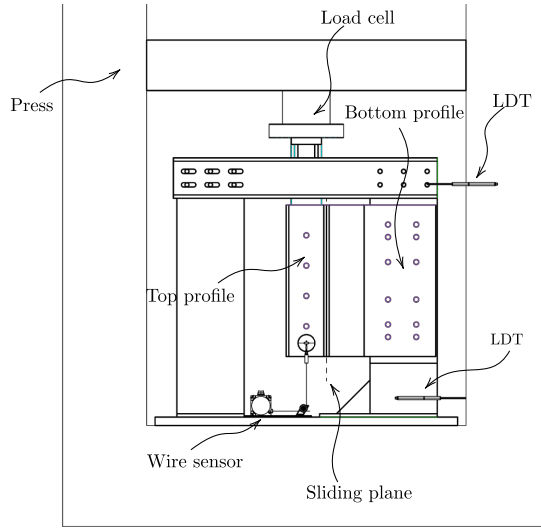

Fig. IV.7. Illustration of the setup elements and measuring acquisition system.

loading protocol originates from the approach in ISO16670 [46], and EN15129 [47] prescriptions: both standards suggest a cyclic protocol with incremental steps of percentages of the ultimate displacement. For the friction connection, the maximum sliding clearance is given by the length of the elongated holes: the ultimate displacement for the tests descends from a geometric property and is set equal to the hole sliding length of 100mm. The choice of this sliding length value derives from the assumption that typical RC frame structures reach failure for an inter-story drift close to 3% of the story height. The common buildings to be retrofitted with the e-CLT system have a story height of approximately 3m. Therefore, the sliding length was chosen to be 100mm, having some tolerance. The load protocols are presented in Tab.IV.2 and in Fig.IV.8.

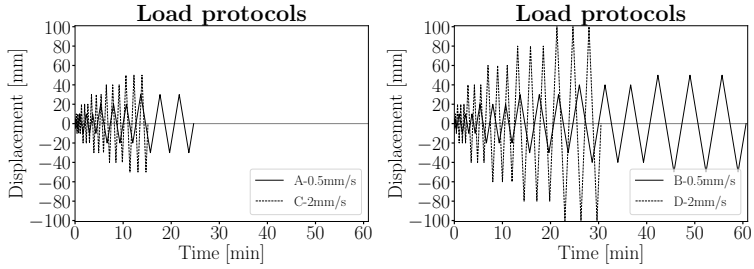

Fig. IV.8. Load protocols: (a) cyclic A 0.5mm/s, cyclic C 2mm/s; (b) cyclic B 0.5mm/s, cyclic D 2mm/s.

IV.3.3 Test overview

Table IV.2 lists the tests carried out in this campaign. The investigation consisted of two main parts. In first instance, for tests STD.1 till STD.4, the authors did not use shim layers or cap plates to examine the steel-to-steel erratic response and determine the consequences of the cap plate absence. In the second part of the tests, the authors included an 8mm cap plate and 2mm aluminum shim layers, as shown in Fig.IV.9, thus reproducing an AFC. The first test was monotonic, with a preload force of the bolts that clamp together the two profiles of the specimen equal to 70% of the bolt ultimate tensile strength, while the others were cyclic with a lower preload force. The lower preload force depended on the testing machine limitations in cyclic testing. Therefore, the authors preloaded the bolts to achieve an approximate 30kN slip force. It is essential to remark that the loading condition is not symmetric, and the specimen presents a complex shape. Therefore, the authors expect the occurrence of a certain deformation level; see [26, 48] for FEM analyses of the specimen. The testing procedure was the following: the bottom profile was mounted on the right column and the top profile was mounted on the T element. Each component was then aligned before inserting and preloading the two bolts that clamp the two profiles together and form the friction connection. A torque wrench was used to give the bolts the preload force, according to the torque method prescriptions of EN1090 [49] and the bolt producer instructions[50].

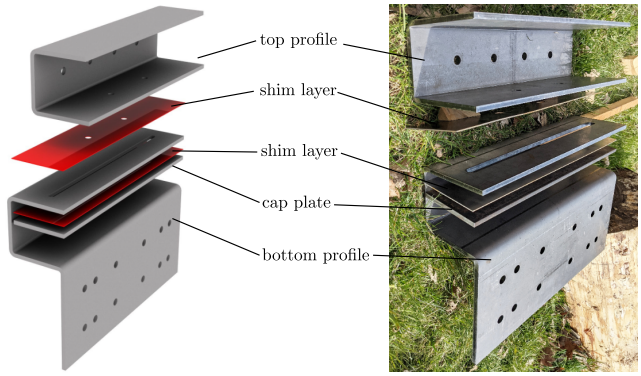

Fig. IV.9. Illustration and photo of the parts of a specimen.

Table IV.2. Test overview

Test Label	Specimen	Protocol	Speed [mm/s]	Shim	Preload [kN]
STD.1	STD_0	Monotonic	4.0	\	80.5
STD.2	STD_1	Cyclic A	0.5	\	24.1
STD.3	STD_1	Cyclic B	0.5	\	24.1
STD.4	STD_1	Cyclic B	0.5	\	24.1
STD.5	STD_2	Cyclic B	0.5	Aluminum	24.1
STD-R.1	STD-R_1	Cyclic B	0.5	Aluminum	24.1
STD-1H.1	STD-1H_1	Cyclic B	0.5	Aluminum	24.1
STD-1H.2	STD-1H_1	Cyclic B	0.5	Aluminum	45.3
ALT.1	ALT_1	Cyclic B	0.5	Aluminum	24.1
ALT.2	ALT_1	Cyclic B	0.5	Aluminum	36.0
ALT.3	ALT_1	Cyclic C	2.0	Aluminum	36.0
ALT.4	ALT_1	Cyclic D	2.0	Aluminum	36.0

Cyclic A: 1x5mm+3x10-20-30mm; speed 0.5 mm/s
Cyclic B: 1x5mm+3x10-20-30-40-50mm; speed 0.5 mm/s
Cyclic C: 1x5mm+3x10-20-30-40-50mm; speed 2 mm/s
Cyclic D: 1x5-10mm+3x20-40-60-80-100mm; speed 2 mm/s

IV.4 Results

This section illustrates the results of the testing campaign. Fig.IV.10, IV.11, IV.12 show the results in graphical form for all the specimens. For each specimen the first graph represents the force displacement loops, which provides insight on the overall behavior of the friction connection. The second graph visualizes the measured force plotted against time, for an enhanced readability of the stability of the force throughout the experiments. The third graph presents the dissipated energy during the testing, which is a useful parameter for the definition of the slip force, since it is an increasing function. Tab.IV.3 presents a summary of the results by reporting significant values, defined in the following paragraphs.
The definition of the slip force F_{slip} from the experimental data is neither straightforward nor unique. The author decided to use the same approach used by [31], which adopts a definition related to the dissipated energy E:

$$E = \sum_{i=0}^{n} E_i = \sum_{i=0}^{n} \left| \frac{F_{i+1} + F_i}{2} \cdot (\delta_{i+1} - \delta_i) \right| \tag{IV.1}$$

where E_i denotes the energy at the $i-$th time step, F_i and δ_i are the force and displacement at the same time step, respectively. The dissipated energy presents a strictly increasing trend, and is therefore a useful unambiguous parameter for the calculations, as opposed to the force value. The cumulative distance of travel D is the sum of the displacement time steps:

$$D = \sum_{i=0}^{n} |\delta_{i+1} - \delta_i| \tag{IV.2}$$

The slip force is defined as the work per unit of length:

$$F_{\text{slip}} = \frac{E}{D} \tag{IV.3}$$

The standard deviation is calculated with reference to the F_{slip} value:

$$F_{sd} = \sqrt{\frac{\sum_{i=0}^{n} |F_i - F_{\text{slip}}|^2}{n-1}} \tag{IV.4}$$

The Coefficient of Variation and the stability parameter λ are calculated as follows:

$$COV = \frac{F_{sd}}{F_{\text{slip}}} \qquad \lambda = \frac{1}{COV} \tag{IV.5}$$

These two values express the loop stability and the sliding behavior nature: a low COV, and thus a high λ value, corresponds to stable performance, resembling

the ideal rectangular shape. The experimental friction coefficient μ is calculated as follows:

$$\mu = \frac{F_{\text{slip}}}{n_s n_b F_P} \tag{IV.6}$$

where F_{slip} is the slip force calculated in Eq.(IV.3), n_s is the number of shear surfaces, n_b is the number of the preloaded bolts and F_P is the preload force from Tab.IV.2.

Table IV.3. Results of cyclic tests

Test	F_{slip} [kN]	F_{sd} [kN]	COV	λ	μ	Preload Loss
STD.1	59.94	12.11	0.20	4.95	0.19	Y
STD.2	10.61	5.62	0.53	1.89	0.11	Y
STD.3	19.99	12.02	0.60	1.66	0.21	N
STD.4	12.00	10.59	0.88	1.13	0.12	Y
STD.5	19.51	14.78	0.76	1.32	0.20	N
STD-R.1	20.49	12.79	0.62	1.60	0.21	N
STD-1H.1	8.10	1.44	0.18	5.62	0.08	Y
STD-1H.2	22.74	8.53	0.38	2.67	0.13	N
ALT.1	18.20	3.62	0.20	5.02	0.19	Y
ALT.2	30.79	7.51	0.24	4.10	0.21	Y
ALT.3	29.57	7.27	0.25	4.07	0.21	Y
ALT.4	28.79	6.80	0.24	4.23	0.20	Y

Figure IV.13 attempts to capture an essential aspect of the tests on friction connections: the definition of F_{slip} is substantially dependent on the loading path, while its value is not constant during the test. The authors presented the final values in Tab.IV.3, related to each test. They also plotted their time-dependency in Fig.IV.13. The x axis represents the displacement step (see Tab.IV.2 for the list of the displacement steps of the various load protocols), while, on the y axis, the circles represent the slip force calculated from the beginning of the test up to a specific displacement step. Figure IV.13 manifests two sorts of scatter: the "horizontal" variation, relative to changes in slip force between successive displacement steps, and the "vertical" variation. The latter derives from the repetition of three cycles at the same displacement step: a appreciable vertical distance between the three circles representing F_{slip} indicates a considerable variation of force during the repetitions of the same displacement step. In Fig.IV.13, the authors also reported the friction coefficients, which follow the same trend of the slip force.

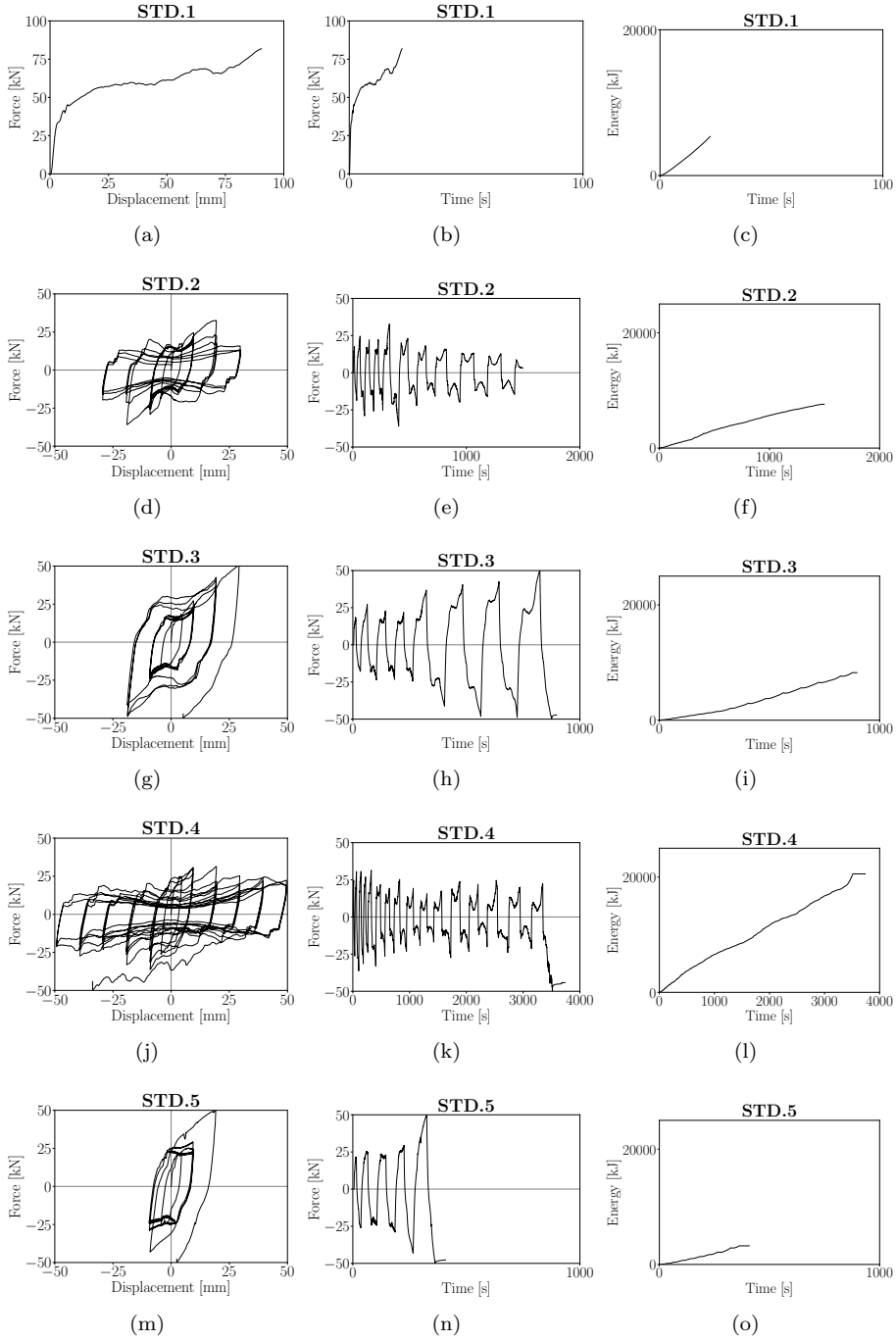

Fig. IV.10. Test results of STD specimens.

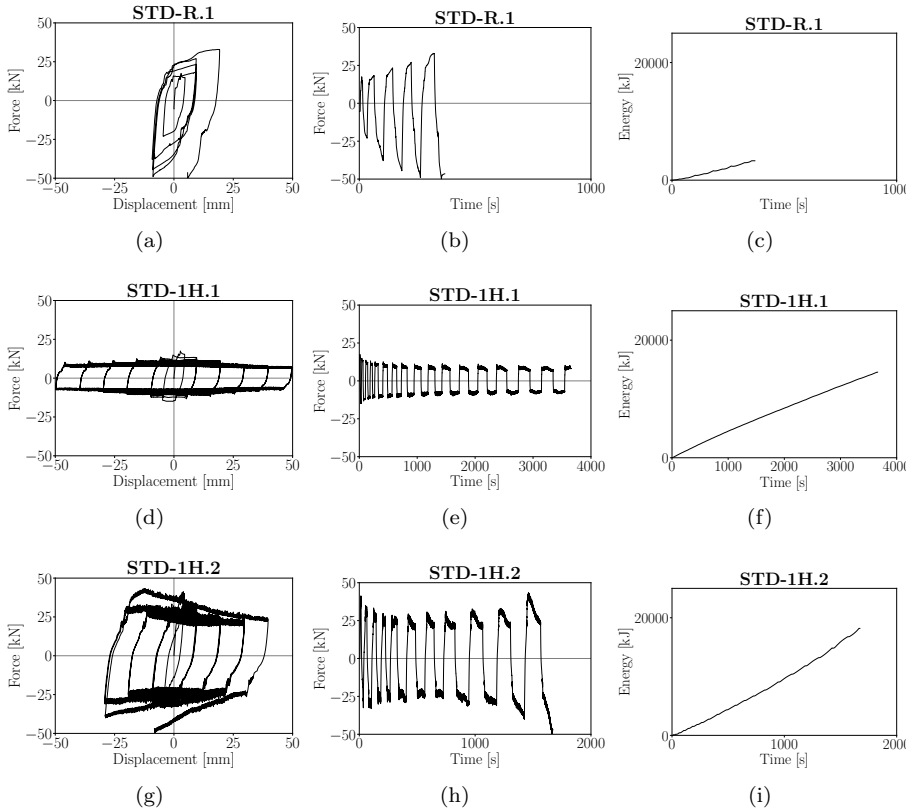

Fig. IV.11. Cyclic test results of STD-R and STD-1H specimens.

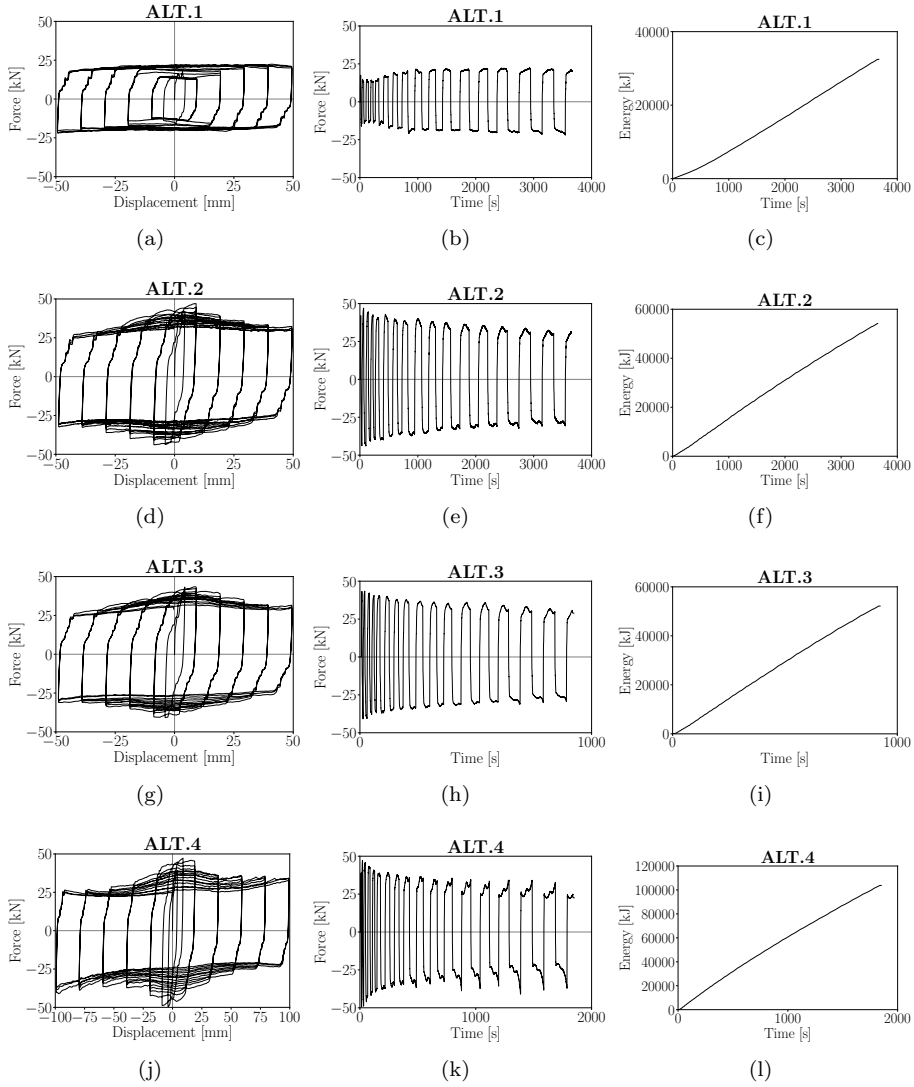

Fig. IV.12. Cyclic test results of ALT specimens.

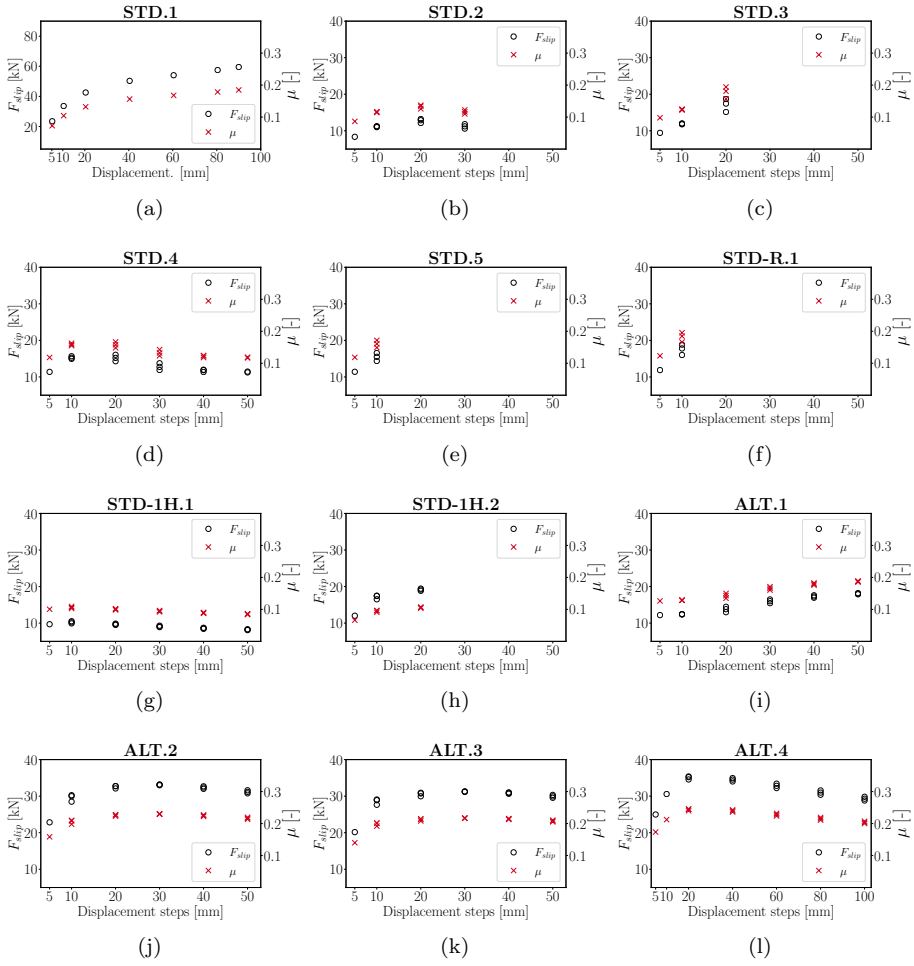

Fig. IV.13. Variation of slip force and friction coefficient during testing.

IV.5 Discussion

The first test, the monotonic STD.1, evidenced the weak point of the STD design from the very beginning. The outward bend of the bottom profile suffered from big deformations, which determined the test to stop. The FEM analysis in [26] also confirm the presence of strong stresses concentrations in that area, additional information is available in [48] and [51]. The load-displacement curve shows that the slip force was approximately 60kN, see Fig.IV.10(a). However, when the deformation of the bottom profile increased, the bolts started pressing against the side of the holes, thus increasing the resisting force. The increased resisting force did not depend on friction solely, but it was a combination of friction and bolts-holes plasticization. The deformations originated from the eccentricity between the applied force and the bend of the bottom profile: the upper part deformed outwards while the lower part deformed inwards, as seen in Fig.IV.14(a). Another significant deformation was a relative "twisting" between the two sliding surfaces, which made the previous effect even worse and was caused by the eccentricity between the two preloaded bolts, also marked in Fig.IV.14(b). Testing of the STD design specimen, despite some expected issues, was important to have a base for comparison with the further improvements. The goal was to understand if, with some improvements and small modifications of the STD design, it was possible to achieve satisfactory mechanical behavior with a design that offers the frontal mounting possibility.

In STD.2-3-4 tests, the preload force was lowered to 30% of the previous values and the speed was also reduced to 0.5mm/s, in order to obtain a lower slip force and minor deformations of the specimen. The curves of these tests, depicted in Fig.IV.10(d)-(g)-(j) and compared in Fig.IV.15, exhibit an extremely erratic shape, with unpredictable behavior: tests STD.2 and STD.4 present similar shapes and level of forces, while STD.3 reached higher forces rapidly, thus causing the stopping of the test before the completion of the whole protocol. Both test STD.2 and STD.4 exhibited preload losses in the bolts at the end of the test, but STD.3 did not. This occurrence may be the motivation for such prominent differences in behavior. In both STD.2 and STD.4 indeed, the hysteresis loops are remarkably similar, presenting a sudden drop in force after the initial peaks, possibly indicating the instant of preload loss. Twisting deformations were more pronounced throughout the whole duration of test STD.3, which was the one that retained the preload till the end of the test, if compared to STD.2 and STD.4. The STD.2 and STD.4 tests also presented twisting deformations, mostly during the initial part of the test. In all these experiments, significant deformations were always present in the outer bend of the bottom profile. The authors also observed a notable scraping of steel between the washers and the sides of the holes.

Test STD.5 had two modifications: an 8mm steel cap plate to limit steel scraping

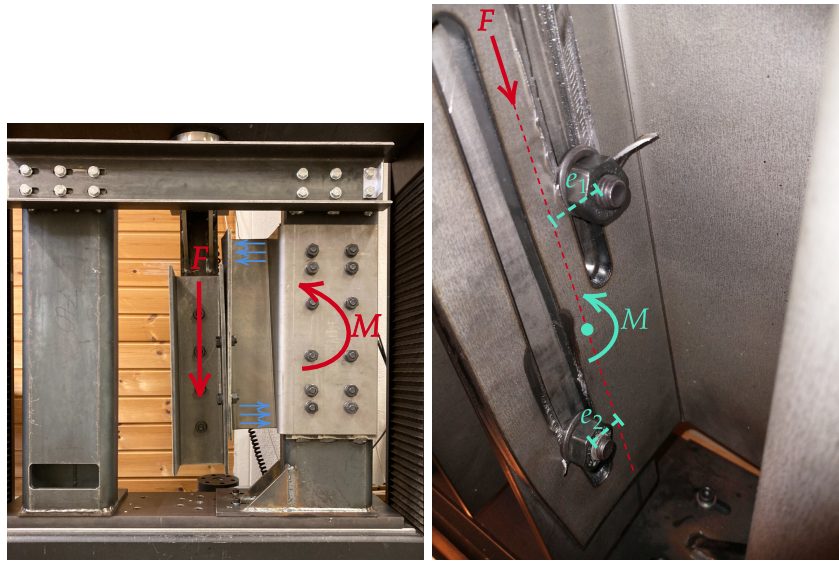

(a) (b)

Fig. IV.14. Test STD.1: schemes illustrating the observed deformations.

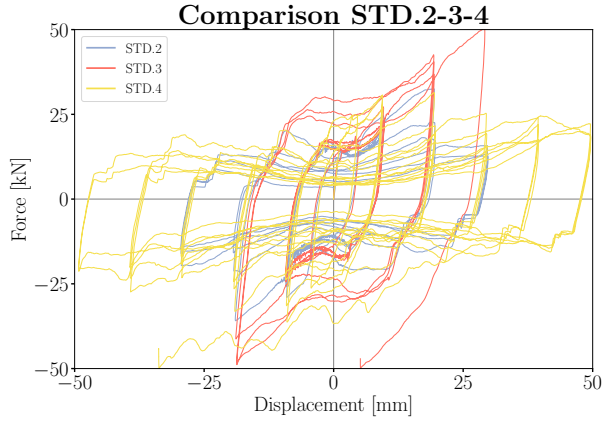

Fig. IV.15. Comparison between the results of tests STD.2, STD.3, STD.4.

and two shim layers made with 2mm thick aluminum to obtain more stable loops. The authors maintained this AFC configuration throughout the rest of the campaign. Nevertheless, the performances of STD.5 were still poor, see Fig.IV.10(m). As observed in the previous cases, STD.5 exhibited considerable deformations and consequent force spikes, which did not allow the completion of the loading protocol. The force continued increasing, with absence of preload losses at the end of the test. Again, the resisting force did not depend on the sole friction, but it was a combination of friction and bolts pushing against the holes. The values of the slip forces and friction coefficients of the STD tests, reported in Fig.IV.13, are then rather approximate, since the tests did not exhibit a pure frictional behavior.

Although the STD-R.1 specimen had additional reinforcements, the behavior was comparable to the STD.5 test, see Fig.IV.11(a). The reinforcement in the box-like part of the specimen contributed to isolate even more the weak spot evidenced during the FEM analyses: the outer bend of the bottom profile. Twisting was also present, and the big deformations and rapid force increase led the experiment to an early stop, as in the previous case.

STD-1H.1 showed an almost rectangular loop behavior, shown in Fig.IV.11(d). Twisting deformation was significantly reduced, indicating that a proper bolt arrangement in a single slotted centered hole effectively mitigated the detrimental phenomena identified for specimens STD and STD-R. The lower force level also determined a lower bending deformation than in previous cases. The preload was lost at the end of the test. This aspect also emerges from observing the value of the slip force, which presents some initial peaks around 16-17kN, later declining to $F_{\text{slip}} = 8.1\text{kN}$, as shown in Tab.IV.3 and Fig.IV.13(g). In the same figure, it is possible to see that the friction coefficient value is unexpectedly small. This value depends on the assumption of the initial preload force value used for calculation, which in reality decreased during the test. In test STD-1H.2, the authors increased the preload to obtain a higher slip force. Still, also higher deformations occurred. Twisting was more evident than in the previous case, even if more limited than in the STD specimens. The bending deformations were quite noticeable during this test, possibly due to the absence of significant preload losses. This phenomenon suggests that higher stresses arose inside the bottom profile. The force rapidly increased to the 50kN limit value of the testing machine during the early cycles, therefore the test stopped before the completion of the whole load protocol C.

ALT specimen showed promising results. The loops in Fig.IV.12(a) closely resemble a rectangular shape, and the force level agrees with analytical predictions. The friction coefficient is in accordance with scientific literature [38], approximately equal to 0.2 for aluminum, as observed from Fig.IV.13(i). Both twisting and bending deformations were almost absent during this test, meaning that the

reduced eccentricity and the single bend played a vital role in obtaining stable loops, confirming the initial FEM results of [26]. The loop shape presents a corner chipping when the load is changing direction: this is common in asymmetrical friction connections [31, 35] and depends on dragging phenomena of the cap plate. The preload force was then increased in the remaining tests on the ALT design, with the goal of reaching a 30kN slip force. ALT.2 results, shown in Fig.IV.12(d), present a lightly less stable behavior. Still, the slip force and friction values agree with the expected ones, as confirmed by Fig.IV.13(j). One significant difference in shape concerning the previous test regards the first cycles. There were lower initial resisting forces in test ALT.1, then stabilizing at higher values close to the slip force. Conversely, there were more prominent peaks in the initial cycles of test ALT.2, which then gradually declined and reached the stable force level. This aspect is also evident when comparing Fig.IV.13(i) and (j): while in the first case, it is possible to seize an increasing trend of the plotted F_{slip} development, in the second case, after the peak, the trend is decreasing. Test ALT.3 included a change of speed: from 0.5 to 2 mm/s. The results prove that the change in speed did not have any noticeable effect on the connection behavior, as highlighted by the comparison in Fig.IV.16, thus confirming one positive feature of friction connections: being independent from the speed of loading. The specimen was also the same as in the previous test, indicating that the connection response does not suffer cumulative damages. Friction coefficient values again agree well with [38], which found a dynamic friction coefficient value of 0.18 for aluminum and a static value of 0.34. The present test provides a friction coefficient value of 0.21 (dynamic condition), and a value of 0.33 when referred to F_{peak} (static initial condition). ALT.4 was the last test, and in this case, the displacement protocol reached the full 100mm sliding capability of the slotted holes. The load-displacement graph shows that up to 50mm, the behavior is the same as the previous tests, while for higher levels of displacements, there is a moderate loop instability. In these last three tests, slight twisting deformation was observed mainly at the change of direction of the load and not continuously as in the STD and STD-R design.

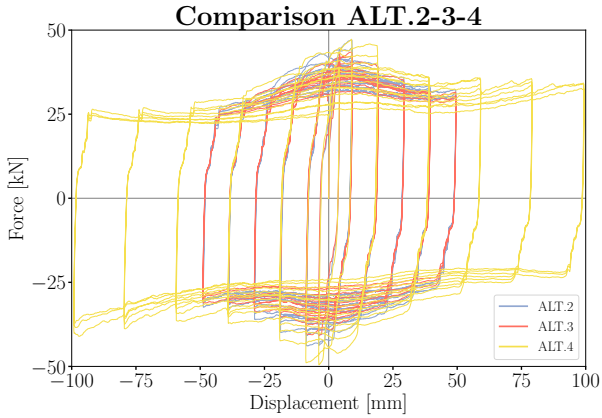

Fig. IV.16. Comparison between the results of tests ALT.2, ALT.3, ALT.4.

IV.6 Friction model

This section presents a possible approach for the simulation of the observed experimental behavior, for inclusion in further non-linear dynamic analysis. The performance of the AFC is mainly related to Coulomb friction. The function defining the friction force must take into account the observed force decrease with cycles:

$$F_{\text{slip}}(\epsilon) = \mu(\epsilon) F_P \,\text{sign}(\dot{d}) \tag{IV.7}$$

where $F_{\text{slip}}(\epsilon)$ is the slip force, F_P is the preload force, $\dot{d}$ the time derivative of the displacement, and ϵ is the cumulated dissipated energy. The friction coefficient is defined as:

$$\mu(\epsilon) = \mu_0(e^{-\xi\epsilon} + 1) \tag{IV.8}$$

where μ_0 and ξ are parameters estimated from the experimental data. As an example of application, Fig.IV.17 shows the superposition of experimental data and simulated model for the test ALT.3, the parameters μ_0=0.33 and $\xi = 0.00005$ were estimated from an ordinary least squares optimization. The proposed model accurately reproduces the experimental behavior, including the effect of decreasing slip force values for higher cycles. The energy dissipation is higher than the experimental value, and this is caused by the non-rectangular shape of the experimental loops, due to the corner chipping effect of asymmetric friction connections. The simple proposed model, on the other hand, generates loops with perfect rectangular shape, thus leading to higher dissipated energy values. The authors neglect this phenomenon at this stage, given the limited impact on the dissipated energy.

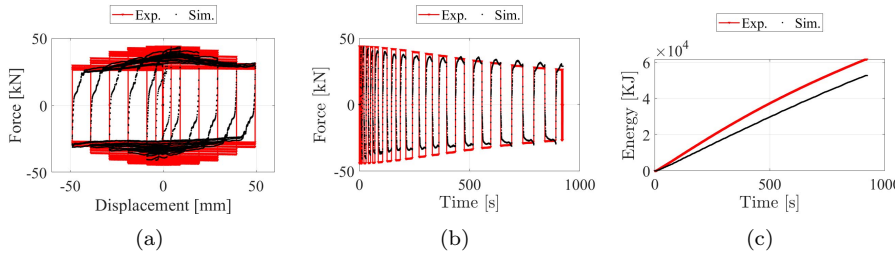

Fig. IV.17. Comparison between experimental data and exponential friction model: (a) Force–Displacement loop; (b) Force–Time function; (c) Cumulated dissipated energy–time function.

IV.7 Conclusion

This paper presents a testing campaign on a novel friction connection (FC) for seismic retrofitting of existing Reinforced-Concrete (RC) frame building. The entire system, called e-CLT, is part of the European Horizon 2020 project e-SAFE (Energy and Seismic AFfordable rEnovation solutions). The seismic retrofitting originates from the installation of CLT panels attached to the outside of a building with innovative friction connections. The connections are Asymmetrical Friction Connections, composed of a couple of cold-bent steel profiles. One steel profile is connected to the CLT panel, while the other to the RC beam. The two profiles are held together by preloaded bolts, which can slide in slotted holes and dissipate energy via friction. This paper focuses on the experimental tests of the FCs for the estimation of their dissipative capacity. The authors carried out an experimental campaign on four different geometries: the standard (STD), two variations -one with reinforcements (STD-R) and one with a single elongated hole (STD-1H)- and an alternative with reduced eccentricity and lower number of bends (ALT). The main findings were that STD and STD-R suffer from major deformations due to bending and twisting, and the reason lies in two features: an intrinsic weakness of the outer bend of the bottom profile, because of the eccentricity, and the presence of two not aligned elongated holes. STD-1H and ALT showed promising results, indicating that the arrangement of a single elongated hole solved some of the deformation problems, and that the reduced eccentricity and lower number of bends of ALT design was effective in isolating the friction behavior. The authors obtained acceptable results using aluminum for the shim layer, whose friction coefficient, nearly equal to 0.2, agree with literature formulations. Aluminum as shim material provided stable hysteresis curves, while its absence caused an erratic

response (e.g. steel-to-steel friction). ALT tests also confirmed the independence from loading speed of the friction connections. A possible modeling strategy is presented, based on an exponential Coulomb friction model, that reproduces the observed experimental behavior. In general then the main conclusions are that:

- the out of plane eccentricity, between the sliding force and the CLT restraint on the bottom profile, and the number of bends play the most important role: a limited depth of the connectors, aimed reducing the eccentricity, and a single bend are effective in limiting unwanted deformations and isolating the friction behavior;
- the arrangement of the bolts in two unaligned slotted holes is cause of additional eccentricities during the sliding movement: a single slotted hole with both bolts aligned is preferable to limit twisting deformations;
- a cap plate and shim layers are necessary to obtain an acceptable loop stability: aluminum shims provided satisfactory frictional behavior with an estimated 0.2 friction coefficient.
- An exponential Coulomb model represent a satisfactory strategy to model the observed experimental results of the AFC.

The major limitation of the experimental campaign presented in this paper is related to the limited number of specimens tested and replications. However, these tests allowed to study the system at the small scale related to the friction connection, which were useful to investigate the potential of the system. The tests confirmed that the performance parameters of the system are related to the geometry: being the eccentricity and the number of bends. As future works, the authors aim at expanding the experimental campaign by investigating the issues arisen during the current campaign: choice of different structural arrangements, use of different materials as shim layers with higher hardness than steel, developing hysteresis models for the complete e-CLT system [52, 53].

Appendix

This section provides the technical drawings of the tested specimen, which include the details on the measure and locations of the holes for the sliding movement. Figure IV.18 shows a technical drawing of the STD specimen, Fig.IV.19 of the STD-R specimen, Fig.IV.20 for the STD-1H specimen and Fig.IV.21 of the ALT specimen.

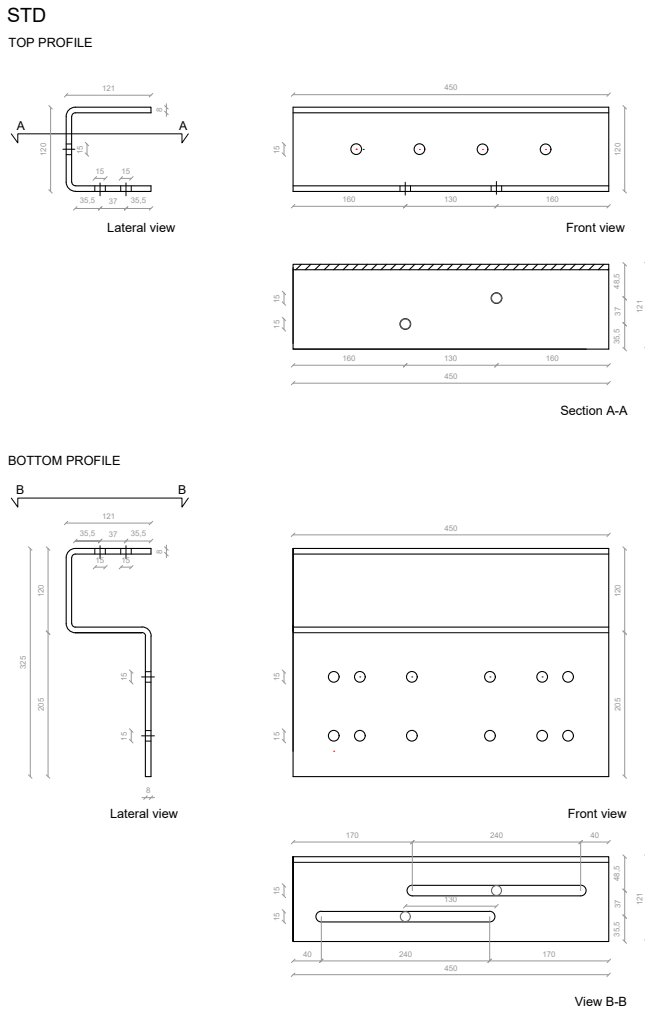

Fig. IV.18. STD specimen, measures in [mm].

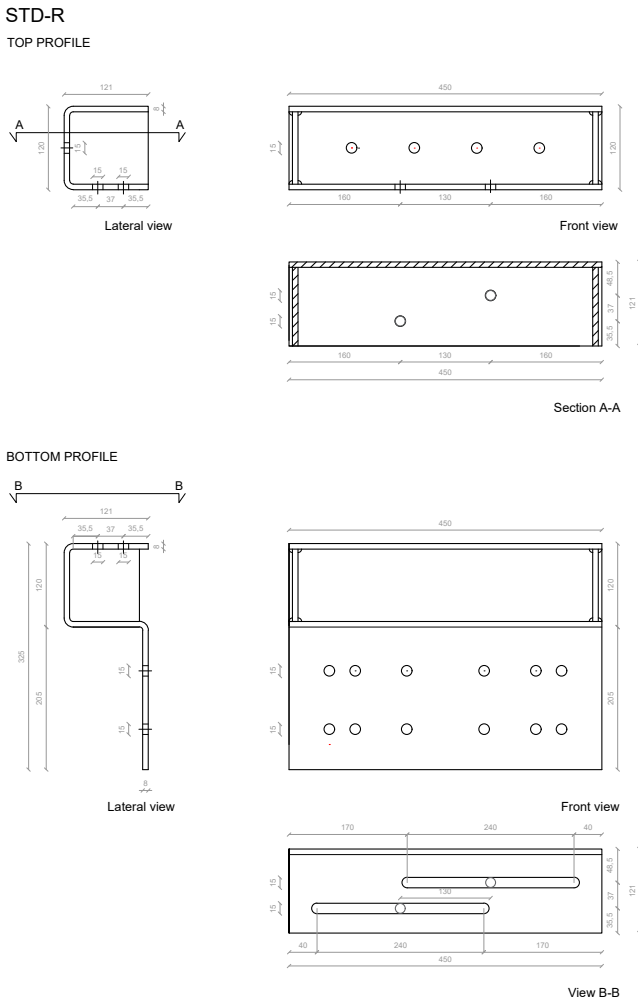

Fig. IV.19. STD-R specimen, measures in [mm].

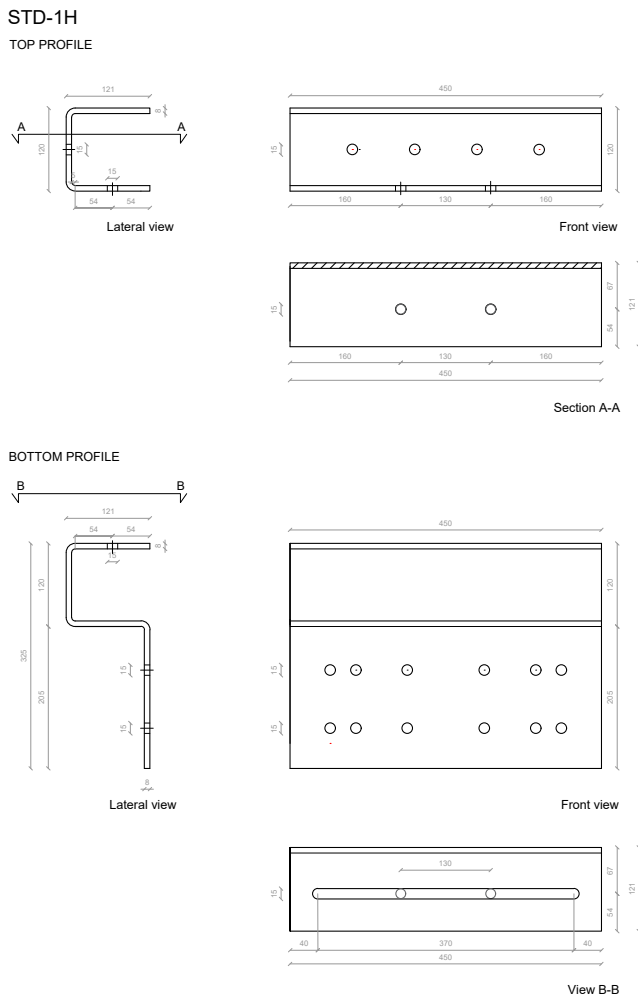

Fig. IV.20. STD-1H specimen, measures in [mm].

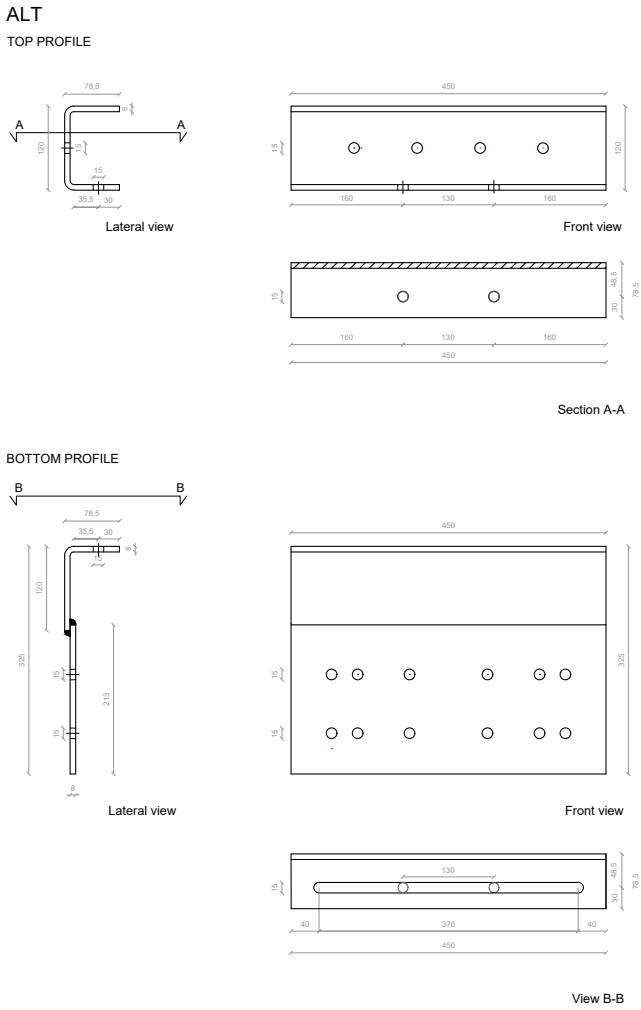

Fig. IV.21. ALT specimen, measures in [mm].

Funding

This paper was carried out in the framework of the "Energy and seismic affordable renovation solutions" (e-SAFE) project, which has received funding from the European Union's Horizon 2020 research and innovation programme under grant agreement No.893135. Neither the Executive Agency for Small and Medium-sized Enterprises (EASME) nor the European Commission is in any way responsible for any use that may be made of the information it contains.

Data availability statement

Some or all data, models, or code that support the findings of this study are available from the corresponding author upon reasonable request.

Acknowledgments

The authors would like to thank: Alberto Moretti and the Italian company Adveco s.r.l. for their relevant and continuous support during the prototyping stage and for providing the specimen for the testing campaign; the master student Mathilde Marthinsen for her precious contribution during the testing campaign and the head engineer of NMBU Øyvind Hansen for his continuous support regarding the design and production of the test setup.

Bibliography

[1] e-SAFE, "Energy and seismic affordable renovation solutions." `https://cordis.europa.eu/project/id/893135`. Accessed: 2021-03-23.

[2] e-SAFE, "Energy and seismic affordable renovation solutions." `http://esafe-buildings.eu/`. `http://esafe-buildings.eu/`.

[3] Horizon 2020, "Reducing energy consumption and carbon footprint by smart and sustainable use." `https://cordis.europa.eu/programme/id/H2020-EU.3.3.1.` Accessed: 2021-03-23.

[4] Istat, *Annuario Statistico Italiano*. Roma: Istituto nazionale di statistica, 2015. `https://www.istat.it/it/files//2015/12/Asi-2015.pdf` Accessed: 2021-03-23.

[5] S. J. Pantazopoulou, S. P. Tastani, G. E. Thermou, T. Triantafillou, G. Monti, D. Bournas, and M. Guadagnini, "Background to the european seismic design provisions for retrofitting rc elements using frp materials," *Structural Concrete*, vol. 17, no. 2, pp. 194–219, 2016.

[6] M. Di Ludovico, A. Prota, C. Moroni, G. Manfredi, and M. Dolce, "Reconstruction process of damaged residential buildings outside historical centres after the l'aquila earthquake: part i—" light damage" reconstruction," *Bulletin of Earthquake Engineering*, vol. 15, no. 2, pp. 667–692, 2017.

[7] N. Caterino, I. Iervolino, G. Manfredi, and E. Cosenza, "Multi-criteria decision making for seismic retrofitting of rc structures," *Journal of Earthquake Engineering*, vol. 12, no. 4, pp. 555–583, 2008.

[8] R. Dubey and P. Kumar, "Experimental study of the effectiveness of retrofitting rc cylindrical columns using self-compacting concrete jackets," *Construction and Building Materials*, vol. 124, pp. 104–117, 2016.

[9] C. Del Vecchio, M. Di Ludovico, A. Balsamo, A. Prota, G. Manfredi, and M. Dolce, "Experimental investigation of exterior rc beam-column joints retrofitted with frp systems," *Journal of Composites for Construction*, vol. 18, no. 4, p. 04014002, 2014.

[10] D. A. Bournas, T. C. Triantafillou, K. Zygouris, and F. Stavropoulos, "Textile-reinforced mortar versus frp jacketing in seismic retrofitting of rc columns with continuous or lap-spliced deformed bars," *Journal of Composites for Construction*, vol. 13, no. 5, pp. 360–371, 2009.

[11] A. Rahimi and M. R. Maheri, "The effects of retrofitting rc frames by x-bracing on the seismic performance of columns," *Engineering Structures*, vol. 173, pp. 813–830, 2018.

[12] A. Rahimi and M. R. Maheri, "The effects of steel x-brace retrofitting of rc frames on the seismic performance of frames and their elements," *Engineering Structures*, vol. 206, p. 110149, 2020.

[13] P. Javadi, A. Tizchang, A. GhafourianHesami, and M. Askari, "A friction-based connection for retrofitting rc frames by steel braced frames," in *Structures*, vol. 24, pp. 627–639, Elsevier, 2020.

[14] L. Di Sarno and G. Manfredi, "Seismic retrofitting with buckling restrained braces: Application to an existing non-ductile rc framed building," *Soil Dynamics and Earthquake Engineering*, vol. 30, no. 11, pp. 1279–1297, 2010.

[15] F. Barbagallo, M. Bosco, E. M. Marino, P. P. Rossi, and P. R. Stramondo, "A multi-performance design method for seismic upgrading of existing rc frames by brbs," *Earthquake Engineering & Structural Dynamics*, vol. 46, no. 7, pp. 1099–1119, 2017.

[16] P. Clemente and G. Buffarini, "Base isolation: design and optimization criteria," *Seismic isolation and protection systems*, vol. 1, no. 1, pp. 17–40, 2010.

[17] M. TahamouliRoudsari, M. Eslamimanesh, A. Entezari, O. Noori, and M. Torkaman, "Experimental assessment of retrofitting rc moment resisting frames with adas and tadas yielding dampers," in *Structures*, vol. 14, pp. 75–87, Elsevier, 2018.

[18] F. Barbagallo, I. Hamashima, H. Hu, M. Kurata, and M. Nakashima, "Base shear capping buildings with graphite-lubricated bases for collapse prevention in extreme earthquakes," *Earthquake Engineering & Structural Dynamics*, vol. 46, no. 6, pp. 1003–1021, 2017.

[19] H.-H. Khoo, C. Clifton, G. MacRae, H. Zhou, and S. Ramhormozian, "Proposed design models for the asymmetric friction connection," *Earthquake Engineering & Structural Dynamics*, vol. 44, no. 8, pp. 1309–1324, 2015.

[20] J. Borzouie, G. MacRae, J. Chase, G. Rodgers, and G. Clifton, "Experimental studies on cyclic performance of column base strong axis–aligned asymmetric friction connections," *Journal of Structural Engineering*, vol. 142, no. 1, p. 04015078, 2016.

[21] A. A. Rad, G. A. MacRae, N. K. Hazaveh, and Q. Ma, "Shake table testing of a low damage steel building with asymmetric friction connections (afc)," *Journal of Constructional Steel Research*, vol. 155, pp. 129–143, 2019.

[22] H.-H. Khoo, C. Clifton, J. Butterworth, and G. MacRae, "Experimental study of full-scale self-centering sliding hinge joint connections with friction ring springs," *Journal of Earthquake Engineering*, vol. 17, no. 7, pp. 972–997, 2013.

[23] A. Björnfot, F. Boggian, A. Nygård, and R. Tomasi, "Strengthening of traditional buildings with slim panels of cross-laminated timber (clt)," in *International Conference on Structural Health Assessment of Timber Structures*, 09 2017.

[24] I. Sustersic and B. Dujic, "Seismic strengthening of existing urm and rc structures using xlam timber panels," in *International conference on Earthquake Engineering*, 01 2013.

[25] F. Stazi, M. Serpilli, G. Maracchini, and A. Pavone, "An experimental and numerical study on clt panels used as infill shear walls for rc buildings retrofit," *Construction and Building Materials*, vol. 211, pp. 605–616, 2019.

[26] C. Tardo, F. Boggian, M. Hatletveit, E. Marino, G. Margani, and R. Tomasi, "Mechanical characterization of energy dissipation devices in retrofit solution of reinforced concrete frames coupled with solid wood panels," in *Proceedings of the 12th International Conference on Structural Analysis of Historical Constructions*, 2020.

[27] G. Margani, G. Evola, C. Tardo, and E. M. Marino, "Energy, seismic, and architectural renovation of rc framed buildings with prefabricated timber panels," *Sustainability*, vol. 12, no. 12, 2020.

[28] M. Latour, G. Rizzano, A. Santiago, and L. S. da Silva, "Experimental response of a low-yielding, self-centering, rocking column base joint with friction dampers," *Soil Dynamics and Earthquake Engineering*, vol. 116, pp. 580–592, 2019.

[29] W. Y. Loo, P. Quenneville, and N. Chouw, "A new type of symmetric slip-friction connector," *Journal of Constructional Steel Research*, vol. 94, pp. 11–22, 2014.

[30] W. Y. Loo, P. Quenneville, and N. Chouw, "A numerical study of the seismic behaviour of timber shear walls with slip-friction connectors," *Engineering Structures*, vol. 34, pp. 233–243, 2012.

[31] W. Loo, P. Quenneville, and N. Chouw, "A new type of symmetric slip-friction connector," *Journal of Constructional Steel Research*, vol. 94, pp. 11–22, 2014.

[32] W. Y. Loo, C. Kun, P. Quenneville, and N. Chouw, "Experimental testing of a rocking timber shear wall with slip-friction connectors," *Earthquake Engineering & Structural Dynamics*, vol. 43, no. 11, pp. 1621–1639, 2014.

[33] W. Y. Loo, P. Quenneville, and N. Chouw, "Rocking timber structure with slip-friction connectors conceptualized as a plastically deformable hinge within a multistory shear wall," *Journal of Structural Engineering*, vol. 142, no. 4, p. E4015010, 2016.

[34] W. Y. Loo, P. Quenneville, and N. Chouw, "The influence of surface preparation and the lubricating effect of mill scale on the performance of slip-friction connectors," *Construction and Building Materials*, vol. 155, pp. 1025–1038, 2017.

[35] D. Fitzgerald, A. Sinha, T. H. Miller, and J. A. Nairn, "Axial slip-friction connections for cross-laminated timber," *Engineering Structures*, vol. 228, p. 111478, 2021.

[36] D. Fitzgerald, T. Miller, A. Sinha, and J. Nairn, "Cross-laminated timber rocking walls with slip-friction connections," *Engineering Structures*, vol. 220, 2020.

[37] J. C. Chanchi Golondrino, G. A. MacRae, J. G. Chase, G. W. Rodgers, and G. C. Clifton, "Seismic behaviour of symmetric friction connections for steel buildings," *Engineering Structures*, vol. 224, p. 111200, 2020.

[38] J. Golondrino, G. MacRae, J. Chase, and G. Rodgers, "Behaviour of asymmetrical friction connections using different shim materials," in *New Zealand Society for Earthquake Engineering Conference*, 2012.

[39] J. Golondrino, G. MacRae, J. Chase, G. Rodgers, and C. Clifton, "Clamping force effects on the behaviour of asymmetrical friction connections (afc)," in *15th World Conference on Earthquake Engineering*, (Lisboa, Portugal), 2012.

[40] J. Golondrino, G. MacRae, J. Chase, G. Rodgers, and C. Clifton, "Effects of the bolt grip length on the behaviour of asymmetrical friction connections (afc)," in *New Zealand Society for Earthquake Engineering Conference*, 2016.

[41] J. C. C. Golondrino, G. A. MacRae, J. G. Chase, G. W. Rodgers, and G. C. Clifton, "Asymmetric friction connection bolt lever arm effects on hysteretic behaviour," *Journal of Earthquake Engineering*, vol. 0, no. 0, pp. 1–22, 2020.

[42] J. C. Chanchi Golondrino, G. A. MacRae, J. G. Chase, G. W. Rodgers, and G. C. Clifton, "Hysteretic behaviour of asymmetrical friction connections using brake pads of d3923," *Structures*, vol. 16, pp. 164–175, 2018.

[43] G. W. Rodgers, R. Herve, G. A. MacRae, J. Chanchi Golondrino, and J. G. Chase, "Dynamic friction coefficient and performance of asymmetric friction connections," *Structures*, vol. 14, pp. 416–423, 2018.

[44] J. C. Chanchi Golondrino, G. A. MacRae, J. G. Chase, G. W. Rodgers, and G. C. Clifton, "Asymmetric friction connection (afc) design for seismic energy dissipation," *Journal of Constructional Steel Research*, vol. 157, pp. 70–81, 2019.

[45] S. Jaisee, F. Yue, and Y. H. Ooi, "A state-of-the-art review on passive friction dampers and their applications," *Engineering Structures*, vol. 235, p. 112022, 2021.

[46] ISO16670, "Timber structures — joints made with mechanical fasteners — quasi-static reversed-cyclic test method," 2003.

[47] EN15129, "Anti-seismic devices," 2018.

[48] M. R. Hatletveit, "Mechanical assessment of a steel dissipating system for RC buildings retrofitting with CLT panels," Master's thesis, Norwegian University of Life Sciences, 2020.

[49] EN1090-2, "Execution of steel structures and aluminium structures - part 2: Technical requirements for steel structures," 2018.

[50] SBE-Varvit, "Structural bolting assemblies en 14399 preloaded assemblies." Accessed: 2021-09-11.

[51] M. B. A. Marthinsen, "Experimental Assessment of a Steel Dissipating System," Master's thesis, Norwegian University of Life Sciences, 2020.

[52] A. Aloisio, R. Alaggio, J. Köhler, and M. Fragiacomo, "Extension of generalized bouc-wen hysteresis modeling of wood joints and structural systems," *Journal of Engineering Mechanics*, vol. 146, no. 3, p. 04020001, 2020.

[53] A. Aloisio, R. Alaggio, and M. Fragiacomo, "Equivalent viscous damping of cross-laminated timber structural archetypes," *Journal of Structural Engineering*, vol. 147, no. 4, p. 04021012, 2021.

V. Experimental and analytical study of friction connection for seismic retrofit with CLT panels

Bibliographic data

F. Boggian, A. Aloisio, and R. Tomasi, "Experimental and analytical study of friction connection for seismic retrofit with CLT panels," *Earthquake Engineering and Structural Dynamics*, 2022. Doi

Contents

abstract

Within the European project e-SAFE (Energy and Seismic AFfordable rEnovation solutions), this paper presents the experimental tests and modeling attempts for a class of Asymmetric Friction Connections (AFC) tested in the laboratories of the Norwegian University of Life Sciences. The AFCs are part of the seismic retrofitting solution, called e-CLT, based on installing Cross-Laminated Timber (CLT) panels in reinforced concrete structures using friction connections. The authors carried out experimental tests on AFCs fixed with screws to a CLT panel to observe the contribution of timber to the total dissipation performance. The investigation is based on 20 cyclic test data with two different setups. The main one includes a CLT panel and screw connection, while the second one isolates the friction behaviour to evaluate the influence of the screw connection. A modified LuGre hysteresis model for friction is developed to simulate the experimental cyclic response of the tested specimen. The model possesses a direct physical meaning, and it explicitly depends on the slip force and the pre-slip stiffness. The optimized model is used to assess the performance of the AFC by varying the pre-slip stiffness and the slip force.

Keywords:

Friction connection; seismic; energy dissipation; renovation; CLT

V.1 Introduction

There are three primary dissipation devices for seismic retrofitting purposes: the Active, Semi-Active and Passive devices [1, 2, 3, 4, 5, 6]. The most used passive dampers are probably the hysteretic devices, generally used for base isolation [7, 8]. However, among hysteretic devices, friction dampers have been gaining more attention in the last few years.

These dampers dissipate seismic energy by mechanical damping through sliding friction with the primary "braking rather than breaking" principle [9]. There is a wide range of applications of friction dampers, from civil to mechanical and avionic engineering [10, 11]. However, there are still a few attempts in using friction dampers for seismic retrofitting of civil structures.

Pall et al. in 1980 [9], was the first to add friction devices as additional damping sources in civil structures. The Limited Slip Bolt (LSB), evolved to the Pall Frictional Damper (PFD), exhibited stable, almost rectangular hysteresis cycles [12, 13]. PFD are conceived for X- and K-bracings. Its worldwide success has confirmed the merits of the PFD. Multiple applications and research papers

are proving the value and efficiency of the PFD [14, 15, 16, 17, 16]. The main drawbacks of PFD are the relatively low capacity (less than 10 kips), the need for high precision work for its manufacture and specialized training for the installation process [18, 19].
In 1989 Fitzgerald et al. [20] devised a friction connection called Slotted Bolted Connection (SBC), characterized by a more straightforward design than the PFD. The proposed SBC worked by sliding channel bracing plate over a gusset plate interconnected by high strength bolts with washers (Belleville spring) for adjusting the bolt tension.
There are two main classes of SBC: the Symmetric and Asymmetric friction connection [21, 22], see Fig.V.1. Both system are based on using three main plates clamped together with pre tensioned bolts, with the central one presenting a slotted hole that allows for the sliding movement. Shim layers of different materials may be present in the two shear plane to improve friction stability. Symmetric Friction Connection (SFC) is a type of SBC where the loading condition is symmetric, so the sliding force is applied to the middle slotted plate and the reaction force is divided equally between the other two plates. Initially proposed by Clifton, Asymmetric Friction Connection (AFC) is another type of SBC [23, 24]. In this case the loading condition is asymmetric: the sliding force is applied to the middle slotted plate but the reaction force is resisted only by one of the other two plates, so the other one act as a cap plate that is simply dragged by the rest of the system [25].
There are already several experimental tests proving the successful hysteretic

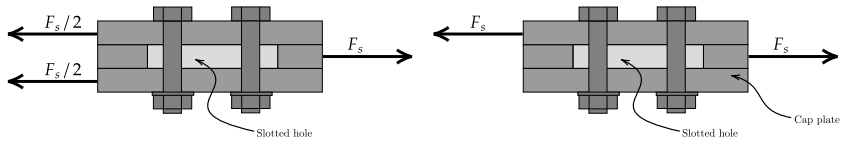

Fig. V.1. (a) Symmetric and (b) Asymmetric Friction connections.

performance of the AFC. This paper discusses a possible application of AFC integrated with CLT panels for the seismic retrofitting of existing RC buildings [26, 27].
AFCs are more commonly applied to steel buildings [28]. Friction devices coupled with other structural components are also known as hybrid systems. Among hybrid devices, the coupling between friction connections and timber embodies a significant innovation in structural engineering. Loo et al. [29] investigated the possibility of using SFC instead of hold-down for restraining timber shear walls against uplift, to cap the force transmitted to the wall, and reduce inelastic damage. The subsequent experimental campaigns by [30, 31] established the effectiveness of SFC on reducing the degradation and pinching phenomena typical

of timber connections. The following studies by [32] pointed to a displacement-based design method for multistory CLT buildings with friction connections. Following [30, 31], Fitzgerald et al. [33] studied the response of SFC connected to a CLT panel [34].
The combined use of CLT panels and AFC for the seismic retrofitting of RC structures has never been investigated so far [35].
In RC buildings with masonry infill, CLT panels can be used in addition, or substitution [36, 37] of existing masonry infill. The main issue related to these interventions is executing an appropriate connection system between the CLT panel and the existing structure. The system suggested by the authors is called e-CLT, see Fig.V.2, and consists of CLT panel attached from the outside of the building while leaving the masonry infills unchanged, without discomfort for the people living inside the building [38]. The CLT panel is not inside the RC frame, as in the masonry infill, but in front of it. So its kinematics and deformation response does not interfere with the RC frame during the seismic excitation. CLT panels are lightweight (around 470 kg/m3), thus not significantly raising the mass of existing buildings. Non secondarily, CLT panels possess a high level of prefabrication and all the benefits of dry interventions. The major innovation of the e-CLT retrofitting intervention stands in the connection system between CLT and the existing building: an AFC.
The AFC is constituted by a couple of steel profiles connected to the existing beam and the CLT panel, clamped together by preloaded bolts. One of the two profiles presents a slotted hole, which enables their mutual sliding. Single CLT panels are connected to the RC beams of the structure by at least two AFC. The possible critical point of this structural arrangement is related to the CLT panel uplift due to its significant in-plane stiffness. The uplift might cause a de-tensioning of the pre-loaded bolts. Therefore, particular attention must be paid to the stiffness of the connection, which should not adsorb the panel rotation. Parallelly, the e-CLT should be designed to withstand out-of-plane forces arising from the out-of-plane behaviour of the masonry infill. However, this aspect is outside the scope of the current research.
The size of the CLT panels is related to that of the bays without openings where they are applied. The e-CLT technology can be combined with non-structural framed panels that may be applied to the walls with openings and are equipped with high-performing windows that replace the existing ones. Both panels integrate insulation materials to improve the energy efficiency of the building and finishing layer. The retrofit system also provides technological solutions to cover the AFC devices after the panels' installation, ensuring their inspection and maintenance [39].
Boggian et al. [40] focused on the shape optimization of the steel profiles and did not study the interaction with the timber component. The experimental

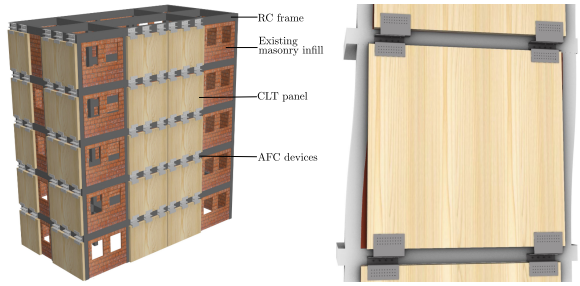

Fig. V.2. e-CLT seismic retrofit system, modified from [40].

activity was directed at isolating the friction behavior of the AFC, representing the innovative part of the system. However, the deformability and damage of the timber connection can potentially undermine the effectiveness of the friction connection. Therefore, the experimental investigation on the interaction between the AFC and the CLT panel should be understood.
Given the above, the main novelties and objectives of this research are:

- Experimental tests of AFC connected to CLT specimens under cyclic loading;
- Comparison between experimental tests on AFC without connection to the CLT specimen to estimate the effect of the connection on the hysteretic response;
- Development of an analytical friction model, derived from the LuGre model, capable of mirroring the stabilization of the friction coefficient as dissipated energy grows; The model is a possible trade-off between model complexity and accuracy.
- Estimate the parameters of the proposed analytical model for each tested specimen using a global optimization algorithm;
- Evaluate the pre-slip stiffness effect and proposal a design formula to predict the lower bounds of the pre-slip stiffness to obtain a correct performance;
- Discussion on the performance of the tested assemblies under multiple repetitions of the same cyclic load protocol.

The paper has the following organization. The second section presents an introduction of the current experimental campaign by highlighting the differences to the previous one detailed in and details the experimental tests, while the third

section deals with the results of the experimental tests. The fifth section deals with the analytical hysteresis modeling and the estimation of the parameters using a global optimization algorithm. The last section addresses the issue of pre-slip stiffness and stability of the dissipated energy. It also compares analytical formulations for predicting the stiffness of the screwed connection.

V.2 Materials and methods

V.2.1 Specimen

The specimen is called HYB (Hybrid), since its design originated from the results of the previous campaign [40]: STD offered the positive feature of the front mounting possibility, while ALT offered better mechanical performances due to the single bend L shape. HYB attempts to combine the best features of the two previous designs: front mounting and simple L shape, see Fig.V.3,V.4. The reader is referred to [40] for the previous campaign, and to [41] for more details on the conceiving of this HYB design.
The specimen is made of two 8mm thick cold bent S355 steel profiles: the anchor profile is connected to the moving head of the press (the existing RC beam for the real world case), while the free profile is connected to the CLT panel. The two profiles are clamped together to form an asymmetric friction connection (AFC) by adding an 8mm steel cap plate and two 2mm aluminum shim layers. The connection between the two profiles is ensured by two high strength M16 10.9 bolts [42], that will slide in a 17mm wide elongated hole. The elongated hole is 100mm long plus some tolerance, and allows for relative sliding between the two profiles. The sliding length was chosen by considering the assumption that typical RC frame reach failure at an inter story drift of 3% of the story height, and a common height value for the type of building object of renovation is 3m.

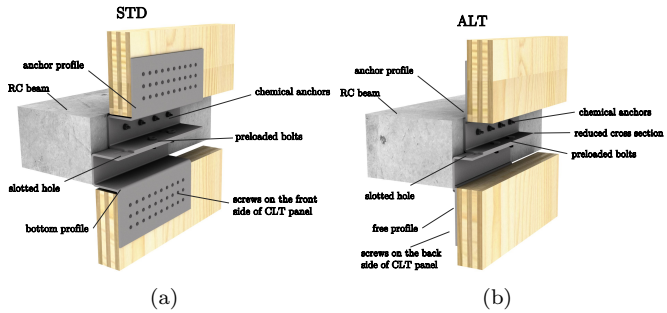

Fig. V.3. Specimen STD and ALT from previous experimental campaign, [40]

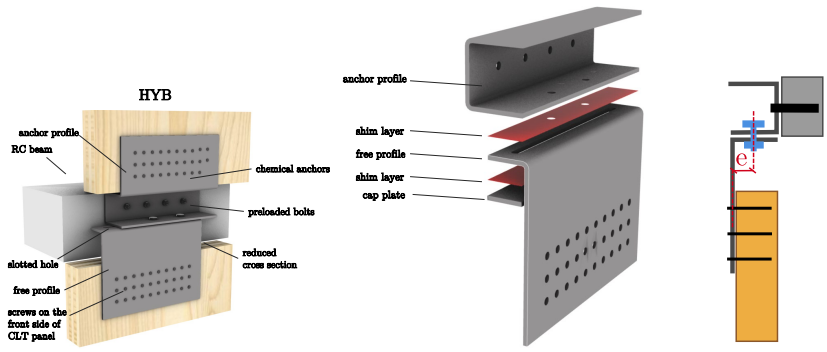

Fig. V.4. Specimen HYB tested in the current experimental campaign: (a) parts of the system in a real building, (b) parts of the specimen used for testing, (c) eccentricity of the specimen.

Three different types of specimen were tested, see Tab.V.1. All had the same overall dimensions and shape, but presented small geometric variations. Specimens HYB (reference design, 3 samples) and HYB_e (1 sample) differed in the eccentricity of the friction connection with respect to the screw connection, see Fig.V.4(c): HYB had the elongated hole in the center of the specimen width, while in HYB_e the elongated hole was moved towards the CLT side, to see if this had an impact on the mechanical behavior. In both cases the free profile presented 33 holes for a screw connection to the CLT panel. The screws were 10x80mm HBS Plate Evo from Rothoblaas [43]. Both these type of specimens were tested in the same setup, with a piece of CLT panel 100mm thick, 5 layers and of dimensions 400x800mm. The specimen HYB_s (1 sample), which had the same eccentricity as the HYB, was used on a different setup: a steel column was used as support for the free profile instead of a CLT panel, thus the hole pattern was different since bolts were used instead of screws. This specimen was made in order to have a direct comparison regarding the effect of the screw connection on the friction behavior of the system.

V.2.2 Setup and load protocol

The tests were carried out in the timber laboratory of the Norwegian University of Life Sciences. The setup comprising the CLT panel can be seen in Fig.V.6, and was devised in order to simulate the sliding movement that would occur in a real building condition. The anchor profile, simplified to a C shape for testing purposes, was rigidly attached to a T shape element connected to the actuator of

Table V.1. Description of the specimens.

Prototype	n	e [mm]	Setup
HYB	3	52.5	with CLT
HYB_e	1	43.5	with CLT
HYB_s	1	52.5	no CLT

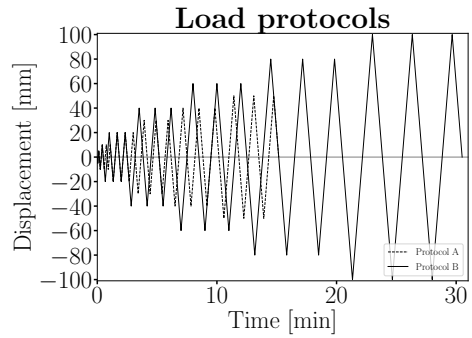

Fig. V.5. Load protocols: Protocol A: 1x5mm+3x10-20-30-40-50mm; 2mm/s; Protocol B: 1x5-10mm+3x20-40-60-80-100mm; 2mm/s.

the press machine. The free profile was connected with screws to the CLT panel, which was held in place by a hold down and UPN profiles connected to base of the press with threaded rods. The hold down was custom made, with 10mm thick steel plates, 22 10x80mm screws for the timber and one M30 bolt at the base. The machine applied a vertical sliding movement, which would be equivalent to the horizontal movement of an RC beam in a real case building. The machine used for the experiments was electro mechanical, and recorded force measures with a load cell of 1200 kN capacity. Measures of displacement were recorded both by the press itself and by an additional wire sensor, attached to the anchor profile and aligned with the actuator. Additional sensors were placed to record the deformations of the screw connection and of the CLT panel. Two LDTs were placed on the free profile, taking vertical measures of the displacement at its center: one was fixed at the base of the press, and the other was fixed to the CLT, thus measuring the relative slip between the steel profile and timber. One inclinometer was placed on the free profile, and another one was placed on the narrow side of the CLT panel. The last LDT was placed on the opposite side at the base of the CLT panel, in order to check the sufficient stiffness of the hold down. A thermocouple measured the temperature on the friction connection. A drawing of the sensors layout and parts of the setup can be seen in Fig.V.7. The setup for the tests on the HYB_s specimen, which was tested without CLT panel to study the influence of the screw connection, was the same as the experiments presented in [40]. The fixed profile was connected to the press in the same way as the previous tests, while the free profile was rigidly connected to a steel column, part of a frame fixed at the base of the press, see Fig.V.8. The load protocol was applied in displacement control, with a constant speed of 2mm/s. The protocol was cyclic, adapted from the prescriptions of EN15129[44], which suggests incremental steps of displacement till reaching the ultimate displacement. In the case of friction connection the ultimate displacement was considered as the maximum sliding clearance of the elongated holes, which was 100mm. The two protocols are visible in Fig. V.5.

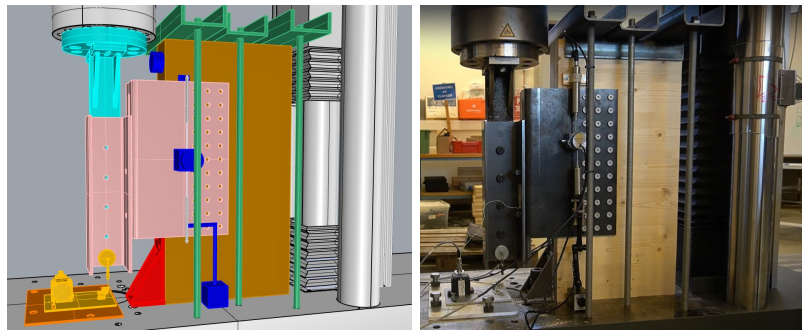

(a) (b)

Fig. V.6. (a) Model of the setup, (b) picture of the setup. In both images the press is pushing down 100mm.

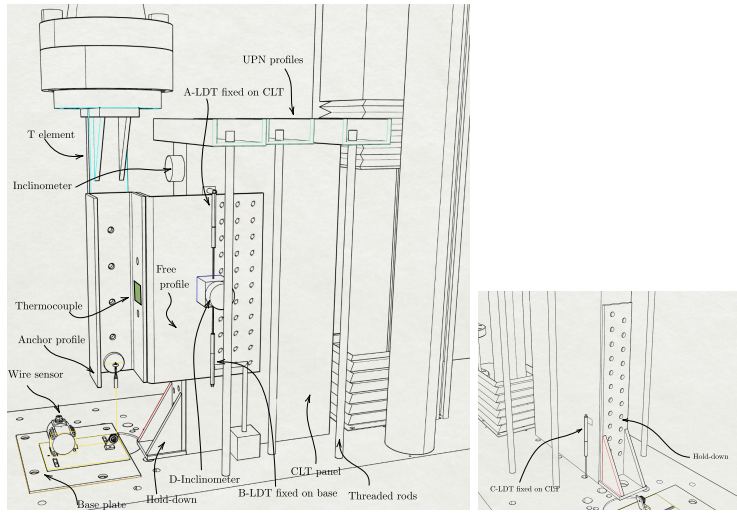

(a) (b)

Fig. V.7. Parts of the CLT setup. The letters associated with some of the sensors help the readability of the results in Fig.V.14.

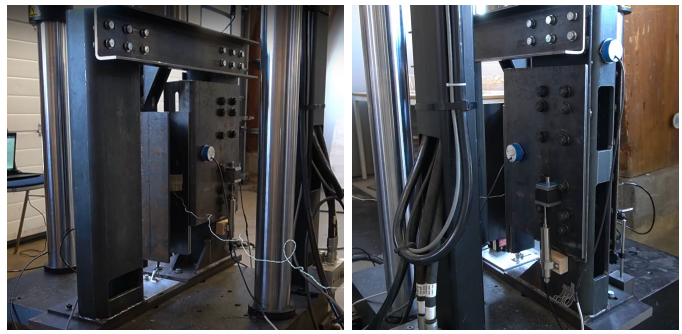

(a) (b)

Fig. V.8. (a) Setup for HYB_s experiments, (b) detail of the free profile bolted to the steel column. In both images the press is pushing down 100mm.

V.2.3 Test overview

Tab.V.2 summarizes the 20 tests that are presented in this paper. The first part of the testing campaign (on specimens with design HYB and HYB_e) was carried out on the main setup that includes the CLT panel. The last 5 tests, on the HYB_s specimen, were performed on the secondary setup which was made of steel and didn't include the CLT panel. The labels of the tests are as follows: ¡name of design¿-¡number of sample¿.¡number of repetition¿, so for example the label *HYB-2.3* indicates the third test on the second sample with HYB design. The preload was set initially to 25kN per bolt, which would yield a sliding force of 20kN, considering a 0.2 friction coefficient of aluminum. The preload value was then increased to 37.5kN, in order to reach a sliding force of 30kN. The preload was applied by using the torque method described in the standard EN1090-2 [45] and following the specification of the bolt producer [46].

V.3 Results and discussion

Fig.V.9,V.10,V.11,V.12 show the results in terms of force-displacement hysteresis loops. The overall behaviour can be assimilated to a rigid-plastic system, which would have a perfectly rectangular shape for an ideal friction connection—the loops exhibit force peaks during the initial cycles. The peaks decrease and stabilize at higher levels of displacements. This phenomenon was also observed in the previous experimental campaign due to degradation agents related to wear phenomena. Indeed the shape of the hysteresis curves tends to flatten after successive repetition on the same specimen, confirming the observed degradation. A visual inspection of the curves does not manifest meaningful differences between HYB specimens and HYB_e specimen, suggesting that the small difference in eccentricity (see Fig.V.4(c) and Tab.V.1) does not play an essential role in the friction behaviour. Therefore, the HYB and HYB_e specimens may be considered equivalent. Interesting remarks arise by comparing the plots of the tests referred to the steel setup, shown in Fig.V.12, and the plots associated with the setup including the CLT panel and screw connection. In both cases, some corner chipping is present, typical of AFCs. However, the loss of energy at the change of loading direction is more prominent in the tests with the CLT panel, implying that the added deformability due to the screw connection modified the friction behaviour to a certain extent and resulted in a loss of dissipated energy. The shape is also more rectangular in the tests without CLT panels. The parts of the hysteresis curve associated with changes of load direction are almost vertical, while the tests including CLT present an S-like shape, more evident in the initial cycles, due to pinching behaviour typical of timber connections.

Tab.V.3 presents the results as values of the slip force and friction coefficient.

Table V.2. Overview of the tests.

Test Label	Specimen	Protocol	Setup	Preload [kN]
HYB-1.1	HYB-1	A	CLT	25.0
HYB-1.2		A	CLT	25.0
HYB-2.1	HYB-2	B	CLT	25.0
HYB-2.2		B	CLT	25.0
HYB-2.3		B	CLT	25.0
HYB-2.4		B	CLT	25.0
HYB-3.1	HYB-3	B	CLT	25.0
HYB-3.2		B	CLT	25.0
HYB-3.3		B	CLT	25.0
HYB-3.4		B	CLT	25.0
HYB_e-1.1	HYB_e-1	B	CLT	25.0
HYB_e-1.2		B	CLT	25.0
HYB_e-1.3		B	CLT	37.5
HYB_e-1.4		B	CLT	37.5
HYB_e-1.5		B	CLT	37.5
HYB_s-1.1	HYB_s-1	B	no CLT	25.0
HYB_s-1.2		B	no CLT	25.0
HYB_s-1.3		B	no CLT	37.5
HYB_s-1.4		B	no CLT	37.5
HYB_s-1.5		B	no CLT	37.5

Protocol A: 1x5mm+3x10-20-30-40-50mm; 2mm/s
Protocol B: 1x5-10mm+3x20-40-60-80-100mm; 2mm/s

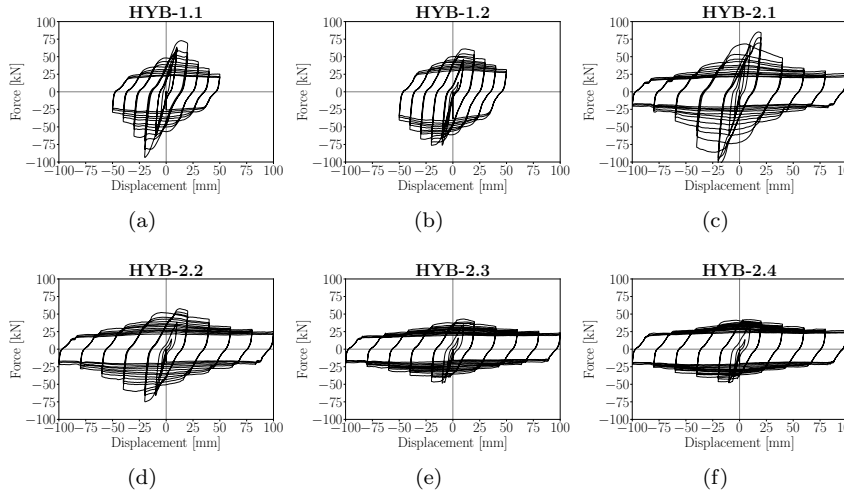

Fig. V.9. Test results of specimen HYB-1 and HYB-2, all with preload 25kN.

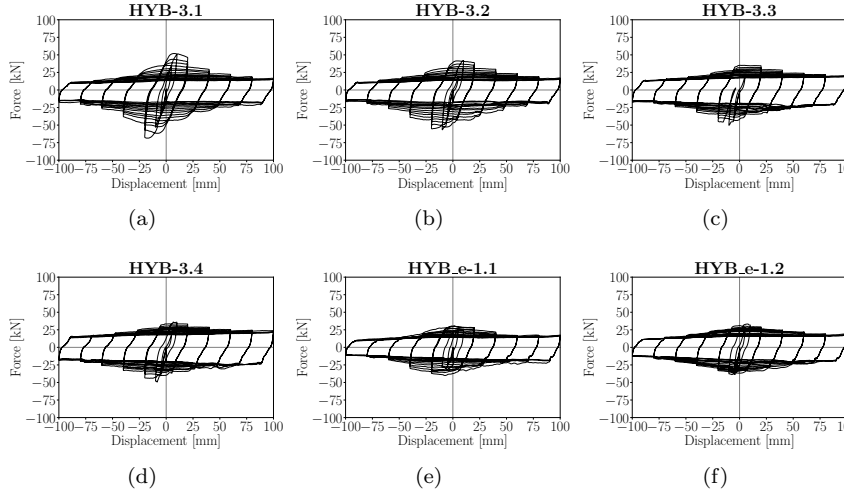

Fig. V.10. Test results of specimen HYB-3 and part of HYB_e.1, all with preload 25kN.

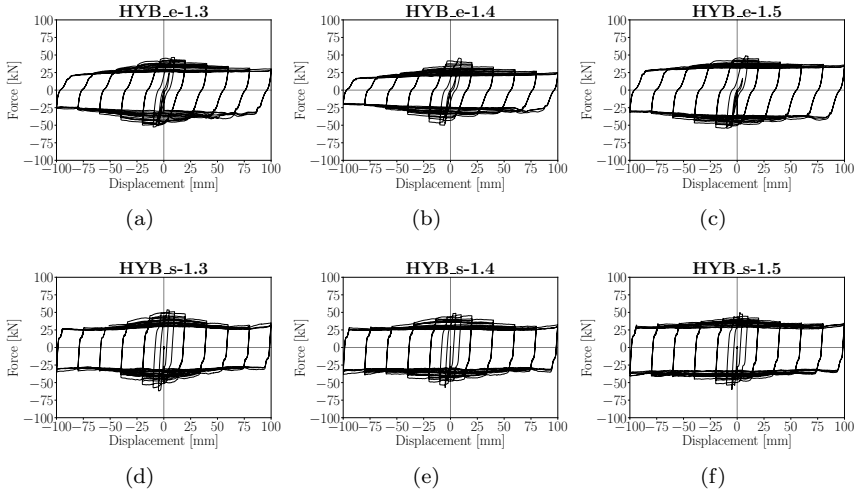

Fig. V.11. Test results for specimen HYB_e-1 HYB_s-1 with preload 37.5kN.

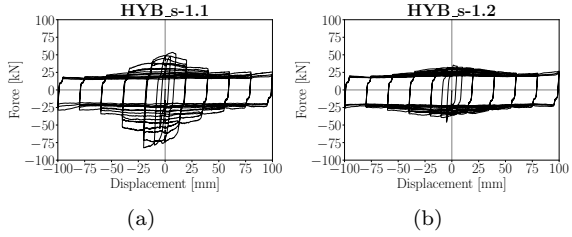

Fig. V.12. Test results for specimen HYB_s-1 with preload 25kN.

The authors adopted the same definition of slip force F_{slip} as [40], which is defined as the dissipated energy E per unit of travel D:

$$E = \sum_{i=0}^{n} E_i = \sum_{i=0}^{n} \left| \frac{F_{i+1} + F_i}{2} \cdot (\delta_{i+1} - \delta_i) \right| \qquad D = \sum_{i=0}^{n} |\delta_{i+1} - \delta_i| \qquad F_{\text{slip}} = \frac{E}{D} \tag{V.1}$$

where E_i denotes the energy at the $i-$th time step, F_i and δ_i are the force and displacement at the same time step, respectively. The dissipated energy is a strictly increasing function, and is thus chosen as parameter for the evaluation of the slip force, as opposed to the force value which varies. The standard deviation and COV are calculated as follows:

$$F_{sd} = \sqrt{\frac{\sum_{i=0}^{n} |F_i - F_{\text{slip}}|^2}{n-1}} \qquad COV = \frac{F_{sd}}{F_{\text{slip}}} \tag{V.2}$$

This parameter synthesizes the stability of the hysteresis loops and the nature of the sliding behavior: a low value of COV corresponds to stable performance, with a loop shape more similar to the ideal rectangle. The experimental friction coefficient μ is evaluated as:

$$\mu = \frac{F_{\text{slip}}}{n_s n_b F_P} \tag{V.3}$$

where F_{slip} is the slip force calculated in Eq.(V.2), $n_s = 2$ is the number of shear surfaces, $n_b = 2$ is the number of the preloaded bolts and F_P is the preload force from Tab.V.2. It's important to note that the definition of slip force, and so the friction coefficient, is dependent on the dissipated energy and thus the displacement imposed as load protocol. Particularly in the case of shorter load protocols, considering the initial force peaks, the calculations may be inaccurate until the connection and the contact areas have stabilized, reaching the real contact area as suggested by [47]. For the data elaboration the authors decided to use only the cycles after 20mm, since the initial part is considered of settlement and not of real friction behavior. Furthermore, in tests including the CLT panel, the displacement adopted was purified from the effect of the timber connection by subtracting the displacement value measured by the LDT A fixed on the CLT, see Fig.V.7(a).

The values of slip force and friction coefficient of specimen HYB-1, reported in Tab.V.3, appear higher than all the others. These aspects confirm that the amplitude and number of the cycles strongly influence the stabilization of the friction behaviour since these tests had a shorter load protocol (see Tab.V.2). Specimen HYB-2, HYB-3, HYB_e all had friction coefficients in line with the expectations for aluminium shims, with an average value for the 13 tests equal to

Table V.3. Results in terms of slip force, standard deviation, coefficient of variation, stability coefficient and friction coefficient.

Test	F_{slip} [kN]	StDev[kN]	COV	μ
HYB-1.1	29.61	12.92	0.44	0.30
HYB-1.2	36.07	14.68	0.41	0.36
mean				0.33
HYB-2.1	28.35	13.70	0.48	0.28
HYB-2.2	26.91	10.35	0.38	0.27
HYB-2.3	22.49	6.91	0.31	0.22
HYB-2.4	25.52	7.40	0.29	0.26
HYB-3.1	19.86	7.98	0.40	0.20
HYB-3.2	19.73	7.52	0.38	0.20
HYB-3.3	20.55	5.67	0.28	0.21
HYB-3.4	21.58	5.73	0.27	0.22
HYB_e-1.1	17.03	5.32	0.31	0.17
HYB_e-1.2	19.21	5.52	0.29	0.19
HYB_e-1.3	30.38	8.15	0.27	0.20
HYB_e-1.4	24.79	6.43	0.26	0.17
HYB_e-1.5	34.41	8.53	0.25	0.23
mean				0.22
HYB_s-1.1	18.94	8.92	0.47	0.19
HYB_s-1.2	23.45	4.28	0.18	0.23
HYB_s-1.3	31.53	5.35	0.17	0.21
HYB_s-1.4	31.25	5.45	0.17	0.21
HYB_s-1.5	33.87	5.12	0.15	0.23
mean				0.21

0.22. This value is similar to the findings of the previous experimental campaign [40], and other values in literature [48]. The tests on the specimen HYB_s, carried out on the setup without CLT panel, show similar friction coefficient values, with a 0.21 average. The friction connection behaves as predicted in both systems, suggesting that the setup, including the CLT panel, does not significantly affect the friction connection. One difference may be found in the stability of the slip force since the tests on the CLT setup generally show higher COVs than the tests on the steel set up, proving that a stiffer connection system is always preferable to obtain a stable friction behaviour. A preliminary remark regards the preloading method according to [45]: the bolts preload is applied by using a torque wrench. Therefore, the accuracy of the initial value influences the resulting slip force used to calculate the friction coefficient. The torque wrench method can be affected by a significant uncertainty due to human error. This fact can result in a preload higher than designed. A misestimation of the slip force could have occurred for specimen HYB-2, which generally has a higher friction coefficient than the other two specimens. Nevertheless, this factor is to be also expected in the building site, where many different operators could be working and installing CLT panels and friction connections. Fig.V.13, for tests HYB-3.1 and HYB-3.2 as an example, highlights the possible misestimation of the actual slip force, and consequently the friction coefficient, being influenced by the loading protocol and showing a decreasing trend towards their final values. In the horizontal axis, the displacement steps of the loading protocol are shown, and for each value of step, three estimates of slip force (or friction coefficient) are shown, corresponding to cycles with the same maximum displacement. A small vertical distance between the markers of the same step indicates that the slip force (or friction coefficient) was not changing between repetitions at the same displacement step. The different displacement steps show the declining trend, which tends to the final value of slip force and friction coefficient. The authors waited for each specimen to cool down before testing again. Therefore the reduction of the friction coefficient within each test depends on both the temperature rising and wear phenomena. Conversely, the initial friction coefficient, observed at each test, depends on the energy dissipated in previous tests. The variation of the friction coefficient due to temperature cannot be eliminated. However, the friction stabilization due to wear phenomena can be reduced by adequately pre-treating the shim layers before installation. Artificial wear could be generated, thus limiting the significant slip force variation.

For brevity, the data recorded by other sensors is shown for the sole HYB-3.1 and HYB.3.2 tests, see Fig.V.14. The plots (a) and (d) display the displacement measured by additional sensors as a function of the displacement input of the loading protocol. Sensor A is the LDT measuring the relative slip between the free profile and the CLT panel. Sensor B records the same quantity but refers to

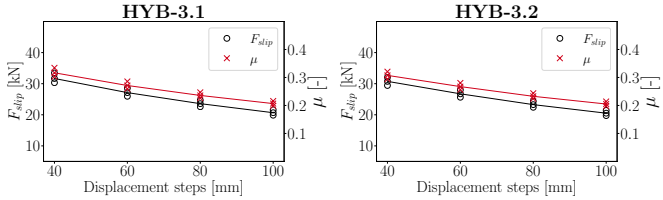

(a) (b)

Fig. V.13. Results of specimen HYB-3, in terms of slip force and friction coefficient, (a) first and (b) second repetition.

the fixed base, thus including the panel elastic deformation. Sensor C is the LDT measuring the uplift, and sensor D is the inclinometer. Fig.V.7 possesses the same notation. Interestingly the shape of these curves closely follows that of the slip force, and as expected, the measure from sensor B is slightly higher than sensor A. Measures from sensor C are almost zero, confirming the adequate stiffness of the hold-down. Plots (b) and (e) use the same measurements, but with the force value on the vertical axis. In this case, the S-shape of the curves is typical of timber connections, characterized by a certain level of pinching. Plots (c) and (f) show the values of the secant stiffness of the timber connection as a function of time. The stiffness was calculated by dividing the peak force at each cycle by the corresponding measure of the LDT A. The values were plotted for each cycle, separating the downwards from the upwards direction. The graphs show that the timber connection suffers from stiffness degradation as the number of cycles increases. The value of stiffness also changes abruptly between downwards and upwards direction after the first repetition, implying an effect from the residual deformations of the first test. This asymmetric behaviour was observed for all specimens following the first repetition in all tests.

Fig.V.15 shows the dissipated energy for tests HYB-3.1 and HYB.3.2, while the respective estimates are reported in Tab.V.4. The total dissipated energy, the black curve in Fig.V.15, was calculated using the displacement measured by the wire sensor during the tests. Parallelly, the friction energy was estimated using displacement values purged from the effect of the screw connection slip, i.e. by subtracting the measure taken by sensor A. This calculation aims to isolate the energy dissipation due to friction. From the plots and the values in the Tab.V.4, it is evident that the two contributions are almost equal, with differences smaller than 3%. This fact suggests that the screw connection was stiff enough and did not reduce the energy dissipation due to friction.

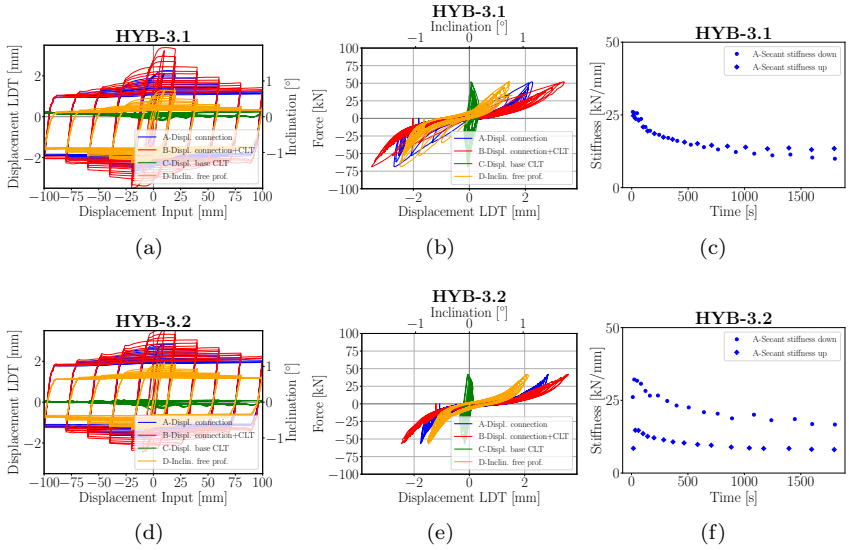

Fig. V.14. Example of results of specimen HYB-3, first and second repetition. Figures (a) and (d) show the displacements/inclination measured by some sensors with reference to the input displacement, Fig.V.6 aids the reader with a labels referring to the sensors considered. Figures (b) and (e) plot the displacements of the sensors and the measured force. Figures (c) and (f) show an estimate of the secant stiffness of the screw connection.

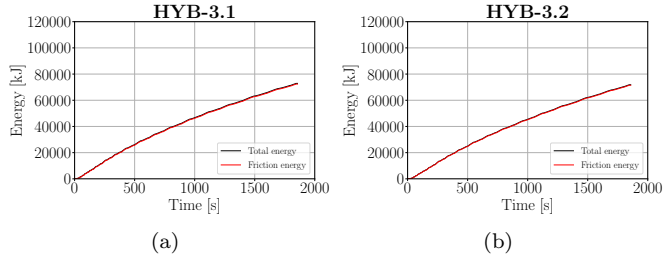

Fig. V.15. Results of specimen HYB-3, in terms of dissipated energy, (a) first and (b) second repetition.

Table V.4. Dissipated Energy

Test	F_{slip} [kN]	Tot. Energy [kJ]	Fric. Energy [kJ]	Diff [%]
HYB-1.1	29.61	48929.59	47763.38	2.38
HYB-1.2	36.07	56849.11	55779.93	1.88
HYB-2.1	28.35	99499.52	98067.97	1.44
HYB-2.2	26.91	94513.16	93538.26	1.03
HYB-2.3	22.49	79627.88	78952.65	0.85
HYB-2.4	25.52	89283.50	88512.00	0.86
HYB-3.1	19.86	72876.99	72361.55	0.71
HYB-3.2	19.73	71847.07	71448.99	0.55
HYB-3.3	20.55	73750.34	73356.27	0.53
HYB-3.4	21.58	76981.71	76594.24	0.50
HYB_e-1.1	17.03	62562.89	62324.80	0.38
HYB_e-1.2	19.21	69662.94	69429.91	0.33
HYB_e-1.3	30.38	107081.30	106635.93	0.42
HYB_e-1.4	24.79	88260.30	87902.15	0.41
HYB_e-1.5	34.41	119802.50	119339.37	0.39
HYB_s-1.1	18.94	91906.66		
HYB_s-1.2	23.45	86867.67		
HYB_s-1.3	31.53	116433.62		
HYB_s-1.4	31.25	115282.31		
HYB_s-1.5	33.87	124091.57		

Table V.5. Dissipated Energy: comparison between the two setups

Test	F_{slip} [kN]	μ	Tot. Energy [kJ]
HYB-2/3/e1.1/2	21.84	0.22	78493.76
HYB_s-1.1/2	21.20	0.21	89387.17
diff [%]	3.08	3.97	12.19
HYB_e-1.3/4/5	29.86	0.20	105048.03
HYB_s-1.3/4/5	32.22	0.22	118602.50
diff [%]	7.32	7.69	11.43

This approach followed for estimating the dissipated energy due to friction, although simple, may still include other possible deformations of the CLT setup, such as elastic deformations of the CLT panel and the rotation of the screwed connection. Then, an indirect way for evaluating and separating the full effect of the CLT presence and screw connection is to compare the results between the two setups with and without the CLT. TabV.5 shows the differences between the two setups in a synthetic way for the specimens with the same load protocol: the first part of the table refers to the tests with a 25kN preload force, the second part to the tests with 37.5kN preload force. The first line shows the mean value of the dissipated energy for the first and second repetitions of tests on the CLT setup (HYB-2.1, HYB-2.2, HYB-3.1, HYB-3.2, HYB_e-1.1, HYB_e-1.2), while the second line lists the same quantities for the steel setup (HYB_s-1.1, HYB_s-1.2). The third line is calculated as the mean value for the third, fourth and fifth repetition of tests on the CLT setup (HYB_e-1.3, HYB_e-1.4, HYB_e-1.5), while the fourth line is the mean for the same repetitions on the steel setup (HYB_s-1.3, HYB_s-1.4, HYB_s-1.5). This comparison enables us to apprehend the fundamental difference between the two setups. While the differences in slip force and friction coefficient are small, minor than 4% and 8% for lower and higher preload, respectively, the difference in dissipated energy is around 12%. This result proves that the timber connection effect is a decrease in dissipated energy compared to a system where only the steel friction connection is present.

V.4 Hysteresis modeling

The authors modeled the experimental cyclic curves using a Duhem-class hysteresis model [49, 50], obtained from the LuGre friction model [51] by introducing a stabilization term of the Coulomb friction and eliminating the Stribeck [52] and viscosity effects which did not manifest in the experimental tests. The slip force can be expressed as:

$$f_s = k_0 z \tag{V.4}$$

where f_s is the slip force, k_0 is the pre-slip stiffness and z is the auxiliary inelastic displacement. The following first-order differential equation governs the evolution of the z variable:

$$\dot{z} = \dot{x}\left[1 - \left(\frac{k_0}{\mu_u h(\epsilon) F_p}\right) z \text{sign}\dot{x}\right]^n \qquad h(\epsilon) \equiv \frac{\mu}{\mu_u} = 1 + \frac{\alpha}{1+\beta\epsilon^\eta} \tag{V.5}$$

where x is the displacement, $\dot{x}$ the derivative of x with respect to time, F_p the preload force, μ_u the stable friction coefficient, $\alpha = \frac{(\mu_i - \mu_u)}{\mu_u} \in [0-1]$ expresses the relative increment of the friction coefficient at the initial stages of deformation (μ_i), β and γ define the shape of stabilization function of the friction coefficient,

ϵ is the dissipated hysteretic energy. Firstly, the authors provide the motivations in choosing this particular hysteresis model, then they validate the model against the experimental data. In the last subsection, the model parameters of the chosen model are estimated from all experimental data using a genetic optimization algorithm.

V.4.1 Motivation in the model selection

The dry kinetic friction, occurring in the tested specimens, can be described by the well-known Coulomb equation:

$$f_s(x, \dot{x}) = \mu F_p \text{sign}\dot{x} \tag{V.6}$$

where μ is the friction coefficient. However, the basic Coulomb model suffers from two severe limitations. It does not model the pre-slip stiffness and it cannot reproduce the corner chipping effect, often significant in friction connections. The pre-slip stiffness derives from the intrinsic deformability of the connection and the shim layers, which deform before the slip triggering. The chipping effect, consisting in the corner smoothing of the hysteresis curve in the un-loading phase also depends on both the shim material and the connection. They exhibit a force delay in the unloading phases, at the first stages of the reversing of the load protocol.
The Coulomb friction model may therefore not be accurate, and the classical Bouc-Wen model could be a valid alternative [53, 54]. Besides, the most used hysteresis model in structural dynamics is the Bouc-Wen, which can reproduce multiple hysteresis phenomena [55]. For a structural element described by a Bouc–Wen class model, the force is written as

$$f_s(x, \dot{x}, z) = \alpha k_0 x + (1 - \alpha) k_0 z \tag{V.7}$$

where α the post-to-preyield stiffness ratio, and k_0 the initial stiffness. In friction connections α is generally very low, since there are no hardening phenomena. The evolution of z is determined by an auxiliary ordinary differential equation

$$\dot{z} = \dot{x}[A - |z|^n \psi(x, \dot{x}, z)] \tag{V.8}$$

where $\dot{z}$ is the derivative of z with respect to time, A a parameter that controls the scale of the hysteresis loops, n controls the sharpness of the hysteresis loops, and $\psi(x, \dot{x})$ a nonlinear function determining other shape features of the hysteresis loop. However, the ψ functions of the original Bouc–Wen model, and the subsequent model developments, like the ones proposed Wang and Wen [56], Song [57], Aloisio [58], are not especially suited for friction connections since they do not possess an explicit dependence on the friction coefficient and the pre-loading force.

Therefore, the Dahl friction model [59], equivalent to the Bouc-Wen model for $n = 1$, is the usual choice in friction modelling. The first-order differential equation governing the evolution of the inelastic displacement in the Dahl friction model is

$$\dot{z} = \dot{x}[1 - z\,\mathrm{sign}\dot{x}]^n \tag{V.9}$$

However, also this model, generally used in friction modelling, does not possess an explicit dependence on the slip force, which must be calibrated by varying the n parameter.

The most general friction model is the LuGre one [51], which originate from the Dahl model and captures the Stribeck ("stick-slip") effect [60, 61]. This model explicits both the Coulomb sliding friction force, and the Stribeck sticking friction force. The following set of equations governs the LuGre model:

$$\dot{z} = \dot{x}\left[1 - z\,\frac{\mathrm{sign}\dot{x}}{g(\dot{x})}\right]^n \qquad k_0 g(\dot{x}) = F_c + (F_s - F_c)\mathrm{e}^{(-\dot{x}/v_s)} \qquad f_s = k_0 z + c_1\dot{z} + c_2\dot{x} \tag{V.10}$$

where c_1 is friction rate effect, c_2 is viscous rate effect, F_c is the Coulomb sliding friction force, F_s is the Stribeck sticking friction force, v_s the Stribeck velocity.

However, the current experimental tests did not evidence the Stribeck phenomenon and manifested a reduction of the friction coefficient as the number of cycles increased.

Therefore, the authors adopted the LuGre model with the following upgrades and simplifications: the Coulomb sliding friction force is set equal to the Stribeck sticking friction force, since there are no stick-slip phenomena, and the rate coefficients c_1 and c_2 are set equal to zero, since the tests are quasi-static and the viscous phenomena are negligible.

The evolution of the friction coefficient is achieved by adopting a stabilization function, dependent on the dissipated hysteretic energy. Initially the authors adopted an exponential function, as they did in [40]. However, the exponential function hardly follows the evolution of the friction coefficient observed in the experimental tests. Accordingly, following the well-known formulation by [62] of the degradation function, the authors observed that the stabilization function closely follows a hyperbolic evolution. Fig.V.16 shows the comparison between experimental data and all three possible modeling approaches presented above. In conclusion, a modification of the LuGre friction model, shown in Eq.V.5, rather than the Bouc-Wen model, is adopted for three main reasons. (i) The LuGre model is is among the most general models in trybology and possesses an explicit dependence on the mechanical parameters (the pre-load force and the friction coefficients, e.g.). (ii) On the contrary, the classical Bouc-Wen model, despite capable of mirroring a wide range of hysteretic phenomena, is characterized by multiple variable with no direct physical meaning. (iii) Additionally, the

parameters of the Bouc-Wen model are redundant, since multiple combination of them can shape the same hysteresis curve [63].

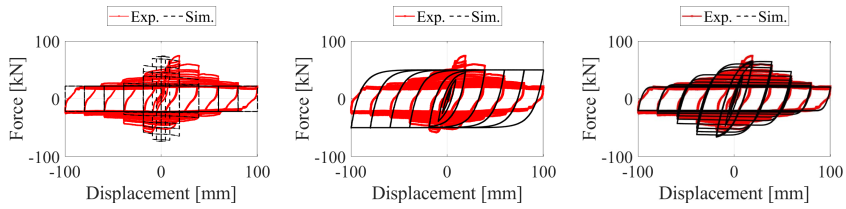

Fig. V.16. Comparison between three hysteresis model in fitting the experimental data of the HYB-2.1 test. The first is the Coulomb model with degradation proposed by [40], the second is the classical Bouc-Wen model, the third is the one implemented in this research shown in Eq.V.5.

V.4.2 Model validation and parameter estimation

Fig.V.17 plots the comparison between the experimental and simulated hysteresis curves using Eq.V.5 in terms of force-displacement, force-time and energy-time functions. The superposition is very accurate, despite the limits and reduced

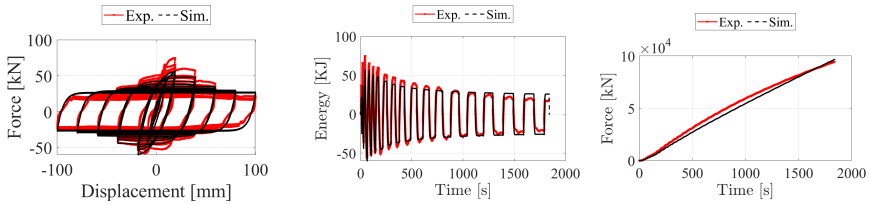

Fig. V.17. Comparison between the experimental and simulated data in terms of force-displacement, force-time and energy-time functions for the HYB-2.1 test.

number of parameters. However, the model has two primary weaknesses: the hysteresis model cannot mirror (i) possible asymmetries in the hysteresis curve and (ii) the peculiar S-like shape during the first stages of loading due to the pinching between the screws and the CLT specimen. However, these two phenomena are not very influential to the structural performance of the AFC. Besides, the asymmetries in the loop should be absent in an actual case application. Though, in the current setup, the CLT specimens are restained by a hold-down, causing

asymmetries in the response. However, despite these two limits, the chosen model accurately seizes the stabilization of the slip force, and the estimated dissipated energy almost overlaps with the experimental curve.
The authors repeated the fitting to all test data and estimated the parameters using a genetic optimization algorithm. Specifically, the experimental force-displacement data are used to calibrate the hysteresis model parameters. The calibration was performed by using the function GA (Genetic Algorithm) of the global optimization toolbox of software MATLAB [64, 65]. The genetic algorithm performs iteration of parameters with the goal of minimizing the following objective function:

$$\text{obj}(\mathbf{p}) = \frac{\sum_{i=1}^{N} | \left[F_{ei} - F_{si}(\mathbf{p})\right] \Delta x_i|}{\sum_{i=1}^{N} |F_{ei} \Delta x_i|} \tag{V.11}$$

where N is the number of data points, $\mathbf{p}$ is the parameter vector containing the hysteresis model parameters, F_{ei} and Δx_i are the experimental data in terms of force and displacement increment respectively and $F_{si}(\mathbf{p})$ is the restoring force of the system simulated with the hysteresis model. Note that the objective function is defined as normalized integral of the difference between experimental force and simulated force. This gives a measure of discrepancy between experimental data and model simulation. The optimization was carried out by defining appropriate lower and upper bounds for the model parameters, based on the physical interpretation of each of them, see Tab.V.6. The parameters and their ranges of variations are: k_0, μ_u, n, α, β, and η. The comparison between the experimental and simulated hysteresis curves in terms of force-displacement, force-time and energy-time functions are shown in the supplementary material. The plots confirm the satisfactory matching between experimental and simulated data anticipated in Fig.V.17. Tab.V.6 is organized in three sections, referring to the three tested specimens. The parameters optimization reveals that the screwed connection significantly reduces the pre-slip stiffness from approximately 15kN/mm to almost 5kN/mm. The effect of a lower eccentricity in the HYB_e typology possibly results in a minor increment of the pre-slip stiffness.
The stable friction coefficient, i.e. the friction coefficient corresponding to the stable cycles, is quite variable, especially after repetitions of the loading protocols. However, it is on average 0.26 for the HYB specimen and 0.23 for HYB_e. It confirms that a lower eccentricity reduces the slip force due to the lacking of parasite bending effects. The average friction coefficient reduces to 0.20 if there is no screwed connection. It may depend on possible lower eccentricity effects, which determine higher slip loads associated with uneven stress distribution. This is coherent with the findings from the experimental tests, even if these values are generally slightly higher due to the fact the LuGre model is fitted to the complete test, without excluding the initial cycles and LDT A measure as was done in the

Table V.6. Optimum parameters of the hysteresis model in Eq.V.5 for each data set.

Label	k_0 [kN/mm]	μ	n	α	β	η
HYB-1.1	5.95	0.25	0.89	4.63	2.19E-07	0.9745
HYB-1.2	5.86	0.30	0.97	2.64	1.86E-07	0.9364
HYB-2.1	5.11	0.22	0.89	4.99	1.17E-07	0.9738
HYB-2.2	5.25	0.26	0.96	4.85	9.57E-08	0.9692
HYB-2.3	4.57	0.22	0.98	3.47	2.57E-07	0.8998
HYB-2.4	4.06	0.29	0.94	1.99	9.57E-08	0.9306
HYB-3.1	5.51	0.22	0.82	4.30	1.66E-07	0.9602
HYB-3.2	5.29	0.23	0.97	4.97	2.32E-07	0.9692
HYB-3.3	5.29	0.28	0.88	1.68	1.03E-07	0.9664
HYB-3.4	4.53	0.28	0.81	1.89	5.25E-07	0.8742
Mean	5.14	0.26	0.91	3.54	2.00E-07	0.95
Variance	0.36	1.13E-03	3.76E-03	1.89	1.67E-14	1.21E-03
HYB_e-1.1	5.64	0.22	1.00	2.47	9.23E-08	1.0000
HYB_e-1.2	5.54	0.24	0.99	2.18	1.16E-07	0.9624
HYB_e-1.3	5.44	0.20	0.84	2.22	2.28E-07	0.8601
HYB_e-1.4	5.26	0.24	0.72	1.53	2.97E-07	0.9039
HYB_e-1.5	5.89	0.22	0.65	1.80	4.50E-07	0.7828
Mean	5.55	0.23	0.84	2.04	2.37E-07	0.90
Variance	0.06	1.99E-04	0.02	0.14	2.12E-14	0.01
HYB_s-1.1	14.50	0.20	0.91	4.79	9.49E-08	0.9226
HYB_s-1.2	14.00	0.22	1.00	1.34	8.76E-07	0.7640
HYB_s-1.3	15.29	0.21	0.97	1.27	5.63E-08	0.8946
HYB_s-1.4	15.49	0.23	0.76	1.70	3.32E-08	0.9604
HYB_s-1.5	19.42	0.15	0.98	3.11	2.94E-07	0.7909
Mean	15.74	0.20	0.92	2.44	2.71E-07	0.87
Variance	4.59	1.04E-03	0.01	2.28	1.25E-13	0.01

experimental part. The n exponent is not very sensitive to the test data since the shape of the hysteresis loop is comparable between tests. The α, and β and η parameters are not highly variable between test data and depend on the friction coefficient evolution as the dissipated energy grows. Therefore, for engineering purposes, the practitioner can use the mean values of the obtained parameters to represent the response of each AFC typology reliably.

V.5 Estimate of the pre-slip stiffness effect

As discussed in [40], the e-CLT system experiences two phases: the stick and the slip phases. During the stick phase, the AFC does not activate, and the total resisting force at the i-th story (f_t) is the summation of the resisting forces of the CLT panel (f_{clt}) and the RC frame (f_{rc}). If the reaction of the CLT panel exceeds the slip force (f_s), the AFC activates, and the total resisting force is the summation of the resisting force of the RC frame and the slip force of the AFC. The e-CLT unit behaves like a parallel system, whose governing equations are:

$$f_t = f_{\text{rc}} + f_{\text{clt}} \quad \text{if} \quad |f_{\text{clt}}| \leq |f_s| \tag{V.12}$$

$$f_t = f_{\text{rc}} + f_s \quad \text{if} \quad |f_{\text{clt}}| > |f_s| \tag{V.13}$$

The conditional statement on the exceeding of the slip force drives the transition between the two stick and slip phases of the response. Given the lateral pre-slip stiffness of the whole system comprising CLT panel-screw connection-steel plates (k_0), the conditional statement can be written in term of the displacement associated with the AFC activation:

$$d_{\text{act}} = \frac{|f_s|}{|k_0|} \tag{V.14}$$

Ideally, the AFC should be undeformable and, if the resisting force attains the slip force, the AFC activates. However, the AFC possesses a pre-slip stiffness (k_0), due to the deformability of the steel profiles and the screw connection. Therefore, the AFC deformation is needed to attain the required slip force level.
Fig.V.18(a) shows the superposition between three simulated hysteresis curves obtained by varying the pre-slip stiffness. Fig.V.18(b) displays the evolution of the percentage dissipated energy, $e_d = \frac{E_d}{E_{d,\infty}}$, where E_d is the dissipated energy and $E_{d,\infty}$ is the dissipated energy corresponding to $k_0 \to \infty$.
The increment of the total dissipated energy is not linear, and tends to an horizontal asymptote. The curve shows a clear bend for a pre-slip stiffness approximately equal to 5 kN/mm, when $e_d = 90\%$. The percentage difference

between the dissipated energy with and without CLT panel is approximately 12%, as shown in Tab.V.5 in the previous section. Therefore, Fig.V.18 is coherent with the experimental findings since it proves that with the considered CLT specimens, the 90% of the dissipation potential is exploited. Consequently, an approximate 10% difference between the cases with and without the CLT specimens is expected. A pre-slip stiffness lower than 5kN/mm leads to a dramatic reduction of the dissipation potential. A pre-slip stiffness higher than 5kN/mm does not cause a meaningful increment of the dissipated energy. Therefore, for a slip force equal to approximately 20kN, the lateral stiffness of the slip connection should not be lower than 5kN/mm.

More generally, in terms of displacement, the activation displacement of the

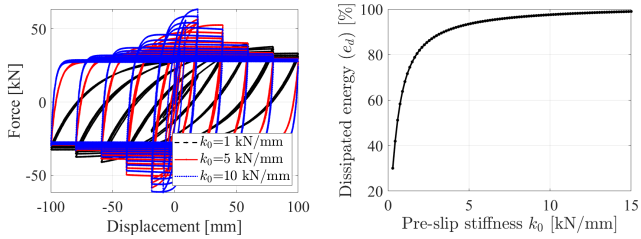

(a) (b)

Fig. V.18. (a) Superposition of hysteresis cycles for different pre-slip stiffess values, (b) Estimate of the percentage dissipated energy, $e_d = \frac{E_d}{E_{d,\infty}}$, where $E_{d,\infty}$ is the dissipated energy corresponding to $k_0 \to \infty$.

tested AFC (d_{act}) should be:

$$d_{\text{act}} < \frac{f_s}{k_0} \approx \frac{20}{5} = 4\text{mm} \text{ if } f_s = 20\text{kN} \tag{V.15}$$

This optimal threshold is valid for an AFC with an approximate 20kN slip force. The authors simulated the cyclic response of different AFCs by varying both the slip force and the pre-slip stiffness to possibly derive a general design rule for the prediction of the minimum activation displacement corresponding to a correct design. Fig.V.19(a) shows the dissipated energy in percentage e_d, as the ratio between the dissipated energy E_d and the maximum dissipated energy ($E_{d,\infty}$) associated to a pre-load stiffness $k_0 \to \infty$. The chosen normalization of E_d allows the simultaneous plotting of curves related to different slip forces. The authors will assume that the optimal AFC performance is associated with a dissipation potential (e_d) equal to 90%. Interestingly, the values of the pre-slip stiffness, corresponding to the intersection between the e_d-k_0 curves and the horizontal

threshold at 90%, plotted against the slip forces do not follow a straight line, see Fig.V.19(b). Therefore, the estimate of the activation displacement equal to 4mm, valid for $f_s = 20kN$, would lead to an overestimation of the pre-slip stiffness. The authors fitted the values of $e_d \approx 90\%$ using a nonlinear least-squares optimization and obtained the following expression for the activation displacement, plotted in Fig.V.19(b):

$$d_{\text{act}} = \frac{f_s}{k_0} \approx 4.5\text{mm} + \frac{f_s[\text{kN}]}{20} \tag{V.16}$$

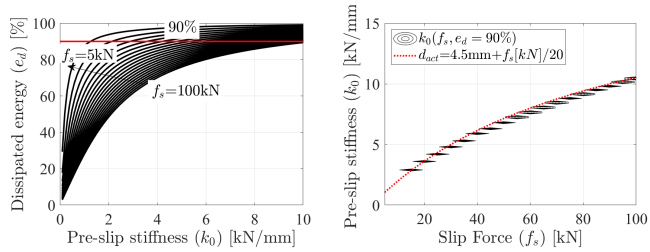

Fig. V.19. (a) Estimate of the percentage dissipated energy for different slip force values, (b) Pre-slip stiffness vs slip force for 90% of dissipated energy.

The activation displacement should rise linearly to the slip force, as the slip force grows. This phenomenon is related to peculiar shape of the hysteresis loop. The maximization of the area inside the loop entails the contemporary increment of the activation displacement as the slip force grows.
In conclusion, the correct design of the AFC requires the estimation of the slip force and the pre-slip stiffness. The slip force derives from the structural design, while the pre-slip stiffness can be determined from Eq.V.16, which provides the activation displacement as a function of the slip-force.

V.5.1 Lateral stiffness of the screw connection

Theoretically, the design pre-slip stiffness can be obtained by using an adequate number and arrangement of screws. However, the pre-slip stiffness is also strongly affected by the intrinsic deformability of the AFC layout rather than only by the screw connection. In this subsection, the contribution of pre-slip stiffness due to the screws has been isolated. The experimental lateral stiffness of the screw connection is compared to the estimates according to the Eurocode 5 and a recent formulation by [66].
According to the current Eurocode [67] the slip modulus (K_{ser}) per shear plane

per fastener under service load for joints made with dowel-type fasteners is related to the mean density ρ_m and the diameter d by the first formula of Eq.V.17. The current formulation lacks parameters such as the length of penetration of the screw into the timber members. An alternative approach to the problem was proposed by [68], in this case the formulation for the slip modulus was derived from an analytical model that considers the screw as a rigid body on elastic springs. Simplified but more accurate formulas to predict the sliding modulus starting from the geometric characteristics and timber member densities of the connection has been derived by [66]. This approach, seen in the second formula of Eq.V.17, are based on an analytical model of beam on elastic foundation taking into account the timber anisotropy and the axial and bending stiffness of the screws:

$$k_{i,EC5} = 2\rho_m^{1.5} d_{ef}/23 \qquad k_{i,DS} = 0.44\rho_m^{1.02} l_p^{0.075} d_{ex}^{1.24} \tag{V.17}$$

where ρ_m is the mean timber density in kg/m^3, d_{ex} is the outer thread diameter, l_p is the length of penetration of the screw into the CLT panel and $d_{ef} = 1.1 d_{in}$ where d_{in} is the screw thread root diameter. The total stiffness of the connection was calculated as an equivalent spring that takes into account the rotational effect of the eccentricity as follows (see also Fig.V.20):

$$K_e = \frac{1}{\frac{1}{K_v} + \frac{e^2}{K_r}} \qquad K_v = \sum_{i=1}^{n_s} k_i \qquad K_r = \sum_{i=1}^{n_s} k_i r_i^2 \tag{V.18}$$

where K_e is the stiffness of the connection evaluated in a point of eccentricity e with respect to the center of rotation of the connection (center of the screws), k_i is the slip modulus of the i^{th} screw, K_v is the equivalent translational slip modulus of all screws, n_s is the number of screws, K_r is the equivalent rotational slip modulus of all screws and r_i is the distance of the i^{th} screw to the center of rotation.

The experimental estimates in Tab.V.7 are calculated as secant values for the first repetition on each specimen, calculated as the average value of the first cycles up to 20mm. Tab.V.8 shows a comparison between the experimental secant stiffness and the two analytical formulations. The comparison proves that the formulation from [66] is closer to the experimental one.

However, the experimental estimates and the predicted values significantly exceed the pre-slip stiffness of the considered AFC connections. Therefore, the design value of the pre-slip stiffness cannot be obtained directly by varying the number and arrangement of the screws. The geometry of the AFC and its layout significantly affects the overall deformability, since the sole stiffness of the screws is five times higher than the pre-slip stiffness of the whole system.

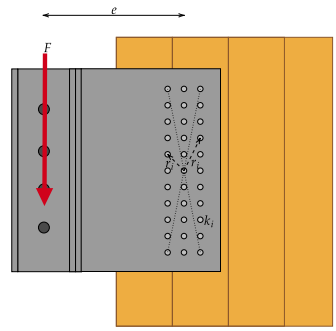

Fig. V.20. Scheme for the evaluation of the stiffness.

Table V.7. Experimental secant stiffness.

Test	K_e [kN/mm]
HYB-1.1	31.50
HYB-2.1	32.34
HYB-3.1	24.67
HYB_e-1.1	22.84
Mean	27.84
St.Dev	4.14

Table V.8. Stiffness values comparison, values in [kN/mm]

Experimental	De Santis [66]	EC5
27.84	31.74	38.29

Accordingly, the pre-slip stiffness should be estimated from a detailed FE model of the connection or experimental test of the complete system configuration, rather than an analytical estimate of the stiffness of the screwed connection from technical standards or well-acknowledged formulations.

V.6 Conclusions

This paper presents the experimental results of cyclic tests on a particular class of asymmetric friction connections (AFC) attached to CLT panels. Following the experimental campaign by Boggian et al. [40], this paper investigates the effect of the screw connection, connecting the AFC to the CLT panel, on the friction performance of the AFC. The main effect of the screw connection is the reduction of the pre-slip stiffness of the AFC. The experimental tests also confirmed the findings by multiple researchers on this topic. The friction coefficient of the AFC tends to stabilize after multiple cycles, possibly due to wear phenomena between the aluminum shims and the steel plates, to an average value of 0.22. Future research will aim at improving the friction coefficient stability by reducing the consequences of wear phenomena by proper pre-treatment of the shim layers surfaces. The effect of the pre-slip stiffness on the AFC performance has been estimated by developing a novel analytical hysteresis model for AFC, obtained from a modification of the Lu-Gre model. The friction coefficient evolution is obtained by adopting a hyperbolic energy-dependent term. The model leads to a satisfactory agreement between experimental and simulated data. Furthermore, the model has been calibrated using a genetic optimization algorithm implemented in Matlab. The proposed model is then used to estimate the effect of the pre-slip stiffness on the AFC performance. The analysis shows that in the considered setup, the AFC with the CLT panel leads to a 90% exploitation of the maximum dissipation potential of the AFC, in full agreement with the experimental results. The maximum dissipated energy corresponds to a pre-slip stiffness tending to infinity. The role of the pre-slip stiffness is crucial to reach optimal energy dissipation. Therefore, the designer must select the pre-slip stiffness and the slip force to maximize the dissipation potential. In the considered specimen, the pre-slip stiffness should not be lower than 5 kN/mm to achieve a 90% of the dissipation potential. The pre-slip stiffness strongly depends on the friction system geometry rather than solely on the number and arrangement of screws. The experimental and analytical estimates of the lateral stiffness of the screwed connection significantly exceed the pre-slip stiffness. Therefore, the number and arrangement of screws are not the sole design parameter for increasing the design pre-slip stiffness. The designer must develop a detailed model of the complete AFC system to provide a reliable estimate of the pre-slip stiffness.

Acknowledgments

The authors would like to thank Scott Brenna, Frode Røsstad, Matteo Manghi, Roar Økseter and Øyvind Hansen for their precious contribution during the testing activity.

Funding

This paper was carried out in the framework of the "Energy and seismic affordable renovation solutions" (e-SAFE) project, which has received funding from the European Union's Horizon 2020 research and innovation programme under grant agreement No.893135. Neither the Executive Agency for Small and Medium-sized Enterprises (EASME) nor the European Commission is in any way responsible for any use that may be made of the information it contains.

Bibliography

[1] D. W. White and Y. Duk Kim, "Unified flexural resistance equations for stability design of steel i-section members: Moment gradient tests," *Journal of Structural Engineering*, vol. 134, no. 9, pp. 1471–1486, 2008.

[2] D. S. Priya, A. Cinitha, P. Umesha, and N. R. Iyer, "A critical review on enhancing the seismic response of buildings with energy dissipation methods," *Journal of Structural Engineering*, vol. 42, no. 3, pp. 78–88, 2015.

[3] B. Spencer Jr and S. Nagarajaiah, "State of the art of structural control," *Journal of structural engineering*, vol. 129, no. 7, pp. 845–856, 2003.

[4] A. Habibi, R. W. Chan, and F. Albermani, "Energy-based design method for seismic retrofitting with passive energy dissipation systems," *Engineering Structures*, vol. 46, pp. 77–86, 2013.

[5] T. E. Saaed, G. Nikolakopoulos, J.-E. Jonasson, and H. Hedlund, "A state-of-the-art review of structural control systems," *Journal of Vibration and Control*, vol. 21, no. 5, pp. 919–937, 2015.

[6] S. Jaisee, F. Yue, and Y. H. Ooi, "A state-of-the-art review on passive friction dampers and their applications," *Engineering Structures*, vol. 235, p. 112022, 2021.

[7] C. Valente, D. Cardone, M. Dolce, and F. Ponzo, "Manside: Shaking table tests of r/c frames with various passive control systems," in *Proc. 12th World Conference on Earthquake Engineering*, 2000.

[8] W.-F. Chen and E. M. Lui, *Handbook of structural engineering*. CRC press, 2005.

[9] A. S. Pall and C. Marsh, "Response of friction damped braced frames," *Journal of the Structural Division*, vol. 108, no. 6, pp. 1313–1323, 1982.

[10] L. Pesaresi, M. Stender, V. Ruffini, and C. Schwingshackl, "Dic measurement of the kinematics of a friction damper for turbine applications," in *Dynamics of Coupled Structures, Volume 4*, pp. 93–101, Springer, 2017.

[11] G. Csaba, "Modelling of a microslip friction damper subjected to translation and rotation," in *Turbo Expo: Power for Land, Sea, and Air*, vol. 78613, p. V004T03A012, American Society of Mechanical Engineers, 1999.

[12] A. S. Pall and C. Marsh, "Friction-damped concrete shearwalls," in *Journal Proceedings*, vol. 78, pp. 187–193, 1981.

[13] A. S. Pall, "Friction devices for aseismic design of buildings," in *4th Canadian Conference on Earthquake Engineering*, pp. 475–484, 1983.

[14] C. Pasquin, N. Leboeuf, R. T. Pall, and A. Pall, "Friction dampers for seismic rehabilitation of eaton's building, montreal," in *13th world conference on earthquake engineering*, pp. 1–2, 2004.

[15] R. Chandra, M. Masand, S. Nandi, C. Tripathi, R. Pall, and A. Pall, "Friction-dampers for seismic control of la gardenia towers south city, gurgaon, india," in *12 th World Conference on Earthquake Engineering, Auckland, New Zealand*, 2000.

[16] A. Pall, S. Vezina, P. Proulx, and R. Pall, "Friction-dampers for seismic control of canadian space agency headquarters," *Earthquake Spectra*, vol. 9, no. 3, pp. 547–557, 1993.

[17] B. Wu, H. Li, L. Lin, and M. Shan, "Seismic retrofit of a city hall in northeast china with frictional energy dissipators," *Journal of Building Structures*, vol. 19, no. 5, pp. 28–36, 1998.

[18] B. Wu, J. Zhang, M. Williams, and J. Ou, "Hysteretic behavior of improved pall-typed frictional dampers," *Engineering Structures*, vol. 27, no. 8, pp. 1258–1267, 2005.

[19] A. Filiatrault and S. Cherry, "Performance evaluation of friction damped braced steel frames under simulated earthquake loads," *Earthquake spectra*, vol. 3, no. 1, pp. 57–78, 1987.

[20] T. Fitzgerald, T. Anagnos, M. Goodson, and T. Zsutty, "Slotted bolted connections in aseismic design for concentrically braced connections," *Earthquake spectra*, vol. 5, no. 2, pp. 383–391, 1989.

[21] M. Latour, G. Rizzano, A. Santiago, and L. S. da Silva, "Experimental response of a low-yielding, self-centering, rocking column base joint with friction dampers," *Soil Dynamics and Earthquake Engineering*, vol. 116, pp. 580–592, 2019.

[22] W. Y. Loo, P. Quenneville, and N. Chouw, "A new type of symmetric slip-friction connector," *Journal of Constructional Steel Research*, vol. 94, pp. 11–22, 2014.

[23] H.-H. Khoo, C. Clifton, G. MacRae, H. Zhou, and S. Ramhormozian, "Proposed design models for the asymmetric friction connection," *Earthquake Engineering & Structural Dynamics*, vol. 44, no. 8, pp. 1309–1324, 2015.

[24] H.-H. Khoo, C. Clifton, J. Butterworth, G. MacRae, and G. Ferguson, "Influence of steel shim hardness on the sliding hinge joint performance," *Journal of Constructional Steel Research*, vol. 72, pp. 119–129, 2012.

[25] H.-J. Kim and C. Christopoulos, "Friction damped posttensioned self-centering steel moment-resisting frames," *Journal of Structural Engineering*, vol. 134, no. 11, pp. 1768–1779, 2008.

[26] A. A. Rad, G. A. MacRae, N. K. Hazaveh, and Q. Ma, "Shake table testing of a low damage steel building with asymmetric friction connections (afc)," *Journal of Constructional Steel Research*, vol. 155, pp. 129–143, 2019.

[27] H.-H. Khoo, C. Clifton, J. Butterworth, and G. MacRae, "Experimental study of full-scale self-centering sliding hinge joint connections with friction ring springs," *Journal of Earthquake Engineering*, vol. 17, no. 7, pp. 972–997, 2013.

[28] J. C. Chanchi Golondrino, G. A. MacRae, J. G. Chase, G. W. Rodgers, and G. C. Clifton, "Seismic behaviour of symmetric friction connections for steel buildings," *Engineering Structures*, vol. 224, p. 111200, 2020.

[29] W. Y. Loo, P. Quenneville, and N. Chouw, "A numerical study of the seismic behaviour of timber shear walls with slip-friction connectors," *Engineering Structures*, vol. 34, pp. 233–243, 2012.

[30] W. Loo, P. Quenneville, and N. Chouw, "A new type of symmetric slip-friction connector," *Journal of Constructional Steel Research*, vol. 94, pp. 11–22, 2014.

[31] W. Y. Loo, C. Kun, P. Quenneville, and N. Chouw, "Experimental testing of a rocking timber shear wall with slip-friction connectors," *Earthquake Engineering & Structural Dynamics*, vol. 43, no. 11, pp. 1621–1639, 2014.

[32] W. Y. Loo, P. Quenneville, and N. Chouw, "Rocking timber structure with slip-friction connectors conceptualized as a plastically deformable hinge within a multistory shear wall," *Journal of Structural Engineering*, vol. 142, no. 4, p. E4015010, 2016.

[33] D. Fitzgerald, A. Sinha, T. H. Miller, and J. A. Nairn, "Axial slip-friction connections for cross-laminated timber," *Engineering Structures*, vol. 228, p. 111478, 2021.

[34] D. Fitzgerald, T. Miller, A. Sinha, and J. Nairn, "Cross-laminated timber rocking walls with slip-friction connections," *Engineering Structures*, vol. 220, 2020.

[35] A. Björnfot, F. Boggian, A. Nygård, and R. Tomasi, "Strengthening of traditional buildings with slim panels of cross-laminated timber (clt)," International Conference on Structural Health Assessment of Timber Structures, 09 2017.

[36] I. Sustersic and B. Dujic, "Seismic strengthening of existing urm and rc structures using xlam timber panels," International conference on Earthquake Engineering, 01 2013.

[37] F. Stazi, M. Serpilli, G. Maracchini, and A. Pavone, "An experimental and numerical study on clt panels used as infill shear walls for rc buildings retrofit," *Construction and Building Materials*, vol. 211, pp. 605–616, 2019.

[38] C. Tardo, F. Boggian, M. Hatletveit, E. Marino, G. Margani, and R. Tomasi, "Mechanical characterization of energy dissipation devices in retrofit solution of reinforced concrete frames coupled with solid wood panels," Proceedings of the 12th International Conference on Structural Analysis of Historical Constructions, 2020.

[39] G. Margani, G. Evola, C. Tardo, and E. M. Marino, "Energy, seismic, and architectural renovation of rc framed buildings with prefabricated timber panels," *Sustainability*, vol. 12, no. 12, 2020.

[40] F. Boggian, C. Tardo, A. Aloisio, E. Marino, and R. Tomasi, "Experimental cyclic response of a novel friction connection for seismic retrofitting of rc buildings with clt panels," *Journal of Structural Engineering*, 2022.

[41] C. Tardo, *Seismic and energy renovation of RC framed buildings with cross-laminated timber panels equipped with innovative friction dampers.* PhD thesis, University of Catania, Italy, 2021.

[42] EN14399-4, "High-strength structural bolting assemblies for preloading - part 4: System hv - hexagon bolt and nut assemblies," 2015.

[43] Rothoblaas, "Screws and connectors for wood-carpentry, structures and outdoor." Accessed: 2022-01-12.

[44] EN15129, "Anti-seismic devices," 2018.

[45] EN1090-2, "Execution of steel structures and aluminium structures - part 2: Technical requirements for steel structures," 2018.

[46] SBE-Varvit, "Structural bolting assemblies en 14399 preloaded assemblies." Accessed: 2022-01-12.

[47] F. P. Bowden, F. P. Bowden, and D. Tabor, *The friction and lubrication of solids*, vol. 1. Oxford university press, 2001.

[48] J. Golondrino, G. MacRae, J. Chase, and G. Rodgers, "Behaviour of asymmetrical friction connections using different shim materials," in *New Zealand Society for Earthquake Engineering Conference*, 2012.

[49] P. Duhem, "Die dauernden aenderungen und die thermodynamik. i," *Zeitschrift für Physikalische Chemie*, vol. 22, no. 1, pp. 545–589, 1897.

[50] V. Hassani, T. Tjahjowidodo, and T. N. Do, "A survey on hysteresis modeling, identification and control," *Mechanical systems and signal processing*, vol. 49, no. 1-2, pp. 209–233, 2014.

[51] C. C. De Wit, H. Olsson, K. J. Astrom, and P. Lischinsky, "A new model for control of systems with friction," *IEEE Transactions on automatic control*, vol. 40, no. 3, pp. 419–425, 1995.

[52] B. Drincic, "Mechanical models of friction that exhibit hysteresis, stick-slip, and the stribeck effect," 2012.

[53] R. Bouc, "Influence du cycle d'hysteresis sur la resonance non lineaire d'un circuit serie," in *Colloq. Inter. du CNRS*, vol. 148, pp. 483–489, 1964.

[54] R. Bouc, "A mathematical model for hysteresis," *Acta Acustica united with Acustica*, vol. 24, no. 1, pp. 16–25, 1971.

[55] Y.-K. Wen, "Method for random vibration of hysteretic systems," *Journal of the engineering mechanics division*, vol. 102, no. 2, pp. 249–263, 1976.

[56] C.-H. Wang and Y.-k. Wen, *Reliability and redundancy of pre-Northridge low-rise steel buildings under seismic excitation.* na, 1998.

[57] J. Song and A. Der Kiureghian, "Generalized bouc–wen model for highly asymmetric hysteresis," *Journal of engineering mechanics*, vol. 132, no. 6, pp. 610–618, 2006.

[58] A. Aloisio, R. Alaggio, J. Köhler, and M. Fragiacomo, "Extension of generalized bouc-wen hysteresis modeling of wood joints and structural systems," *Journal of Engineering Mechanics*, vol. 146, no. 3, p. 04020001, 2020.

[59] P. R. Dahl, "A solid friction model," tech. rep., Aerospace Corp El Segundo Ca, 1968.

[60] M. F. Mohammad Naser and F. Ikhouane, "Consistency of the duhem model with hysteresis," *Mathematical Problems in Engineering*, vol. 2013, 2013.

[61] A. Visintin, "Mathematical models of hysteresis," in *Modelling and Optimization of Distributed Parameter Systems Applications to Engineering*, pp. 71–80, Springer, 1996.

[62] T. T. Baber and Y.-K. Wen, "Random vibration of hysteretic, degrading systems," *Journal of the Engineering Mechanics Division*, vol. 107, no. 6, pp. 1069–1087, 1981.

[63] M. Ismail, F. Ikhouane, and J. Rodellar, "The hysteresis bouc-wen model, a survey," *Archives of computational methods in engineering*, vol. 16, no. 2, pp. 161–188, 2009.

[64] M. Pelliciari, G. C. Marano, T. Cuoghi, B. Briseghella, D. Lavorato, and A. M. Tarantino, "Parameter identification of degrading and pinched hysteretic systems using a modified bouc–wen model," *Structure and Infrastructure Engineering*, vol. 14, no. 12, pp. 1573–1585, 2018.

[65] S. Sirotti, M. Pelliciari, F. Di Trapani, B. Briseghella, G. Carlo Marano, C. Nuti, and A. M. Tarantino, "Development and validation of new bouc–wen data-driven hysteresis model for masonry infilled rc frames," *Journal of Engineering Mechanics*, vol. 147, no. 11, p. 04021092, 2021.

[66] Y. De Santis and M. Fragiacomo, "Timber-to-timber and steel-to-timber screw connections: Derivation of the slip modulus via beam on elastic foundation model," *Engineering Structures*, vol. 244, p. 112798, 2021.

[67] EN1995-1.1, "5-1. eurocode 5: Design of timber structures–part 1-1: General rules and rules for buildings," *European Committee for Standardization (CEN)*, 2004.

[68] U. A. Girhammar, N. Jacquier, and B. Källsner, "Stiffness model for inclined screws in shear-tension mode in timber-to-timber joints," *Engineering structures*, vol. 136, pp. 580–595, 2017.

. List of publications

Scopus profile `https://www.scopus.com/authid/detail.uri?authorId=57210106957`
Researchgate Profile `https://www.researchgate.net/profile/Francesco-Boggian`

Shear Walls - codification

[1] A. Björnfot, F. Boggian, A. Nygård, and R. Tomasi, "Strengthening of traditional buildings with slim panels of cross-laminated timber (clt)," in *International Conference on Structural Health Assessment of Timber Structures*, 09 2017. Link.

[2] F. Boggian, M. Andreolli, and R. Tomasi, "Cross laminated timber (clt) beams loaded in plane: testing stiffness and shear strength," *Frontiers in Built Environment*, vol. 5, p. 58, 2019. Doi.

[3] F. Boggian, E. Ricci, A. Salenikovich, R. Springhetti, and R. Tomasi, "Deflections of light timber frame shear wall segments: Validation of a standard proposal," in *Proceedings of the World Conference of Timber Engineering-WCTE*, (Chile), 2021. Link.

[4] A. Aloisio, F. Boggian, R. Tomasi, and M. Fragiacomo, "Reliability-based assessment of ltf and clt shear walls under in-plane seismic loading using a modified bouc-wen hysteresis model," *ASCE-ASME Journal of Risk and Uncertainty in Engineering Systems, Part A: Civil Engineering*, vol. 7, 2021. Doi.

[5] A. Aloisio, F. Boggian, R. Tomasi, and M. Fragiacomo, "The role of the hold-down in the capacity model of ltf and clt shear walls based on the experimental lateral response," *Construction and Building Materials*, vol. 289, 2021. Doi.

[6] A. Aloisio, F. Boggian, and R. Tomasi, "Plastic deformation contributions of clt and ltf shear walls: development of an analytical capacity model," in *Proceedings of the World Conference of Timber Engineering-WCTE*, (Oslo, Norway), 2023. Abstract accepted.

[7] F. Boggian, A. Aloisio, J. Bjørkedal, H. Østraat Sævareid, and R. Tomasi, "Elastic displacement of timber shear walls: parametric analysis for ltf and clt," in *Proceedings of the World Conference of Timber Engineering-WCTE*, (Oslo, Norway), 2023. Abstract accepted.

[8] F. Boggian, A. Aloisio, H. Østraat Sævareid, J. Bjørkedal, and R. Tomasi, "Analysis and enhancement of the new eurocode 5 formulations for the lateral elastic deformation of ltf and clt walls," *Structures*, vol. x, 2022. Doi.

Shear walls - Renovation

[1] C. Tardo, F. Boggian, M. Hatletveit, E. Marino, G. Margani, and R. Tomasi, "Mechanical characterization of energy dissipation devices in retrofit solution of reinforced concrete frames coupled with solid wood panels," in *Proceedings of the 12th International Conference on Structural Analysis of Historical Constructions*, 2020. Doi.

[2] F. Boggian, C. Tardo, A. Aloisio, E. Marino, and R. Tomasi, "Experimental cyclic response of a novel friction connection for seismic retrofitting of rc buildings with clt panels," *Journal of Structural Engineering*, 2022. Doi.

[3] A. Aloisio, F. Boggian, and R. Tomasi, "Optimization of the slip force in a novel friction-based connection for the e-clt technology," in *Proceedings of COMPDYN2021- Computational Methods in Structural Dynamics and Earthquake Engineering*, 2021. Doi.

[4] A. Aloisio, F. Boggian, and R. Tomasi, "Design of a novel seismic retrofitting system for rc structures based on asymmetric friction connections and clt panels," *Engineering Structures*, vol. 254, 2022. Doi.

[5] C. Tardo, F. Boggian, G. Evola, E. Marino, G. Margani, and R. Tomasi, "Innovazione: riqualificazione sismica ed energetica di edifici in c.a. mediante pannelli xlam." Ingenio-WEB. Link.

[6] F. Boggian, A. Aloisio, M. Pelliciari, S. Sirotti, and R. Tomasi, "Restoration of existing rc frame buildings with clt panels: experimental and numerical study on innovative connection system," in *Proceedings of ICSA2022 - International Conference on Structures and Architecture*, 2022.

[7] A. Aloisio, M. Pelliciari, S. Sirotti, F. Boggian, and R. Tomasi, "Optimization of the structural coupling between rc frames, clt shear walls and asymmetric friction connections," *Bulletin of Earthquake Engineering*, 2022. Doi.

[8] F. Boggian, A. Aloisio, and R. Tomasi, "Experimental and analytical study of friction connection for seismic retrofit with clt panels," *Earthquake Engineering and Structural Dynamics*, 2022. Doi.

[9] A. Aloisio, A. Contento, F. Boggian, and R. Tomasi, "Probabilistic friction model for aluminium–steel Asymmetric Friction Connections (AFC)," *Engineering Structures*, 2023. Doi.

[10] F. Boggian, A. Aloisio, and R. Tomasi, "Cyclic tests on an innovative friction dissipative device for seismic retrofit with clt panels," in *Proceedings of*

the World Conference of Timber Engineering-WCTE, (Oslo, Norway), 2023. Abstract accepted.

[11] F. Boggian, C. Tardo, A. Aloisio, F. Rizzo, S. Barattucci, L. Pozza, C. Mazzotti, E. Marino, G. Margani, and R. Tomasi, "Technological development of a novel friction connector for seismic renovation using clt panels," in *Proceedings of the World Conference of Timber Engineering-WCTE*, (Oslo, Norway), 2023. Abstract accepted.

[12] A. Aloisio, A. Contento, F. Boggian, and R. Tomasi, "Asymmetric friction connections (afc): temperature dependent probabilistic friction model," in *Proceedings of the World Conference of Timber Engineering-WCTE*, (Oslo, Norway), 2023. Abstract accepted.

This research is inserted in the topic of timber buildings. Many construction systems are available for building using timber, with the two main systems in residential ambit being Cross Laminated Timber (CLT) and Light Timber Frame (LTF). Both systems reckon on the presence of shear walls to bear the effects of horizontal loads like seismic events or wind. This thesis deals with timber shear walls and is divided into two parts: the first part is related to the design rules for ultimate and serviceability limit states to be included upcoming versions of the building codes, while the second part presents a novel use of CLT walls as seismic renovation for existing buildings, as part of a European project. The first part of the thesis, which is presented in three papers, is closely related to the process of producing new building codes, and aims at an easier integration between research and codification. The three papers cover the following topics: the behaviour of CLT panels under in-plane shear loading, the evaluation of the displacement at the top of LTF walls subjected to horizontal loads and a comparison between the lateral behaviour and capacity models for LTF and CLT shearwalls. The second part of the thesis deals with the use of CLT shear walls as a mean for the retrofit of existing buildings. The need for sustainable renovation solutions and improvement of the performance of existing buildings is at the base of the European project e-Safe. The project presents a multidisciplinary approach on building renovation, from a mechanical, energetic, technological, and architectural point of view. In this thesis the focus is on the seismic retrofit system called e-CLT: a CLT panel is attached to the outside of existing buildings with a novel connector that acts as friction dissipation device, thus offering additional energy dissipation in case of strong earthquakes. Two papers are included to illustrate the research on the new friction connection: the first presents the initial experimental campaign on a simplified steel setup to focus on the friction behaviour, while the second presents a following testing campaign that includes a CLT panel and the study of the influence of the timber-to-steel connection on the friction behaviour.

Francesco Boggian is civil engineer and studied at the Department of Civil, Environmental and Mechanical Engineering of the University of Trento, Italy. His principal research interest is the structural behaviour of timber products in constructions, focusing on Cross Laminated Timber (CLT) and Light Timber Frame (LTF) buildings. He studied the lateral behaviour of timber shear walls. He worked on the European project e-Safe in collaboration with the Norwegian University of Life Sciences: a multidisciplinary approach to building renovation. He focused on the development and testing of a novel friction connection used for attaching CLT panels to existing buildings for seismic retrofit purposes.